Simulating the impacts of climate on rivers, irrigation and crops in South Asia

Camilla Therese Mathison

Submitted in accordance with the requirements for the degree of
Doctor of Philosophy

The University of Leeds
School of Earth and Environment

May 2019

The candidate confirms that the work submitted is her own, except where work which has formed part of jointly authored publications has been included. The contribution of the candidate and the other authors to this work has been explicitly indicated below. The candidate confirms that appropriate credit has been given within the thesis where reference has been made to the work of others.

The work in Chapter 2 of the thesis has appeared in publication as follows:
Mathison, C, Wiltshire, A. J., Falloon, P., and Challinor, A. J.(2015), *South Asia river flow projections and their implications for water resources*, Hydrol. Earth Syst. Sci., 19, 4783-4810, https://doi.org/10.5194/hess-19-4783-2015, 2015

The Regional climate simulations I completed as part of the HighNoon EU FP7 project form the basis of the research in this publication. I processed the data to run the river routing, wrote the manuscript, produced all figures and conducted the analysis presented in this paper. This paper was improved by comments and suggestions from the co-authors on drafts of the paper and reviewers during the peer review process.

The work in Chapter 3 of the thesis has appeared in publication as follows:
Mathison, C., Deva, C., Falloon, P., and Challinor, A. J.(2018), *Estimating sowing and harvest dates based on the Asian summer monsoon*, Earth Syst. Dynam., 9, 563-592, https://doi.org/10.5194/esd-9-563-2018, 2018

I devised a new method to calculate sowing and harvest dates based on the main meteorological phenomena for the region to improve the input data being used. I completed the analysis, produced all figures and wrote the manuscript. Chetan Deva provided gridded India observations which made the method possible. This paper was improved by comments and suggestions from the co-authors on drafts of the paper and reviewers during the peer review process.

The work in Chapter 4 of the thesis is currently in review, it is currently available in this discussion publication as follows:
Mathison, C., Challinor, A. J., Deva, C., Falloon, P., Garrigues, S., Moulin, S., Williams, K. and Wiltshire, A. J. *Developing a sequential cropping capability in the JULESvn5.2 land–surface model*, Geosci. Model Dev. Discuss., https://doi.org/10.5194/gmd-2019-85, in review, 2019.

I wrote and implemented the new code in the model to include a double cropping capability in JULES. I tested the code, developed the India suite of simulations and added crops to the Avignon suite of simulations. I completed all simulations, produced all figures and completed the analysis. Discussions with A. Wiltshire helped with the interpretation of the

results, particularly for the India sites and C. Deva provided gridded India observations which made comparisons of model yields against observed yield possible for the India points. S. Garrigues and S. Moulin provided expertise on the Avignon site and observations for running and evaluating JULES at the Avignon site, including flux and biomass observations. Thanks to the INRA EMMAH laboratory at Avignon (France) in charge of the flux and remote sensing site for the supply of this data. K. William provided code to generate the crop ancillaries for the simulations, an initial suite for the Avignon site without the crop model and help with parameter settings. This paper was improved by comments and suggestions from the co-authors on drafts of the paper

Acknowledgements

This PhD has been a long, rewarding, sometimes stressful but ultimately a great and worthwhile experience with support from many people along the way. I would like to acknowledge those people here.

Firstly I would like to thank my supervisors: Pete Falloon and Andy Challinor for creating the opportunity for me to do a PhD with Leeds University and providing guidance throughout the project. Thank you to the Met Office for allowing me the time and both the Hadley Centre Climate Programme (HCCP) and the EU FP7 High End cLimate Impacts and eXtremes (HELIX) project for providing funding to allow me to complete this project. Thank you to Michelle Lesnianski at Leeds and Tracy Noyce at the Met Office for being on hand to help answer all my administration queries. I would also like to thank my co-authors on the papers that make up three chapters of this thesis and my work colleagues, who have heard about nothing else for the last few years. Thanks also to the Impacts modelling development team and Earth system and mitigation science team at the Met Office and the Climate impacts group at Leeds for interesting and helpful conversations that helped me throughout the project.

Thanks to my family, particularly my husband Colin and my parents, Karen and Terry. They have been a constant source of support to me all the way through the project. Thanks also to my children, Finlay and Catriona, for providing a welcome distraction during the most challenging times and for whom this PhD has been ongoing for their entire life so far.

Abstract

The effect of increasing green house gases (GHGs) is already changing the worlds climate, increasing atmospheric temperatures and affecting the land-surface, for example, by changing water availability and the viability of crops. These direct and indirect climate change impacts interact with each other, thereby increasing or decreasing the overall impact of a changing climate. South Asia (SA) is a region with complex orography, ranging from high glaciated mountains, the headwaters for large rivers that flow through several countries to feed vast lowland deltas. The region has extensive irrigation systems that support an intensive agricultural industry. These features, together with a highly variable climate, make SA vulnerable to climate change and important for developing understanding of interactions between land-surface climate impacts.

This thesis develops simulations to study the interactions between water resources and crop production for SA using a land surface model. Analysis of SA river flows from regional climate model (RCM) simulations indicate an increasing water resource toward 2100. However this RCM does not include abstraction or irrigation. The Joint UK Land Environment Simulator (JULES) represents rivers but irrigation and crops require development to represent key features of the SA crop calendar; these include: the correct growing season inputs for crops, the capability to simulate several crops in rotation during a single growing period (sequential cropping) and crop specific irrigation.

This thesis addresses the main development needs for representing the SA region. A method is presented for estimating sowing and harvest dates for SA based on the dominating climatological phenomena, the Asian Summer Monsoon (ASM). This method provides a more accurate alternative to the global datasets of cropping calendars than is currently available and generates more representative inputs for climate impact assessments. In order to model the SA cropping system more accurately, the development and implementation of sequential cropping in JULES with crop specific irrigation is presented to develop simulations to understand how changes in the SA climate could affect water resources and crops. Finally I present simulations in which all of the individual developments from this thesis are brought together; these show the progress that has been made towards simulations that enable analysis of the impacts of climate on rivers, irrigation and crops for SA in a fully integrated way.

Contents

List of Figures

List of Tables

Abbreviations

AgMIP	Agricultural Model Intercomparison Project
APHRODITE	Asian Precipitation-Highly Resolved Observational Data Integration Towards the Evaluation of Water Resources
AR4	IPCC 4th assessment report
AR5	IPCC 5th assessment report
a.s.l.	Above sea level
ASM	Asian summer monsoon
CMIP	Coupled Model Intercomparison Project
DGVM	Dynamic global vegetation model
ECHAM5	Climate model from the Max Planck Institute
ECMWF	European Centre for Medium Range Weather Forecasts
ERAint	ERA-interim reanalysis product from ECMWF
ESM	Earth System Model
EU FP7	European Union Funding Programme 7
GCM	General Circulation Model

GDP	Gross Domestic Product
GGCMI	Global Gridded Crop Model Inter-comparison
GHG	Green House Gas
GLAM	General Large Area Model
GRDC	Global Runoff Data Centre
HadAM3	Met Office Hadley Centre atmospheric model
HadCM3	3rd version of the Met Office Hadley Centre Climate Model
HadRM3	Hadley Centre Regional Climate Model
HELIX	High End cLimate Impacts and eXtremes
HNRCMs	HighNoon Regional Climate Models
IAMs	Integrated Assessment Models
ICRISAT	International Crops Research Institute for the Semi-Arid Tropics
IGP	Indo-Gangetic Plain
IPCC	Intergovernmental Panel on Climate Change
ISIMIP	Inter-Sectoral Impact Model Intercomparison Project
JULES	Joint UK Land Environment Simulator
JULES-IM	JULES standalone impacts model
KDE	Kernal Density Estimation
LSMs	Land surface models
LPJml	LundPotsdamJena managed land

MinAg	Ministry of Agriculture and Farmers Welfare, Government of India
MOSESv2.2	Met Office Surface Exchange scheme version 2.2
MMM	multi-model mean
NPPI	Normalized Pentad Precipitation Index
pdfs	Probability density functions
RCM	Regional Climate Model
REMO	Regional model from the Max Planck Institute
SA	South Asia
SD	Standard Deviation
STN-30p	Simulated Topological Network at 30 min resolution
SSA	Sub-Saharan Africa
SRES A1B	Scenario A1B from the Special Report on Emissions Scenarios
SWAT	Soil Water Assessment tool
TRIP	Total Runoff Integrating Pathways river-routing scheme
VMD	Vietnam Mekong Delta
VPD	Vapour Pressure Deficit

Chapter 1

Introduction

The observed increases in greenhouse gas (GHG) concentrations and the subsequent increase in temperatures are already having an impact on climate around the world. The complexity of the climate system means that climate change impacts individual regions differently, affecting both the average, variability and extremes of climate. Awareness of these impacts has resulted in a growing interest in their effect on food and water security. This has driven demand for climate impact assessments and therefore model development, for simulating the impacts of climate on food production and water resources (*Frieler et al.*, 2015).

Christensen et al. (2013) highlight that a direct effect of increased CO_2 concentrations can increase crop yields by increasing productivity. The impact of higher GHG concentrations, such as high temperatures and drought, can also reduce yields due to heat stress; this is likely to be a problem in tropical regions where the temperatures are already at or above the physiological maxima for crops (*Gornall et al.*, 2010). Direct impacts of climate can lead to other indirect effects. For example, higher average growing season temperatures may affect the rate a crop matures and cause a reduction in yield by shortening the growing season (*Hussain et al.*, 2018, *Waha et al.*, 2013, *Gornall et al.*, 2010). Other downstream impacts from increased temperatures could include increasing evaporation and transpiration costs or changes in the distribution of rainfall that lead to prolonged dry spells (*Hewitson et al.*, 2014); both of which could have an impact on the demand for water for irrigation (*Fischer et al.*, 2007, *Boonwichai et al.*, 2018). Rainfall distribution alone could be important, *Challinor et al.* (2004) found that even where the total rainfall amount stays the same, changes in the distribution of rainfall during the growing season strongly affected groundnut crop yield.

The relationship between climate impacts can be highly non-linear and therefore have a larger combined effect than seen individually (*Halladay and Good*, 2017). Agriculture acts to both influence and be influenced by the regional climate, for example, via the local effect of methane emissions from rice paddies (*Betts*, 2005). Large scale irrigation systems modify the local climate through evaporation (*Tuinenburg et al.*,

2014, *Harding et al.*, 2013) or affecting the radiation and energy balance at the surface, thereby affecting the surface temperature and humidity (*Kang and Eltahir*, 2018). Croplands cover a large proportion of the earth surface and therefore could have a significant influence on the response of the land surface to climate change. For example, higher CO_2 emissions are widely reported to cause a reduction in transpiration via reduced stomatal opening, thereby reducing the moisture flux from the surface (*Falloon and Betts*, 2010).

It is usual for studies regarding the impacts of climate to be sector specific, with each using different methods to understand the likely impacts to that sector. Usually the process for simulating the impacts of climate is unidirectional, with atmospheric models used to drive downstream offline models that simulate separate aspects of the land-surface, thereby using different models for crops and hydrology. This approach will always have caveats and limitations, not least of these is the missing feedbacks between the land–surface and the atmosphere, for example, allowing the croplands to modify the atmosphere through evaporation. This also means that there is little to link the impacts of two related sectors that are in reality affected not only by climate but also by each other (*Betts*, 2005). The Inter-Sectoral Impact Model Intercomparison Project (ISIMIP– *Warszawski et al.*, 2013, 2014) has highlighted the importance of these links between sectors and has developed frameworks to encourage modellers to develop their models with these in mind.

An integrated approach is common in understanding human influences on climate change and mitigation of greenhouse gases (*Schwanitz*, 2013), involving the use of Integrated Assessment Models (IAMs). For example, IAMs are used by economists to understand the links between the climate, social and economic factors to determine future climate change and the effectiveness of climate policy (*van Vuuren et al.*, 2011). They are often complicated because of all the different processes being represented. Inevitably this leads to compromises in the representation of some of the more complex areas. For example in terms of resolution, IAMs often aggregate geographical areas using economic metrics like GDP or they neglect the daily to monthly timescales (*Schwanitz*, 2013). IAMs are usually constructed with a very specific purpose in mind and therefore the choices made are affected by this. An economist would require a complex economic representation while an energy company might require a more complex demand and supply model (*Schwanitz*, 2013). Often IAMs use a simplified representation of the climate system and they are typically deterministic using a best guess approach to uncertainty (*Ackerman et al.*, 2009). On the other hand, *Lontzek et al.* (2015) applies a stochastic approach to study the economic impacts of climate tipping points. Nevertheless these simplified representations of the carbon cycle and climate can lead to large variations in outcomes (*van Vuuren et al.*, 2011).

The growing interest in climate change and food security has influenced the development of crop models for use in future climate impact assessments (*Frieler et al.*, 2017)

and encouraged large intercomparison projects such as the Agricultural Model Intercomparison and Improvement Project (AgMIP– *Rivington and Koo*, 2010, *Rosenzweig et al.*, 2013, 2014) and the Global Gridded Crop Model Inter-comparison (GGCMI– *Elliott et al.*, 2015). These large projects have developed frameworks to try to gain the most from this offline approach, encouraging and focussing model development by highlighting where models need to improve. For example as part of the AgMIP project, *Maiorano et al.* (2017) shows that improving the response of wheat to heat stress in 15 models reduces the uncertainty range in the model yields. These projects have also encouraged climate modellers to output relevant data from larger more complex models that are needed to run downstream sector specific models.

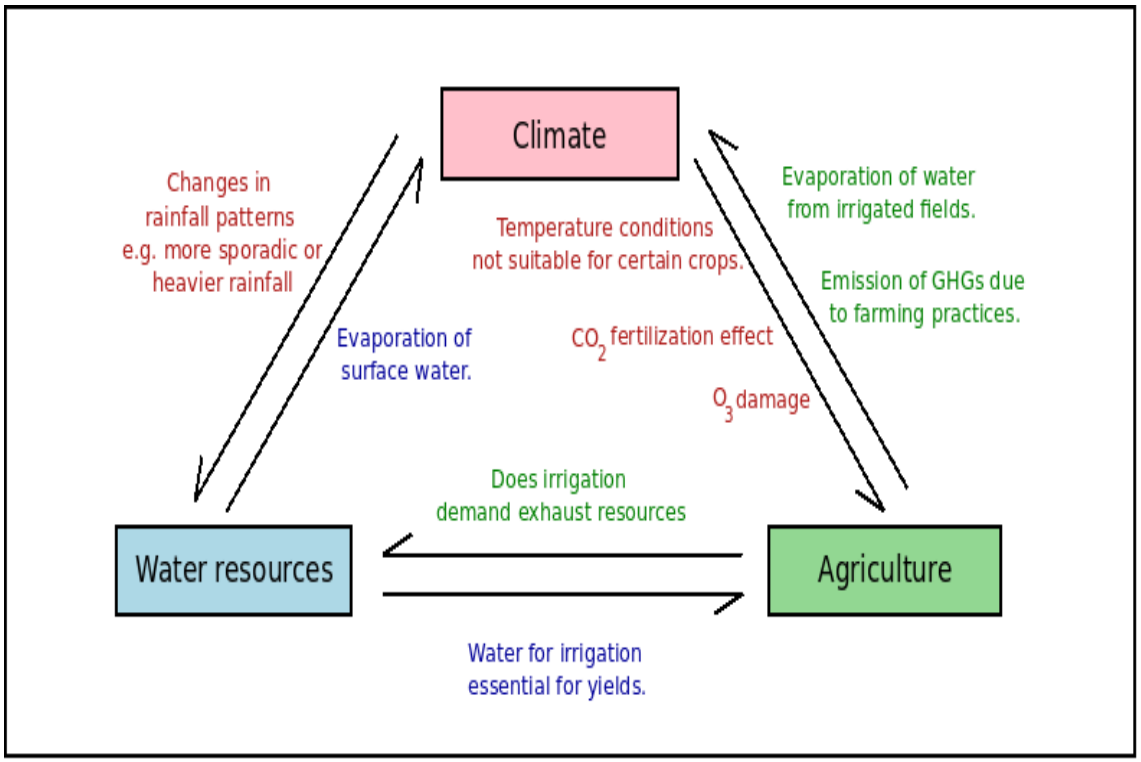

Figure 1.1: A flowchart summarizing the interactions between climate, irrigation and agriculture.

Betts (2005) highlights the need for an integrated or online approach to create more robust climate projections for crops, for example where the crop model is part of the land surface scheme and is therefore run as part of the larger climate model (*Osborne et al.*, 2007, 2015). The interactions between climate, water resources and agriculture are summarized by the flowchart shown in Fig. 1.1. The crop model could then take advantage of the high temporal resolution data from the climate model and the crops could feed back on the atmosphere and thereby affect the regional climate. *Betts* (2005) suggests that the implementation of crop and hydrology models into offline versions of land-surface models that are also used within climate models would be a significant step

towards a crop model that is a fully integrated part of a climate model. *Gornall et al.* (2010) highlight the interactions between climate, water resources and agriculture and the variation between these interactions for different regions. In their global analysis *Gornall et al.* (2010) highlight the uncertainties for the South Asia region particularly, with changes to the seasonality of river flows affected by increases in temperature and therefore snowmelt and precipitation. Any increases in water resources during times of excess can only have a positive impact on agriculture if it is stored during these periods; otherwise it could be lost to the oceans in the form of increased river flows and runoff.

The main aim of this thesis is to use a model that is both a standalone model, and the land–surface scheme within climate simulations, to make progress towards this more integrated approach for understanding climate impacts for a region where inter-sector interactions are important, namely South Asia. Global datasets are not readily available for all the different sectors, both for setting up the simulations and evaluating them. In this thesis the missing elements needed for simulating the impacts of climate for a particular region are identifed; methods to address these are then proposed and demonstrated in Chapters 2, 3 and 4. Chapter 5 applies these methods to a present day simulation to develop simulations of the impacts of climate on water resources and crop production. A more detailed description of each chapter is provided in Sect. 1.5. The study region selected for this analysis has the following characteristics:

- the region is already being strongly affected by the impacts of climate today,
- there are data available to both set up and evaluate simulations and
- there is a real need for more information on climate impacts.

The remainder of this chapter is structured as follows. The study region is introduced in Sect. 1.1 of this Chapter. The model is introduced in Sect. 1.2 and the climate forcing data that is used throughout this thesis is described in Sect. 1.3. An outline of the thesis providing more details on each chapter is provided in Sect. 1.5.

1.1 South Asia

South Asia (SA) is a region which has already experienced significant climate impacts, with parts of SA experiencing disasters such as tropical cyclones, storm surges, coastal erosion or flooding almost annually (*Rahman et al.*, 2019, *Mirza*, 2002). The impacts of climate are many and varied across SA, including: droughts, heatwaves, lightening strikes, cyclones, landslides, flash floods and salt water intrusion into agricultural lands. Bangladesh is particularly vulnerable to coastal climate impacts due to its low lying, relatively flat orography and coastline. The three large rivers (Ganges, Brahmaputra and the Meghna) that flow through Bangladesh to the Bay of Bengal, also represent a significant and increasing flood risk (*Mohammed et al.*, 2018). In general, the population

of SA is large and forecast to increase to more than 2 billion by 2050, with India alone accounting for 1.66 billion (*United Nations*, 2013, 2017). Almost 25 % of the Bangladesh population, which equates to more than 38 million people, live in these vulnerable coastal locations and are likely to be affected by these climate impacts (*Rahman et al.*, 2019). In recent times, floods particularly have displaced large numbers of people from their homes (*Dhar and Nandargi*, 2000). However, droughts are also likely to be an increasing problem for parts of SA as the mean global temperature increases (*Naumann et al.*, 2018). The SA region relies on industries with a high demand for water, including agriculture and hydroelectricity generation (*Rasul et al.*, 2019). The effect of climate on the demand for water resources from all sectors in SA is discussed in Chapter 2.

The economy of SA is expanding, with the per capita GDP of the region doubling over the last 10 years (from 957 USD in 2008 to 1840 USD in 2018). Yet 400 million people do not have access to electricity and 200 million face chronic food shortages or little access to fresh water or sanitation (*Rasul et al.*, 2019). *Rasul et al.* (2019) argues that increased resource scarcity, together with the growing demand for water for energy, food and other competing uses, highlights the need for integrated solutions for SA. These solutions would be coordinated across sectors to provide water for multiple uses, starting as a resource for generating hydropower, later being used for agricultural use, for making water navigable or sustaining fisheries. Currently, Nepal stores less than 1 % of its water for use later in the year (*Biswas*, 2008). However, there are plans for building reservoirs, with a total capacity of 121 km^3, equivalent to 18 % of the total annual flow of the Ganges (*Biswas*, 2008).

The terrain and climate of SA are extreme in their diversity. From the high mountainous glaciated regions of the Himalaya to vast lowland deltas, where large rivers cross multiple borders and enter both the Bay of Bengal and the Arabian sea. The climate is highly variable both temporally and spatially. Some parts of SA have surplus water (*Dhar and Nandargi*, 2000); while others, for example the north-west of the Indian subcontinent have extended periods of very low rainfall (*Thatte*, 2018). These factors contribute to making this part of the world highly vulnerable to climate change and therefore an important region to study. In addition to this vulnerability to climate, the SA land–surface has many features in a relatively limited area that are likely to be affected by the climate and by each other. Glaciers, large rivers and intensive irrigation systems together with a significant proportion of land devoted to agriculture and crop cultivation, are just some of the characteristics that make this an interesting region. These aspects of the land surface could usefully be considered together, as they interact and affect each other, but are often evaluated using separate models in a more sectoral approach (*Rasul et al.*, 2019). Although such individual models are highly specific and detailed they could miss important links and feedbacks from other parts of the land–surface, such as how much surface water is available and what is the demand for water for irrigation. In the remainder of this section water resources, including rivers and

irrigation, are discussed in Sect. 1.1.1 and crops are discussed in Sect.1.1.2.

1.1.1 Water resources

The Asian Summer Monsoon (ASM) is a major feature of the South Asian climate occurring during the months of June–September (*Goswami and Xavier*, 2005). The ASM is main source of fresh water for this region. There is also a contribution to water resources from glacial melt, which is likely to be important outside the ASM period when river flows are usually lower (*Mathison et al.*, 2013). Recent studies have cast doubt on the reliability of both the ASM (*Hewitson et al.*, 2014, *Christensen et al.*, 2013, 2007) and glacial melt (*Shannon et al.*, 2019, *Fujita and Nuimura*, 2011, *Bolch et al.*, 2012, *Gardelle et al.*, 2013) for future water resources for this region. The influence of glaciers on water resources for SA is discussed further in Chapter 2.

Rivers are an important source of irrigation water. Of the major basins in Northern India: the Indus, Ganges and Brahmaputra; the Indus basin has the largest proportion of water sourced from surface sources (i.e. rivers and lakes) with a larger contribution from glacial melt than the other two (*Biemans et al.*, 2013, *Immerzeel et al.*, 2010). A significant proportion, approximately 80 % of India's total demand for water is for the agricultural industry for irrigation. This means total water extractions from both surface and groundwater are large in this region (*Biemans et al.*, 2013). The gross irrigated area in SA has increased significantly: for India alone this has increased from 76 million ha in 2000-2001 to a provisional figure of 96 million ha in 2014-2015 (*Bodh et al.*, 2017). *Biemans et al.* (2013) uses the LundPotsdamJena managed Land model (LPJml – *Bondeau et al.*, 2007) to simulate changes in water resources for food production in five South Asian river basins. They find that for the Indus over 90 % of the crop production depends on irrigated land, which means a reduction in availability of water for irrigation could put yields at risk in this part of India. A significant proportion of the irrigation water for the Ganges, Godavari and Krishna basins comes from ground water, without which crop production in these basins would be severely impacted (*Biemans et al.*, 2013). Ground water is less renewable than surface water, but this resource is often heavily utilized, even when normal rainfall is observed because of pollution and mismanagement of surface waters (*Rodell et al.*, 2009). A key water resource in SA includes canals: these have been constructed all over India, three states in Northern India that account for 30 % of the water used for canal irrigation include Haryana, Punjab and Uttar Pradesh (*Narayanamoorthy*, 2018). Water tanks are also used in regions such as Tamil Nadu (*Anbumozhi et al.*, 2001).

The EU FP7 project, High End cLimate Impacts and eXtremes (HELIX) assessed a range of climate impacts and adaptation at different global warming levels (between 1.5 and 6$^{\circ}C$) using a new 60km resolution global model, HadGEM3A-GA3.0. As part of HELIX *Betts et al.* (2018) focussed on the hydrological impacts of climate change across the world, generally finding large differences between ensemble members for some

regions. However, for the Ganges there is agreement between most ensemble members for an increase in river flows, which represents more than a doubling of river flows at a $2°C$ global warming level. This agrees with the findings in the analysis of SA river flows presented as part of this thesis in Chapter 2, which uses 25km resolution regional climate model simulations described in Sect. 1.3 to provide runoff to a river routing scheme. This also shows that the Ganges could experience a doubling of river flow towards the 2100s.

1.1.2 Crops

One of the main features of the crops in SA is the use of the sequential cropping system, which makes the most efficient use of limited resources and space in order to maximize yield potential and lower the risk of complete crop failure. Sequential cropping is also referred to as multiple cropping and is discussed in Chapter 4. The Indo-Gangetic plains (IGP) traditionally provide the staple crops of rice and wheat in rotation (*Aggarwal et al.*, 2000) for India and SA as a whole; the continued success of these crops is therefore important for the food security of the region and can be severely affected by water availability. The two main seasons in SA agriculture correspond to summer and winter/spring growing seasons respectively; these are kharif and rabi. Kharif crops include rice, which is usually sown during the monsoon, and harvested in the autumn. Rabi crops include wheat, which is mainly cultivated during the dry season (*Erenstein and Laxmi*, 2008, *Singh et al.*, 2014) and is therefore irrigated. This crop rotation is discussed further in Chapter 3 and simulated in Chapter 4 of this thesis.

Biemans et al. (2016) found that including multiple cropping in a SA version of LPJml improved the simulations of the demand for water from irrigation, particularly the timing of the demand. This highlights the close relationship between crops and water resources and the importance of being able to simulate the two together. The model providing the basis for a more integrated approach to understanding climate impacts on water and crops in this thesis is introduced in Sect. 1.2.

1.2 The JULES land surface model

Chapter 4 of this thesis uses the Joint UK Land Environment Simulator (JULES) model described in detail in (*Best et al.*, 2011, *Clark et al.*, 2011). The relevant parts of JULES for this thesis are described in Chapter 4. JULES is the main land surface scheme used with the Met Office weather and climate models. JULES is a dual-purpose model, intended for both use as a standalone impacts model (JULES-IM) and as the land surface scheme in larger coupled simulations such as earth system models (ESMs eg. HadGEM2-ES; *Collins et al.*, 2011), global climate models GCMs e.g. (HadGEM3- *Williams et al.*, 2018a) and regional climate models (RCMs e.g. HadRM3- *Jones et al.*, 2004). JULES-IM and the larger coupled models are therefore based on the same code

structure, which reduces potential inconsistencies between them (*Betts*, 2005). JULES in these larger models allows feedbacks from the land surface to have an effect on the atmosphere, but simulations are often complex and require significant computational resource. JULES-IM on the other hand has a smaller demand for computer resource, because it models only the land surface processes and the associated fluxes. This means that, although feedbacks are unable to influence the atmosphere (and vice-versa) as this is prescribed from the driving data, it is possible to include additional processes that are not yet possible within most of the coupled models and study the impact of these processes on surface fluxes, e.g. crops and irrigation. The land–surface schemes in these larger simulations cannot currently include crops or irrigation which could be important for extensive cropland areas and regions with intensive irrigaton. The availability of JULES-IM means smaller more focussed studies are possible that include multiple aspects of the land-surface response to climate change in one simulation. JULES-IM allows a full evaluation of the influence of new model developments on the land-surface before they are implemented in larger more complicated simulations.

JULES is a process-based model that simulates the fluxes of carbon, water, energy and momentum between the land-surface and the atmosphere. JULES represents both vegetation (including natural vegetation and crops) and non-vegetation surface types including; urban areas, bare soil, lakes, and ice. With the exception of the ice tile all these tiles can co-exist within a gridbox so that a fraction of the surface within each gridbox is allocated between surface types. For the ice tile a grid box must be either completely covered in ice or not (*Shannon et al.*, 2019). JULES treats each vegetation type as a separate tile within a gridbox, with each one represented individually with its own set of parameters and properties, such that each tile has a separate energy balance. The forcing air temperature, humidity and windspeed are prescribed for the gridbox as a whole for a given height. Below the surface the soil type is also uniform across each gridbox (where the number of soil tiles is set to one). JULES-IM represents many different aspects of the land–surface, including river flows, irrigation and crops; these are individually important in terms of climate impacts but their impact on each other cannot be separated easily. In the remainder of this section the representation of each of these in JULES-IM are described in more detail.

1.2.1 River flow and glaciers in JULES

In this thesis, river flows in JULES are routed using the 0.5° Total Runoff Integrating Pathways river routing scheme (TRIP; *Oki and Sud*, 1998); this is the same scheme that is used in Chapter 2 as a post processing step, prior to being included in an official release of JULES. In this configuration, the TRIP routing scheme takes the 25km gridbox runoff from the RCM and converts it into river flow for comparison with river gauge observations. TRIP is described in more detail in Chapter 2. Previous studies that use TRIP successfully with GCMS such as HadCM3 and HadGEM1, improving

the seasonality of river flows for many major rivers (*Falloon et al.*, 2007, 2011), are also discussed in Chapter 2. The TRIP model has been shown to agree well with observed river flow gauge data (*Oki et al.*, 1999) and largely showed good skill when comparing runoff from several land surface models (*Morse et al.*, 2009). Using TRIP ensures the river flow forcing is consistent with the atmospheric forcing; however, it also assumes that all runoff is routed to the river network and as such there is no net aquifer recharge/discharge. This may not be the case in regions with significant ground water extraction which is subsequently lost though evaporation and transported out of the basin.

Representation of glaciers in JULES is a new development that is currently implemented in a branch of JULES vn4.7; this is presented in *Shannon et al.* (2019). The implementation of elevation bands in JULES together with a glaciated and unglaciated elevated tile allows the variation in glacial coverage up the mountain to be represented. Both glaciated and unglaciated elevated tiles can accumulate snow, represented in JULES using a full energy balance snow pack scheme; however, the glaciated tile can gain mass through accumulation and freezing of water and lose mass through sublimation and melting (*Shannon et al.*, 2019). These developments allow JULES to simulate changes in the mass balance of glaciers, which can move the terminus of a glacier higher up the mountain. However, this development does not include the dynamical processes needed to move the glacier down the mountain, i.e. glacier dynamics (*Shannon et al.*, 2019).

TRIP is already included in the current SA configuration presented in Chapter 5; however, further work is needed to successfully merge the glacier developments into this configuration. Including the glacier model development presented in *Shannon et al.* (2019) in a SA configuration of JULES-IM would be interesting and valuable future work, providing a more complete representation of the water resources for this region.

1.2.2 Irrigation in JULES

Irrigation in JULES is implemented in two stages. The first stage is to implement irrigation demand; setting only irrigation demand means that the water applied to the soil is unlimited by availability. All of the irrigation schemes in JULES add water to the top two soil levels (*Gedney et al.*, 2014; see Supplementary information) to ensure that the soil moisture is at a critical point (often the field capacity); this means that the vegetation does not experience water stress (*Williams and Falloon*, 2015, *Williams et al.*, 2017). Using the unlimited irrigation demand simulates potential yield (*Williams and Falloon*, 2015) in the absence of a yield gap parameter, which would account for the impact of differing nutrient levels, pests, diseases and non-optimal management (*Challinor et al.*, 2004).

The second stage for implementing the irrigation in JULES is to limit the irrigation according to water availability. When water is limited in JULES, water for irrigation

is taken first from the deep soil (surface groundwater) store. In this thesis surface groundwater is represented by a TOPMODEL-based approach in JULES (*Best et al.*, 2011, *Clark and Gedney*, 2008); this allows the lowest regions to become saturated first, using a topographic index to define the upstream area and the local slope and thereby determine which areas flood first. The TOPMODEL approach includes a deep soil layer in JULES, with a simplified representation of water fluxes. This deep soil layer occurs below the standard 4 soil levels (which occur at 0.1, 0.25, 0.65 and 2.0 m), i.e. below 3.0 m (*Best et al.*, 2011). When there is no more water available from this deep soil layer, then resource is taken from the river storage. Tiles are only then irrigated, provided water is available, up to the critical point. The critical point allows vegetation to maintain un-water-stressed transpiration at values below field capacity, i.e. the soil moisture held in the soil after any excess has drained away. In JULES this is defined as a matrix water potential of -33 kPa (*Best et al.*, 2011, *Cox et al.*, 1999).

Limiting the irrigation according to water availability is useful for understanding the impact of water availability on crop yields. *Halladay* (2018) assesses the performance of interactive hydrological and agricultural impacts for Brazil using JULES with both limited and unlimited irrigation, ensuring irrigation of specific tiles by introducing a new irrigated tile for c3 and c4 grasses. *Halladay* (2018) finds that JULES underestimates the irrigation demand for Brazil especially where the demand is highest. This happens whether irrigation is limited or not and is probably because JULES does not account for inefficiency of the irrigation system used. Irrigation efficiency is a particular problem for SA (*Biemans et al.*, 2013) and this would be a useful development for JULES; however, it is not included in JULES currently. There are three irrigation schemes available in JULES. In this thesis the scheme that requires the crop model is used (i.e. the number of crop tiles must be greater than 0); therefore for irrigation to occur, the crop must be sown. This means that irrigation only occurs during the crop season. In Chapter 4 of this thesis the irrigation scheme in JULES is extended in a branch of JULES vn5.2 so that irrigation can be more easily restricted to specific tiles. This development is intended for implementation in a future JULES release.

1.2.3 Crops in JULES

The parametrisation of crops in JULES (JULES-crop) is described in detail in *Osborne et al.* (2015) and *Williams et al.* (2017). The main aim of JULES-crop is to improve the simulation of land-atmosphere interactions where crops are a major feature of the land-surface (*Osborne et al.*, 2015). JULES-crop is intended for use both in JULES and JULES-IM (*Osborne et al.*, 2015). Each crop is represented by an additional separate tile within JULES-crop with four main crops included in the *Osborne et al.* (2015) JULES configuration; these are wheat, maize, soybean and rice. JULES-crop requires a sowing date, representing the start of the growing season and two thermal times that represent the growing season length. The thermal times contol the rate that

the crop develops through the stages of: sowing to emergence, emergence to flowering and flowering to maturity. In this thesis the concept of thermal time and effective temperature are introduced in Chapter 3, while the relevant JULES-crop equations for this study are discussed in Chapter 4.

There have been a number of studies that use JULES-crop within the JULES-IM infrastructure including *Williams et al.* (2018b, 2017) and *Williams and Falloon* (2015); although the aim of using JULES-crop fully integrated into a global climate model has not to date been realized, due to the complexity in setting up global coupled simulations that include crops. JULES-crop currently simulates a single crop per year by default, which is typical of many crop models, especially those used for global and regional applications (*Biemans et al.*, 2016). In Chapter 4 of this thesis the crop model is extended in a branch of JULES at vn5.2 to include the sequential cropping system, as with the modifications to irrigation (discussed in Sect. 1.2.2), this is also intended for implementation into a future release of JULES.

1.3 Data

This thesis uses 25 km resolution climate data for the SA region from the EU HighNoon project. The focus of the HighNoon project was on the water resources of Northern India but the RCM simulations were for the whole of the Indian subcontinent including the high Himalaya (25° N, 79° E–32° N, 88° E). This data is described in this thesis in Chapters 2 (Section 2.2 *Mathison et al.*, 2015) and 3 (Section 3.6 *Mathison et al.*, 2018), as well as a number of previous publications (*Kumar et al.*, 2013, *Mathison et al.*, 2013). The RCMs in the HighNoon project were run using GCM data from HadCM3 and ECHAM5 which were both considered to have a good representation of the monsoon (*Kumar et al.*, 2013, *Annamalai et al.*, 2007, *Mathison et al.*, 2013). The HighNoon RCMS (HNRCMs) are from the Coupled Model Intercomparison Project 3 (CMIP3), which contributed to the Intergovernmental Panel on Climate Change (IPCC) 4th assessment report (AR4- *Christensen et al.*, 2007). The HNRCMs also use the A1B SRES scenario (*Nakicenovic et al.*, 2000) from the same generation of models and simulations. Even though the SRES scenarios are almost 20 years old, they are no less probable than any of the more recent RCP scenarios from later CMIP simulations. In addition, their relevance to more recent work is maintained through projects like the HELIX project (Sect. 1.1.1). The HELIX Specific Warming Levels (SWLs) shift the focus from the particular climate scenario being used to a realization of what the world will look like at each of these SWLs of 1.5, 2, 4 and 6°C *Gohar et al.* (2017). These SWLs are used in Chapter 3 of this thesis.

Since AR4, the 5th assessment report (AR5- *Christensen et al.*, 2013) using output from the 5th CMIP (CMIP5), has been published. CMIP5 models include many model developments that were unavailable for CMIP3. Compared with CMIP3, many of the

CMIP5 models have increased horizontal and vertical resolution, while some also include a more complete representation of the carbon cycle and aerosols. However, the ASM remains a challenging phenomenon to simulate (*Sperber et al.*, 2013), with a large spread across the CMIP5 ensemble and many of them underestimating the monsoon rainfall (*Hagos et al.*, 2019). *Sperber et al.* (2013) evaluates the simulation of the ASM in 22 CMIP3 and 25 CMIP5 models. The CMIP5 multi-model mean (MMM) is more skillfull in terms of variability (interannual and interseasonal) and annual cycle than the CMIP3 MMM, although no one single model is better for all metrics. Unfortunately the comparison between CMIP3 and CMIP5 models for the monsoon onset and retreat does not include the ECHAM5 and HadCM3 CMIP3 models (the GCMs that provide the boundary conditions in this thesis) due to a lack of available data. However, *Annamalai et al.* (2007) show that the monsoon precipitation climatologies from the CMIP3 HadCM3 and ECHAM5 simulations are reasonable. *Sperber et al.* (2013) suggests that the CMIP3 and CMIP5 ensembles should arguably be used together to investigate climate change impacts because they are so similar in terms of their ASM skill. During the HighNoon project there were relatively few simulations at 25 km resolution with the correct outputs to run JULES. However, now a few years on, there are more equivalent resolution simulations of SA available using CMIP5 data (*Janes et al.*, 2019). The availability of these downscaled CMIP5 simulations has great potential for future work on this region using a combined CMIP5 and CMIP3 ensemble.

The 6th Coupled Model Intercomparison Project, CMIP6, has grown considerably even since CMIP5, requiring a new experimental design. CMIP now includes many more models, representing more processes and focussing on a wider range of questions, to further understanding of both the present and future climate (*Eyring et al.*, 2016a). The simulations for CMIP6 are currently in progress (July 2019), with most of the essential simulations (referred to as DECK and historical), likely to be completed by the Autumn of 2019. Together with the new CMIP6 structure, there is also more of a focus on model evaluation, with a new framework for CMIP6 to improve understanding of how past CMIPs relate to more recent ones (*Eyring et al.*, 2016b). This framework will be especially useful where there are systematic model errors or processes not captured well by the models.

1.4 Uncertainty and errors

In this thesis, boundary conditions from a GCM are used to drive an RCM, which in turn provides climate data to a land surface model like JULES or river routing model such as TRIP. This is seen as an interim step on the way to a more integrated approach for impacts with crops and irrigation part of a fully coupled system. RCMs are run at a higher resolution than their driving GCMs and therefore often improve simulations of precipitation; as discussed in Chapter 2. However, RCMs still have biases that are

either inherited from the GCM or due to the parameterization of regional processes in the RCMs themselves (*Brown et al.*, 2014). Biases in RCMs and GCMs can affect the usability of the output data for studying climate impacts (*Papadimitriou et al.*, 2017). Current approaches tend to bias correct specific variables from the GCMs or RCMs that are used to drive impacts models, namely temperature and precipitation. This bias correction step is seen as essential to ensure that future impacts projections are realistic. *Papadimitriou et al.* (2017) suggest that in addition to precipitation and temperature, radiation and humidity should also be bias corrected, particularly for hydrological applications. Where impacts models are run as an integral part of larger model simulations, this approach to bias correction will no longer be possible and an alternative approach will be needed. Bias correction may then need to be implemented as a post-processing step. In this thesis no bias correction is carried out on the GCM or RCM data before it is used to run TRIP or JULES.

There are also uncertainties associated with the models that use climate data from the RCM. TRIP for example, is a very simple representation of the movement of water down a river channel. Other routing models might represent this movement in a more complex way, which may or may not reduce the uncertainty compared with using TRIP. JULES on the other hand, is a complex model, representing many different aspects of the land-surface. JULES has evolved from version 2.2 of the Met Office Surface Exchange Scheme (MOSESv2.2, *Essery et al.*, 2003), the land-surface representation used in the RCM simulations described in this thesis in Chapter 2. There have been many releases of JULES since MOSESv2.2, which have included many developments that have fixed bugs and introduced new processes. Because of these developments, there may be more inconsistencies between the representation of the land-surface in the RCM and in JULES. A version of the RCM that included JULES rather than MOSESv2.2, would have more in common with the standalone version of JULES, especially in terms of code structure; this would minimise inconsistences between the impact's projections and the RCM.

1.5 Thesis aims and structure

In this section more detail is provided on the individual chapters of the thesis and how they contribute towards the main aim of the thesis to develop a more integrated approach to understanding the impacts of climate in SA. The important components of the thesis are summarised in the schematic shown in Fig. 1.2. The individual components of river routing, crops (*Osborne et al.*, 2015) and irrigation and their availability in JULES are discussed in Sect. 1.2, these are relatively recent additions to the official JULES trunk and therefore have not been tested for the SA region either individually or all together in a single simulation. In this thesis essential developments that are needed to provide a more realistic representation of the SA region are presented and

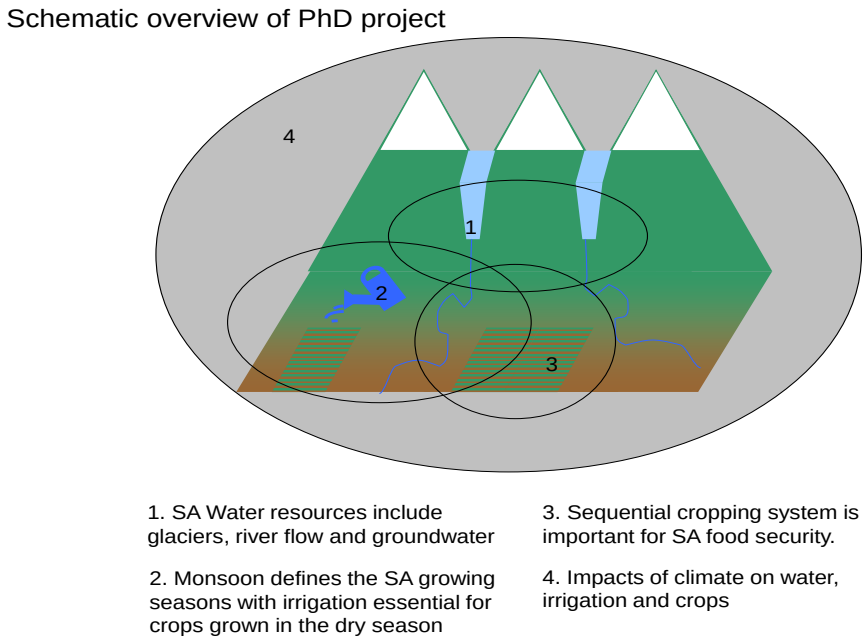

Figure 1.2: A schematic overview of the thesis.

evaluated. These developments will enable a more complete understanding of the impacts of climate on the SA region and are presented in a series of published papers provided in Chapters 2, 3 and 4.

The aim of Chapter 2 is to analyse the RCM river flows across the Himalaya and understand how useful these simulations are for understanding how river flows could change in SA in the future. *Mathison et al.* (2015) presents regional climate projections of river flow for the SA region by analysing river flows for 12 river gauges across the Himalayan arc. These gauges are selected to characterize the changing conditions from west to east across the Himalayan arc considering the present day river flows, where possible comparing against observations, and the potential changes in river flows and their implications for future surface water resources for the region. In this analysis, the RCM data described in Sect. 1.3 is used to provide runoff to the TRIP river routing scheme; this demonstrates that the ability to route the RCM river flow adds value to the RCM data and enables the limitations of the RCM data to be more fully understood. TRIP is now available in the official JULES code providing consistency between the simulations presented here and other simulations that use JULES with river routing.

Initial SA simulations using irrigation and crops for the whole of SA (not shown here) highlighted problems with the SA sowing and harvest dates being used both for the present day and with their application to future climate. In addition, recent work in climate–crop impact studies seeking to quantify uncertainty from the quality and scale

of input data found that, for global scale simulations, planting dates are a significant source of uncertainty (*Frieler et al.*, 2017, *Elliott et al.*, 2015). On this basis the aim of Chapter 3 is to provide a more accurate alternative to the global datasets of cropping calendars than is currently available and generate more representative inputs for climate impact assessments for SA. The uncertainty surrounding sowing and harvest dates within crop models is particularly important for regions where high-resolution data are unavailable or, as is the case in future climate runs, where no data are available at all. This method estimates the crop sowing and harvest dates, for rice and wheat, using the ASM onset and retreat from the model. This ensures that the sowing and harvest date remains consistent with the internal model climate so the crops are still growing at the optimum time even in future simulations.

A key feature of agriculture in SA is the use of the sequential cropping system (also known as multiple or double cropping). This practise involves growing two or more crops on the same field in a given year or growing period (*Liu et al.*, 2013, *Waha et al.*, 2013). Currently there are few land surface models (LSMs) that are able to simulate sequential cropping, but the capability is needed for understanding the resource requirement of this region both today and in the future. On this basis the main objective of Chapter 4 is to develop and implement sequential cropping in JULES and demonstrate that it grows two crops within one growing season. Chapter 4 evaluates the new implementation of sequential cropping in JULES against a site in Avignon (France, *Garrigues et al.* (2015, 2018)) to show that the method provides a realistic representation of the real land surface at Avignon. The same method is applied to four locations in the North Indian states of Uttar Pradesh and Bihar, representing a tropical region with a large variation in growing conditions.

Chapter 5 is the first implementation of all of the methods presented in Chapters 2 to 4 in one regional integrated study. Therefore the JULES simulations included in this chapter include TRIP river flows (implemented in JULES outside of this thesis - see Chapter 2), an extended irrigation scheme to allow irrigation only on specific tiles and an enhanced version of the crop model to enable sequential cropping (implemented in a branch of JULES at version 5.2 - see Chapter 4). The method for estimating the sowing and harvest dates, described in Chapter 3 is used for calculating the thermal time requirement for the rice–wheat rotation in these simulations. This chapter includes two simulations: The first one is limited by water availability, therefore linking the rivers and groundwater to irrigation and the second is not linked to the rivers and ground water and is therefore referred to as unlimited. The aim of Chapter 5 is to demonstrate that an integrated impact simulation is possible that links the agriculture and water sectors and shows promising results. These are prototype simulations rather than a complete solution suitable for informing policy decisions. Chapter 6 summarises the progress made toward simulating integrated impacts for SA, now possible as a result of the analyses presented in Chapters 2 to 5 of this thesis. Chapter 6 also discusses

the next steps that are needed beyond this thesis to achieve integrated simulations of future climate change impacts on multiple sectors for SA.

References

Ackerman, F., S. J. DeCanio, R. B. Howarth, and K. Sheeran (2009), Limitations of integrated assessment models of climate change, *Climatic Change*, *95*(3), 297–315, doi:10.1007/s10584-009-9570-x. 1

Aggarwal, P., K. Talukdar, and R. Mall (2000), Potential yields of rice-wheat system in the indo-gangetic plains of india, *Rice-wheat consortium paper series*, *10*, 16. 1.1.2

Anbumozhi, V., K. Matsumoto, and E. Yamaji (2001), Sustaining agriculture through modernization of irrigation tanks: An opportunity and challenge for Tamilnadu, India, *Agricultural Engineering International, vol. III (2001)*, 1–11. 1.1.1

Annamalai, H., K. Hamilton, and K. Sperber (2007), The South Asian summer monsoon and its relationship with ENSO in the IPCC AR4 simulations, *Journal of Climate*, *20*(6), 1071–1092, doi:10.1175/JCLI4035.1. 1.3

Best, M. J., M. Pryor, D. B. Clark, G. G. Rooney, R. L. H. Essery, C. B. Ménard, J. M. Edwards, M. A. Hendry, A. Porson, N. Gedney, L. M. Mercado, S. Sitch, E. Blyth, O. Boucher, P. M. Cox, C. S. B. Grimmond, and R. J. Harding (2011), The joint uk land environment simulator (JULES), model description, part 1: Energy and water fluxes, *Geoscientific Model Development*, *4*(3), 677–699, doi:10.5194/gmd-4-677-2011. 1.2, 1.2.2

Betts, R. A. (2005), Integrated approaches to climate-crop modelling: needs and challenges, *Philosophical transactions of the Royal Society of London. Series B, Biological sciences*, *360*, 2049–65, doi:10.1098/rstb.2005.1739. 1, 1, 1.2

Betts, R. A., L. Alfieri, C. Bradshaw, J. Caesar, L. Feyen, P. Friedlingstein, L. Gohar, A. Koutroulis, K. Lewis, C. Morfopoulos, L. Papadimitriou, K. J. Richardson, I. Tsanis, and K. Wyser (2018), Changes in climate extremes, fresh water availability and vulnerability to food insecurity projected at $1.5°c$ and $2°c$ global warming with a higher-resolution global climate model, *Philosophical Transactions of the Royal Society A: Mathematical, Physical and Engineering Sciences*, *376*, doi:10.1098/rsta.2016.0452. 1.1.1

Biemans, H., L. Speelman, F. Ludwig, E. Moors, A. Wiltshire, P. Kumar, D. Gerten, and P. Kabat (2013), Future water resources for food production in five South Asian river basins and potential for adaptation - a modeling study, *Science of The Total Environment*, *468-469, Supplement*(0), S117–S131, doi:10.1016/j.scitotenv.2013.05.092. 1.1.1, 1.2.2

Biemans, H., C. Siderius, A. Mishra, and B. Ahmad (2016), Crop-specific seasonal estimates of irrigation-water demand in south asia, *Hydrology and Earth System Sciences*, *20*(5), 1971–1982, doi:10.5194/hess-20-1971-2016. 1.1.2, 1.2.3

Biswas, A. K. (2008), *Management of Ganges-Brahmaputra-Meghna System: Way Forward*, pp. 143–164, Springer Berlin Heidelberg. 1.1

Bodh, S. P. C., M. S. Singla, S. A. Sharma, S. M. Yadav, M. N. Arora, S. S. Dawar, M. S. Virmani, and S. Rinku (2017), Agricultural statistics at a glance 2017, *Ministry of Agriculture & Farmers welfare, Directorate of Economics and Statistics*. 1.1.1

Bolch, T., A. Kulkarni, Kääb, C. Huggel, F. Paul, J. G. Cogley, H. Frey, J. S. Kargel, K. Fujita, M. Scheel, S. Bajracharya, and M. Stoffel (2012), The state and fate of himalayan glaciers, *Science*, *336*(6079), 310–314, doi:10.1126/science.1215828. 1.1.1

Bondeau, A., P. C. Smith, S. Zaehle, S. Schaphoff, W. Lucht, W. Cramer, D. Gerten, H. Lotze-Campen, C. Müller, M. Reichstein, and B. Smith (2007), Modelling the role of agriculture for the 20th century global terrestrial carbon balance, *Global Change Biology*, *13*(3), 679–706, doi:10.1111/j.1365-2486.2006.01305.x. 1.1.1

Boonwichai, S., S. Shrestha, M. S. Babel, S. Weesakul, and A. Datta (2018), Climate change impacts on irrigation water requirement, crop water productivity and rice yield in the songkhram river basin, thailand, *Journal of Cleaner Production*, *198*, 1157–1164, doi:10.1016/j.jclepro.2018.07.146. 1

Brown, S. J., J. M. Murphy, D. M. H. Sexton, and G. R. Harris (2014), Climate projections of future extreme events accounting for modelling uncertainties and historical simulation biases, *Climate Dynamics*, *43*, doi:10.1007/s00382-014-2080-1. 1.4

Challinor, A., T. Wheeler, P. Craufurd, J. Slingo, and D. Grimes (2004), Design and optimisation of a large-area process-based model for annual crops, *Agricultural and Forest Meteorology*, *124*(1-2), 99–120, doi:10.1016/j.agrformet.2004.01.002. 1, 1.2.2

Christensen, J., B. Hewitson, A. Busuioc, A. Chen, X. Gao, I. Held, R. Jones, R. Kolli, W.-T. Kwon, R. Laprise, V. M. na Rueda, L. Mearns, C. Menendez, J. Räisänen, A. Rinke, A. Sarr, and P. Whetton (2007), Regional climate projections. in: Climate change 2007: The physical science basis. contribution of working group i, *Fourth Assessment Report of the Intergovernmental Panel on Climate Change*. 1.1.1, 1.3

Christensen, J., K. Krishna-Kumar, E. Aldrian, S.-I. An, I. Cavalcanti, M. de Castro, W. Dong, P. Goswami, A. Hall, J. Kanyanga, A. Kitoh, J. Kossin, N.-C. Lau, J. Renwick, D. Stephenson, S.-P. Xie, and T. Zhou (2013), *Climate Phenomena and their Relevance for Future Regional Climate Change*, book section 14, pp. 1217–1308, Cambridge University Press, doi:10.1017/CBO9781107415324.028. 1, 1.1.1, 1.3

Clark, D. B., and N. Gedney (2008), Representing the effects of subgrid variability of soil moisture on runoff generation in a land surface model, *Journal of Geophysical Research*, *113*, doi:10.1029/2007JD008940. 1.2.2

Clark, D. B., L. M. Mercado, S. Sitch, C. D. Jones, N. Gedney, M. J. Best, M. Pryor, G. G. Rooney, R. L. H. Essery, E. Blyth, O. Boucher, R. J. Harding, C. Huntingford, and P. M. Cox (2011), The joint uk land environment simulator (JULES), model description, part 2: Carbon fluxes and vegetation dynamics, *Geoscientific Model Development*, *4*(3), 701–722, doi:10.5194/gmd-4-701-2011. 1.2

Collins, W. J., N. Bellouin, M. Doutriaux-Boucher, N. Gedney, P. Halloran, T. Hinton, J. Hughes, C. D. Jones, M. Joshi, S. Liddicoat, G. Martin, F. O'Connor, J. Rae, C. Senior, S. Sitch, I. Totterdell, A. Wiltshire, and S. Woodward (2011), Development and evaluation of an earth-system model – hadgem2, *Geoscientific Model Development*, *4*(4), 1051–1075, doi:10.5194/gmd-4-1051-2011. 1.2

Cox, P. M., R. A. R. A. Betts, C. B. Bunton, R. L. H. Essery, P. R. Rowntree, and J. Smith (1999), The impact of new land surface physics on the gcm simulation of climate and climate sensitivity, *Climate Dynamics*, *15*(3), 183–203, doi:10.1007/s003820050276. 1.2.2

Dhar, O., and S. Nandargi (2000), A study of floods in the brahmaputra basin in india, *International Journal of Climatology*, *20*(7), 771–781, doi:10.1002/1097-0088(20000615)20:7¡771::AID-JOC518¿3.0.CO;2-Z. 1.1

Elliott, J., C. Müller, D. Deryng, J. Chryssanthacopoulos, K. Boote, M. Büchner, I. Foster, M. Glotter, J. Heinke, T. Iizumi, R. C. Izaurralde, N. D. Mueller, D. K. Ray, C. Rosenzweig, A. C. Ruane, and J. Sheffield (2015), The global gridded crop

model intercomparison: data and modeling protocols for phase 1 (v1.0), *Geoscientific Model Development*, *8*(2), 261–277, doi:10.5194/gmd-8-261-2015. 1, 1.5

Erenstein, O., and V. Laxmi (2008), Zero tillage impacts in india's rice-wheat systems: A review, *Soil and Tillage Research*, *100*, 1–14, doi:10.1016/j.still.2008.05.001. 1.1.2

Essery, R. L. H., M. J. Best, R. A. Betts, P. M. Cox, and C. Taylor (2003), Explicit representation of subgrid heterogeneity in a GCM land surface scheme, *Journal of Hydrometeorology*, *4*, 530–543. 1.4

Eyring, V., S. Bony, G. A. Meehl, C. A. Senior, B. Stevens, R. J. Stouffer, and K. E. Taylor (2016a), Overview of the Coupled Model Intercomparison Project Phase 6 (CMIP6) experimental design and organization, *Geoscientific Model Development*, *9*, 1937–1958, doi:10.5194/gmd-9-1937-2016. 1.3

Eyring, V., P. J. Gleckler, C. Heinze, R. J. Stouffer, K. E. Taylor, V. Balaji, E. Guilyardi, S. Joussaume, S. Kindermann, B. N. Lawrence, G. A. Meehl, M. Righi, and D. N. Williams (2016b), Towards improved and more routine earth system model evaluation in cmip, *Earth System Dynamics*, *7*(4), 813–830, doi:10.5194/esd-7-813-2016. 1.3

Falloon, P., and R. Betts (2010), Climate impacts on european agriculture and water management in the context of adaptation and mitigation – the importance of an integrated approach, *Science of The Total Environment*, *408*(23), 5667 – 5687, doi:10.1016/j.scitotenv.2009.05.002, special Section: Integrating Water and Agricultural Management Under Climate Change. 1

Falloon, P., R. Betts, and C. Bunton (2007), New global river routing scheme in the unified model, *Hadley Centre Technical Note*, *72*. 1.2.1

Falloon, P., R. A. Betts, A. Wiltshire, R. Dankers, C. Mathison, D. McNeall, P. Bates, and M. Trigg (2011), Validation of river flows in hadgem1 and hadcm3 with the trip river flow model, *Journal of Hydrometeorology*, *12*, 1157–1180, doi:10.1175/2011JHM1388.1. 1.2.1

Fischer, G., F. N. Tubiello, H. van Velthuizen, and D. A. Wiberg (2007), Climate change impacts on irrigation water requirements: Effects of mitigation, 1990–2080, *Technological Forecasting and Social Change*, *74*(7), 1083–1107, doi:10.1016/j.techfore.2006.05.021, greenhouse Gases-Integrated Assessment. 1

Frieler, K., A. Levermann, J. Elliott, J. Heinke, A. Arneth, M. F. P. Bierkens, P. Ciais, D. B. Clark, D. Deryng, P. Döll, P. Falloon, B. Fekete, C. Folberth, A. D. Friend, C. Gellhorn, S. N. Gosling, I. Haddeland, N. Khabarov, M. Lomas, Y. Masaki, K. Nishina, K. Neumann, T. Oki, R. Pavlick, A. C.Ruane, E. Schmid, C. Schmitz, T. Stacke, E. Stehfest, Q. Tang, D. Wisser, V. Huber, F. Piontek, L. Warszawski, J. Schewe, H. Lotze-Campen, and H. J. Schellnhuber (2015), A framework for the cross-sectoral integration of multi-model impact projections: land use decisions under climate impacts uncertainties, *Earth System Dynamics*, *6*(2), 447–460, doi:10.5194/esd-6-447-2015. 1

Frieler, K., S. Lange, F. Piontek, C. P. O. Reyer, J. Schewe, L. Warszawski, F. Zhao, L. Chini, S. Denvil, K. Emanuel, T. Geiger, K. Halladay, G. Hurtt, M. Mengel, D. Murakami, S. Ostberg, A. Popp, R. Riva, M. Stevanovic, T. Suzuki, J. Volkholz, E. Burke, P. Ciais, K. Ebi, T. D. Eddy, J. Elliott, E. Galbraith, S. N. Gosling, F. Hattermann, T. Hickler, J. Hinkel, C. Hof, V. Huber, J. Jägermeyr, V. Krysanova, R. Marcé, H. Müller Schmied, I. Mouratiadou, D. Pierson, D. P. Tittensor, R. Vautard, M. van Vliet, M. F. Biber, R. A. Betts, B. L. Bodirsky, D. Deryng, S. Frolking, C. D. Jones, H. K. Lotze, H. Lotze-Campen, R. Sahajpal, K. Thonicke, H. Tian, and Y. Yamagata (2017), Assessing the impacts of 1.5°c global warming – simulation protocol of the inter-sectoral impact model intercomparison project (isimip2b), *Geoscientific Model Development*, *10*(12), 4321–4345, doi:10.5194/gmd-10-4321-2017. 1, 1.5

Fujita, K., and T. Nuimura (2011), Spatially heterogeneous wastage of Himalayan glaciers, *Proceedings of the National Academy of Sciences*, *108*(34), 14,011–14,014. 1.1.1

Gardelle, J., E. Berthier, Y. Arnaud, and A. Kääb (2013), Region-wide glacier mass balances over the Pamir-Karakoram-Himalaya during 1999-2011, *The Cryosphere*, *7*(4), 1263–1286, doi:10.5194/tc-7-1263-2013. 1.1.1

Garrigues, S., A. Olioso, J. Calvet, E. Martin, S. Lafont, S. Moulin, A. Chanzy, O. Marloie, S. Buis, V. Desfonds, N. Bertrand, and D. Renard (2015), Evaluation of land surface model simulations of evapotranspiration over a 12-year crop succession: impact of soil hydraulic and vegetation properties, *Hydrology and Earth System Sciences*, *19*(7), 3109–3131, doi:10.5194/hess-19-3109-2015. 1.5

Garrigues, S., A. Boone, B. Decharme, A. Olioso, C. Albergel, J.-C. Calvet, S. Moulin, S. Buis, and E. Martin (2018), Impacts of the soil water transfer parameterization on the simulation of evapotranspiration over a 14-year mediterranean crop succession, *Journal of Hydrometeorology*, *19*(1), 3–25, doi:10.1175/JHM-D-17-0058.1. 1.5

Gedney, N., C. Huntingford, G. P. Weedon, N. Bellouin, O. Boucher, and P. M. Cox (2014), Detection of solar dimming and brightening effects on northern hemisphere river flow, *Nature geoscience*, *7*, 796–800, doi:10.1038/ngeo2263. 1.2.2

Gohar, L., J. Lowe, and D. Bernie (2017), The impact of bias correction and model selection on passing temperature thresholds, *Journal of Geophysical Research: Atmospheres*, *122*(22), 12,045–12,061, doi:10.1002/2017JD026797, 2017JD026797. 1.3

Gornall, J., R. Betts, E. Burke, R. Clark, J. Camp, K. Willett, and A. Wiltshire (2010), Implications of climate change for agricultural productivity in the early twenty-first century, *Philosphical Transactions of the Royal Society B: Biological Sciences*, *365*, 2973–2989, doi:10.1098/rstb.2010.0158. 1, 1

Goswami, B., and P. K. Xavier (2005), Dynamics of "internal" interannual variability of the Indian summer monsoon in a GCM, *Journal of Geophysical Research: Atmospheres*, *110*(D24), doi:10.1029/2005JD006042. 1.1.1

Hagos, S., L. R. Leung, M. Ashfaq, and K. Balaguru (2019), South asian monsoon precipitation in cmip5: a link between inter-model spread and the representations of tropical convection, *Climate Dynamics*, *52*(1), 1049–1061. 1.3

Halladay, K. (2018), Assessment of performance of interactive hydrological and agricultural impacts for brazil, *Climate Science to Services Project – Brazil, Met Office Hadley Centre, Exeter, UK*. 1.2.2

Halladay, K., and P. Good (2017), Non-linear interactions between co_2 radiative and physiological effects on amazonian evapotranspiration in an earth system model, *Climate Dynamics*, *49*(7), 2471–2490, doi:10.1007/s00382-016-3449-0. 1

Harding, R., E. Blyth, O. Tuinenburg, and A. Wiltshire (2013), Land atmosphere feedbacks and their role in the water resources of the ganges basin, *Science of The Total Environment*, *468-469, Supplement*(0), S85–S92, doi:10.1016/j.scitotenv.2013.03.016, changing water resources availability in Northern India with respect to Himalayan glacier retreat and changing monsoon patterns: consequences and adaptation. 1

Hewitson, B., A. C. Janetos, T. R. Carter, F. Giorgi, R. G. Jones, W. T. Kwon, L. O. Mearns, E. L. F. Schipper, and M. van Aalst (2014), *Climate Phenomena and their Relevance for Future Regional Climate Change*, book section 14, pp. 1133–1197, Cambridge University Press, doi:10.1017/CBO9781107415324.028. 1, 1.1.1

Hussain, J., T. Khaliq, A. Ahmad, and J. Akhtar (2018), Performance of four crop model for simulations of wheat phenology, leaf growth, biomass and yield across planting dates, *PLOS ONE*, *13*(6), 1–14, doi:10.1371/journal.pone.0197546. 1

Immerzeel, W. W., L. van Beek, and M. Bierkens (2010), Climate change will affect the Asian water towers, *Science*, *328*(5984), 1382–1385, doi:10.1126/science.1183188. 1.1.1

Janes, T., F. McGrath, I. Macadam, and R. Jones (2019), High-resolution climate projections for south asia to inform climate impacts and adaptation studies in the ganges-brahmaputra-meghna and mahanadi deltas, *Science of The Total Environment*, *650*, 1499–1520, doi:10.1016/j.scitotenv.2018.08.376. 1.3

Jones, R. G., M. Noguer, D. C. Hassell, D. Hudson, S. S. Wilson, G. J. Jenkins, and J. F. Mitchell (2004), Generating high resolution climate change scenarios using PRECIS, *Met Office Hadley Centre, Exeter, UK*, pp. 0–40. 1.2

Kang, S., and E. A. B. Eltahir (2018), North china plain threatened by deadly heatwaves due to climate change and irrigation, *Nature Communications*, *9*, doi:10.1038/s41467-018-05252-y. 1

Kumar, P., A. Wiltshire, C. Mathison, S. Asharaf, B. Ahrens, P. Lucas-Picher, J. H. Christensen, A. Gobiet, F. Saeed, S. Hagemann, and D. Jacob (2013), Downscaled climate change projections with uncertainty assessment over India using a high resolution multi-model approach, *Science of The Total Environment*, *468-469, Supplement*(0), S18–S30, doi:10.1016/j.scitotenv.2013.01.051, changing water resources availability in Northern India with respect to Himalayan glacier retreat and changing monsoon patterns: consequences and adaptation. 1.3

Liu, L., X. Xu, D. Zhuang, X. Chen, and S. Li (2013), Changes in the potential multiple cropping system in response to climate change in china from 1960–2010, *PLoS ONE*, *8*(12), doi:10.1371/JOURNAL.PONE.0080990. 1.5

Lontzek, T. S., Y. Cai, K. L. Judd, and T. M. Lenton (2015), Stochastic integrated assessment of climate tipping points indicates the need for strict climatepolicy, *Nature Climate Change*, *5*, 441–444, doi:10.1038/nclimate2570. 1

Maiorano, A., P. Martre, S. Asseng, F. Ewert, C. Müller, R. P. Rötter, A. C. Ruane, M. A. Semenov, D. Wallach, E. Wang, P. D. Alderman, B. T. Kassie, C. Biernath, B. Basso, D. Cammarano, A. J. Challinor, J. Doltra, B. Dumont, E. E. Rezaei, S. Gayler, K. C. Kersebaum, B. A. Kimball, A.-K. Koehler, B. Liu, G. J. OLeary, J. E. Olesen, M. J. Ottman, E. Priesack, M. Reynolds, P. Stratonovitch, T. Streck, P. J. Thorburn, K. Waha, G. W. Wall, J. W. White, Z. Zhao, and Y. Zhu (2017), Crop model improvement reduces the uncertainty of the response to temperature of multi-model ensembles, *Field Crops Research*, *202*, 5–20, doi:10.1016/j.fcr.2016.05.001. 1

Mathison, C., A. Wiltshire, A. Dimri, P. Falloon, D. Jacob, P. Kumar, E. Moors, J. Ridley, C. Siderius, M. Stoffel, and T. Yasunari (2013), Regional projections of North Indian climate for adaptation studies, *Science of The Total Environment*, *468-469, Supplement*(0), S4–S17, doi:10.1016/j.scitotenv.2012.04.066. 1.1.1, 1.3

Mathison, C., A. J. Wiltshire, P. Falloon, and A. J. Challinor (2015), South asia river-flow projections and their implications for water resources, *Hydrology and Earth System Sciences*, *19*(12), 4783–4810, doi:10.5194/hess-19-4783-2015. 1.3, 1.5

Mathison, C., C. Deva, P. Falloon, and A. J. Challinor (2018), Estimating sowing and harvest dates based on the asian summer monsoon, *Earth System Dynamics*, *9*(2), 563–592, doi:10.5194/esd-9-563-2018. 1.3

Mirza, M. M. Q. (2002), Global warming and changes in the probability of occurrence of floods in bangladesh and implications, *Global Environmental Change*, *12*(2), 127–138, doi:10.1016/S0959-3780(02)00002-X. 1.1

Mohammed, K., A. K. M. S. Islam, G. M. T. Islam, L. Alfieri, M. J. U. Khan, S. K. Bala, and M. K. Das (2018), Future floods in bangladesh under 1.5c, 2c, and 4c global warming scenarios, *Journal of Hydrologic Engineering*, *23*(12), 04018,050, doi:10.1061/(ASCE)HE.1943-5584.0001705. 1.1

Morse, A., C. Prentice, and T. Carter (2009), Assessments of climate change impacts, *Ensembles: Climate change and its impacts: Summary of research and results from the ENSEMBLES project*, pp. 107–129. 1.2.1

Nakicenovic, N., J. Alcamo, A. Grubler, K. Riahi, R. Roehrl, H.-H. Rogner, and N. Victor (2000), Special report on emissions scenarios (SRES), *A Special Report of Working Group III of the Intergovernmental Panel on Climate Change*, Last access April 2017editor:Nebojsa Nakicenovic and Rob Swart. 1.3

Narayanamoorthy, A. (2018), Financial performance of indias irrigation sector: a historical analysis, *International Journal of Water Resources Development*, *34*(1), 116–131, doi:10.1080/07900627.2017.1298998. 1.1.1

Naumann, G., L. Alfieri, K. Wyser, L. Mentaschi, R. A. Betts, H. Carrao, J. Spinoni, J. Vogt, and L. Feyen (2018), Global changes in drought conditions under different levels of warming, *Geophysical Research Letters*, *45*(7), 3285–3296, doi:10.1002/2017GL076521. 1.1

Oki, T., and Y. C. Sud (1998), Design of total runoff integrating pathways (TRIP). a global river channel network, *Earth Interactions*, *2*, 1–37, doi:10.1175/1087-3562(1998)002¡0001:DOTRIP¿2.3.CO;2. 1.2.1

Oki, T., T. Nishimura, and P. Dirmeyer (1999), Assessment of annual runoff from land surface models using Total Runoff Integrating Pathways (TRIP), *Journal of the Meteorological Society of Japan. Ser. II*, *77*(1B), 235–255, doi:10.1080/02626668509490989. 1.2.1

Osborne, T., J. Gornall, J. Hooker, K. Williams, A. Wiltshire, R. Betts, and T. Wheeler (2015), Jules-crop: a parametrisation of crops in the joint uk land environment simulator, *Geoscientific Model Development*, *8*(4), 1139–1155, doi:10.5194/gmd-8-1139-2015. 1, 1.2.3, 1.5

Osborne, T. M., D. M. Lawrence, A. J. Challinor, J. M. Slingo, and T. R. Wheeler (2007), Development and assessment of a coupled crop-climate model, *Global Change Biology*, *13*(1), 169–183, doi:10.1111/j.1365-2486.2006.01274.x. 1

Papadimitriou, L., A. Koutroulis, M. G. Grillakis, and I. Tsanis (2017), The effect of gcm biases on global runoff simulations of a land surface model, *Hydrology and Earth System Sciences*, *21*(9), 4379–4401, doi:10.5194/hess-21-4379-2017. 1.4

Rahman, S., A. K. M. S. Islam, P. Saha, A. R. Tazkia, Y. Krien, F. Durand, L. Testut, G. M. T. Islam, and S. K. Bala (2019), Projected changes of inundation of cyclonic storms in the ganges–brahmaputra–meghna delta of bangladesh due to slr by 2100, *Journal of Earth System Science*, *128*(6), 145, doi:10.1007/s12040-019-1184-8. 1.1

Rasul, G., N. Neupane, A. Hussain, and B. Pasakhala (2019), Beyond hydropower: towards an integrated solution for water, energy and food security in south asia, *International Journal of Water Resources Development*, *1*(1), 1–25, doi:10.1080/07900627.2019.1579705. 1.1

Rivington, M., and J. Koo (2010), Report on the meta-analysis of crop modelling for climate change and food security survey, *Climate Change, Agriculture and Food Security Challenge Program of the CGIAR*. 1

Rodell, M., I. Velicogna, and J. Famiglietti (2009), Satellite-based estimates of groundwater depletion in India, *Nature*, *460*(7258), 999 – 1002, doi:10.1038/nature08238. 1.1.1

Rosenzweig, C., J. Jones, J. Hatfield, A. Ruane, K. Boote, P. Thorburn, J. Antle, G. Nelson, C. Porter, S. Janssen, S. Asseng, B. Basso, F. Ewert, D. Wallach, G. Baigorria, and J. Winter (2013), The agricultural model intercomparison and improvement project (agmip): Protocols and pilot studies, *Agricultural and Forest Meteorology*, *170*, 166–182, doi:10.1016/j.agrformet.2012.09.011, agricultural prediction using climate model ensembles. 1

Rosenzweig, C., J. Elliott, D. Deryng, A. C. Ruane, C. Müller, A. Arneth, K. J. Boote, C. Folberth, M. Glotter, N. Khabarov, K. Neumann, F. Piontek, T. A. M. Pugh, E. Schmid, E. Stehfest, H. Yang, and J. W. Jones (2014), Assessing agricultural risks of climate change in the 21st century in a global gridded crop model intercomparison, *Proceedings of the National Academy of Sciences*, *111*(9), 3268–3273, doi:10.1073/pnas.1222463110. 1

Schwanitz, V. J. (2013), Evaluating integrated assessment models of global climate change, *Environmental Modelling & Software*, *50*, 120–131, doi:10.1016/j.envsoft.2013.09.005. 1

Shannon, S., R. Smith, A. Wiltshire, T. Payne, M. Huss, R. Betts, J. Caesar, A. Koutroulis, D. Jones, and S. Harrison (2019), Global glacier volume projections under high-end climate change scenarios, *The Cryosphere*, *13*(1), 325–350, doi:10.5194/tc-13-325-2019. 1.1.1, 1.2, 1.2.1

Singh, D. K., P. Kumar, and A. K. Bhardwaj (2014), Evaluation of agronomic management practices on farmers' fields under rice-wheat cropping system in northern india, *International Journal of Agronomy*, *2014*, 5, doi:10.1155/2014/740656. 1.1.2

Sperber, K. R., H. Annamalai, I.-S. Kang, A. Kitoh, A. Moise, A. Turner, B. Wang, and T. Zhou (2013), The asian summer monsoon: an intercomparison of cmip5 vs. cmip3 simulations of the late 20th century, *Climate Dynamics*, *41*(9), 2711–2744, doi:10.1007/s00382-012-1607-6. 1.3

Thatte, C. D. (2018), Water resources development in india, *International Journal of Water Resources Development*, *34*(1), 16–27, doi:10.1080/07900627.2017.1364987. 1.1

Tuinenburg, O. A., R. W. A. Hutjes, T. Stacke, A. Wiltshire, and P. Lucas-Picher (2014), Effects of irrigation in india on the atmospheric water budget., *Journal of Hydrometeorology*, *15*, 1028–1050, doi:10.1175/JHM-D-13-078.1. 1

United Nations (2013), Fertility levels and trends as assessed in the 2012 revision of world population prospects, *Department of Economic and Social Affairs, Population Division*. 1.1

United Nations (2017), World population prospects: The 2017 revision, key findings and advance tables. working paper no. esa/p/wp/248, *Department of Economic and Social Affairs, Population Division*. 1.1

van Vuuren, D. P., J. Lowe, E. Stehfest, L. Gohar, A. F. Hof, C. Hope, R. Warren, M. Meinshausen, and G.-K. Plattner (2011), How well do integrated assessment models simulate climate change?, *Climatic Change*, *104*(2), 255–285, doi:10.1007/s10584-009-9764-2. 1

Waha, K., C. Müller, A. Bondeau, J. Dietrich, P. Kurukulasuriya, J. Heinke, and H. Lotze-Campen (2013), Adaptation to climate change through the choice of cropping system and sowing date in sub-saharan africa, *Global Environmental Change*, *23*(1), 130–143, doi:10.1016/j.gloenvcha.2012.11.001. 1, 1.5

Warszawski, L., A. Friend, S. Ostberg, K. Frieler, W. Lucht, S. Schaphoff, D. Beerling, P. Cadule, P. Ciais, D. B. Clark, R. Kahana, A. Ito, R. Keribin, A. Kleidon, M. Lomas, K. Nishina, R. Pavlick, T. T. Rademacher, M. Buechner, F. Piontek, J. Schewe, O. Serdeczny, and H. J. Schellnhuber (2013), A multi-model analysis of risk of ecosystem shifts under climate change, *Environmental Research Letters*, *8*(4), 044,018. 1

Warszawski, L., K. Frieler, V. Huber, F. Piontek, O. Serdeczny, and J. Schewe (2014), The inter-sectoral impact model intercomparison project (isi-mip):project framework, *Proceedings of the National Academy of Sciences*, *111*(9), 3228–3232, doi:10.1073/pnas.1312330110. 1

Williams, K., J. Gornall, A. Harper, A. Wiltshire, D. Hemming, T. Quaife, T. Arkebauer, and D. Scoby (2017), Evaluation of jules-crop performance against site observations of irrigated maize from mead, nebraska, *Geoscientific Model Development*, *10*(3), 1291–1320, doi:10.5194/gmd-10-1291-2017. 1.2.2, 1.2.3

Williams, K. D., D. Copsey, E. W. Blockley, A. Bodas-Salcedo, D. Calvert, R. Comer, P. Davis, T. Graham, H. T. Hewitt, R. Hill, P. Hyder, S. Ineson, T. C. Johns, A. B. Keen, R. W. Lee, A. Megann, S. F. Milton, J. G. L. Rae, M. J. Roberts, A. A. Scaife, R. Schiemann, D. Storkey, L. Thorpe, I. G. Watterson, D. N. Walters, A. West, R. A. Wood, T. Woollings, and P. K. Xavier (2018a), The met office global coupled model 3.0 and 3.1 (gc3.0 and gc3.1) configurations, *Journal of Advances in Modeling Earth Systems*, *10*(2), 357–380, doi:10.1002/2017MS001115. 1.2

Williams, K. E., and P. D. Falloon (2015), Sources of interannual yield variability in jules-crop and implications for forcing with seasonal weather forecasts, *Geoscientific Model Development Discussions*, *8*(6), 4599–4621, doi:10.5194/gmdd-8-4599-2015. 1.2.2, 1.2.3

Williams, K. E., A. B. Harper, C. Huntingford, L. M. Mercado, C. T. Mathison, P. D. Falloon, P. M. Cox, and J. Kim (2018b), Revisiting the first islscp field experiment to evaluate water stress in julesv5.0, *Geoscientific Model Development Discussions*, *2018*, 1–47, doi:10.5194/gmd-2018-210. 1.2.3

Chapter 2

South Asia river flow projections and their implications for water resources

Camilla T. Mathison[1,2], Andy J Wiltshire [1], Pete Falloon [1] and Andrew. J Challinor [2]

[1] *Met Office Hadley Centre, FitzRoy Road, Exeter, EX1 3PB, UK*
[2] *School of Earth and Environment, Institute for Climate and Atmospheric Science, University of Leeds, Leeds, LS2 9AT, UK*

South Asia is a region with a large and rising population, a high dependence on water intense industries, such as agriculture and a highly variable climate. In recent years, fears over the changing Asian Summer Monsoon (ASM) and rapidly retreating glaciers, together with increasing demands for water resources, have caused concern over the reliability of water resources and the potential impact on intensely irrigated crops in this region. Despite these concerns, there is a lack of climate simulations with a high enough resolution to capture the complex orography and water resource analysis is limited by a lack of observations of the water cycle for the region. In this paper we present the first 25 km resolution regional climate projections of river flow for the South Asia region. Two global climate models (GCMs), which represent the ASM reasonably well are downscaled (1960–2100) using a regional climate model (RCM). In the absence of robust observations, ERA-interim reanalysis is also downscaled providing a constrained estimate of the water balance for the region for comparison against the GCMs (1990–2006). The RCM river flow is routed using a river-routing model to allow analysis of present day and future river flows through comparison with available river gauge observations. We examine how useful these simulations are for understanding potential changes in water resources for the South Asia region. In general the downscaled GCMs capture the seasonality of the river flows but over-estimate the maximum river flows

compared to the observations, probably due to a positive rainfall bias and a lack of abstraction in the model. The simulations suggest an increasing trend in annual mean river flows for some of the river gauges in this analysis, in some cases almost doubling by the end of the century. The future maximum river flow rates still occur during the ASM period, with a magnitude in some cases greater than the present day natural variability. Increases in river flow could mean additional water resource for irrigation, the largest usage of water in this region, but has implications in terms of inundation risk. These projected increases could be more than countered by changes in demand due to depleted groundwater, increases in domestic use or expansion of water intense industries. Including missing hydrological processes in the model would make these projections more robust, but could also change the sign of the projections.

2.1 Introduction

South Asia, the Indo-Gangetic plain in particular, is a region of rapid socio-economic change where both population growth and climate change are expected to have a large impact on available water resource and food security. The region is home to almost 1.6 billion people and the population is forecast to increase to more than 2 billion by 2050 (*United Nations*, 2013). The economy of this region is rural and highly dependent on climate sensitive sectors such as the agricultural and horticultural industry, characterised by a large demand for water resources. As a result, over the coming decades, the demand for water from all sectors (domestic, agricultural and industrial) is likely to increase (*Gupta and Deshpande*, 2004, *Kumar et al.*, 2005).

The climate of South Asia is dominated by the Asian Summer Monsoon (ASM), with much of the water resource across the region provided by this climatological phenomena during the months of June–September (*Goswami and Xavier*, 2005). The contribution from glacial melt to water resources is less certain but likely to be important outside the ASM period during periods of low river flow (*Mathison et al.*, 2013). Glaciers and seasonal snowpacks are natural hydrological buffers releasing water during the drier periods, such as spring and autumn, when the flows of some catchments in this region are at their lowest. Similarly they may act to buffer interannual variability as well releasing water during warmer drier years and accumulating during wetter colder years (*Barnett et al.*, 2005). However, *Kaser et al.* (2010) show that the influence of glacial melt reduces with distance downstream, as other influences such as evaporation and precipitation increase in importance. *Immerzeel et al.* (2010) found that by the 2050s the main upstream water supply could decrease due to a reduction in snow and glacial melt (reductions of 8 % for the upper Indus and more than 18 % for the Ganges and Brahmaputra). Meltwater plays an important role for the Indus and Brahmaputra particularly, accounting for a larger percentage of the downstream flow than the Ganges (where meltwater is approximately 10 % of the downstream flow). However *Immerzeel*

et al. (2010) also show that these reductions in melt water are offset by an increase in precipitation in all three basins. *Immerzeel et al.* (2010) use coarse resolution general circulation models (GCMs) known to have difficulties in capturing monsoon precipitation and in estimating the relationship between daily mean temperature and melting of snow and ice.

Recent studies have highlighted uncertainty in both glacier mass balance and ASM rainfall. *Fujita and Nuimura* (2011) show a negative mass balance for three benchmark glaciers in the Nepal Himalaya. *Bolch et al.* (2012) and *Gardelle et al.* (2013) highlight losses more generally from western, eastern and central Himalayan glaciers. These observed changes in Himalayan glaciers can be attributed to the increase in temperature already experienced across the region, with warming more pronounced at higher elevations and during winter months (*Shrestha and Aryal*, 2011). There are however some glaciers in the Karakoram region showing increases in mass which has been attributed to a decrease in temperature for this region (*Bolch et al.*, 2012, *Gardelle et al.*, 2013). Projections of future glacial change are challenging due to poor understanding of glacial processes, diversity in climate extremes and the complex orography of the region (*Bolch et al.*, 2012). Complex orography contributes to other processes such as avalanching and therefore debris cover. The relationship between debris cover and melt is complex with a wide variety of responses across different glaciers across the Himalayan arc (*Gardelle et al.*, 2013). The thickness of debris cover is widely thought to significantly affect the response of the glacier to climate, with thick debris cover tending to slow down surface melting (*Bolch et al.*, 2012, *Scherler et al.*, 2011). However on the regional scale *Kääb et al.* (2012) found, using satellite data, similar thinning rates between clean and debris covered ice despite insulation by debris cover at some sites. *Kääb et al.* (2012) suggest that the insulating effect of debris layers with thicknesses exceeding a few centimetres depends on the continuity of the coverage. Therefore changes in the thickness of debris across a glacier could change the melt rate on a local scale even across a single glacier tongue.

The ASM is also uncertain: *Christensen et al.* (2007) highlight two climate features that could influence the ASM, including a general weakening of monsoonal flows while enhanced moisture convergence could increase precipitation. Any reduction in water availability from either resource is likely to put more pressure on groundwater resources, which is not sustainable in the longer term (*Rodell et al.*, 2009). There is some disagreement in the literature regarding the main effects of climate change on this region. *Gregory et al.* (2005) suggest that the availability and quality of ground water for irrigation could be more important factors influencing food security than the direct effects of climate change, particularly for India. However, *Aggarwal et al.* (2012) suggest that an increase in extremes (both temperature and precipitation) could lead to instability in food production and it is this variability in food production that is potentially the most significant effect of climate change for the South Asia region.

Despite the general uncertainty in the reliability of water resources and the impacts of climate change for this region, there are few simulations available with a high enough resolution for capturing the complex topography of the Himalayan region. The water balance for the South Asia region as a whole is generally poorly understood with limited observing networks and data availability for both precipitation and river flows presenting a real challenge for validating models and estimates of water balance. This analysis seeks to use regional climate simulations to develop our understanding of the water cycle for the region in the context of the complete climate system, while acknowledging that more needs to be done to address the missing hydrological processes in the model. Regional Climate Model (RCM) simulations are a widely used method across climate science for downscaling GCMs, including the regional IPCC assessment but are used in many other regional climate projects (*Christensen et al.*, 2007, *Murphy et al.*, 2009, *Jacob et al.*, 2007). RCMs are based on the same physical equations as GCMs and therefore represent the climate system for the region being modelled including the carbon and water cycle as completely as possible. Although there are some limitations due to missing processes, their higher resolution allows a better representation of the regional scale processes; especially in regions of complex topography such as the Himalaya (*Lucas-Picher et al.*, 2011). RCMs are designed to maintain the conservation of water, mass, energy and momentum, essential for analysis on climate timescales. *Lucas-Picher et al.* (2011) conduct a comprehensive assessment of four RCMs run over South Asia demonstrating their ability to capture the monsoon; this analysis includes the RCM used here. *Mathison et al.* (2013) compare GCM and RCM outputs for temperature and precipitation specifically for the RCM used in this analysis.

Perhaps due to the lack of adequate resolution regional climate simulations available for this region, there are relatively few studies that consider the value of downscaling using RCMs for hydrological applications. However *Akhtar et al.* (2008) found that RCM data produced better results when used with a hydrological model than using poor-quality observation data; this implies greater confidence in the RCM simulated meteorology than available observational data for this region (*Wiltshire*, 2014). Therefore in the literature hydrological analysis is typically at the global scale using GCMs coupled with hydrological models (*Milly et al.*, 2005, *Hirabayashi et al.*, 2008, *Falloon et al.*, 2011, *Wiltshire et al.*, 2013a,b) or at the basin scale using stand-alone hydrological models (*Singh and Kumar*, 1997, *Singh and Bengtsson*, 2005, *Singh et al.*, 2008, *Seidel et al.*, 2000) such as the Soil Water Assessment Tool (SWAT – *Arnold et al.*, 1998). Weather data in SWAT is either simulated within the model using a weather generator or taken from observations of daily precipitation and maximum/minimum temperature (*Nyeko*, 2015). This approach may be appropriate for small domains within which there is consistency in rainfall patterns but may not be suitable for large domains in South Asia due to the high temporal and spatial variability in precipitation across the region (*Hijioka et al.*, 2014). *Gosain et al.* (2006) use the SWAT model with 50 km

resolution daily RCM weather data to conduct a climate change impact assessment of the hydrology of several individual basins over India for two 20-year periods representing the present day (1981-2000) and future (2041-2060). *Gosain et al.* (2006) compare the differences between the two periods, rather than focussing on absolute values, to find that climate change causes an increase in precipitation, river flow and evaporation for the Ganges basin. High variability across basins and sub-basins means that parts of the Ganges basin could experience seasonal or regular water-stressed conditions under climate change (*Gosain et al.*, 2006) although it is not clear exactly which climate change scenario has been used for these simulations. There are more examples of the application of RCMs for hydrological analysis for other regions such as the UK and Europe. *Kay et al.* (2006) use 25km RCM data in a catchment-based rainfall-runoff model to estimate the flood frequency of small UK river basins to good effect. *Dankers et al.* (2007) use an RCM to evaluate the benefits of using high spatial resolution climate information for the Danube basin. *Sampson et al.* (2014) have also demonstrated the importance of the resolution of precipitation data for a region of Ireland for hydrological impact modelling.

The typical domain and resolution of RCM simulations enables the analysis of areas spanning multiple river basins covering a larger area than is usually possible with hydrological models. This means that there is consistent forcing across different basins. The use of the RCM generated runoff within the hydrological model also preserves the consistency of the projections with atmospheric forcing, which is not possible if the runoff is derived within a hydrological model. However, there are few regional river flow analyses currently available, where these consistencies are maintained. *Biemans et al.* (2013) analyse the RCM projections used in this analysis in terms of water availability for food production for selected river basins, using a coupled hydrology and dynamic vegetation model; however, so far no specific analysis of river flows has been done for these RCMs. Therefore we present the first 25 km resolution regional climate projections of river flow for the South Asia region by using RCM generated runoff within a routing model to estimate river flow thereby enabling consistency to be maintained across basins and with the driving climate scenario. This is a new application of the highest resolution RCM data currently available for this region, to enable analysis of the impacts of climate on river flows in conjunction with the strategic sampling of climate variability from selected GCMs. We use a novel approach to the consideration of variability of river flows through analysis of the upper and lower parts of the distribution, in addition to the mean flows.

The aim of this analysis is to examine how useful RCM simulations are for understanding how river flows could change in South Asia in the future. Irrigation is an important part of the agricultural industry for this part of the world, with the Indo-Gangetic plains traditionally providing the staple crops of rice and wheat (*Aggarwal et al.*, 2000) for India and South Asia as a whole; the continued success of these crops

is therefore important for the food and water security of the region. We discuss the potential implications of projected changes in the water resources needed to maintain yields of these crops in a changing climate. The models, observations and the analysis used are described in Sect. 2.2, while a brief evaluation of the driving data and the river flow analysis is presented in Sect. 2.3. The implications of the potential changes in river flows on water resources and conclusions are discussed in Sects. 2.4 and 2.5 respectively.

2.2 Methodology

2.2.1 Models

Figure 2.1 summarises the methodology described in this section in a flow chart, highlighting the main stages in the generation of the presented river flow projections and the approximate resolution of the model data used.

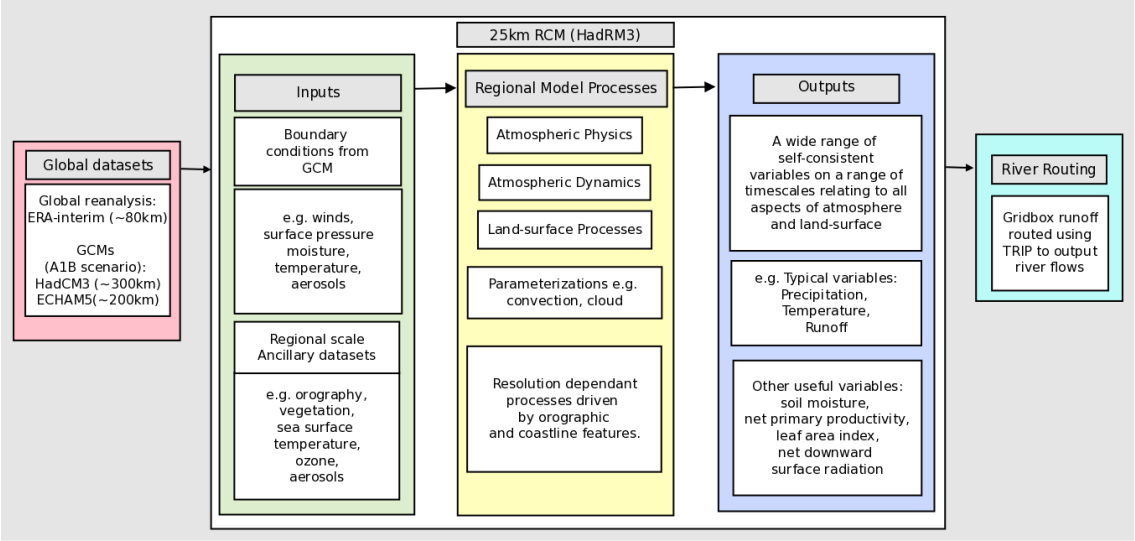

Figure 2.1: A flow chart showing the methodology for the presented analysis

2.2.1.1 GCM and RCM forcing

This analysis utilizes 25 km resolution regional climate modelling of the Indian subcontinent to provide simulations across the Hindu-Kush Karakoram Himalaya mountain belt. These RCM simulations form part of the ensemble produced for the EU-HighNoon project (referred to hereafter as HNRCMs), for the whole of the Indian subcontinent (25° N, 79° E–32° N, 88° E), for the period 1960–2100. The other simulations in the HighNoon ensemble, which used another RCM, the Regional Model from the Max Planck Institute for Meteorology (REMO – *Jacob et al.*, 2007) were unavailable for use in this analysis. Therefore one RCM, the HadRM3 RCM (*Jones et al.*, 2004) is used to

generate the river flow projections presented here. While the additional RCM would be useful here, analysis of the ERAint driven HadRM3 and REMO simulations over the Western Himalaya by *Dimri et al.* (2013) show that both models run at 25 km resolution over comparable domains have similar distributions of precipitation, temperature and interannual variablility, despite having different representations of orography. Analysis of the complete HighNoon ensemble for the Ganges/Brahmaputra basin in *Mathison et al.* (2013) also indicate a small spread between HNRCMs for the 30-year mean climatologies of temperature. Precipitation is more variable for this basin, with a larger spread between HNRCMs. However the RCM uncertainty defined by these two models (REMO and HadRM3) is still smaller than the climate uncertainty represented by the selected GCMs with the influence of the GCM on the projections of precipitation as great as the variability between RCMs (*Kumar et al.*, 2013). Therefore the most important contribution to the input uncertainty is from the GCM (*Akhtar et al.*, 2008) and using two GCMs to provide boundary data to one RCM provides a better estimate of climate uncertainty than using a single GCM to drive two RCMs, which would be the computational equivalent. On this basis we use HadRM3 driven by two carefully selected GCMs for this analysis. However other RCMs, not yet applied to this region could produce different projections.

In order to sample climate uncertainty, we use two GCM simulations that have been shown to capture a range of temperatures and variability in precipitation similar to the AR4 ensemble for Asia (*Christensen et al.*, 2007). Although using just two ensemble members is unlikely to capture the full range of uncertainty of a larger ensemble, the two models used for these simulations have been shown to capture the main features of the large-scale circulation particularly the ASM (*Kumar et al.*, 2013, *Annamalai et al.*, 2007, *Mathison et al.*, 2013), which is not true of all GCMs. The experimental design of the HighNoon ensemble compromises between the need for higher resolution climate information for the region and the need for a number of ensemble members to provide a range of uncertainty. The length of the simulations needed and the limited number of GCMs that are able to simulate the ASM also affect the number of ensemble members. These factors are all important given the limited computational resources available. The GCMs: the third version of the Met Office Hadley Centre Climate Model (HadCM3 – *Pope et al.*, 2000, *Gordon et al.*, 2000; a version of the Met Office Unified Model) and ECHAM5 (3rd realization – *Roeckner et al.*, 2003) are downscaled using the HadRM3 RCM (*Jones et al.*, 2004). These two GCMs capture the uncertainty in the sign of the projected change in precipitation with one showing an increase (HadCM3) and the other a decrease (ECHAM5). This feature is a key reason for the selection of these two GCMs. In addition to the GCMs, ERA-interim data (*Simmons et al.*, 2007, *Dee et al.*, 2011) is also downscaled using the HadRM3 RCM. ERA-Interim is reanalysis product that combines model and observations to provide a constrained estimate of the water balance of the region. The ERAinterim simulation has also been shown to

capture the role of steep topography on moisture transport fluxes and vertical flow for the western Himalayas (*Dimri et al.*, 2013). Therefore, for this region, where there is a lack of robust observations, particularly of the water cycle (see Sects. 2.2.3.1 and 2.3.1), it provides a useful benchmark against which to compare the GCM driven simulations. A similar approach is described in a previous study by *Wiltshire* (2014).

These RCM simulations are currently the finest resolution climate modelling available for this region (*Mathison et al.*, 2013, *Moors et al.*, 2011, *Kumar et al.*, 2013). HadRM3 has 19 atmospheric levels and the lateral atmospheric boundary conditions are updated 3 hourly and interpolated to a 150 s timestep. These simulations include a detailed representation of the land surface in the form of version 2.2 of the Met Office Surface Exchange Scheme (MOSESv2.2, *Essery et al.*, 2003), which includes a full physical energy-balance snow model (*Lucas-Picher et al.*, 2011). MOSESv2.2 treats subgrid land-cover heterogeneity explicitly with separate surface temperatures, radiative fluxes (long wave and shortwave), heat fluxes (sensible, latent and ground), canopy moisture contents, snow masses and snowmelt rates computed for each surface type in a grid box (*Essery et al.*, 2001). However the air temperature, humidity and wind speed above the surface are treated as homogenous across the gridbox and precipitation is applied uniformly over the different surface types of each gridbox.

The relationship between the precipitation and the generation of runoff is complicated, depending on not only the intensity, duration and distribution of the rainfall but also the characteristics of the surface. The infiltration capacity of the soil, the vegetation cover, steepness of the orography within the catchment and the size of the catchment are important influencing factors on runoff generation (*Linsley et al.*, 1982). In GCMs and even 25 km RCMs such as the one presented here, the resolution is often too coarse to explicitly model the large variations of soil moisture and runoff within a catchment and therefore the major processes are parameterized (*Gedney and Cox*, 2003). The method used within MOSES2.2 for generating surface and subsurface runoff across a gridbox is through partitioning the precipitation into interception by vegetation canopies, throughfall, runoff and infiltration for each surface type (*Essery et al.*, 2003). The *Dolman and Gregory* (1992) infiltration excess mechanism generates surface runoff; this assumes an exponential distribution of point rainfall rate across the fraction of the catchment where it is raining (*Clark and Gedney*, 2008). Moisture fluxes are allowed between soil layers; these are calculated using the Darcy equation, with the water going into the top layer defined by the gridbox average and any excess removed by lateral flow (*Essery et al.*, 2001). Excess moisture in the bottom soil layer drains from the bottom of the soil column at a rate equal to the hydraulic conductivity of the bottom layer as subsurface runoff (*Clark and Gedney*, 2008). The performance of MOSESv2.2 is discussed in the context of a GCM in *Essery et al.* (2001), however no formal assessment of MOSESv2.2 and the runoff generation in particular has been done for the RCM.

2.2.1.2 River routing model

In this analysis the simulated 25km gridbox runoff is converted into river flow using the 0.5° Total Runoff Integrating Pathways river routing scheme (TRIP; *Oki and Sud*, 1998) as a post-processing step. TRIP is a simple model that moves water along a predefined 0.5° river network; the Simulated Topological Network at 30 min resolution (STN-30p, version 6.01; *Vörösmarty et al.*, 2000a,b, *Fekete et al.*, 2001) in order to provide mean runoff per unit area of the basin; this can be compared directly with river gauge observations. TRIP has been used previously in *Falloon et al.* (2011), which used GCM outputs directly to assess the skill of a global river-routing scheme. The TRIP model has been shown to agree well with observed river flow gauge data (*Oki et al.*, 1999) and largely showed good skill when comparing runoff from several land surface models (*Morse et al.*, 2009). Implementation of TRIP in two GCMs; HadCM3 and HadGEM1 is described by *Falloon et al.* (2007) and was found to improve the seasonality of the river flows into the ocean for most of the major rivers. Using TRIP ensures the river flow forcing is consistent with the atmospheric forcing, however it also assumes that all runoff is routed to the river network and as such there is no net aquifer recharge/discharge. This may not be the case in regions with significant ground water extraction, which is subsequently lost though evaporation and transported out of the basin.

These simulations do not include representation of extraction, reservoirs or dams. Many of the river gauges used in this analysis and described in Section 2.2.2 are located at large dams along rivers in these basins and therefore the comparison between the simulations and the river gauges could be affected by these large features. Extraction, particularly for irrigation purposes is large in this region (*Biemans et al.*, 2013); this means that the extraction-evaporation and subsequent recycling of water in a catchment (*Harding et al.*, 2013, *Tuinenburg et al.*, 2014) is not considered in this analysis. The routed runoff of the HNRCM simulations are generally referred to hereafter using only the global driving data abbreviations; ERAint, ECHAM5 and HadCM3 (except Sect. 2.3.1 where we refer to the HadCM3 GCM and ERAint datasets before downscaling).

2.2.1.3 Emission Scenario

These simulations use the SRES A1B scenario (*Nakicenovic et al.*, 2000). The SRES scenarios were devised according to the production of greenhouse gases and aerosol precursor emissions as part of the AR4 IPCC report (*Christensen et al.*, 2007). The A1 storyline and scenario family represents a future world of very rapid economic growth, global population that peaks in mid-century and declines thereafter, and rapid introduction of new and more efficient technologies. The A1B scenario specifically, represents this future world where there is balance across energy sources i.e. a mixture

of fossil and non-fossil fuels (*Nakicenovic et al.*, 2000). This scenario does not represent changes in landuse, which remains fixed through the duration of these simulations. This is useful for understanding the effect of climate change in the absence of any adaptation.

2.2.2 Observations

This analysis uses observations of precipitation and river flow to assess the present day RCM hydrology. The precipitation observations are from the Asian Precipitation-Highly Resolved Observational Data Integration Towards the Evaluation of Water Resources (APHRODITE – *Yatagai et al.*, 2012) dataset. APHRODITE is a daily, 0.25° resolution gridded dataset.

The river flow analysis focuses on a selection of river gauges from the Global Runoff Data Centre (*GRDC*, 2014) that are located within the three major river basins for South Asia; the Indus and the Ganges/Brahmaputra. These gauges provide observations, which are used, in addition to downscaled ERA-interim river flows, to evaluate the downscaled GCM river flows. The selection of these river gauges aims to illustrate from the perspective of river flows, as modelled in an RCM, that the influence of the ASM on precipitation totals increases, from west to east and north to south across the Himalayan mountain range, while that of western disturbances reduces (*Wiltshire*, 2014, *Dimri et al.*, 2013, *Ridley et al.*, 2013, *Collins et al.*, 2013). The differing influences across the Himalayan arc result in complex regional differences in sensitivity to climate change; with western regions dominated by non-monsoonal winter precipitation and therefore potentially less susceptible to reductions in annual snowfall (*Wiltshire*, 2014, *Kapnick et al.*, 2014). A brief geographical description of the rivers and the chosen gauges is given in this section, their locations are shown in Fig. 2.2 and listed in Table 2.1 (including the abbreviations shown in Fig. 2.2 and the gauge location in terms of latitude and longitude).

The Indus, originates at an elevation of more than 5000 m in western Tibet on the northern slopes of the Himalayas, flowing through the mountainous regions of India and Pakistan to the west of the Himalayas. The upper part of the Indus basin is greatly influenced by western disturbances, which contribute late winter snowfall to the largest glaciers and snow fields outside the polar regions; the meltwaters from these have a crucial role in defining the water resource of the Indus basin (*Wescoat Jr*, 1991). In this analysis the Attock gauge is the furthest upstream and the Kotri gauge, located further downstream provide observations on the main trunk of the Indus river. The Chenab river, located in the Panjnad basin and in this analysis represented by the Panjnad gauge, is a major eastern tributary of the Indus, originating in the Indian state of Himachal Pradesh. In the upper parts of the Chenab sub-basin western disturbances contribute considerably to precipitation while the foothills are also influenced by the ASM (*Wescoat Jr*, 1991).

The Ganges river originates on southern slopes of the Himalayas (*Thenkabail et al.*,

2005) and traverses thousands of kilometres before joining with the Brahmaputra in Bangladesh and emptying into the Bay of Bengal (*Mirza et al.*, 1998). The Ganges basin has a population density 10 times the global average making it the most populated river basin in the world (*Johnston and Smakhtin*, 2014), it covers 1.09 $million\,km^2$ with 79 % in India, 13 % in Nepal, 4 % in Bangladesh and 4 % in China (*Harding et al.*, 2013). The main trunk of the Ganges is represented in this analysis by the gauge at the Farakka barrage, located at the India–Bangladeshi border, to the East of the Himalayas. The Bhagirathi river, located in "the Upper Ganga basin", is one of the main head streams of the Ganges. The Bhagirathi river originates from Gaumukh 3920 $m\,a.s.l.$ at the terminus of the Gangotri glacier in Uttarakhand, India (*Bajracharya and Shrestha*, 2011). The Tehri dam is located on this tributary, providing the most central data point on the Himalayan arc in this analysis (not a GRDC gauge).

The Karnali river (also known as Ghaghara), drains from the Himalaya originating in Nepal flowing across the border to India where it drains into the Ganges. The Karnali is the largest river in Nepal and a major tributary of the Ganges (*Bajracharya and Shrestha*, 2011) accounting for approximately 11 % of the Ganges discharge, 5 % of its area and 12 % of its snowfall in the HNRCMs. Two of the river gauges in this analysis; the Benighat and the Chisapani are located on this river. Two other sub-catchments complete those covering the Ganges basin; the Narayani river (or Gandaki River, represented here by the Devghat river gauge); reportedly very dependant on glaciers at low flow times of the year with over 1700 glaciers covering more than 2200 km^2 (*Bajracharya and Shrestha*, 2011). The Arun river, part of the Koshi river basin originates in Tibet, flows south through the Himalayas to Nepal. The Arun, represented in this analysis by the Turkeghat gauge joins the Koshi river, which flows in a southwest direction as a tributary of the Ganges.

The Brahmaputra originates from the glaciers of Mount Kailash at more than 5000 $m\,a.s.l.$, on the northern side of the Himalayas in Tibet flowing into India, and Bangladesh before merging with the Padma in the Ganges Delta. The Brahmaputra is prone to flooding due to its surrounding orography and the amount of rainfall the catchment receives (*Dhar and Nandargi*, 2000). The Brahmaputra is represented in this analysis by three gauges; Yangcun, the highest upstream gauge, Pandas in the middle and Bahadurabad furthest downstream but above the merge with the Padma.

There are no known observation errors for the GRDC observations (personal communication, GRDC). Estimates of observation errors for river gauges vary in the literature with a recommendation in *Falloon et al.* (2011) for GCMs to be consistently within 20 % of the observations while *Oki et al.* (1999) suggest that errors of 5 % at the 95 % confidence interval might be expected. *McMillan et al.* (2010) propose a method for quantifying the uncertainty in river discharge measurements by defining confidence bounds. In this analysis, these methods are hindered by the lack of observations concurrent with the model simulations. Therefore the method for approximating the inter-

annual variability in this analysis is based on the model variability and is described in Sect. 2.2.3.

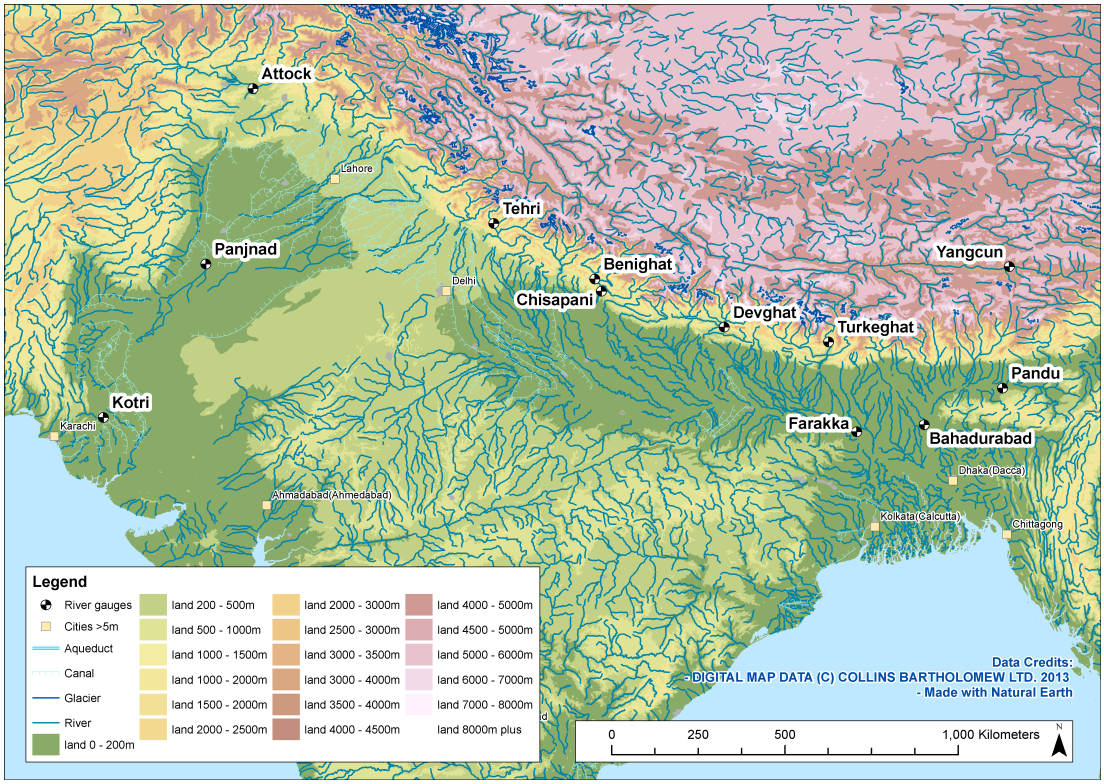

Figure 2.2: A map showing the locations of the river gauges used in this analysis.

Map abbreviation	River name	Gauge name	Latitude	Longitude	Years of data
IND_KOT	Indus	Kotri	25.37	68.37	14u (1950–1978)
IND_ATT	Indus	Attock	33.9	72.25	6c (1973–1979)
CHE_PAN	Chenab	Panjnad	29.35	71.03	6c (1973–1979)
BHA_TEH	Bhagirathi	Tehri Dam	30.4	78.5	3c (2001–2004)
KAR_BEN	Karnali River	Benighat	28.96	81.12	25u (1963–1993)
KAR_CHI	Karnali River	Chisapani	28.64	81.29	31c (1962–1993)
NAR_DEV	Narayani	Devghat	27.71	84.43	23u (1963–1993)
ARU_TUR	Arun	Turkeghat	27.33	87.19	10c (1976–1986)
GAN_FAR	Ganges	Farakka	25.0	87.92	18u (1950–1973)
BRA_BAH	Brahmaputra	Bahadurabad	25.18	89.67	12u (1969–1992)
BRA_YAN	Brahmaputra	Yangcun	29.28	91.88	21u (1956–1982)
BRA_PAN	Brahmaputra	Pandu	26.13	91.7	13u (1956–1979)

Table 2.1: Table listing the rivers and gauges (including their location) used in this analysis; all the observations shown here are from GRDC. The abbreviations used in Fig. 2.2 are given in column one. The Years of data column includes the number of years that data is available since 1950 with c to denote where data is continuous and u to show where the data is available for that number of years but not as a continuous dataset.

2.2.3 Methods

There are two stages to the analysis presented, comparison of the simulations with observations (for both RCM precipitation and river flows) and analysis of future climate. The comparison against observations aims to assess if the RCM reproduces the regional hydrology in terms of precipitation and river flow compared with available observations. The objective of the analysis of future climate is to understand how these simulations compare against the present day high and low flows i.e. present day natural variability. In this section we describe the methods used in each stage of the analysis; the comparison against observations is described in Sect. 2.2.3.1 and the analysis of future river flows in Sect. 2.2.3.2.

2.2.3.1 Comparison against observations

The total precipitation from each of the downscaled GCM simulations are compared against a downscaled ERAinterim simulation and APHRODITE observations. This comparison is on the basin scale, focussing on the basins included in the river flow analysis (see Sect. 2.2.2); the Indus and the Ganges/Brahmaputra. The TRIP model basin boundaries for each of these basins are shown in Fig. 2.4. The Ganges and Brahmaputra catchments are considered together in this analysis as these rivers join together in the Ganges Delta and are not clearly delineated in TRIP (see Fig. 2.4b). The precipitation patterns for each basin are useful for understanding the changes in the river flows within the catchments although rain gauges in the APHRODITE dataset are particularly sparse at higher elevations (see *Yatagai et al.*, 2012, Fig. 1). This leads to underestimation of the basin wide water budgets particularly for mountainous regions (*Andermann et al.*, 2011). This is confirmed by *Immerzeel et al.* (2015) for the Indus basin where they find a high altitude precipitation of up to ten times higher than current gridded datasets is needed to close the water balance for this basin. We compare the observations and simulations in terms of their annual timeseries and the climatology for each basin. The climatologies are calculated using the 1971-2000 period for HadCM3 and ECHAM5 and 1990-2006 for the ERAint simulation in order to capture a typical seasonal cycle for each simulation and basin.

This analysis is repeated for river flows in Sect. 2.3.2 for each of the 12 gauges described in Sect. 2.2.2. We also calculate the 1.5 standard deviation (SD) over a 30 year period to define the interannual variability. A value of plus 1.5 SD indicates an approx 1 in 10 year wet event, a value of minus 1.5 SD indicates a 1 in 10 year dry event. This approach is taken to indicate the possible impact of such a change under the hypothesis that current socio-economic levels of climate adaptation can cope with a 1 in 10 year events. The change driving mechanism could be anthropogenic climate or decadal variability. This assumes that interannual variability is independent of climate change whether that is due to decadal variability or externally forced change. In this context it

is indicative of the timing and magnitude of possible changes under the A1B emissions scenario. More work and ensemble members would be required to control for the role of decadal variability while the substantial computation expense in running high-resolution RCM experiments currently precludes the use of initial condition ensembles.

2.2.3.2 Future analysis

In Sect. 2.3.3 we use the annual timeseries of the whole simulation period to highlight any trends in future precipitation, evaporation (at the basin scale) and river flows (for each gauge) over the century. We also calculate the climatologies for two future 30-year periods; 2040-2070 (referred to as the 2050s) and 2068-2098 (referred to as the 2080s). The monthly climatology for the two periods is compared against the 1971-2000 range of natural variability. The purpose of the climatology analysis is twofold. The first objective is to establish if there is any change in the seasonality of the river flow. The second objective is to establish if there is any increase in the future 30-year mean river flows that is outside the present day variability, thereby indicating an increase in future events that are equivalent to the 1971-2000 1 in 10 year wet (dry) events (see Sect. 2.3.3.1).

Analysis of the 30 year mean is useful for understanding the general climatology of the region but often it is the periods of high and low river flow that are critical in terms of water resources. *Mathison et al.* (2013) highlight the importance of potential changes in the seasonal maximum and minimum river flows for the agricultural sector. The analysis in Sect. 2.3.3.2 uses Kernal Density Estimation (KDE, *Scott*, 2009, *Silverman*, 1986) to calculate the probability density functions (pdfs) of the river flows for each river gauge and 30 year period. The main aim of this analysis is to establish if there is any change in the distribution of the highest and lowest river flows for the 2050s and 2080s compared with the 1971-2000 period (see Sect. 2.3.3.2). Given these distributions, we then attempt to quantify the changes in highest and lowest river flows for the two future periods by focussing on the changes in the lowest and highest 10 % of flows using two different approaches. In the first approach in Sect. 2.3.3.3 we apply the upper and lower 10% of river flows for the 1971-2000 period as thresholds for the 2050s and 2080s. In Sect. 2.3.3.4, we take the principle of the threshold analysis one step further by calculating the 10th and 90th percentile threshold for each decade, simulation and gauge. The aim of this second approach is to establish if there is any systematic change in the upper and lower parts of the distribution through the century.

2.3 Results

The results are divided into three sections. Precipitation has a key influence on river flows; therefore, in Sect. 2.3.1, we consider the previous evaluation of the HNRCM simulations comparing the RCM precipitation for major South Asia basins with observations

and ERAint. In Sect. 2.3.2 we focus on river flows themselves for 12 gauges within these basins distributed across the Himalayan arc. The methods used in Sect. 2.3.1 and 2.3.2 are described in Sect. 2.2.3.1). In Sect. 2.3.3 we analyse the future projections of precipitation, evaporation and river flow to understand the water cycle of the region (see Sect. 2.2.3.2 for the methods used).

2.3.1 Comparison of present day driving data with observations

The HNRCM simulations have been evaluated in several previous publications. *Lucas-Picher et al.* (2011) evaluates the ability of RCMs to capture the ASM using ERA-40 data. *Kumar et al.* (2013) analysed the HNRCMs forced with ERA-Interim data. The GCM and HNRCM simulations are also evaluated against a range of observations for the Ganges/Brahmaputra river basin in *Mathison et al.* (2013). Figure 2.3 shows the observed spatial distribution of total precipitation for the monsoon period (June to September *Goswami and Xavier*, 2005) together with the HadCM3 and ERAint prior to and post downscaling. The HNRCMs (Figure 2.3 d and e) improve the spatial distribution of precipitation and therefore compare well with the observations shown in Figure 2.3c. This is highlighted by the additional detail shown in the precipitation fields through comparison of the pre-downscaled datasets for the HadCM3 GCM (Figure 2.3a) with those downscaled using HadRM3 (Figure 2.3e). This comparison is also possible for the downscaled ERA-interim reanalysis dataset shown in Figure 2.3d, which also shows an improved precipitation representation compared with the pre-downscaled dataset (Figure 2.3b). The higher resolution orography used in the 25km RCMs is more able than the much coarser resolution datasets to capture the particularly varied terrain of this region and the effects of this on the precipitation distribution.

In general the HNRCM simulations capture the spatial characteristics of the ASM, successfully reproducing regions of high convective precipitation, maximum land rainfall and the rain shadow over the east coast of India (*Kumar et al.*, 2013). Through adequately representing the spatial precipitation characteristics across the region, the areas of maximum and minimum precipitation can have a direct impact on the river flows for the appropriate basin. This is shown by the improvement in the timing and magnitude of the maximum precipitation for the RCM (HadRM3) compared with the GCM (HadCM3) shown in Fig. 2.6c (Indus) and Fig. 2.6d (Ganges/Brahmaputra). The RCMs are also able to reproduce the interannual variability of the region, although they underestimate the magnitude of the variation (*Kumar et al.*, 2013). The GCMs in the AR4 ensemble tend to exhibit cold and wet biases compared to observations both globally (*Nohara et al.*, 2006) and for South Asia (*Christensen et al.*, 2007). Although these are generally reduced in the RCM simulations there is a cold bias in the RCM that is probably carried over from the larger bias in the GCMs (*Mathison et al.*, 2013, *Kumar et al.*, 2013).

The remaining analysis focuses on the downscaled simulations of HadCM3, ECHAM5

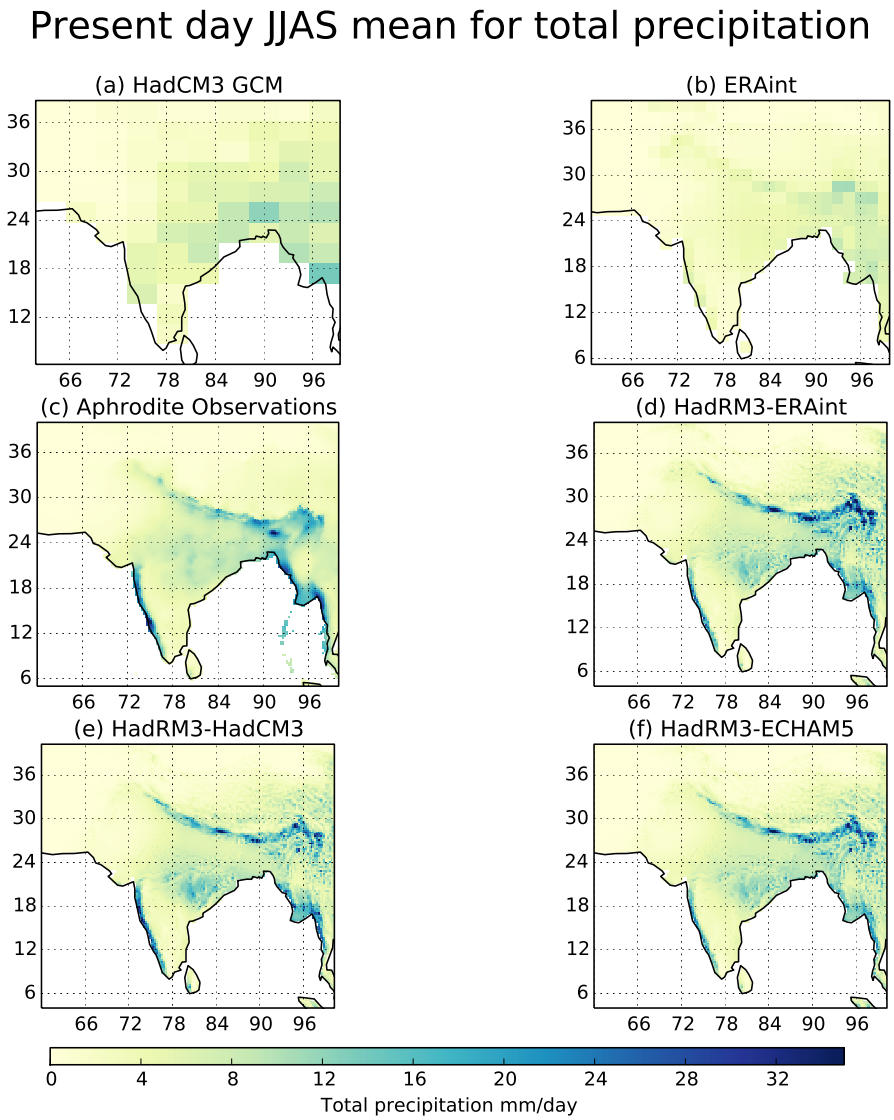

Figure 2.3: The spatial distribution of the seasonal mean total precipitation for the monsoon period (June, July, August, September) for the HadCM3 GCM (a), ERAint (b), APHRODITE observations (c) and the three HadRM3 simulations; HadRM3-ERAint (d), HadRM3-HadCM3 (e) and HadRM3-ECHAM5 (f).

and ERAint using the HadRM3 RCM. The RCM simulations shown in Fig. 2.6 appear to overestimate the seasonal cycle of total precipitation compared with the APHRODITE observations; this is highlighted by the annual mean of the total precipitation shown in Fig. 2.5. However, given the limitations of the observations at high elevations discussed in Sect. 2.2.3.1, we compare HadCM3 and ECHAM5 against an ERAint simulation. The annual mean precipitation (Fig. 2.5), the monthly precipitation climatology (Fig. 2.6) and the annual mean evaporation (Fig. 2.7) show that, for these catchments, the ERAint simulation lies between the two HighNoon ensemble members for much of the year. However, during peak periods of precipitation the magnitude of total

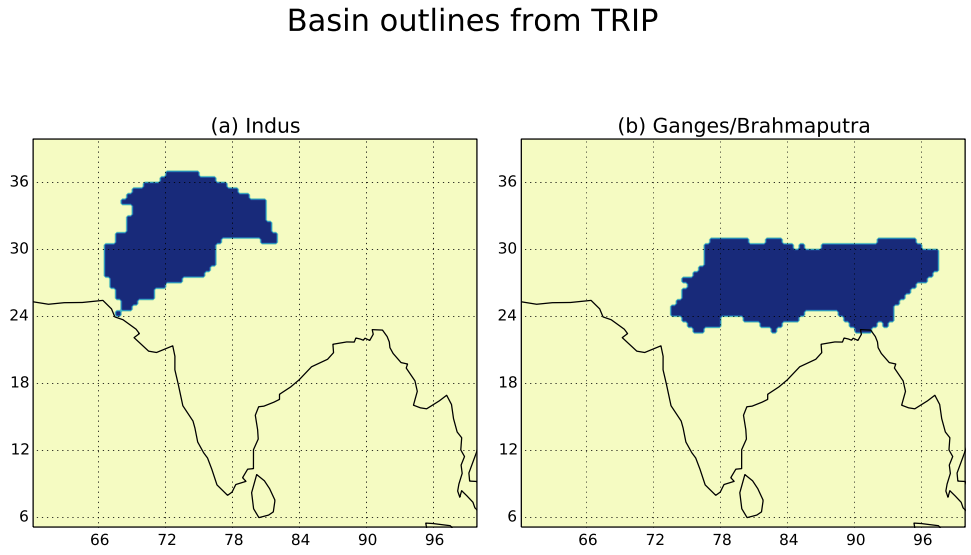

Figure 2.4: The outline of the basins within the TRIP model; Indus (a) and Ganges/Brahmaputra (b).

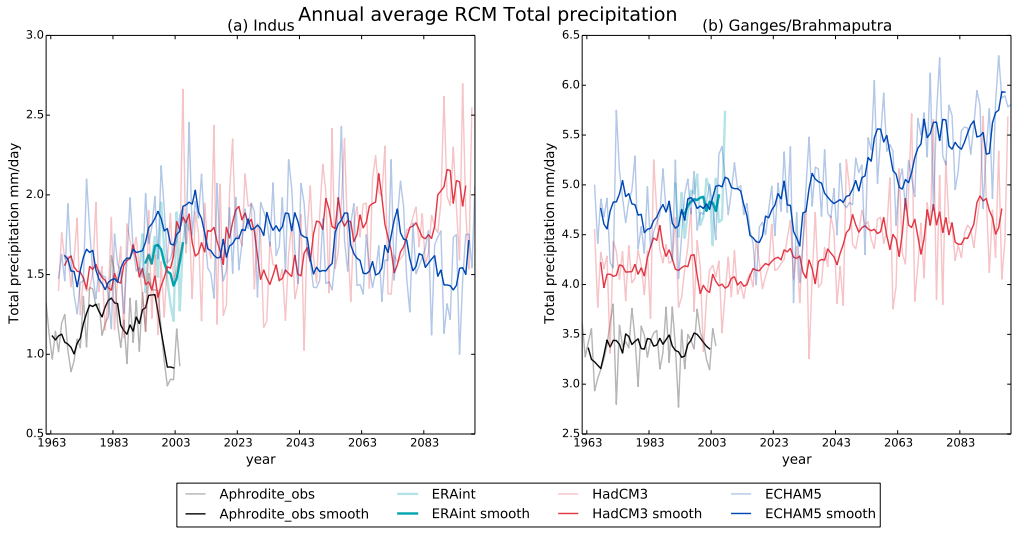

Figure 2.5: Annual mean total precipitation for the Indus (a) and Ganges/Brahmaputra (b) catchments for each model run (HadCM3 – red, ECHAM5 – blue, ERAint – cyan lines) plotted against APHRODITE observations (black line). Paler observations are annual averages and darker lines are a 5-year rolling smoothed average. See sect. 2.6 for Addendum plot with additional observations

precipitation for ERAint is larger.

The seasonal cycles of total precipitation are distinctly different between the basins

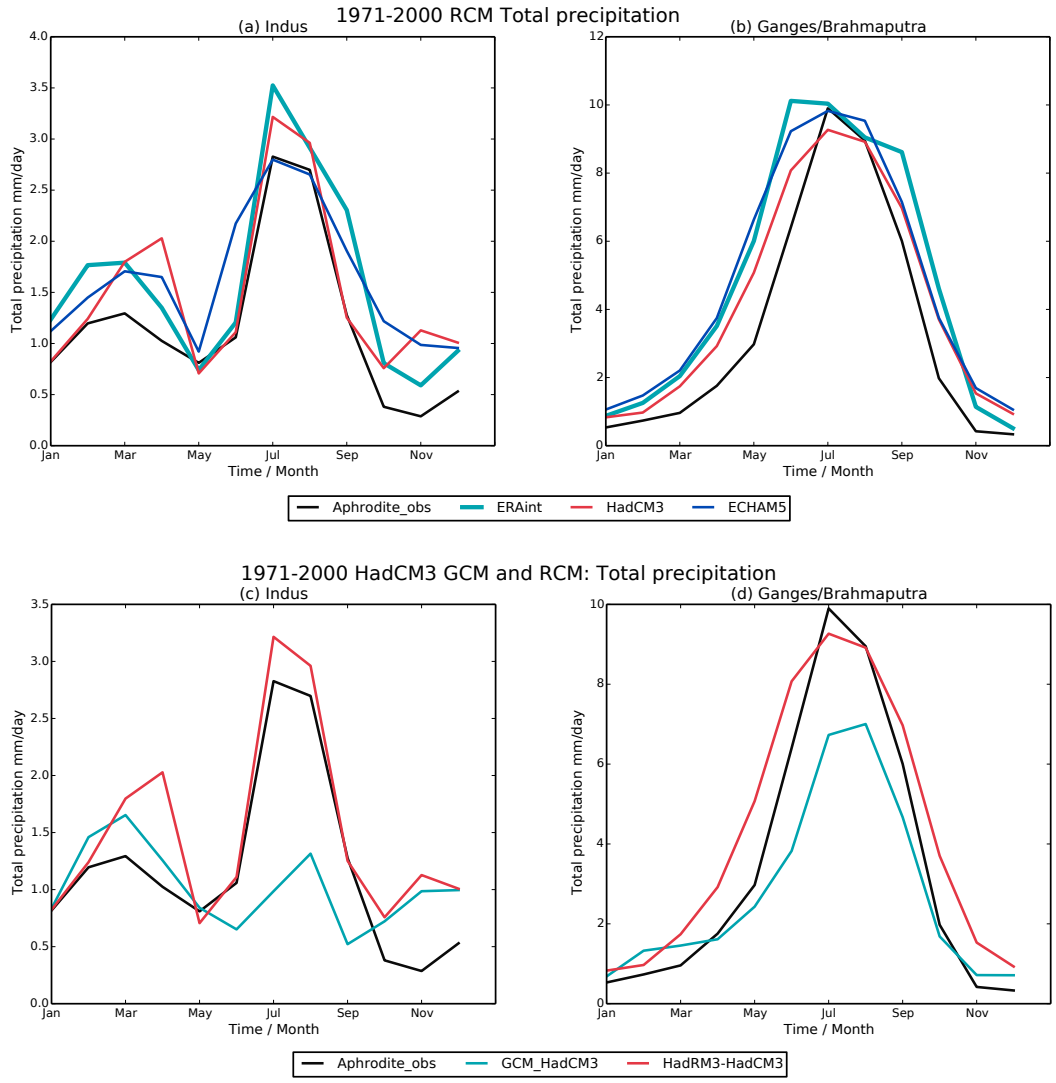

Figure 2.6: Seasonal cycle of total precipitation for the Indus (a and c) and Ganges/Brahmaputra (b and d) catchments. The RCM simulations are shown in plots a and b (HadCM3 – red, ECHAM5 – blue, ERAint – cyan lines). A comparison of the HadCM3 GCM (cyan line) and HadCM3-HadRM3 (red line) seasonal cycles are shown in plots c and d. APHRODITE observations are also shown (black line) on all plots.

shown. The Indus basin (Fig. 2.6a), indicates two periods of precipitation; one smaller peak between January and May and another larger one between July and September. The timings of the largest peak compare well, however the smaller peak occurs later than both ERAint and APHRODITE for ECHAM5 and HadCM3. The magnitude of the peaks in precipitation in the APHRODITE observations are consistently lower throughout the year than the simulations. The magnitude of the ERAint total precipitation is typically the largest while the ECHAM5 simulation is the lowest and closest to the APHRODITE observations. HadCM3 is between ECHAM5 and ERAint for most of the year. In contrast the Ganges/Brahmaputra catchment (Fig. 2.6b) has

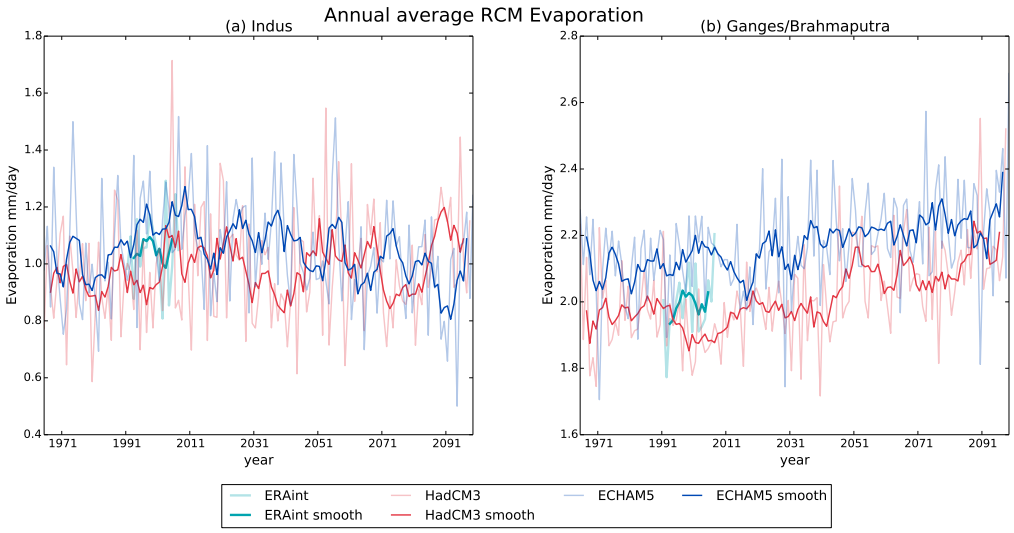

Figure 2.7: Annual mean evaporation for the Indus (a) and Ganges/Brahmaputra (b) catchments for each model run (HadCM3 – red, ECHAM5 – blue, ERAint – cyan lines) from 1971–2100. Paler lines are annual averages and darker lines are a 5-year rolling smoothed average.

one strong peak between July and September. In general this seasonal cycle is captured reasonably well by the simulations, both in terms of magnitude and timing of the highest period of precipitation. However there is a tendency for the simulations to overestimate rainfall between January and June compared to the observations, thus lengthening the wet season (*Mathison et al.*, 2013). *Mathison et al.* (2013) also show that in these simulations, the region of maximum precipitation along the Himalayan foothills is displaced slightly to the north of that shown in the observations. One explanation for this could be that the peak in total precipitation is due to the distribution of observations already discussed. Alternatively it could be due to the model resolution, which may still be too coarse to adequately capture the influence of the orography on the region of maximum precipitation. The downscaled ERAint simulation also indicates a higher total precipitation for January–May that is within the range of uncertainty of the GCM driven simulations. However for the remainder of the monsoon period, ERAint has a higher total precipitation than the GCM driven simulations. Fig. 2.3d illustrates this, showing a slightly larger and more intense area of maximum rainfall over the eastern Himalayas for the downscaled ERAint simulation than shown in the other RCM simulations (Fig. 2.3e and f) or APHRODITE (Fig. 2.3c).

2.3.2 Present day modelled river flows

In this section we compare present day modelled river flows with observations and a downscaled ERAint simulation using annual average river flows (see Fig. 2.8) and monthly climatologies (see Fig. 2.9). It is clear from Fig. 2.8 that observed river flow data is generally limited, which makes statistical analysis of the observations difficult.

River flow data for this region is considered sensitive and is therefore not readily available, particularly for the present day. For each of the gauges shown here, there are generally several complete years of data but often the time the data was collected pre-dates the start of the model run. The ERAint simulation is also shown (cyan line-ERAint) to provide a benchmark in the absence of well-constrained observations (See Sect. 2.3.1). The comparison between the model and observations shown in Figs. 2.8 and 2.9 is therefore to establish if the model and observations are comparable in terms of the average seasonal cycle and mean river flow rate without over-interpreting how well they replicate the observations. The Tehri Dam on the Bhagirathi river is not a GRDC gauge therefore observations are not shown. Observations for this gauge were received via personal communication from the Tehri Dam operator and therefore could not be adequately referenced.

The Kotri gauge on the Indus (Fig. 2.9a) and the Yangcun gauge on the Brahmaputra (Fig. 2.9k) are the only two gauges where the modelled river flow is higher than the observations and not within the estimated variability (1.5 SD) of the region. The ERAint simulation is also outside the estimated variability (1.5 SD) for the Benighat gauge on the Karnali river (Fig. 2.9e). The differences in these gauges are also reflected in the annual mean river flows (Fig. 2.8) for these river gauges, which are higher than observed. The high bias in modelled river flow at the Kotri gauge could be due to the extraction of water, which is not included in the model. The Indus has the largest irrigation scheme in the world and a semi-arid climate (*Immerzeel et al.*, 2015), which means the extraction rate for this basin is large (*Biemans et al.*, 2013). This gauge is also located relatively close to the river mouth to the west of the Himalayas (see Fig. 2.2 and Table 2.1), therefore the river flows are less likely to be affected by the ASM and more likely to be affected by meltwater from winter precipitation. The Yangcun gauge is a more upstream gauge and the differences between the model and observations for this gauge are more likely to be related to the precipitation distribution. Fig. 2.3 shows a region of intense precipitation in the simulations (Fig. 2.3d, e and f) for the ASM period close to this gauge. The APHRODITE data (Fig. 2.3c) also shows a region of higher rainfall although this is not as large as that shown for the simulations. This could be having a direct effect on the river flow.

The other two gauges on the Brahmaputra are located downstream of the Yangcun gauge; the Pandu (Fig. 2.9j) and Bahadurabad (Fig. 2.9l). At these two gauges, the seasonal cycle of river flow has a very broad peak particularly in the modelled river flows compared to the other gauges. In the simulations the snowfall climatology for the Ganges/Brahmaputra basin (not shown) has a similar seasonal cycle to that of the river flow for the Bahadurabad and the Pandu gauges. It is therefore likely that the broad peak in river flow is related to the broad peak in snowfall and subsequent snowmelt. The Pandu gauge is also one of only two gauges where the modelled river flow is less than the observations for at least part of the year, the other being the

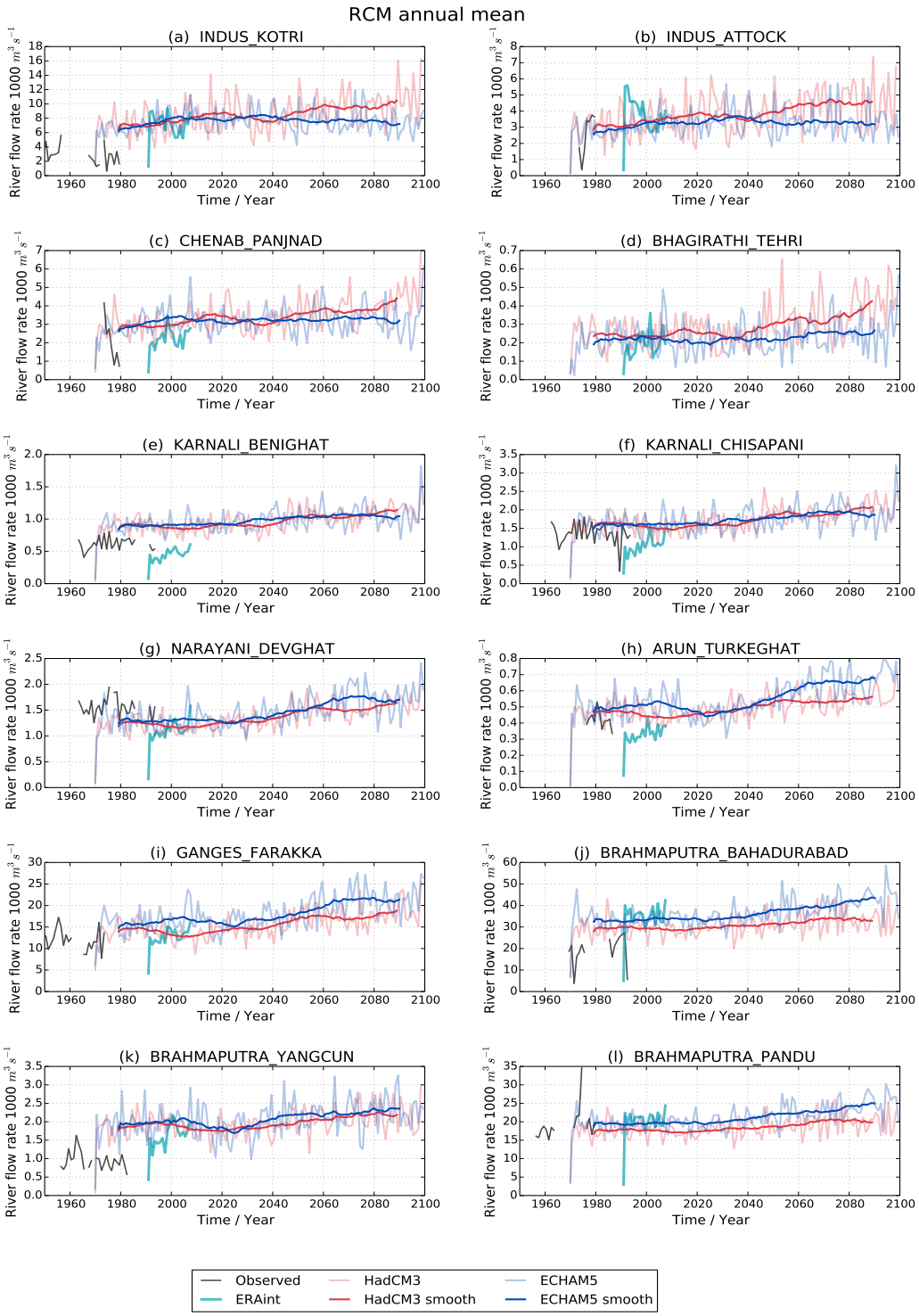

Figure 2.8: Timeseries of river flows showing available observations (black) and RCM runs (HadCM3 – red, ECHAM5 – blue, ERAint – cyan lines) from 1971–2100. Paler lines are annual averages and darker lines are a 20-year rolling smoothed average.

Devghat gauge on the Narayani river (Fig. 2.9g). Both of these gauges are located in the Himalayan foothills close to the region of simulated maximum total precipitation.

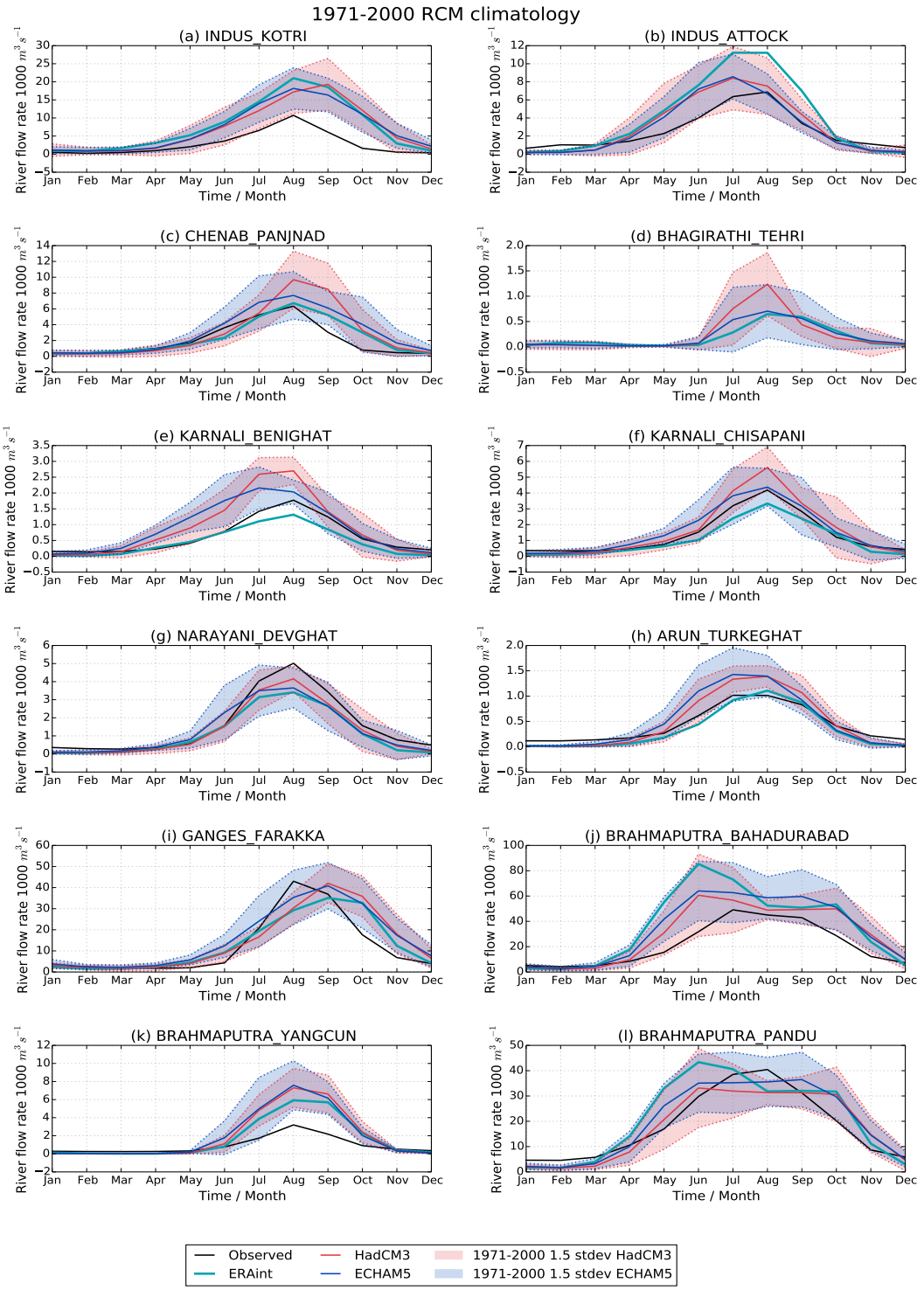

Figure 2.9: Seasonal cycle of river flow at individual river gauges; observed (black solid line) and for each of the RCMs (HadCM3 – red, ECHAM5 – blue, ERAint – cyan lines) for 1971–2000; with shaded regions showing 1.5 SD from the mean for the two simulations for the same period.

If the simulations put the location of this maximum below these gauges this could cause the river flows at the gauges to be lower than observed. The river flow on the main trunk of the Ganges at the Farakka barrage (shown in Fig. 2.9i), is a reasonable approximation to the observations in terms of magnitude; however, the timing of the peak flow seems to be later in the models. It could be argued this also happens in some of the other gauges, although it is more noticeable for the Farakka barrage. All the gauges shown here are for glacierized river basins. Snow fields and snow melt are represented in the simulations in this analysis and will therefore replicate some aspects of melt affecting river flow. However glacial melt is not explicitly represented in the RCM used for these simulations. Including glacial processes specifically could act to reduce runoff because more snow is stored as ice or increase runoff where there is an increased melting (*Bolch et al.*, 2012). Therefore including glacial processes could be important for the timing and magnitude of the maximum and minimum river flows for these catchments.

2.3.3 Future river flows

In this section we consider the future HNRCM simulations. Figure 2.5 highlights the variability in the future projections of total precipitation for South Asia between basins. In these simulations the Ganges/Brahmaputra catchment shows an increasing trend in total precipitation and there is considerable variation between the simulations (Fig. 2.5b). The Indus basin (Fig. 2.5a), however, has a much flatter trajectory to 2100 and the simulations are more similar. The annual timeseries of evaporation (Fig. 2.7) over these catchments shows a similar picture, with an increasing trend for the Ganges/Brahmaputra basin (Fig. 2.7b) but no real trend for the Indus (Fig. 2.7a). The annual mean runoff efficiency (not shown), defined here as the ratio of annual runoff (streamflow per unit area) to annual precipitation, shows no real trend for either basin. The trends in river flow (see Fig. 2.8) vary between gauges, although none indicate decreasing river flows. There is an upward trend in river flows at some of the gauges, in particular, the Narayani-Devghat (Fig. 2.8g), Arun-Turkeghat (Fig. 2.8h) and Ganges-Farakka (Fig. 2.8i). These gauges suggest an upward trend toward the 2100s that actually represents a doubling of the river flow rate. The increase in river flow for the Narayani-Devghat gauge (Fig. 2.8g) are consistent with analysis by *Shrestha and Aryal* (2011) using a hydrological model for the Narayani basin. Ganges-Farakka is the most downstream gauge in the Ganges/Brahmaputra basin in this river flow analysis, therefore providing an approximation for the whole Ganges basin. These simulations show an increase in precipitation for the Ganges/Brahmaputra basin of approximately 20 % (See Fig. 2.5) and an increase of approximately 10 % in evaporation (See Fig. 2.7), over the course of the century. This suggests the changes in runoff over the Ganges catchment are predominantly driven by precipitation on the annual scale. However regional analysis by *Jhajharia et al.* (2012) covering the humid northeastern part of

India and a global analysis by *McVicar et al.* (2012) suggest there has been a decline in the evaporation caused by lighter surface winds and reduced radiation. A future reduction in evaporation could also contribute to future increases in runoff. Analysis using a conceptual hydrological model by *Singh and Bengtsson* (2005) suggests that the type of precipitation being received at different elevations and the changes in melt and evaporation from snowpacks in a warmer climate could also be important for changes in runoff.

2.3.3.1 Climatology analysis

In this section we use climatologies to compare future river flows with the present day interannual variability (defined in Sect. 2.2.3.1). South Asia is a very variable region, yet these models suggest the future mean river flow could lie outside the present day variability for peak flows for some of the gauges in this study. This could have important implications for water resources for the region. The gauges that show an increase in maximum river flows (see Fig. 2.10) are mainly those in the middle of the Himalayan arc (see Fig. 2.2). The seasonal cycle for the westernmost (Indus gauges) and the easternmost (Brahmaputra gauges) are typically still within the range of present day variability. This could be due to the changes in the influence on river flow from west to east becoming more influenced by the ASM and less by western disturbances, with basins in the centre of the Himalayas and to the north influenced by both phenomena. Figure 2.10 also suggests that the maximum river flows still occur mainly during the ASM for many of the gauges shown.

2.3.3.2 High and low flow analysis

The analysis of the high and low flows is of particular importance to water resources and future availability, therefore in this section we calculate the distributions of the river flows for each of the gauges (see Sect. 2.2.3.2). These are shown in the form of probability density functions (pdfs) in Fig. 2.11 for the 1971–2000, 2050s and the 2080s. Figure 2.11 illustrates how the lowest flows dominate the distributions for each of the three periods. In most of the gauges 1971–2000 period has the highest frequency of the lowest flows, the curves then tend to flatten in the middle of the distribution before tailing off toward zero for the highest flows. The two future periods also follow a similar trajectory, although in general there is a reduction in the frequency of the lowest flows and an increase in the magnitude of the highest flows for all of the gauges and both simulations towards 2100.

The Yangcun gauge on the Brahmaputra (Fig. 2.11k) shows the least change of all the gauges between the 1971–2000 period, future periods and simulations. The distributions for the gauges downstream of Yangcun; the Pandu (Fig. 2.11l) and the Bahadurabad (Fig. 2.11j) are notable for their differences from all the other gauges.

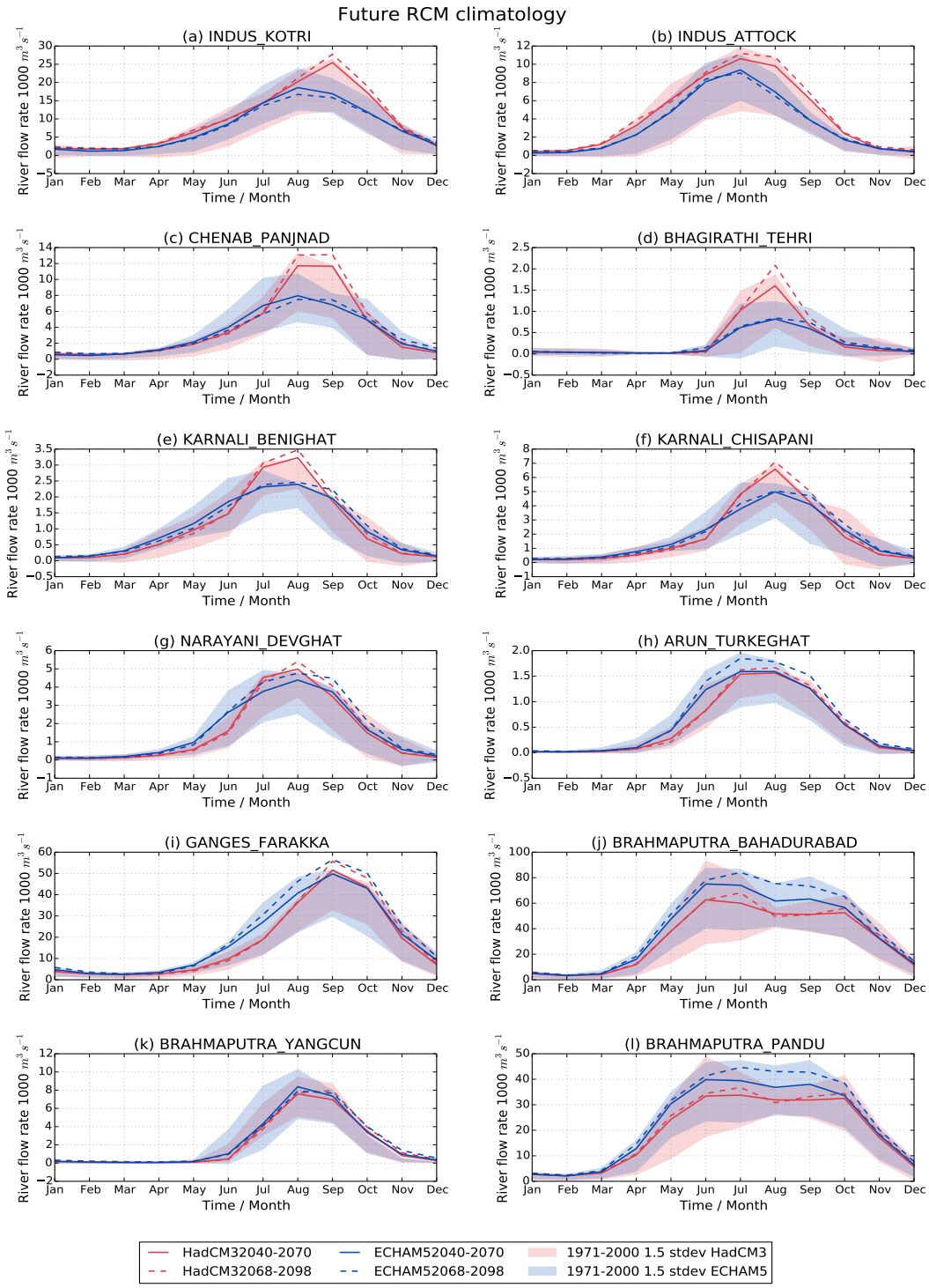

Figure 2.10: Seasonal cycle of river flow in each of the RCMs (HadCM3 – red, ECHAM5 – blue) for the two future periods: 2050s (solid lines) and 2080s (dashed lines), with shaded regions showing 1.5 SD from the mean for 1971–2000 for each river gauge.

All the other gauges shown have a single peak toward the lower end of the river flow distribution. The Pandu and Bahadurabad gauges have two distinct peaks in frequency

with a second peak occurring toward the middle of the distribution, where the distribution for most other gauges flattens out. This is consistent with the broader peak in the 30-year mean seasonal cycle shown for these gauges in Fig. 2.10 and is probably similarly explained by snowmelt (see Sect. 2.3.2). In some of the other gauges there is a small increase in the middle of the river flow distribution but this tends to be smaller and restricted to the two future periods e.g. the two Karnali river gauges (Fig. 2.11e and f).

2.3.3.3 Threshold analysis

The pdfs shown in Fig. 2.11 and described in Sect. 2.3.3.2 suggest future changes in the lower and upper ends of the river flow distribution. In this section we consider these parts of the distribution in order to confirm this pattern. We compare the two future periods (2050s and 2080s) against the 1971–2000 period explicitly using thresholds defined by the 10th and 90th percentiles for this present day period and for each river gauge. Graphical examples from the results of this analysis are shown for all three periods (historical (a), 2050s (b), 2080s (c)) for the Farakka Barrage on the River Ganges in Fig. 2.12 and Fig. 2.13. In Fig. 2.12 the number of months where river flow is below the present day 10th percentile reduces in each of the future decades. However for flows greater than the present day 90th percentile there is an increase in each of the future decades (Fig. 2.13). Table 2.2 illustrates that the patterns shown in Figs. 2.12 and 2.13 are generally true for almost every other gauge in the analysis. The Tehri Dam (Bhagirathi) is the only exception of the gauges shown in Table 2.2, showing an increase of 12 % in the number of incidences where the river flow is less than the 1971–2000 10th percentile for the 2080s. This is mainly due to the ECHAM5 model, which has a high number of incidences. The Yangcun gauge (Brahmaputra) is the only gauge where there is no change in the number of incidences where the river flow is less than the 10th percentile for 1971–2000 in either of the future periods. This is probably because the lowest river flows are already very low at this gauge.

At every gauge there is an increase in the number of incidences where river flows are greater than the 90th percentile for 1971–2000 for the two future periods. Several of the gauges have increases in the number of events above the 90th percentile for the 1971–2000 period of more than 100 %. This confirms the conclusions drawn visually from the analysis in Fig. 2.11 that the general distributions move toward the higher flows for these gauges and simulations.

2.3.3.4 Decadal percentile analysis

The annual timeseries shown in Fig. 2.8 is very variable and systematic changes throughout the century could be masked by this variability. On the basis that there are changes in the upper and lower parts of the future river flow distributions, the 10th and 90th

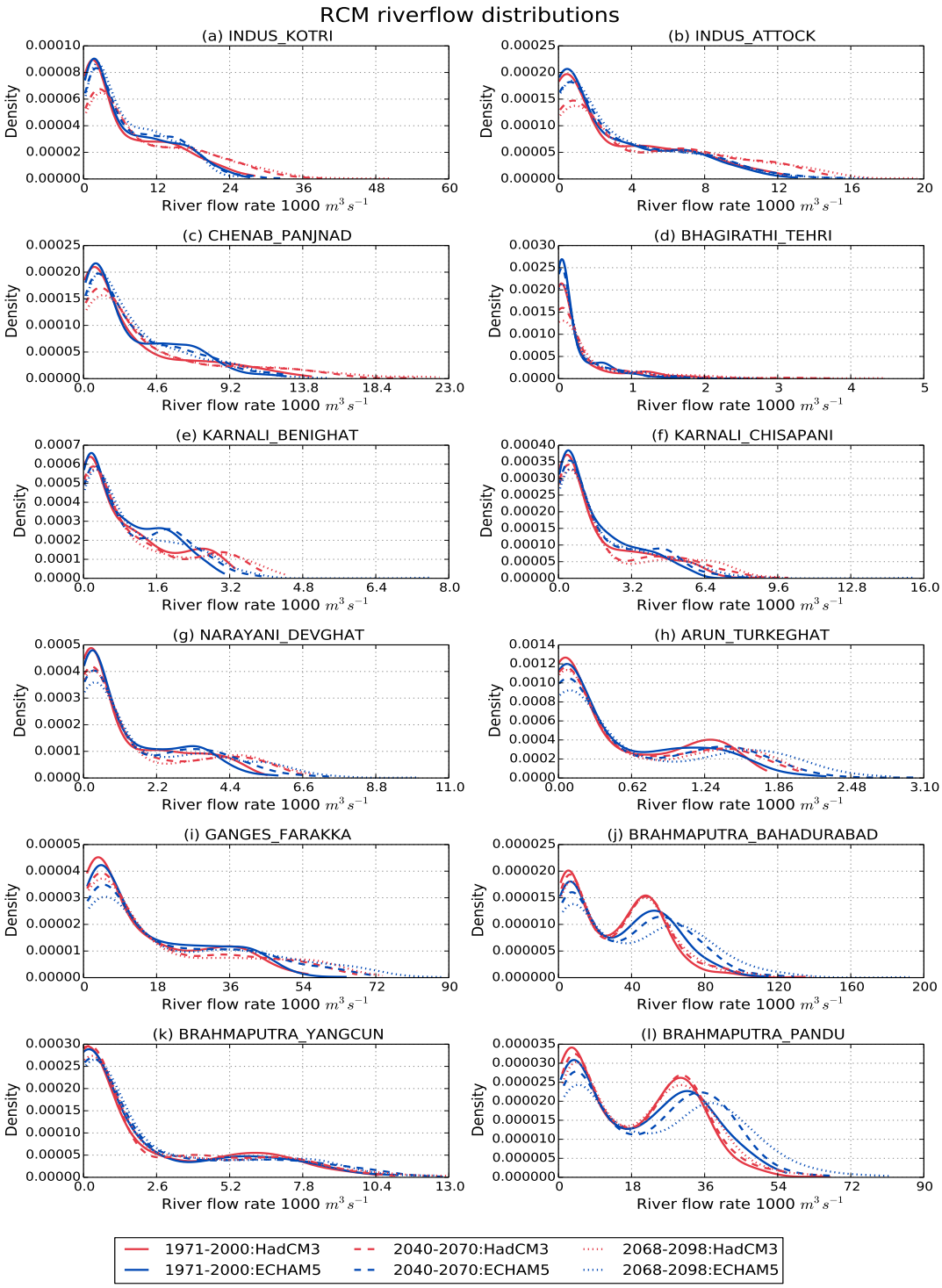

Figure 2.11: The distribution of the river flow in the HadCM3 and ECHAM5 (HadCM3 – red, ECHAM5 – blue) runs for three periods: historical (1971–2000 – solid lines) and two future periods (2050s – dashed lines and 2080s – dotted lines) plotted as a pdf for each river gauge.

percentiles for each decade and each simulation are calculated. At the lower end of the distribution, there is little change in the 10th percentile (not shown) for most of the

River	Gauge	< 10th percentile % change		> 90th percentile % change	
		2050s	2080s	2050s	2080s
Indus	Kotri	−55.4	−89.2	60.8	55.4
Indus	Attock	−70.3	−95.9	70.3	81.1
Karnali River	Benighat	−39.2	−73.0	63.5	81.1
Karnali River	Chisapani	−27.0	−56.8	60.8	79.7
Narayani	Devghat	−21.6	−54.1	75.7	110.8
Arun	Turkeghat	−63.5	−90.5	66.2	116.2
Brahmaputra	Yangcun	0	0	20.3	36.5
Brahmaputra	Pandu	−59.5	−79.7	47.3	113.5
Brahmaputra	Bahadurabad	−48.6	−64.9	67.6	114.9
Ganges	Farakka	−36.5	−52.7	68.9	102.7
Bhagirathi	Tehri Dam	−4.1	**12.2***	13.5	41.9
Chenab	Panjnad	−58.1	−83.8	43.2	50.0

Table 2.2: Table showing the average percentage change for the two models in the number of times the modelled river flow is less than the 10th percentile and greater than the 90th percentile of the 1970–2000 period for the 2050s and 2080s future periods. * This value is the only positive value in the table.

gauges, probably because of very low flows at the lowest times of the year. Only the Pandu and Bahadurabad gauges on the Brahmaputra and the Farakka gauge on the Ganges show a non-zero value for the lowest 10 % of river flows through to the 2100s. These three gauges indicate a slight increase for the 10th percentile for each decade through to 2100.

The 90th percentile values (Fig. 2.14) are generally much more variable throughout the century than those for the 10th percentile to the 2100s. We consider the gauges according to their location across the Himalayan arc from west to east (see Fig. 2.2). The HadCM3 simulation projects an increase in river flows for the most westerly gauges in this analysis; Attock and Kotri gauges located on the Indus (see Fig. 2.14a and b) and the Chenab-Panjnad gauge (see Fig. 2.14c). ECHAM5, on the other hand, shows a much flatter trajectory for these gauges. This may be explained by the HadCM3 simulation depicting an increase in the occurance of western disturbances and an increase in total snowfall, which is not simulated by ECHAM5 (*Ridley et al.*, 2013).

The gauges located toward the middle of the Himalayan arc generally show increases across the decades to 2100 in both models; these are the Bhagirathi-Tehri (Fig. 2.14d), both Karnali river gauges (Benighat - Fig. 2.14e and Chisapani-Fig. 2.14f), Narayani-Devghat and Arun-Turkeghat (Fig. 2.14g and h). There is very close agreement between the two simulations for the Narayani-Devghat, Arun-Turkeghat (Fig. 2.14g and h) and Bhagirathi-Tehri (Fig. 2.14d) gauges, with the former two showing less variability between decades than the others in the analysis. The Karnali-Benighat gauge (Fig. 2.14e) also has less variability between the decades. However, there is a systematic difference between the two simulations, which remains fairly constant across the decades. From the subset of gauges in this analysis that are the most central on the Himalayan arc, the Karnali-Chisapani gauge (Fig. 2.14f) has the largest variability between simulations

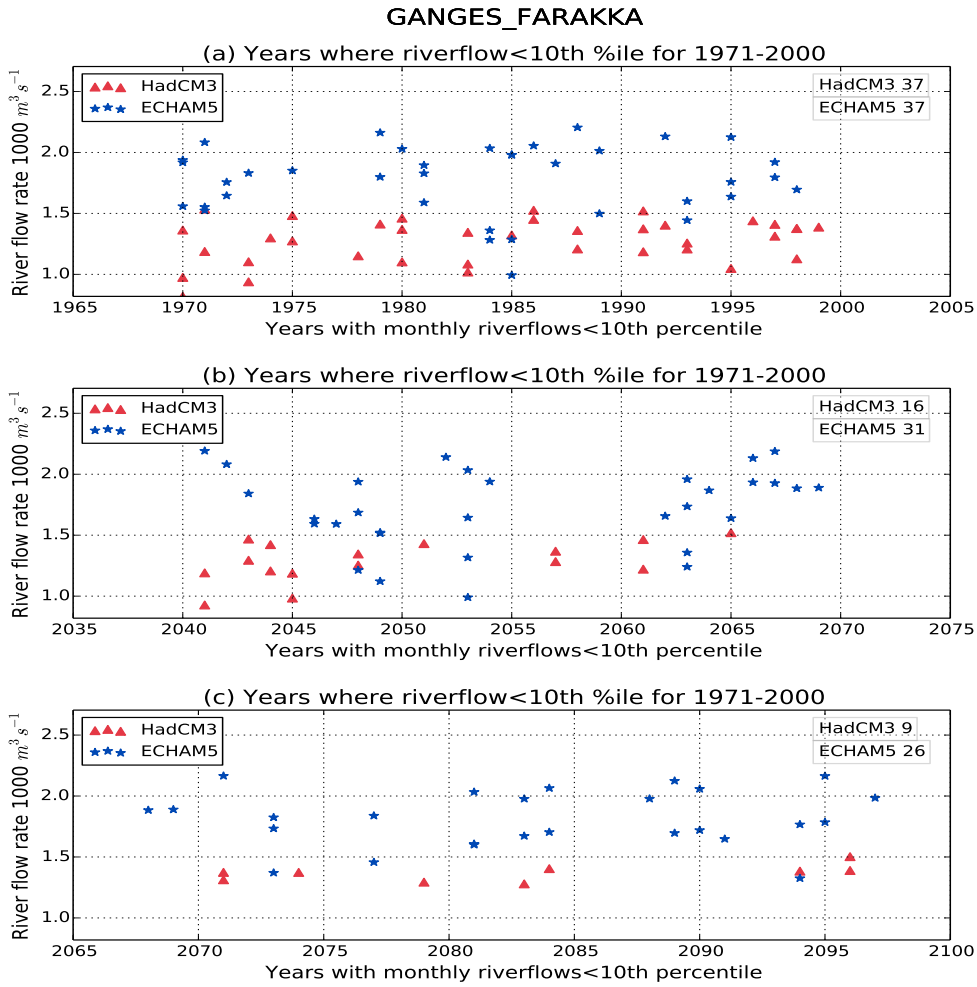

Figure 2.12: Comparison of the lowest 10 % of monthly river flows at the Farakka barrage on the Ganges river against the 10th percentile for the 1971–2000 period for 1971–2000 (top), 2050s (middle) and 2080s (bottom) for HadCM3 (red triangles) and ECHAM5 (blue stars). Each star or triangle represents a month within the 30 year period where the value is less than the 10th percentile of the 1971-2000 period with the total number for each of the simulations given in the top right corner of each plot.

and decades. However this gauge still shows an increase overall in both simulations with a steeper increase for HadCM3 than ECHAM5. The closer agreement between simulations at these more central gauges may be due to the reducing influence of the western disturbances in the HadCM3 simulation from west to east across the Himalaya therefore resulting in smaller differences between the the two simulations.

The Farakka-Ganges gauge (Fig. 2.14i) and two of the Brahmaputra gauges – Bahadurabad (Fig. 2.14j) and Pandu (Fig. 2.14l), represent three of the most easterly river gauges in the analysis. These gauges show an increase in both simulations through to the 2100s, in this case more pronounced in ECHAM5 than HadCM3 for these two Brahmaputra gauges. There is much closer agreement between the two simulations at

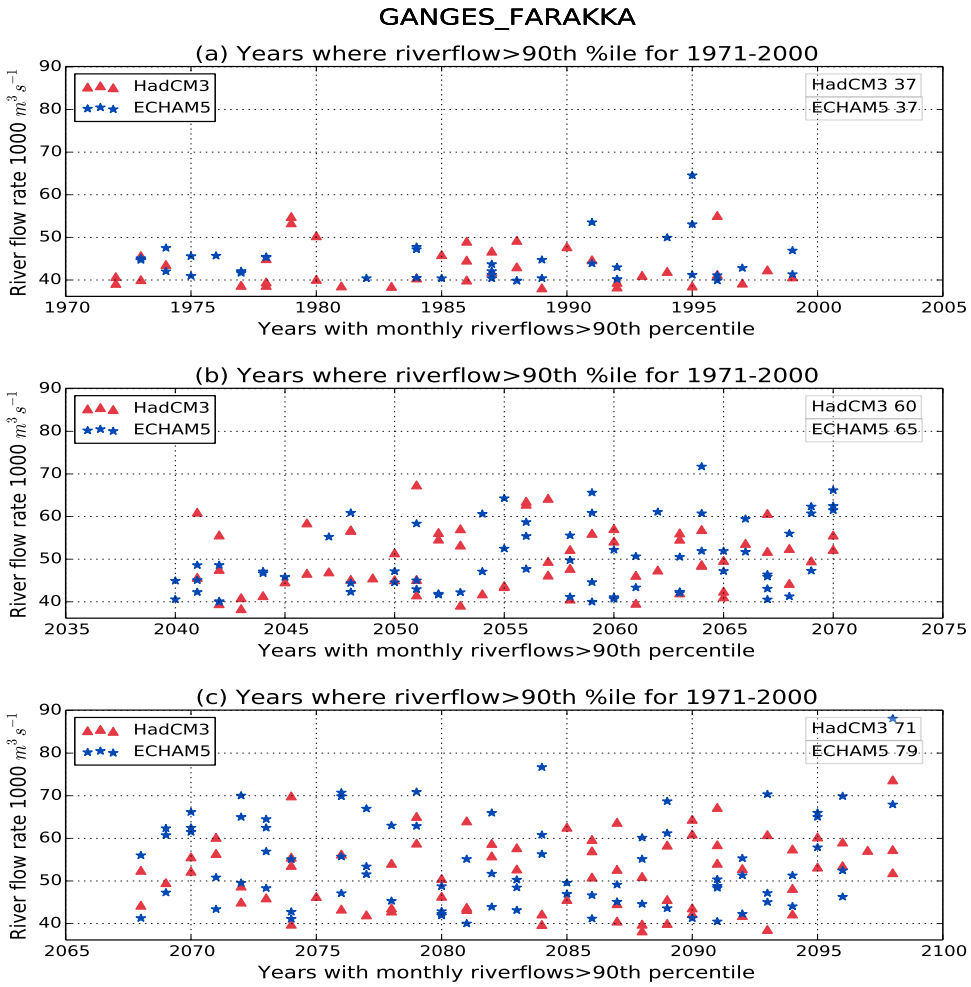

Figure 2.13: Comparison of the highest 10 % of monthly river flows at the Farakka barrage on the Ganges river against the 90th percentile for the 1971–2000 period for 1971–2000 (top), 2050s (middle) and 2080s (bottom) for HadCM3 (red triangles) and ECHAM5 (blue stars). Each star or triangle represents a month within the 30 year period where the value is greater than the 90th percentile of the 1971-2000 period with the total number for each of the simulations given in the top right corner of each plot.

the Farakka-Ganges gauge (Fig. 2.14i), which is located slightly further west than the two Brahmaputra gauges. The other Brahmaputra gauge, the Yangcun (Fig. 2.14k) is very variable through the century, there is a period with consecutive decades of increasing river flows in the middle of the century but over the whole century neither model shows a consistent change.

This analysis shows that neither simulation is consistently showing a systematic increase in the 90th percentile of river flows across all the gauges. Instead it highlights the changing conditions and the different behaviour of the two simulations across the Himalayan arc.

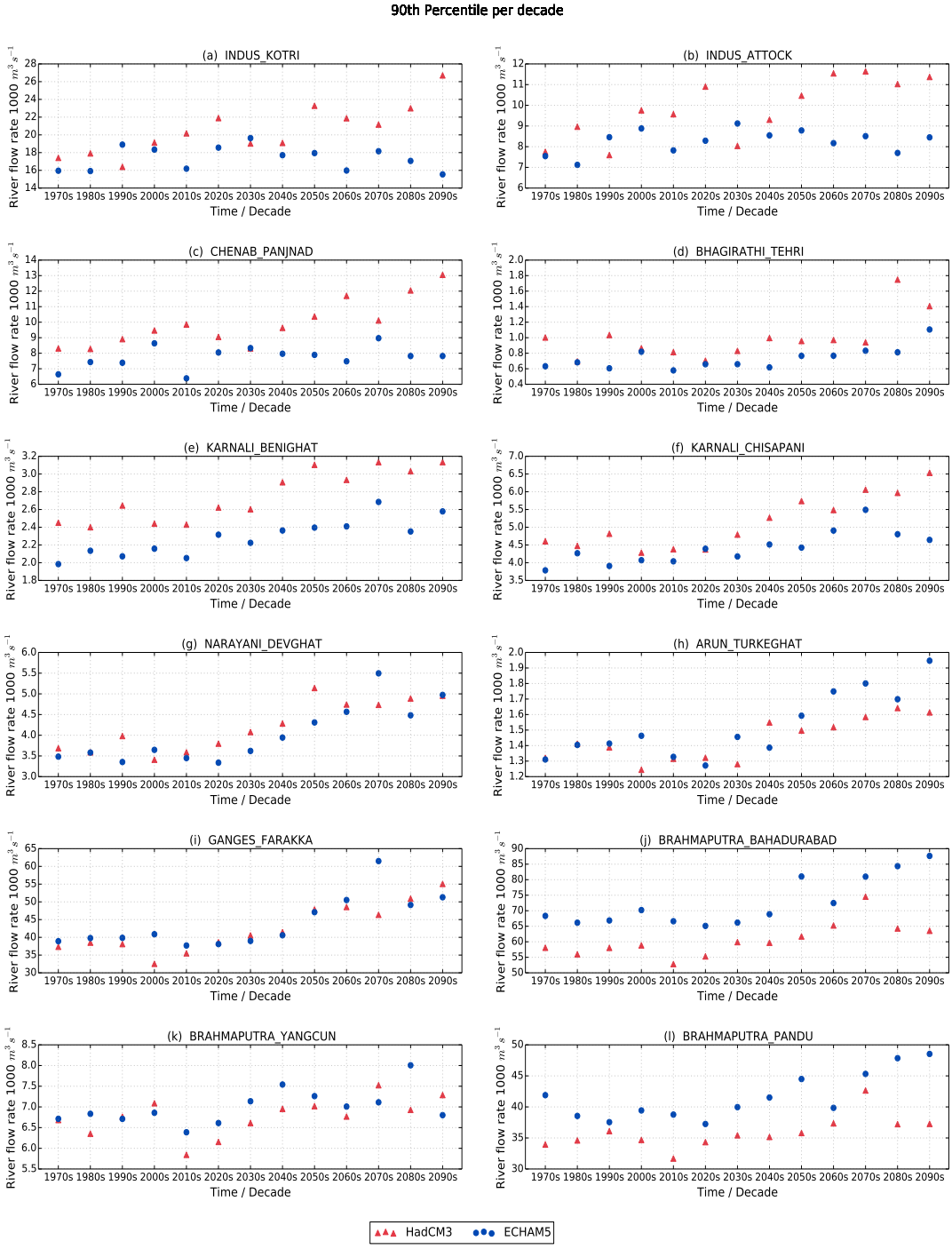

Figure 2.14: The 90th percentile of river flow for each decade for HadCM3 (red triangles) and ECHAM5 (blue circles) for each river gauge.

2.4 Implications of changes in future river flows

In this section we consider the implications of the projected future changes in river flows for South Asia on water resources. We highlight the broader challenges facing the region and where the current RCMs need development to represent key processes for this region. The key points from this discussion are summarised in Table 2.3. In the present day, water resources in South Asia are complicated, precariously balanced between excess and shortage. Parts of South Asia receive some of the largest volumes of precipitation in the world and are therefore at frequent risk of flooding and yet others regularly endure water stress. The complexity is increased by the competition between states and countries for resources from rivers that flow large distances crossing state and country borders, each with their own demands on resource. There is a considerable gap between the amount of water resource flowing through South Asia and the actual usable amount (*Aggarwal et al.*, 2012), for example the total flow for the Brahmaputra basin is approximately $629\,km^3$ of which only $24\,km^3$ is usable (*Kumar et al.*, 2005). There is therefore huge potential for improvements in the efficiency of systems for irrigation and domestic water supply that could ease pressures on water resources, currently and predicted, as demand increases.

In the last $50\,years$ there have already been efficiency improvements, such as development of irrigation systems and use of high yielding-water efficient crop varieties. These improvements have fuelled the rapid development in agriculture across South Asia, making the region more self-sustained and alleviating poverty (*Kumar et al.*, 2005). However these advances have also had a large impact on the regions river ecosystems resulting in habitat loss, reduced biodiversity (*Sarkar et al.*, 2012) and water pollution (*Vörösmarty et al.*, 2010). Historically arbitrary thresholds based on a percentage of the annual mean flow have been used to estimate minimum flows, but these simplistic estimates do not take account of the flow variability that is crucial for sustaining river ecosystems (*Arthington et al.*, 2006, *Smakhtin et al.*, 2006), referred to as environmental flows. Environmental flows are defined by *Smakhtin and Anputhas* (2006) as the ecologically acceptable flow regime designed to maintain a river in an agreed or predetermined state. The variability in river flows through the year have important ecological significance; for example low flows are important for algae control and therefore maintaining water quality. High flows are important for wetland flooding and preserving the river channel. When considering the implications of future changes in climate on river flows and therefore surface water resources, estimates of flow variability and minimum flows are an important consideration. However these are not easily quantified in general terms with many methods requiring calibration for applications to different regions and basins. In our simulations there is an intensification of the seasonal cycle and therefore an increase in the flow variability and a reduction in the occurrance of the lowest flows. These changes could have implications for the

Types of change	Implications for water resources	Adaptation options	Other issues
Large annual variability	Abundance some years and scarcity in others make it difficult to plan budgets for different users.	Building storage capacity e.g. rainwater harvesting. Improvement of irrigation systems. Development of water efficient, high yielding crop varieties.	Type of water storage is important e.g. reservoirs/dams have both political and ecological implications. Developing new crops takes time.
Changes in peak flow – timing and magnitude	Increases in peak flows could be postive for irrigation and domestic supply but could increase the risk of flooding. Peak flows occurring later and/or decreases in peak flows could reduce availability of water for irrigation at crucial crop development stages negatively impacting yields.	Improving river channel capacity. Diverting excess water to a different valley. Storing the excess water for low flow periods e.g. through rainwater harvesting. Improving drainage and water recycling. Adopting varieties of crops that grow when water for irrigation is more readily available.	Flood protection levels do not match demographic trends so vulnerability to flooding remains high in this region (*Gupta et al.*, 2003). Market development for new crops takes time.
Changes in low flows – timing and magnitude	Increases in the magnitude of the low flows could be positive for irrigation and domestic supply. Decreases could mean less resource available for irrigation leading to reduced yields.	Adaptations to avoid flooding during peak flow periods could provide resource during low flow periods. Development of water efficient, high yielding crop varieties.	

Table 2.3: Table of implications of changes in water resources.

biodiversity of these catchments.

In India the domestic requirement for water is the highest priority but is only 5 % of the total demand. Irrigation is the second highest priority accounting for a much greater proportion, approximately 80 % of India's total demand for water. A significant proportion of domestic and irrigation resource comes from both ground and surface water. *Biemans et al.* (2013) study future water resources for food production using LPJml and the HNRCMs. LPJml also simulates ground water extractions (*Biemans et al.*, 2013); these are thought to be important for the Indus and parts of the Ganges, but not the Brahmaputra. The LPJml simulated extraction varies considerably between basins: the largest occuring in the Indus ($343\,km^3\,year^{-1}$) followed by the Ganges ($281\,km^3\,year^{-1}$) and Brahmaputra ($45\,km^3\,year^{-1}$). The Brahmaputra has the smallest percentage of irrigated crop production (approximately 40 %) followed by the Ganges (less than 75 %) and the Indus where more than 90 % of crop production

is on irrigated land. The Indus has the largest proportion of water sourced from rivers and lakes of the three basins and the largest proportion of the river flow is glacial melt (*Immerzeel et al.*, 2010).

Wiltshire et al. (2013a) use a perturbed physics ensemble of HadCM3 GCM simulations (*Murphy et al.*, 2004) and find an increase in water resources for South Asia at the annual timescale due to climate change. The analysis shown here shows a similar result with increases in river flow, particularly the magnitudes of the higher river flows at these gauges, in some cases above the range of variability used for this analysis (1.5 SD). However, the analysis shown here on the monthly timescale, also highlights that these increases in resource tend to occur during the ASM, when river flow is at its maximum. This could mean that the benefits of an increase in water resource may not be realised due to the timing of this increase within the year. Although these projected changes in river flow are not critical for water resources they could still be beneficial where there is the capacity to store the additional flow for use during periods of low flow. Additional water storage capacity for example through rainwater harvesting, could greatly increase the useable water resource for the Ganges–Brahmaputra catchments (*Kumar et al.*, 2005) and potentially alleviate the increased risk of flooding during the ASM when rainfall is most persistent and rivers are already at their peak flow. South Asia, even in the current climate, is particularly susceptible to flooding due to the high temporal and spatial variability of rainfall of the region. It is estimated that approximately 20 % of Bangladesh floods annually (*Mirza*, 2002). Several studies have highlighted increases in both the extremes (*Sharma*, 2012, *Rajeevan et al.*, 2008, *Goswami et al.*, 2006, *Joshi and Rajeevan*, 2006) and the variability (*Gupta et al.*, 2005) of precipitation in recent years that cause extreme rainfall events resulting in catastrophic levels of river flooding. Over 30 million people in India alone are affected by floods and more than 1500 lives are lost each year (*Gupta et al.*, 2003), the economic cost of flooding is also considerable with the cumulative flood related losses estimated to be of the order of USD 16 billion between 1978 and 2006 (*Singh and Kumar*, 2013).

The timing of the peak flows of major rivers in this region is also very important in terms of flooding. In 1998 the peak flows of the Ganges and the Brahmaputra rivers occurred within 2 days of each other resulting in devastating flooding across the entire central region of Bangladesh. Approximately 70 % of the country was inundated, the flood waters then remained above danger levels for more than 60 days (*Mirza*, 2002). This event caused extensive loss of life and livelihood in terms of damaged crops, fisheries and property and the slow recedance of flood waters hindered the relief operation and recovery of the region. This analysis does not suggest any change to the timing of the peak flows, only the magnitude. However given the high probability of two rivers in this region having coincident peak flows in any given year (*Mirza*, 2002) and the likelihood that severe flooding will result, an increase in the magnitude of the peak could still be significant. Flooding can have a large impact on crops, for

example in Bangladesh over 30 % of the total flood related damages are due to the loss of crops. The estimated crop damage from the 1998 floods was estimated to be 3.0 million t (*Gain et al.*, 2013). The slow receding of flood water can also mean the ground is not in a suitable condition to sow the next crop, restricting the growing time and potentially affecting crop yields for the following year. On the other hand a limited amount of flooding could also be a benefit, particularly for rice crops. Inundation of clear water can benefit crop yield, due to the fertilization effect of nitrogen producing blue-green algae in the water (*Mirza et al.*, 2003).

In our simulations the reduced occurrence of the lowest flows could translate into an increase in the surface water resource in this region especially during periods when the river flows are traditionally very low. This could mean that the current and increasing pressure on ground water (*Rodell et al.*, 2009) may be alleviated in future years. Alternatively increases in the lowest flows may enable adaptation to a changing climate and the modification of irrigation practises. Current projections of future climate suggest that temperatures could also increase for this region (*Cruz et al.*, 2007). Increasing temperatures poses a threat to crop yields of a different kind because this is a region where temperatures are already at a physiological maxima for some crops (*Gornall et al.*, 2010). Rice yield, for example, is adversely affected by temperatures above 35 °C at the critical flowering stage of its development (*Yoshida*, 1981). Wheat yields could also be affected by rising temperatures, with estimated losses of 4–5 million tonnes per degree of temperature rise through the growing period (*Aggarwal et al.*, 2012). Additional water resource for irrigation at previously low flow times of the year could allow sowing to take place at a different time of the year in order to avoid the highest temperatures, thereby reducing the likelihood of crop failure. However with increasing variability and extremes, a potential feature of the future climate for this region (*Hijioka et al.*, 2014), there is also the increased risk of longer periods with below average rainfall and potentially more incidences of drought. This could lead to additional demand for water for irrigation to prevent crops becoming water stressed (*Aggarwal et al.*, 2012). There may also be increases in demand from other sources other than agriculture, for example the increasing population (*United Nations*, 2013) or the reduced availability of ground water of an acceptable quality for domestic use (*Gregory et al.*, 2005). Any of these factors, either individually or combined, could effectively cancel out any or all increases in resource from increased river flow due to climate change.

In addition there are a number of processes missing from the models used for these simulations that could change the sign of the projected changes. There is no irrigation included in these simulations, which could be important particularly on the basin scale. The impacts of extensive irrigation on the atmosphere are complex but could have a positive impact on water availability (*Harding et al.*, 2013) due to evaporation and water being recycled within the basin. *Tuinenburg et al.* (2014) estimate that up to

35 % of additional evaporation is recycled within the Ganges basin. This means that this part of the regional water cycle is not accounted for in these simulations. There is also no representation of glaciers which could act to increase or reduce river flows depending on the occurance of negative or positive mass balance respectively. In these simulations snowmelt is represented, however representing glacial processes as snowmelt could act to enhance the seasonal cycle in the simulated river flows for both present day and future projections as snow melts more readily than ice. These simulations also do not explicitly include groundwater, primarily focusing on river flows. Groundwater is a highly exploited part of water resources for South Asia. Representation of this would give a more complete picture of the total water resources for this region.

2.5 Conclusions

We present the first 25 km resolution regional climate projections of river flow for the South Asia region. A sub-selection of the HNRCMs are used to provide runoff to a river routing model in order to provide river flow rate, which can be compared directly with ERAInt and any available river gauge data for the South Asia region. This analysis focuses on the major South Asia river basins, which originate in the glaciated Hindu-Kush Karakoram Himalaya; the Ganges/Brahmaputra and the Indus. The aim of this analysis is firstly to understand the river flows in the ECHAM5 and HadCM3 simulations and secondly examine how useful they are for understanding the changes in water resources for South Asia. We also consider what the projected changes in river flow to the 2100s might mean for water resources across the Himalaya region.

The driving GCMs (ECHAM5 and HadCM3) have previously been shown to capture a range of temperatures and variability in precipitation similar to the AR4 ensemble for the much larger domain of Asia (*Christensen et al.*, 2007). However using just two ensemble members cannot capture the full range of these larger ensembles. In this analysis the seasonal cycle of precipitation, a key influence on river flows, is captured reasonably well for the downscaled GCMs compared to both observations and the downscaled ERAint simulation. Although observed precipitation is lower than in the model the underestimation inherrent in precipitation observations at higher elevations are likely to be an important factor for this analysis, which includes the high Himalaya.

A number of GRDC gauge stations (*GRDC*, 2014), selected to capture the range of conditions across the Himalayan arc and sample the major river basins, provide observations of river flow for comparison against the HNRCM simulations. The lack of recent river flow data limited the gauges that could be selected for analysis. In the absence of robust observations we use a downscaled ERAint simulation in addition to the available observations to provide a useful benchmark against which to compare the downscaled GCM simulations. In general there is a tendancy for overestimation of river flow rate across the selected gauges compared with GRDC observations; however,

comparison against the ERAint simulation is more mixed with some gauges showing higher and others with lower river flows than ERAInt. In general most of the simulations broadly agree with observations and ERAint to within the range of natural variability (of 1.5 SD) and agree on the periods of highest and lowest river flow. Therefore the RCM is able to capture the main features of both the climate and hydrology of this region for the present day.

The future projections indicate an increase in surface water resources, with river flow rates at some of the gauges almost doubled by the end of the century. These increases in river flow occur for the gauges in the Ganges/Brahmaputra basin, which also shows an increasing trend in both evaporation and precipitation. Therefore the changes in river flow are likely to be mainly driven by precipitation on the annual scale, which more than counters the evaporation caused by increasing temperatures in the model. This is consistent with other analyses of precipitation, which also use the A1B climate scenario (*Nepal and Shrestha*, 2015), which is a useful result. The trajectories of the annual average river flow, evaporation and precipitation for the Indus are much flatter, showing little or no trend.

The increases in the annual mean river flows are reflected in the seasonal cycles of river flow for the two future periods (2050s and 2080s), which indicate that most of the changes occur during peak flow periods. Some of the gauges toward the middle of the Himalayan arc show changes above the range of present day natural variability. This could be due to the increasing influence of the ASM and reducing influence of western disturbances from west to east having an additive effect. The gauges located furthest west and east in this analysis lie within the present day natural variability. There were also differences between the two simulations across the Himalayan arc with HadCM3 suggesting increases in river flow at the upper end of the distribution for western gauges that was not evident in ECHAM5. The analysis shown here does not suggest a systematic change in the models for the timing of the maximum and minimum river flows relative to the present day suggesting an overall increase in water resources at the top and bottom of the distribution. This has positive and negative implications with potentially more resource during usually water scarce periods. However there are also implications in terms of increased future flood risk during periods where the river flow is particularly high. Increases in maximum flows for rivers in this region could be important in terms of loss of life, livelihoods, particularly agriculture and damage to infrastructure.

While this analysis suggests increasing surface water resources due to climate change, there are a number of other factors that could affect this result, both in terms of this analysis and uncertainties surrounding the region itself. The South Asia region is changing rapidly, therefore other factors could have a large effect on water resources for this region. A rising population, expansion of industry (other than agriculture) and the continued depletion of ground water could change the demand for surface water

resource from other parts of the South Asia economy. In addition increasing variability of an already changeable climate could lead to extended periods throughout the year of rainfall below the annual average, leading to an increase in demand for irrigation resource. In terms of this analysis, this is only one RCM and another RCM could produce a different result. Also there are missing hydrological processes in the RCM and river flow model that could impact the river flows directly. The RCM and river flow model do not include abstraction and irrigation, groundwater recharge or explicitly include glacial processes and their contribution to river flow. Including glacial processes in the form of a glacier model together with river routing within the land-surface representation will be useful to establish if the contribution from glaciers changes the timing and/or magnitude of both the lowest and highest flows in these gauges. Likewise including representation of water extraction (both from rivers and groundwater) particularly for irrigation, the biggest user of water in the region, will help to provide a more complete picture of the demand for water resources for the South Asia region. Including irrigation and therefore the associated evaporation will capture part of the water cycle not possible with the current model and maintain the regional water balance. Including representation of these processes in the RCM or river flow model would improve the robustness of the future projections of water resources and further our understanding of the water balance for this region. These processes could have a large impact on the water balance in the model, potentially changing the sign of the projected changes in river flow. Understanding the interactions between availability of water resources, irrigation and food production for this region by using a more integrated approach, such as that used in *Biemans et al.* (2013) may also help with understanding how pressures on resources could change with time. In support of this work and others, there is also a need for good quality observations of both precipitation and river flow available for long enough time periods to conduct robust water resource assessments for this region.

2.6 Addendum: Comparison of precipitation against observations

Figure 2.15 shows the annual mean timeseries of precipitation for South Asia to compliment Fig. 2.3 and Fig. 2.5. The maps of the climatological average of the total monsoon precipitation for each of the driving GCMs, the APHRODITE observations and the RCM simulations (Fig. 2.3) highlight the benefits of increased horizontal resolution for representing rainfall. However, Fig. 2.3 does not show the considerable variability of precipitation for South Asia from year to year. The large interannual variability of the South Asia region is shown by the timeseries of the annual mean precipitation for the observed datasets: APHRODITE (black solid line - *Yatagai et al.*, 2012), GPCPv2.3 (black dashed line - *Adler et al.*, 2003) and TRMM_3B43_7 (purple line - *Huffman et al.*, 2007) (Fig. 2.15). The average annual precipitation for the

RCM simulations are also shown in Fig 2.15; the interannual variability in the RCMS is arguably too large compared to observations. The considerable uncertainty in the observed precipitation for the South Asia region is highlighted by the difference between the GPCP/TRMM datasets and APHRODITE in Fig. 2.15. The TRMM_3B43_7 dataset and the GPCPv2.3 observations shown are not independent of each other, which is why they are so similar

The GRDC river gauge observations are not provided with an observational uncertainty, due to the variety across its network of gauges. The quality control is the responsibility of the provider, which is largely due to the age of the gauges and the data from the IGP. *Falloon et al.* (2011) choose a threshold of 20% as a reasonable estimate for a GCM to be able to achieve consistently and a threshold of 10% as statistically indistinguishable from observations. This level is also consistant with observational errors of 5% at the 95% confidence interval quoted by *Oki et al.* (1999).

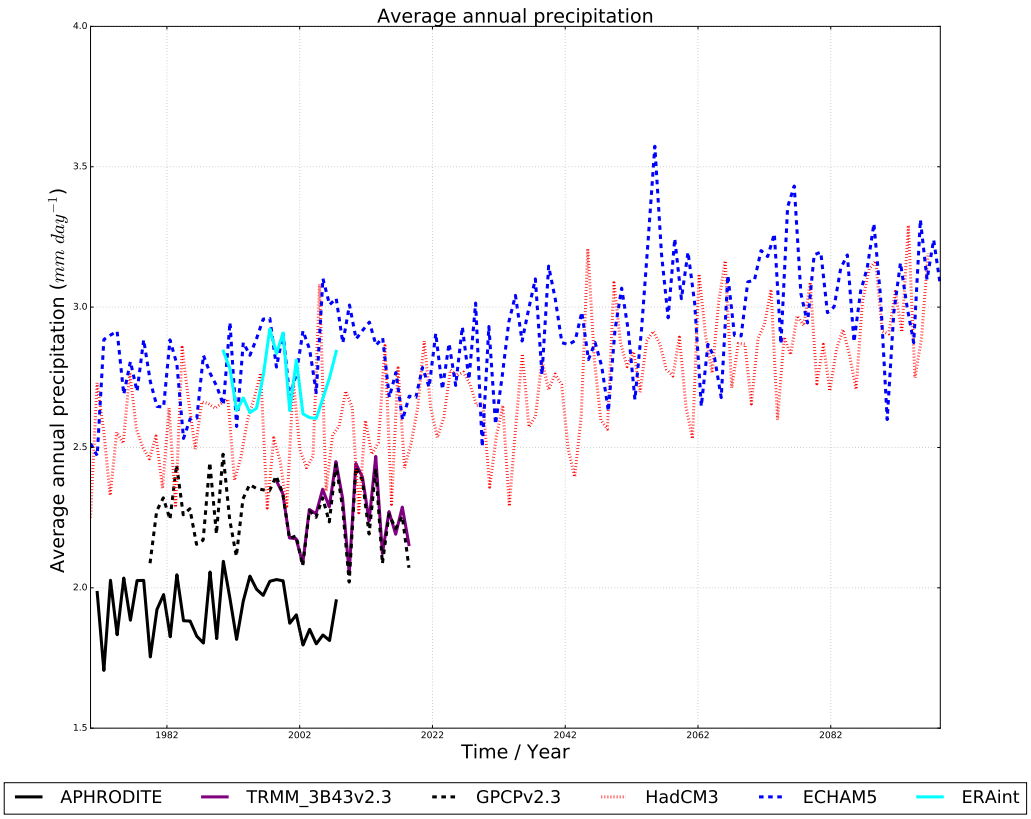

Figure 2.15: Annual mean precipitation for South Asia for each model run (HadCM3 – red, ECHAM5 – blue, ERAint – cyan lines) plotted against APHRODITE observations (solid black line), TRMM observations (purple solid line) and GPCP observations (dashed black line). GPCP observations are provided by the NOAA/OAR/ESRL PSD, Boulder, Colorado, USA, from their Web site at https://www.esrl.noaa.gov/psd/.

References

Adler, R. F., G. J. Huffman, A. Chang, R. Ferraro, P.-P. Xie, J. Janowiak, B. Rudolf, U. Schneider, S. Curtis, D. Bolvin, A. Gruber, J. Susskind, P. Arkin, and E. Nelkin (2003), The version-2 global precipitation climatology project (gpcp) monthly precipitation analysis (1979-present), *Journal of Hydrometeorology*, *4*(6), 1147–1167, doi:10.1175/1525-7541(2003)004¡1147:TVGPCP¿2.0.CO;2. 2.6

Aggarwal, P., K. Talukdar, and R. Mall (2000), Potential yields of rice-wheat system in the indo-gangetic plains of india, *Rice-wheat consortium paper series*, *10*, 16. 2.1

Aggarwal, P., K. Palanisami, M. Khanna, and K. Kakumanu (2012), Climate change and food security of India: adaptation strategies for the irrigation sector, *World Agriculture*, *3*(1), 20–26. 2.1, 2.4, 2.4

Akhtar, M., N. Ahmad, and M. Booij (2008), The impact of climate change on the water resources of hindukush-karakorum-himalaya region under different glacier coverage scenarios, *Journal of Hydrology*, *355*(1-4), 148–163, doi:10.1016/j.jhydrol.2008.03.015. 2.1, 2.2.1.1

Andermann, C., S. Bonnet, and R. Gloaguen (2011), Evaluation of precipitation data sets along the himalayan front, *Geochemistry, Geophysics, Geosystems*, *12*(7), doi:10.1029/2011GC003513. 2.2.3.1

Annamalai, H., K. Hamilton, and K. Sperber (2007), The South Asian summer monsoon and its relationship with ENSO in the IPCC AR4 simulations, *Journal of Climate*, *20*(6), 1071–1092, doi:10.1175/JCLI4035.1. 2.2.1.1

Arnold, J. G., R. Srinivasan, R. S. Muttiah, and J. R. Williams (1998), Large area hydrologic modeling and assessment part i: Model development1, *JAWRA Journal of the American Water Resources Association*, *34*(1), 73–89, doi:10.1111/j.1752-1688.1998.tb05961.x. 2.1

Arthington, A. H., S. E. Bunn, N. L. Poff, and R. J. Naiman (2006), The challenge of providing environmental flow rules to sustain river ecosystems, *Ecological Applications*, *16*, 1311–1318, doi:10.1890/1051-0761(2006)016[1311:TCOPEF]2.0.CO;2. 2.4

Bajracharya, S., and B. Shrestha (2011), The status of glaciers in the Hindu Kush-Himalayan region, *Kathmandu:ICIMOD*. 2.2.2

Barnett, T., J. Adam, and D. Lettenmaier (2005), Potential impacts of a warming climate on water availability in snow-dominated regions, *Nature*, *438*(7066), 303–309, doi:10.1038/nature04141. 2.1

Biemans, H., L. Speelman, F. Ludwig, E. Moors, A. Wiltshire, P. Kumar, D. Gerten, and P. Kabat (2013), Future water resources for food production in five South Asian river basins and potential for adaptation - a modeling study, *Science of The Total Environment*, *468-469, Supplement*(0), S117–S131, doi:10.1016/j.scitotenv.2013.05.092. 2.1, 2.2.1.2, 2.3.2, 2.4, 2.5

Bolch, T., A. Kulkarni, Kääb, C. Huggel, F. Paul, J. G. Cogley, H. Frey, J. S. Kargel, K. Fujita, M. Scheel, S. Bajracharya, and M. Stoffel (2012), The state and fate of himalayan glaciers, *Science*, *336*(6079), 310–314, doi:10.1126/science.1215828. 2.1, 2.3.2

Christensen, J., B. Hewitson, A. Busuioc, A. Chen, X. Gao, I. Held, R. Jones, R. Kolli, W.-T. Kwon, R. Laprise, V. M. na Rueda, L. Mearns, C. Menendez, J. Räisänen, A. Rinke, A. Sarr, and P. Whetton (2007), Regional climate projections. in: Climate change 2007: The physical science basis. contribution of working group i, *Fourth Assessment Report of the Intergovernmental Panel on Climate Change*. 2.1, 2.2.1.1, 2.2.1.3, 2.3.1, 2.5

Clark, D. B., and N. Gedney (2008), Representing the effects of subgrid variability of soil moisture on runoff generation in a land surface model, *Journal of Geophysical Research*, *113*, doi:10.1029/2007JD008940. 2.2.1.1

Collins, D. N., J. L. Davenport, and M. Stoffel (2013), Climatic variation and runoff from partially-glacierised himalayan tributary basins of the ganges, *Science of The Total Environment*, *468-469, Supplement*, S48–S59, doi:10.1016/j.scitotenv.2013.10.126, changing water resources availability in Northern India with respect to Himalayan glacier retreat and changing monsoon patterns: consequences and adaptation. 2.2.2

Cruz, R., H. Harasawa, M. Lal, S. Wu, Y. Anokhin, B. Punsalmaa, Y. Honda, M. Jafari, C. Li, and N. Huu Ninh (2007), Asia. climate change 2007: Impacts, adaptation and vulnerability. contribution of working group ii, *Fourth Assessment Report of the Intergovernmental Panel on Climate Change*, pp. 469–506. 2.4

Dankers, R., O. B. Christensen, L. Feyen, M. Kalas, and A. de Roo (2007), Evaluation of very high-resolution climate model data for simulating flood hazards in the upper danube basin, *Journal of Hydrology*, *347*(3-4), 319–331, doi:10.1016/j.jhydrol.2007.09.055. 2.1

Dee, D. P., S. M. Uppala, A. J. Simmons, P. Berrisford, P. Poli, S. Kobayashi, U. Andrae, M. A. Balmaseda, G. B. P., Bauer, P. Bechtold, A. C. M. Beljaars, L. van de Berg, J. Bidlot, N. Bormann, C. Delsol, R. Dragani, M. Fuentes, A. J. Geer, L. Haimberger, S. B. Healy, H. Hersbach, E. V. Hólm, L. Isaksen, P. Kållberg, M. Köhler, M. Matricardi, A. P. McNally, B. M. Monge-Sanz, J.-J. Morcrette, B.-K. Park, C. Peubey, P. de Rosnay, C. Tavolato, J.-N. Thépaut, and F. Vitart (2011), The era-interim reanalysis: configuration and performance of the data assimilation system, *Quarterly Journal of the Royal Meteorological Society*, *137*(656), 553–597, doi:10.1002/qj.828. 2.2.1.1

Dhar, O., and S. Nandargi (2000), A study of floods in the brahmaputra basin in india, *International Journal of Climatology*, *20*(7), 771–781, doi:10.1002/1097-0088(20000615)20:7¡771::AID-JOC518¿3.0.CO;2-Z. 2.2.2

Dimri, A., T. Yasunari, A. Wiltshire, P. Kumar, C. Mathison, J. Ridley, and D. Jacob (2013), Application of regional climate models to the Indian winter monsoon over the western Himalayas, *Science of The Total Environment*, *468*, S36–S47. 2.2.1.1, 2.2.2

Dolman, A. J., and D. Gregory (1992), The parametrization of rainfall interception in gcms, *Quarterly Journal of the Royal Meteorological Society*, *118*(505), 455–467, doi:10.1002/qj.49711850504. 2.2.1.1

Essery, R. L. H., M. J. Best, and P. M. Cox (2001), Moses 2.2 technical documentation, *Hadley Centre Technical Note*, *30*. 2.2.1.1

Essery, R. L. H., M. J. Best, R. A. Betts, P. M. Cox, and C. Taylor (2003), Explicit representation of subgrid heterogeneity in a GCM land surface scheme, *Journal of Hydrometeorology*, *4*, 530–543. 2.2.1.1

Falloon, P., R. Betts, and C. Bunton (2007), New global river routing scheme in the unified model, *Hadley Centre Technical Note*, *72*. 2.2.1.2

Falloon, P., R. A. Betts, A. Wiltshire, R. Dankers, C. Mathison, D. McNeall, P. Bates, and M. Trigg (2011), Validation of river flows in hadgem1 and hadcm3 with the trip river flow model, *Journal of Hydrometeorology*, *12*, 1157–1180, doi:10.1175/2011JHM1388.1. 2.1, 2.2.1.2, 2.2.2, 2.6

Fekete, B. M., C. J. Vörösmarty, and R. B. Lammers (2001), Scaling gridded river networks for macroscale hydrology: Development, analysis, and control of error, *Water Resources Research*, *37*, 1955–1967, doi:10.1029/2001WR900024. 2.2.1.2

Fujita, K., and T. Nuimura (2011), Spatially heterogeneous wastage of Himalayan glaciers, *Proceedings of the National Academy of Sciences*, *108*(34), 14,011–14,014. 2.1

Gain, A. K., H. Apel, F. G. Renaud, and C. Giupponi (2013), Thresholds of hydrologic flow regime of a river and investigation of climate change impact the case of the lower brahmaputra river basin, *Climatic Change*, *120*(1-2), 463–475, doi:10.1007/s10584-013-0800-x. 2.4

Gardelle, J., E. Berthier, Y. Arnaud, and A. Kääb (2013), Region-wide glacier mass balances over the Pamir-Karakoram-Himalaya during 1999-2011, *The Cryosphere*, *7*(4), 1263–1286, doi:10.5194/tc-7-1263-2013. 2.1

Gedney, N., and P. Cox (2003), The sensitivity of global climate model simulations to the representation of soil moisture heterogeneity, *Journal of Hydrometeorology*, *4*, 1265–1275, doi:10.1175/1525-7541(2003)004¡1265:TSOGCM¿2.0.CO;2. 2.2.1.1

Gordon, C., C. Cooper, C. A. Senior, H. Banks, J. M. Gregory, T. C. Johns, J. F. B. Mitchell, and R. A. Wood (2000), The simulation of sst, sea ice extents and ocean heat transports in a version of the hadley centre coupled model without flux adjustments, *Climate Dynamics*, *16*(2-3), 147–168, doi:10.1007/s003820050010. 2.2.1.1

Gornall, J., R. Betts, E. Burke, R. Clark, J. Camp, K. Willett, and A. Wiltshire (2010), Implications of climate change for agricultural productivity in the early twenty-first century, *Philosphical Transactions of the Royal Society B: Biological Sciences*, *365*, 2973–2989, doi:10.1098/rstb.2010.0158. 2.4

Gosain, A. K., S. Rao, and D. Basuray (2006), Climate change impact assessment on hydrology of Indian river basins, *Current Science*, *90*, 346–353. 2.1

Goswami, B., and P. K. Xavier (2005), Dynamics of "internal" interannual variability of the Indian summer monsoon in a GCM, *Journal of Geophysical Research: Atmospheres*, *110*(D24), doi:10.1029/2005JD006042. 2.1, 2.3.1

Goswami, B. N., V. Venugopal, D. Sengupta, M. S. Madhusoodanan, and P. K. Xavier (2006), Increasing trend of extreme rain events over india in a warming environment, *Science*, *314*(5804), 1442–1445, doi:10.1126/science.1132027. 2.4

GRDC (2014), The global runoff data centre, *D-56002 Koblenz, Germany, edited*. 2.2.2, 2.5

Gregory, P., J. Ingram, and M. Brklacich (2005), Climate change and food security, *Philosophical Transactions of the Royal Society B: Biological Sciences*, *360*(1463), 2139–2148, doi:10.1098/rstb.2005.1745. 2.1, 2.4

Gupta, A. D., M. S. Babel, X. Albert, and O. Mark (2005), Water sector of bangladesh in the context of integrated water resources management: A review, *International Journal of Water Resources Development*, *21*(2), 385–398, doi:10.1080/07900620500037818. 2.4

Gupta, S., and D. Deshpande (2004), Water for India in 2050: first order assessment of available options, *Current Science*, *86*(9), 1216–1224. 2.1

Gupta, S., A. Javed, and D. Datt (2003), Economics of flood protection in india, *Natural Hazards*, *28*(1), 199–210. **??**, 2.4

Harding, R., E. Blyth, O. Tuinenburg, and A. Wiltshire (2013), Land atmosphere feedbacks and their role in the water resources of the ganges basin, *Science of The Total Environment*, *468-469, Supplement*(0), S85–S92, doi:10.1016/j.scitotenv.2013.03.016, changing water resources availability in Northern India with respect to Himalayan glacier retreat and changing monsoon patterns: consequences and adaptation. 2.2.1.2, 2.2.2, 2.4

Hijioka, Y., E. Lin, J. Pereira, R. Corlett, X. Cui, G. Insarov, R. Lasco, E. Lindgren, and A. Surjan (2014), Asia. in: Climate change 2014: Impacts, adaptation, and vulnerability. part b: Regional aspects. contribution of working group ii, *Fifth Assessment Report of the Intergovernmental Panel on Climate Change*, pp. 1327–1370. 2.1, 2.4

Hirabayashi, Y., S. Kanae, S. Emori, T. Oki, and M. Kimoto (2008), Global projections of changing risks of floods and droughts in a changing climate, *Hydrological Sciences Journal*, *53*(4), 754–772. 2.1

Huffman, G. J., D. T. Bolvin, E. J. Nelkin, D. B. Wolff, R. F. Adler, G. Gu, Y. Hong, K. P. Bowman, and E. F. Stocker (2007), The trmm multisatellite precipitation analysis (tmpa): Quasi-global, multiyear, combined-sensor precipitation estimates at fine scales, *Journal of Hydrometeorology*, *8*(1), 38–55, doi:10.1175/JHM560.1. 2.6

Immerzeel, W. W., L. van Beek, and M. Bierkens (2010), Climate change will affect the Asian water towers, *Science*, *328*(5984), 1382–1385, doi:10.1126/science.1183188. 2.1, 2.4

Immerzeel, W. W., N. Wanders, A. F. Lutz, J. M. Shea, and M. F. P. Bierkens (2015), Reconciling high altitude precipitation in the upper indus basin with glacier mass balances and runoff, *Hydrology and Earth System Sciences Discussions*, *12*(5), 4755–4784, doi:10.5194/hessd-12-4755-2015. 2.2.3.1, 2.3.2

Jacob, D., L. Bärring, O. B. Christensen, J. H. Christensen, M. de Castro, M. Déqué, F. Giorgi, S. Hagemann, M. Hirschi, R. Jones, E. Kjellström, G. Lenderink, B. Rockel, E. Sánchez, C. Schär, S. I. Seneviratne, S. Somot, A. van Ulden, and B. van den Hurk (2007), An inter-comparison of regional climate models for europe: model performance in present-day climate, *Climatic Change*, *81*(1), 31–52, doi:10.1007/s10584-006-9213-4. 2.1, 2.2.1.1

Jhajharia, D., Y. Dinpashoh, E. Kahya, V. P. Singh, and A. Fakheri-Fard (2012), Trends in reference evapotranspiration in the humid region of northeast india, *Hydrological Processes*, *26*(3), 421–435, doi:10.1002/hyp.8140. 2.3.3

Johnston, R., and V. Smakhtin (2014), Hydrological modeling of large river basins: How much is enough?, *Water Resources Management*, *28*(10), 2695–2730, doi:10.1007/s11269-014-0637-8. 2.2.2

Jones, R. G., M. Noguer, D. C. Hassell, D. Hudson, S. S. Wilson, G. J. Jenkins, and J. F. Mitchell (2004), Generating high resolution climate change scenarios using PRECIS, *Met Office Hadley Centre, Exeter, UK*, pp. 0–40. 2.2.1.1

Joshi, U., and M. Rajeevan (2006), Trends in precipitation extremes over India, *National Climate Centre Research report*, *3*. 2.4

Kääb, A., E. Berthier, C. Nuth, J. Gardelle, and Y. Arnaud (2012), Contrasting patterns of early twenty-first-century glacier mass change in the Himalayas, *Nature*, *488*, 495–498, doi:10.1038/nature11324. 2.1

Kapnick, S. B., T. L. Delworth, M. Ashfaq, S. Malyshev, and P. C. D. Milly (2014), Snowfall less sensitive to warming in karakoram than in himalayas due to a unique seasonal cycle, *Nature Geoscience*, *7*(11), 834–840, doi:10.1038/ngeo2269. 2.2.2

Kaser, G., M. Großhauser, and B. Marzeion (2010), Contribution potential of glaciers to water availability in different climate regimes, *Proceedings of the National Academy of Sciences*, *107*(47), 20,223–20,227, doi:10.1073/pnas.1008162107. 2.1

Kay, A. L., N. S. Reynard, and R. G. Jones (2006), RCM rainfall for UK flood frequency estimation. i. method and validation, *Journal of Hydrology*, *318*(1-4), 151–162, doi:10.1016/j.jhydrol.2005.06.012. 2.1

Kumar, P., A. Wiltshire, C. Mathison, S. Asharaf, B. Ahrens, P. Lucas-Picher, J. H. Christensen, A. Gobiet, F. Saeed, S. Hagemann, and D. Jacob (2013), Downscaled climate change projections with uncertainty assessment over India using a high resolution multi-model approach, *Science of The Total Environment*, *468-469, Supplement*(0), S18–S30, doi:10.1016/j.scitotenv.2013.01.051, changing water resources availability in Northern India with respect to Himalayan glacier retreat and changing monsoon patterns: consequences and adaptation. 2.2.1.1, 2.3.1

Kumar, R., R. Singh, and K. Sharma (2005), Water resources of India, *Current Science*, *89*(5), 794–811. 2.1, 2.4, 2.4

Linsley, R., M. Kohler, and J. Paulhus (1982), *Hydrology for Engineers*, McGraw-Hill series in water resources and environmental engineering, McGraw-Hill. 2.2.1.1

Lucas-Picher, P., J. H. Christensen, F. Saeed, P. Kumar, S. Asharaf, B. Ahrens, A. J. Wiltshire, D. Jacob, and S. Hagemann (2011), Can regional climate models represent the Indian monsoon?, *Journal of Hydrometeorology*, *12*, 849–868, doi:10.1175/2011JHM1327.1. 2.1, 2.2.1.1, 2.3.1

Mathison, C., A. Wiltshire, A. Dimri, P. Falloon, D. Jacob, P. Kumar, E. Moors, J. Ridley, C. Siderius, M. Stoffel, and T. Yasunari (2013), Regional projections of North Indian climate for adaptation studies, *Science of The Total Environment*, *468-469, Supplement*(0), S4–S17, doi:10.1016/j.scitotenv.2012.04.066. 2.1, 2.2.1.1, 2.2.3.2, 2.3.1, 2.3.1

McMillan, H., J. Freer, F. Pappenberger, T. Krueger, and M. Clark (2010), Impacts of uncertain river flow data on rainfall-runoff model calibration and discharge predictions, *Hydrological Processes*, *24*(10), 1270–1284. 2.2.2

McVicar, T. R., M. L. Roderick, R. J. Donohue, L. T. Li, T. G. V. Niel, A. Thomas, J. Grieser, D. Jhajharia, Y. Himri, N. M. Mahowald, A. V. Mescherskaya, A. C. Kruger, S. Rehman, and Y. Dinpashoh (2012), Global review and synthesis of trends in observed terrestrial near-surface wind speeds: Implications for evaporation, *Journal of Hydrology*, *416-417*, 182–205, doi:10.1016/j.jhydrol.2011.10.024. 2.3.3

Milly, P. C. D., K. A. Dunne, and A. Vechhia (2005), Global pattern of trends in streamflow and water availability in a changing climate, *Nature*, *438*, 347–350. 2.1

Mirza, M. M. Q. (2002), Global warming and changes in the probability of occurrence of floods in bangladesh and implications, *Global Environmental Change*, *12*(2), 127–138, doi:10.1016/S0959-3780(02)00002-X. 2.4

Mirza, M. M. Q., R. Warrick, N. Ericksen, and G. Kenny (1998), Trends and persistence in precipitation in the ganges, brahmaputra and meghna river basins, *Hydrological Sciences Journal*, *43*(6), 845–858, doi:10.1080/02626669809492182. 2.2.2

Mirza, M. M. Q., R. A. Warrick, and N. J. Ericksen (2003), The implications of climate change on floods of the ganges, brahmaputra and meghna rivers in bangladesh, *Climatic Change*, *57*(3), 287–318, doi:10.1023/A:1022825915791. 2.4

Moors, E. J., A. Groot, H. Biemans, C. T. van Scheltinga, C. Siderius, M. Stoffel, C. Huggel, A. Wiltshire, C. Mathison, J. Ridley, D. Jacob, P. Kumar, S. Bhadwal, A. Gosain, and D. N. Collins (2011), Adaptation to changing water resources in the Ganges basin, northern India, *Environmental Science & Policy*, *14*(7), 758–769, doi:10.1016/j.envsci.2011.03.005, adapting to Climate Change: Reducing Water-related Risks in Europe. 2.2.1.1

Morse, A., C. Prentice, and T. Carter (2009), Assessments of climate change impacts, *Ensembles: Climate change and its impacts: Summary of research and results from the ENSEMBLES project*, pp. 107–129. 2.2.1.2

Murphy, J. M., D. M. H. Sexton, D. N. Barnett, G. S. Jones, M. J. Webb, M. Collins, and D. A. Stainforth (2004), Quantification of modelling uncertainties in a large ensemble of climate change simulations, *Nature*, *430*, 768–772, doi:10.1038/nature02771. 2.4

Murphy, J. M., D. M. H. Sexton, G. J. Jenkins, P. M. Boorman, B. B. B. Booth, C. C. Brown, R. T. Clark, M. Collins, G. R. Harris, E. J. Kendon, R. A. Betts, S. J. Brown, T. P. Howard, K. A. Humphrey, M. P. McCarthy, R. E. McDonald, A. Stephens, C. Wallace, R. Warren, R. Wilby, and R. A. Wood (2009), Uk climate projections science report: Climate change projections., *Met Office Hadley Centre*, pp. 124–131. 2.1

Nakicenovic, N., J. Alcamo, A. Grubler, K. Riahi, R. Roehrl, H.-H. Rogner, and N. Victor (2000), Special report on emissions scenarios (SRES), *A Special Report of Working Group III of the Intergovernmental Panel on Climate Change*, Last access April 2017editor:Nebojsa Nakicenovic and Rob Swart. 2.2.1.3

Nepal, S., and A. B. Shrestha (2015), Impact of climate change on the hydrological regime of the indus, ganges and brahmaputra river basins: a review of the literature, *International Journal of Water Resources Development*, *31*(2), 201–218, doi:10.1080/07900627.2015.1030494. 2.5

Nohara, D., A. Kitoh, M. Hosaka, and T. Oki (2006), Impact of climate change on river discharge projected by multimodel ensemble, *Journal of Hydrometeorology*, *7*, 1076–1089, doi:10.1175/JHM531.1. 2.3.1

Nyeko, M. (2015), Hydrologic modelling of data scarce basin with swat model: Capabilities and limitations, *Water Resources Management*, *29*(1), 81–94, doi:10.1007/s11269-014-0828-3. 2.1

Oki, T., and Y. C. Sud (1998), Design of total runoff integrating pathways (TRIP). a global river channel network, *Earth Interactions*, *2*, 1–37, doi:10.1175/1087-3562(1998)002¡0001:DOTRIP¿2.3.CO;2. 2.2.1.2

Oki, T., T. Nishimura, and P. Dirmeyer (1999), Assessment of annual runoff from land surface models using Total Runoff Integrating Pathways (TRIP), *Journal of the Meteorological Society of Japan. Ser. II*, *77*(1B), 235–255, doi:10.1080/02626668509490989. 2.2.1.2, 2.2.2, 2.6

Pope, V., M. L. Gallani, P. R. Rowntree, and R. A. Stratton (2000), The impact of new physical parametrizations in the hadley centre climate model: Hadam3, *Climate Dynamics*, *16*(2-3), 123–146, doi:10.1007/s003820050009. 2.2.1.1

Rajeevan, M., J. Bhate, and A. K.Jaswal (2008), Analysis of variability and trends of extreme rainfall events over india using 104 years of gridded daily rainfall data, *Geophysical Research Letters*, *35*(18), doi:10.1029/2008GL035143. 2.4

Ridley, J., A. Wiltshire, and C. Mathison (2013), More frequent occurrence of westerly disturbances in Karakoram up to 2100, *Science of The Total Environment*, *468-469, Supplement*(0), S31–S35, doi:10.1016/j.scitotenv.2013.03.074, changing water resources availability in Northern India with respect to Himalayan glacier retreat and changing monsoon patterns: consequences and adaptation. 2.2.2, 2.3.3.4

Rodell, M., I. Velicogna, and J. Famiglietti (2009), Satellite-based estimates of groundwater depletion in India, *Nature*, *460*(7258), 999 – 1002, doi:10.1038/nature08238. 2.1, 2.4

Roeckner, E., G. Bäuml, L. Bonaventura, R. Brokopf, M. Esch, M. Giorgetta, S. Hagemann, I. Kirchner, L. Kornblueh, E. Manzini, A. Rhodin, U. Schlese, U. Schulzweida, and A. Tompkins (2003), The atmospheric general circulation model ECHAM 5. PART I: Model description, *Max Planck Institute for Meteorology Rep. 349*. 2.2.1.1

Sampson, C. C., T. Fewtrell, F. O'Loughlin, F. Pappenberger, P. B. Bates, J. E. Freer, and H. L. Cloke (2014), The impact of uncertain precipitation data on insurance loss estimates using a flood catastrophe model, *Hydrology and Earth System Sciences*, *18*(6), 2305–2324, doi:10.5194/hess-18-2305-2014. 2.1

Sarkar, U. K., A. K.Pathak, R. K. Sinha, K. Sivakumar, A. K. Pandian, A. Pandey, V. K. Dubey, and W. S. Lakra (2012), Freshwater fish biodiversity in the river ganga (india): changing pattern, threats and conservation perspectives, *Reviews in Fish Biology and Fisheries*, *22*(1), 251–272, doi:10.1007/s11160-011-9218-6. 2.4

Scherler, D., B. Bookhagen, and M. Strecker (2011), Spatially variable response of Himalayan glaciers to climate change affected by debris cover, *Nature Geoscience*, *4*(0), 156–159, doi:10.1038/ngeo1068. 2.1

Scott, D. W. (2009), *Multivariate density estimation: theory, practice, and visualization*, vol. 383, John Wiley & Sons, New Jersey. 2.2.3.2

Seidel, K., J. Martinec, and M. F. Baumgartner (2000), Modelling runoff and impact of climate change in large himalayan basins, in *International Conference on Integrated Water Resources Management (ICIWRM)*, pp. 19–21, Citeseer. 2.1

Sharma, D. (2012), Situation analysis of flood disaster in south and southeast Asia - a need of integrated approach, *International Journal of Science, Environment and Technology*, *1*(3), 167–173. 2.4

Shrestha, A. B., and R. Aryal (2011), Climate change in nepal and its impact on himalayan glaciers, *Regional Environmental Change*, *11*(1), 65–77, doi:10.1007/s10113-010-0174-9. 2.1, 2.3.3

Silverman, B. (1986), Density estimation for statistics and data analysis, *Monographs on Statistics and Applied Probability*, *26*. 2.2.3.2

Simmons, A., S. Uppala, D. Dee, and S. Kobayashi (2007), Era-interim: New ecmwf reanalysis products from 1989 onwards., *ECMWF Newsletter - Winter 2006/07*, *110*, 25–35. 2.2.1.1

Singh, O., and M. Kumar (2013), Flood events, fatalities and damages in india from 1978 to 2006, *Natural Hazards*, *69*(3), 1815–1834. 2.4

Singh, P., and L. Bengtsson (2005), Impact of warmer climate on melt and evaporation for the rainfed, snowfed and glacierfed basins in the Himalayan region, *Journal of Hydrology*, *300*(1-4), 140–154, doi:10.1016/j.jhydrol.2004.06.005. 2.1, 2.3.3

Singh, P., and N. Kumar (1997), Impact assessment of climate change on the hydrological response of a snow and glacier melt runoff dominated himalayan river, *Journal of Hydrology*, *193*(1-4), 316–350, doi:10.1016/S0022-1694(96)03142-3. 2.1

Singh, P., U. K. Haritashya, and N. Kumar (2008), Modelling and estimation of different components of streamflow for gangotri glacier basin, himalayas, *Hydrological Sciences Journal*, *53*(2), 309–322, doi:10.1623/hysj.53.2.309. 2.1

Smakhtin, V., and M. Anputhas (2006), An assessment of environmental flow requirements of Indian river basins, *IWMI Research Report 107*. 2.4

Smakhtin, V. U., R. L. Shilpakar, and D. A. Hughes (2006), Hydrology-based assessment of environmental flows: an example from Nepal, *Hydrological Sciences Journal*, *51*(2), 207–222, doi:10.1623/hysj.51.2.207. 2.4

Thenkabail, P. S., M. Schull, and H. Turral (2005), Ganges and indus river basin land use/land cover LULC) and irrigated area mapping using continuous streams of MODIS data, *Remote Sensing of Environment*, *95*(3), 317–341, doi:10.1016/j.rse.2004.12.018. 2.2.2

Tuinenburg, O. A., R. W. A. Hutjes, T. Stacke, A. Wiltshire, and P. Lucas-Picher (2014), Effects of irrigation in india on the atmospheric water budget., *Journal of Hydrometeorology*, *15*, 1028–1050, doi:10.1175/JHM-D-13-078.1. 2.2.1.2, 2.4

United Nations (2013), Fertility levels and trends as assessed in the 2012 revision of world population prospects, *Department of Economic and Social Affairs, Population Division*. 2.1, 2.4

Vörösmarty, C., B. Fekete, M. Meybeck, and R. Lammers (2000a), Geomorphometric attributes of the global system of rivers at 30-minute spatial resolution, *Journal of Hydrology*, *237*(1-2), 17–39, doi:10.1016/S0022-1694(00)00282-1. 2.2.1.2

Vörösmarty, C., B. Fekete, M. Meybeck, and R. Lammers (2000b), Global system of rivers: Its role in organizing continental land mass and defining land-to-ocean linkages, *Global Biogeochemical Cycles*, *14*(2), 599–621, doi:10.1029/1999GB900092. 2.2.1.2

Vörösmarty, C. J., P. B. McIntyre, M. O. Gessner, D. Dudgeon, A. Prusevich, P. Green, S. Glidden, S. E. Bunn, C. A. Sullivan, C. R. Liermann, and P. M. Davies (2010), Global threats to human water security and river biodiversity, *Nature*, *467*, 555–561, doi:10.1038/nature09440. 2.4

Wescoat Jr, J. (1991), Managing the indus river basin in light of climate change: Four conceptual approaches, *Global Environmental Change*, *1*(5), 381 – 395, doi:10.1016/0959-3780(91)90004-D. 2.2.2

Wiltshire, A. (2014), Climate change implications for the glaciers of the Hindu-Kush, Karakoram and Himalayan region, *The Cryosphere*, *8*(3), 941–958, doi:10.5194/tc-8-941-2014. 2.1, 2.2.1.1, 2.2.2

Wiltshire, A., J. Gornall, B. Booth, E. Dennis, P. Falloon, G. Kay, D. McNeall, C. McSweeney, and R. Betts (2013a), The importance of population, climate change and co_2 plant physiological forcing in determining future global water stress, *Global Environmental Change*, *23*(5), 1083–1097, doi:10.1016/j.gloenvcha.2013.06.005. 2.1, 2.4

Wiltshire, A. J., G. Kay, J. L. Gornall, and R. A. Betts (2013b), The impact of climate, co_2 and population on regional food and water resources in the 2050s, *Sustainability*, *5*, 2129–2151, doi:10.3390/su5052129. 2.1

Yatagai, A., K. Kamiguchi, O. Arakawa, A. Hamada, N. Yasutomi, and A. Kitoh (2012), Aphrodite: constructing a long-term daily gridded precipitation dataset for asia based on a dense network of rain gauges., *Bulletin of the American Meteorological Society*, *93*, 1401–1415, doi:10.1175/BAMS-D-11-00122.1. 2.2.2, 2.2.3.1, 2.6

Yoshida, S. (1981), *Fundamentals of rice crop science*, 1-269 pp., Manila, Philipines. 2.4

Chapter 3

Estimating sowing and harvest dates based on the Asian Summer Monsoon

Camilla T. Mathison[1,2], Chetan Deva[1,2], Pete Falloon[1] and Andrew J. Challinor

[1] *Met Office, FitzRoy Road, Exeter, EX1 3PB, UK*
[2] *School of Earth and Environment, Institute for Climate and Atmospheric Science, University of Leeds, Leeds, LS2 9AT, UK*

Sowing and harvest dates are a significant source of uncertainty within crop models especially for regions where high-resolution data are unavailable or, as is the case in future climate runs, where no data are available at all. Global datasets are not always able to distinguish when wheat is grown in tropical and sub-tropical regions, they are also often coarse in resolution. South Asia is one such region where large spatial variation means higher resolution datasets are needed, together with greater clarity for the timing of the main wheat growing season. Agriculture in South Asia is closely associated with the dominating climatological phenomenon, the Asian Summer Monsoon (ASM). Rice and wheat are two highly important crops for the region, rice being mainly cultivated in the wet season during the summer monsoon months and wheat during the dry winter. We present a method for estimating the crop sowing and harvest dates, for rice and wheat, using the ASM onset and retreat. The aim of this method is to provide a more accurate alternative to the global datasets of cropping calendars than is currently available and generate more representative inputs for climate impact assessments.

We first demonstrate that there is skill in the model prediction of monsoon onset and retreat for two downscaled General Circulation Models (GCMs) by comparing modelled precipitation with observations. We then calculate and apply sowing and harvest rules

for rice and wheat for each simulation to climatological estimates of the monsoon onset and retreat for a present day period. We show that this method reproduces the present day sowing and harvest dates for most parts of India. Application of the method to two future simulations demonstrates that the estimated sowing and harvest dates are successfully modified to ensure that the growing season remains consistent with the internal model climate. The study therefore provides a useful way of modelling potential growing season adaptations to changes in future climate.

3.1 Introduction

Field studies dominate the modelling literature on crops and agriculture. Many crop models are developed and applied at the field scale using site specific observations to drive models and optimize outputs. The growing awareness of climate change and the likely impact this will have on food production has generated a demand for regional and global assessments of climate impacts on food security through for example, projects such as Agricultural Model Intercomparison and Improvement Project (AgMIP– *Rivington and Koo*, 2010, *Rosenzweig et al.*, 2013, 2014), the Inter-Sectoral Impact Model Intercomparison Project (ISIMIP– *Warszawski et al.*, 2013, 2014) and Global Gridded Crop Model Inter-comparison (GGCMI– *Elliott et al.*, 2015). Recent work in such climate–crop impact studies has sought to quantify uncertainty from the quality and scale of input data. A result from this work is that, for global scale simulations, planting dates are a significant source of uncertainty (*Frieler et al.*, 2017, *Elliott et al.*, 2015).

Aside from their use in modelling studies, deciding when to plant crops is a significant challenge, particularly in water scarce regions such as parts of Sub-Saharan Africa (SSA- *Waongo et al.*, 2014), South and South East Asia (*Kotera et al.*, 2014). These regions have crop sowing dates that are closely associated with the onset of the rainy season. Any prolonged dry spells of more than two weeks after sowing could have serious consequences, leading to crop failure or significant yield reduction, because top soil layers dry out preventing germination (*Laux et al.*, 2008). For large parts of SSA deciding when to sow determines the length of the crop duration for the agricultural season and is therefore an important tactical decision (*Waongo et al.*, 2014).

Planting dates can be determined using a number of different methods; for example, *Kotera et al.* (2014) propose a cropping calendar model for rice cultivation in the Vietnam Mekong Delta (VMD). The *Kotera et al.* (2014) model estimates the sowing date based on the the suitability of the land for crops given any flooding, salt water intrusion or erratic monsoon rains; these are important factors for the water resources of the VMD region. Alternatively *Laux et al.* (2008, 2010) use a fuzzy logic-based algorithm developed to estimate the onset of the rainy season in order to examine the impact of the planting date for the SSA. In the General Large Area Model (GLAM– *Challinor et al.*, 2004), the sowing date can be estimated by the model based on the soil

moisture conditions, with the crop sown when surface soil moisture exceeds a specified threshold during a given time window and crop emergence occurring a specified time after sowing. *Waha et al.* (2012) base their estimates of sowing dates at the global scale on climatic conditions and crop specific temperature thresholds, therefore providing a suitable method for taking climate change into account. However the *Waha et al.* (2012) method is not really intended for use in irrigated multiple cropping regions. *Elliott et al.* (2015) describe how sowing dates are defined in the GGCMI project. The GGCMI protocols use a combination of *Sacks et al.* (2010), *Portmann et al.* (2010) and model data to define sowing dates, thus highlighting the challenges in defining a complete, accurate dataset of sowing and harvest dates. This has influenced and driven the development and application of crop models on broader scales. In this study we are considering the whole South Asia region; this is a large scale problem with complicated cropping patterns, which means that assumptions and generalizations need to be made across a region with a wide variety of climatic conditions and cropping environments (soils etc). *Waha et al.* (2013) highlight that global crop calendars such as those used in the GGCMI often only report individual crops, therefore limiting their usefulness for regions with multiple cropping systems.

The growing interest in climate change and food security has influenced the development of crop models for use in future climate impact assessments (*Frieler et al.*, 2017); this represents a different challenge for crop models in terms of the input data used. ISIMIP simulations use time varying crop management data until 2005 after which the data are held fixed at 2005 levels for the remainder of the simulations (*Frieler et al.*, 2017). Fixing crop management to present day practices is not really suitable for adaptation studies (*van Bussel et al.*, 2015). The assumption that there will be no large shifts in climate, causing sowing and harvest dates to change significantly from the present day, could lead to the sowing and harvesting of crops in the model in the future at unrealistic times of the year. Thus the appropriate sowing and harvest dates used in future simulations depends on the intended application for the simulations. In many adaptation studies, impacts without adaptation are assessed using present day estimates of sowing dates, then the sowing dates are adjusted in response to climate change to assess the benefits of adaptation (*Lobell*, 2014). *Challinor et al.* (2018) suggest using autonomous adaptation in simulations in order to avoid overestimating the effects of adaptation. On this basis there is a requirement for estimates of sowing and harvest dates for climate simulations that remain consistent with the future model climate. Thus, making estimates of sowing and harvest dates important not only for understanding the present day, but also for use in future simulations especially when considering potential adaptation to climate change.

Agriculture in South Asia is dominated by the Asian Summer Monsoon (ASM). Kharif and Rabi are the two main seasons in South Asian agriculture and these correspond to summer and winter/spring growing seasons respectively. Rice-wheat systems

are a major crop rotation across South Asia. Kharif crops include rice, which is usually sown during the monsoon, and harvested in the autumn. Sowing and harvest dates for rice cultivated during the Kharif season vary between states, with rice traditionally sown in some locations with the first rains of the monsoon, while other regions such as eastern parts of the Indo Gangetic Plain (IGP) tend to plant rice late into June when the monsoon is fully established (*Erenstein and Laxmi*, 2008). Rabi crops include wheat, which is mainly cultivated during the dry season (*Erenstein and Laxmi*, 2008, *Singh et al.*, 2014). The close association of the sowing dates of these crops and the ASM offer the potential for a new method of defining the cropping calendar for this important rotation.

Rice-wheat systems, particularly those in Pakistan (*Erenstein et al.*, 2008) and the Indo Gangetic Plain (IGP), tend to plant varieties like Basmati that take a long time to mature (*Erenstein and Laxmi*, 2008). Since this delays wheat planting, this has a direct impact on wheat yield. In the Eastern IGP this is a particular problem as the season for which wheat is viable is relatively short (*Erenstein and Laxmi*, 2008, *Laik et al.*, 2014, *Jat et al.*, 2014). Any delay between the rice harvest and wheat planting can have a large impact on the success of the wheat crop, as this will reduce the time available before the temperatures get too high for the successful cultivation of wheat (*Joshi et al.*, 2007). The time between the rice harvest and wheat sowing also depends on the time it takes to ensure the soil is in a suitable condition for wheat sowing after the rice harvest. *Erenstein and Laxmi* (2008) describe the zero-tillage approach which allows for a reduced turn-around time between the harvest of rice and sowing of wheat. Potential avenues by which the uncertainty from sowing and harvest dates can be reduced in inputs to crop simulations include:

- The use of higher resolution regional data sets of recorded sowing and harvest dates for crop calendars rather than existing global data sets.
- The use of new methods for estimating crop calendars in the absence of higher resolution regional data sets.

3.1.1 Motivation

The correct representation of the crop duration within crop models are crucial for the interpretation of the important outputs from the model. For example if the datasets used for sowing and harvest dates are inaccurate, the simulations could grow crops during the wrong season, thereby affecting the reliability of the simulated water use and crop yield. The main differences between the regional *Bodh et al.* (2015) dataset and the global *Sacks et al.* (2010) data are for spring wheat. Spring wheat grown in winter is misclassified as winter wheat in the *Sacks et al.* (2010) data. This is discussed by *Sacks et al.* (2010) as a potential limitation when using the data for tropical and subtropical regions. Spring wheat is the more common type of wheat grown in the

South Asia region (*Hodson and White*, 2007) because minimum temperatures there are not low enough to allow vernalization to take place, which is needed for winter varieties of wheat (*Sacks et al.*, 2010, *Yan et al.*, 2015).

Figure 3.1 shows the averaged rice (green rectangles) and wheat (orange rectangles) growing season durations for *Sacks et al.* (2010) (diagonal hatching) and the *Bodh et al.* (2015) dataset (perpendicular hatching - labeled MinAg) overlaid on the present day South Asia averaged precipitation climatology and estimates of the monsoon onset and retreat. This illustrates the differences between the *Bodh et al.* (2015) and *Sacks et al.* (2010) datasets showing that in *Sacks et al.* (2010), the main growing period for both rice and wheat appears to be during the monsoon. While rice is usually grown during the monsoon it is not typical that wheat should be grown during this period for this region. The growing season durations for the *Bodh et al.* (2015) dataset (Fig. 3.1 - perpendicular hatching rectangles labeled MinAg) are more typical of this region with rice (green) growing during the monsoon and wheat (orange) growing during the dry season. Figure 3.1 highlights that where a global dataset is unable to establish exactly when wheat is grown in tropical regions, an alternative is needed.

Crop models such as those described by *Challinor et al.* (2003, 2004) and *Osborne et al.* (2015) require sowing information such as a sowing date or a sowing window, with the crop model integrating an effective temperature over time as the crop develops. The effective temperature is a function of air or leaf temperature and differs between models. The integrated effective temperature in each development stage is referred to as the thermal time of that development stage (*Cannell and Smith*, 1983, *McMaster and Wilhelm*, 1997) (there may also be an additional photoperiod length dependence). The thermal time in each development stage is typically set by the user, and can be calibrated to simulate different varietal properties. Where these varietal properties are unavailable e.g. for the global analysis in *Osborne et al.* (2015), in order to mimic the spatial variation in the choice of crop variety, these thermal times were determined from sowing and harvest dates and the temperature climatology which allowed them to vary spatially. This ensures that during the simulation, the crop develops over the course of the crop season starting at the sowing date and ending at approximately the harvest date (i.e. the harvest date is the average over the course of climatological period used).

The use of this predefined thermal time ancillary drives the requirement for providing both a sowing and harvest date. Reliable high resolution datasets for sowing and harvest dates are often unavailable for either the region or the time period that is needed. In addition there is a demand for sowing and harvest dates that maintain consistency with the model climate. Therefore, in this paper we propose a new method, outlined in Fig 3.2, for estimating sowing and harvest dates for use in the large-scale modelling of the rice-wheat rotation in South Asia using estimates of monsoon onset and retreat. This method does not require large amounts of data and the user can elect to use either the sowing input data or if needed, both sowing and harvest data to run

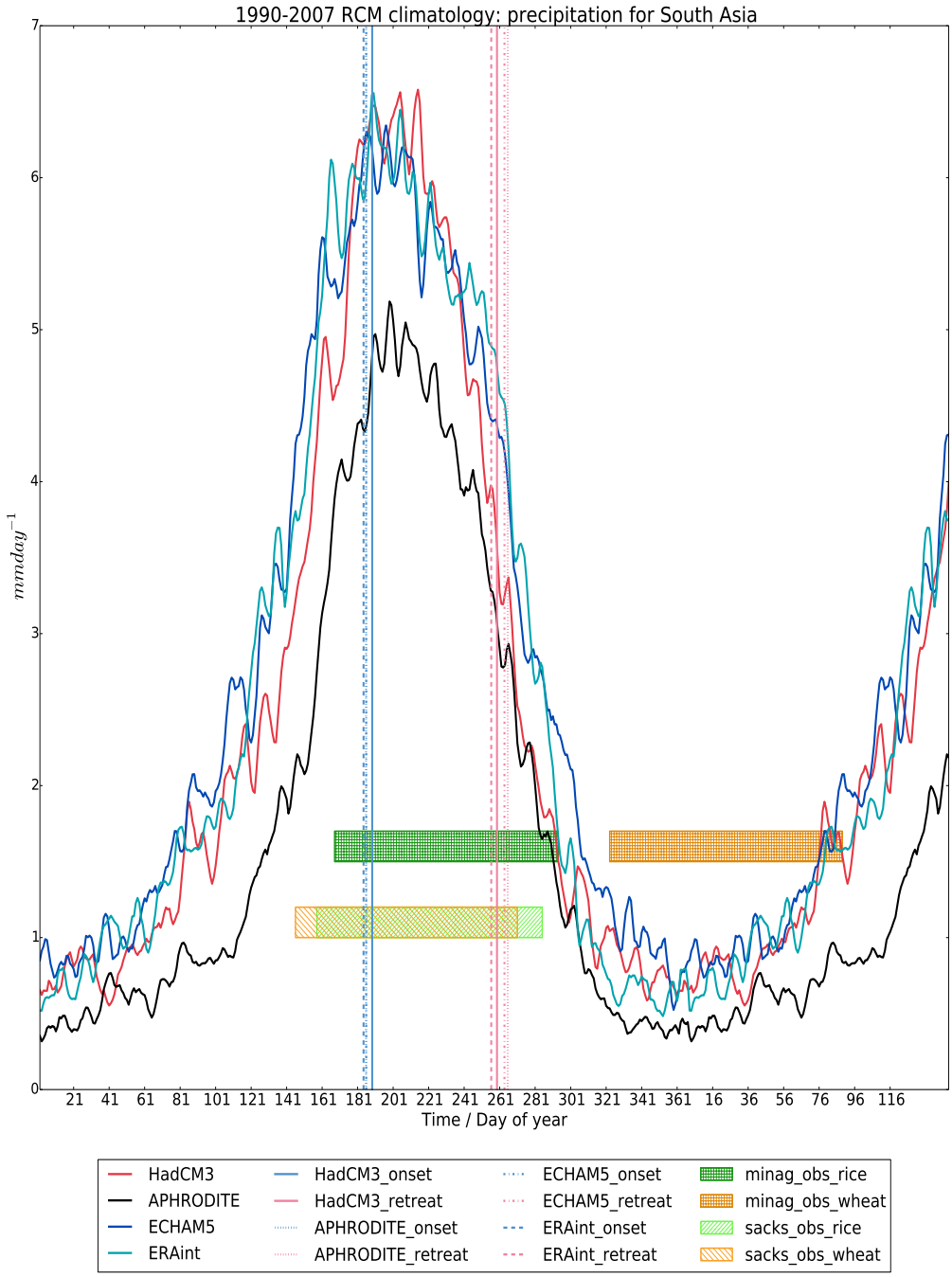

Figure 3.1: The one and a half year precipitation climatology for the 1990–2007 period averaged for South Asia for each simulation (ERAint-cyan line, ECHAM5-blue line, HadCM3-red line) and APHRODITE observations (black line) using a 5-day smoothed rolling mean. Also shown are the growing seasons also averaged for 1990–2007 for South Asia for wheat (orange) and rice (green) from two datasets; *Sacks et al.* (2010) (diagonal hatching-labeled sacks) and *Bodh et al.* (2015) (perpendicular hatching-labeled minag) and the monsoon onset (blue vertical lines) and retreat (pink vertical lines) from each of the simulations (APHRODITE-dotted, ERAint-dashed, HadCM3-solid, ECHAM5-dash dot).

their chosen crop model. The main objectives of this study are:

- To develop a method for determining sowing and harvest dates for modelling the rice-wheat rotation in South Asia based on the ASM.
- To test the method in current and future climates.

We therefore present the methodology in Sect. 3.2. We show the proposed method is viable and show it works in Sect. 3.3. Discussion of the results and conclusions are provided in Sect. 3.4 and Sect. 3.5 respectively.

3.2 Methodology

The methodology is summarized in the flow chart in Fig. 3.2. The model datasets, described in detail in Sect. 3.6 of the Appendix, include General Circulation Models (GCMs) and a Regional Climate Model (RCM). GCMs provide spatially consistent boundary data to an RCM, which generates 25km regional fields (Fig. 3.2 blue boxes). The two GCMs used in this analysis were specifically selected because they were able to capture main features of the ASM (Sect. 3.6 of the Appendix). RCMs are based on the same physical equations as GCMs and therefore represent the entire climate system including the carbon and water cycle. Their higher resolution allows a better representation of the regional-scale processes adding detail to fields like precipitation (*Mathison et al.*, 2015). The individual RCM simulations (also called HNRCMS - see Appendix Sect. 3.6) used in this analysis are referred to using their global driving data abbreviations; HadCM3, ECHAM5 and ERAint as described in Appendix Sect. 3.6. Precipitation fields are used to generate a precipitation climatology which are used to calculate monsoon statistics (Sect. 3.2.2) from which sowing and harvest dates are estimated; shown by the pink rectangles (Sect. 3.2.3). These estimated sowing and harvest dates are referred to as relative monsoon sowing and harvest dates (Fig. 3.2). Observations are used throughout the process to ensure the method is viable and produces sensible results, these are described in Sect. 3.2.1 and shown by the green boxes.

3.2.1 Observations

In order to demonstrate the viability of the methodology outlined in Fig. 3.2 we compare the simulated precipitation with observations from the Asian Precipitation-Highly Resolved Observational Data Integration Towards the Evaluation of Water Resources (APHRODITE –*Yatagai et al.*, 2012) dataset in Section 3.2.2.1. APHRODITE is a daily, 0.25° resolution land only gridded dataset that is also used in *Mathison et al.* (2015) to show that the RCMs in this analysis capture the general hydrology of the region. The monsoon is a highly variable and complex phenomenon that currently not

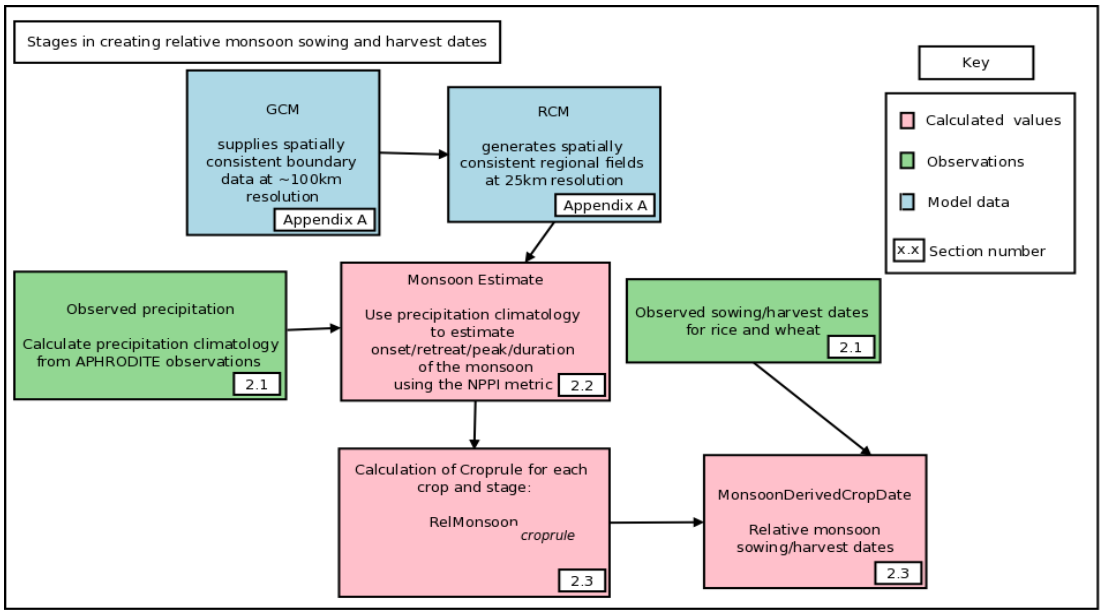

Figure 3.2: A flow chart summarizing the methodology. The blue rectangles represent datasets that are used within the methodology, green rectangles represent observations and pink rectangles represent any calculations parts of the methodology.

all climate models are able to represent; this may mean that some climate models would not yet be suitable for using with this method, which relies on a good representation of the monsoon. The method presented in Fig. 3.2 will become more robust with improving representations of the monsoon in climate models.

The datasets used for sowing and harvest dates include a global dataset, *Sacks et al.* (2010) and a regional dataset, *Bodh et al.* (2015) from the Government of India, Ministry of Agriculture & Farmers welfare. The *Bodh et al.* (2015) data is referred to from here on as MinAg data. The MinAg observations of sowing and harvest dates for rice and wheat are given as a range of days of year. The midpoints of these observed ranges are calculated and compared against the midpoints of the model pentads for onset and retreat in day of year. As a post-processing step the differences are then masked using crop areas from the International Crops Research Institute For The Semi-arid Tropics (*ICRISAT*, 2015) so that only the areas where rice or wheat are grown are considered.

3.2.2 Estimating monsoon onset and retreat

There are a wide variety of metrics for estimating the monsoon onset and retreat. Some are specific to agriculture and include representation of breaks in the monsoon (*Moron and Robertson*, 2014). More general metrics include a combination of meteorological variables such as 850hPa wind and precipitation as in *Martin et al.* (2000), or only use precipitation, such as in *Sperber et al.* (2013) and the Normalized Pentad Precipitation Index (NPPI) (*Lucas-Picher et al.*, 2011). The NPPI and *Sperber et al.* (2013) methods both use a long term climatological average of precipitation because the model data are

too noisy to calculate the monsoon statistics per year. Agricultural specific definitions of monsoon onset and retreat represent breaks in the monsoon which can adversely affect the germination of crops. However these metrics are not as effective when used in conjunction with long term average precipitation fields such as those used here. This is probably because the breaks that occur in the monsoon are quite variable from year to year and are smoothed out within the climatology. The approach by *Sperber et al.* (2013) defines monsoon onset as the pentad where the relative rainfall exceeds 5 mm day^{-1} during the May–September period. However, *Sperber et al.* (2013) regrid to the GPCP rainfall dataset (*Huffman et al.*, 2001) which is much coarser resolution than the APHRODITE data used here. The NPPI metric uses Eq. 3.1 to estimate monsoon onset, retreat, peak and duration.

$$NPPI = \frac{P - P_{min}}{P_{max} - P_{min}} \tag{3.1}$$

where P is the unsmoothed pentad precipitation climatology and P_{min} and P_{max} are the annual minimum and maximum at each gridbox respectively. The monsoon onset is then defined as the pentad in which the NPPI exceeds 0.618 for the first time and withdrawal as the last time the NPPI drops below this threshold in the year. The NPPI only reaches a value of 1.0 once in the annual cycle which corresponds to the monsoon peak. In the NPPI method the only regridding that takes place is to ensure the model and observations are on the same grid, as they are both 25km resolution there is no loss of resolution in doing this. The threshold for NPPI is also independent of the resolution of the data which is not the case for the *Sperber et al.* (2013) method. The NPPI metric has been successfully applied previously by *Lucas-Picher et al.* (2011) to analyse the monsoon of models of a similar resolution to the simulations used here (Fig 3.2). Therefore in this analysis, in the same way that *Lucas-Picher et al.* (2011) uses the 1981–2000 climatology, we use a 1990–2017 climatology. The pentad provided by the NPPI is representative of the climatological period and therefore cannot be compared to a particular year; however the pentad can be used to find the 5-day window for the climatological period where onset and retreat typically occur which can then be compared to APHRODITE observations also averaged for that period. We use the NPPI metric to calculate the pentad of the monsoon onset, retreat, peak and duration for the APHRODITE observations and the three HNRCM simulations.

3.2.2.1 Comparison of model monsoon onset and retreat with precipitation observations

Figure 3.3 shows plots of the onset (left column) and the retreat (right column) of the South Asian Summer Monsoon as defined using the NPPI described in Sect. 3.2.2. The NPPI index for the climatology of the APHRODITE precipitation observations (*Yatagai et al.*, 2012) are shown in plots (a) and (b) of Fig. 3.3 for comparison with the

precipitation climatology for each of the HNRCMs shown; ERAint (c and d), HadCM3 (e and f) and ECHAM5 (g and h). The white regions are areas where the threshold was exceeded at the first pentad; this implies the monsoon had already started at the first pentad which suggests a model bias and therefore these regions were masked out. Figure 3.4 shows the differences between the model onset (retreat) and APHRODITE onset (retreat) for each model. On average the difference between the monsoon onset in APHRODITE and the HNRCM simulations is between 1 and 7 days and the difference between the retreat in APHRODITE and the HNRCM simulations is between 4 and 10 days. However there are regions where the differences between the APHRODITE monsoon statistics are much larger than this; these are highlighted by the darker red and blue regions in Fig. 3.4. In general for most of India the HNRCMS are within 25 days of the APHRODITE observations, with the regions where the differences are larger explained by different monsoon characteristics, for example the South of India and the Bangladesh region (this is discussed further in Sect. 3.4.1).

3.2.3 Calculating sowing and harvest dates from monsoon characteristics

We use estimates of the monsoon onset and retreat together with present day rules on sowing and harvest for rice and wheat, referred to as crop rules to calculate the sowing and harvest dates relative to the monsoon (Fig. 3.2). This method allows any crop model that uses, for example, a driving dataset similar to APHRODITE or the HNRCMs, to derive sowing and harvest dates that are consistent with the monsoon of the driving data (Fig. 3.2). Thus growing the crop at the appropriate time of the year i.e rice is kept during the monsoon period and wheat is sown and harvested during the dry season. The monsoon is a highly variable phenomenon; however the use of a long term average (climatology) to calculate the monsoon statistics smooths out their large inter-annual variability. This highlights the consistency between the sowing and harvest dates and the monsoon statistics. Therefore we do not expect the monsoon statistics to be exactly the same as the observed sowing and harvest dates. Rather, this method relies on consistency between the climatological estimate of the monsoon statistics and the sowing and harvest dates across the region. The introduction of a croprule then moves the monsoon statistic to more closely reflect the observed sowing and harvest dates. This means that, even if the difference between the most relevant monsoon statistic and the observed sowing or harvest date is large then the difference is similar across India. Although these sowing and harvest events may not always be dictated entirely by the monsoon, it provides the broader seasonality associated with the crop seasons in this region. The consistency between the crop practices and the monsoon statistics across the region provides the empirical relationship exploited here to estimate the sowing and harvest dates for use in both present day and future crop

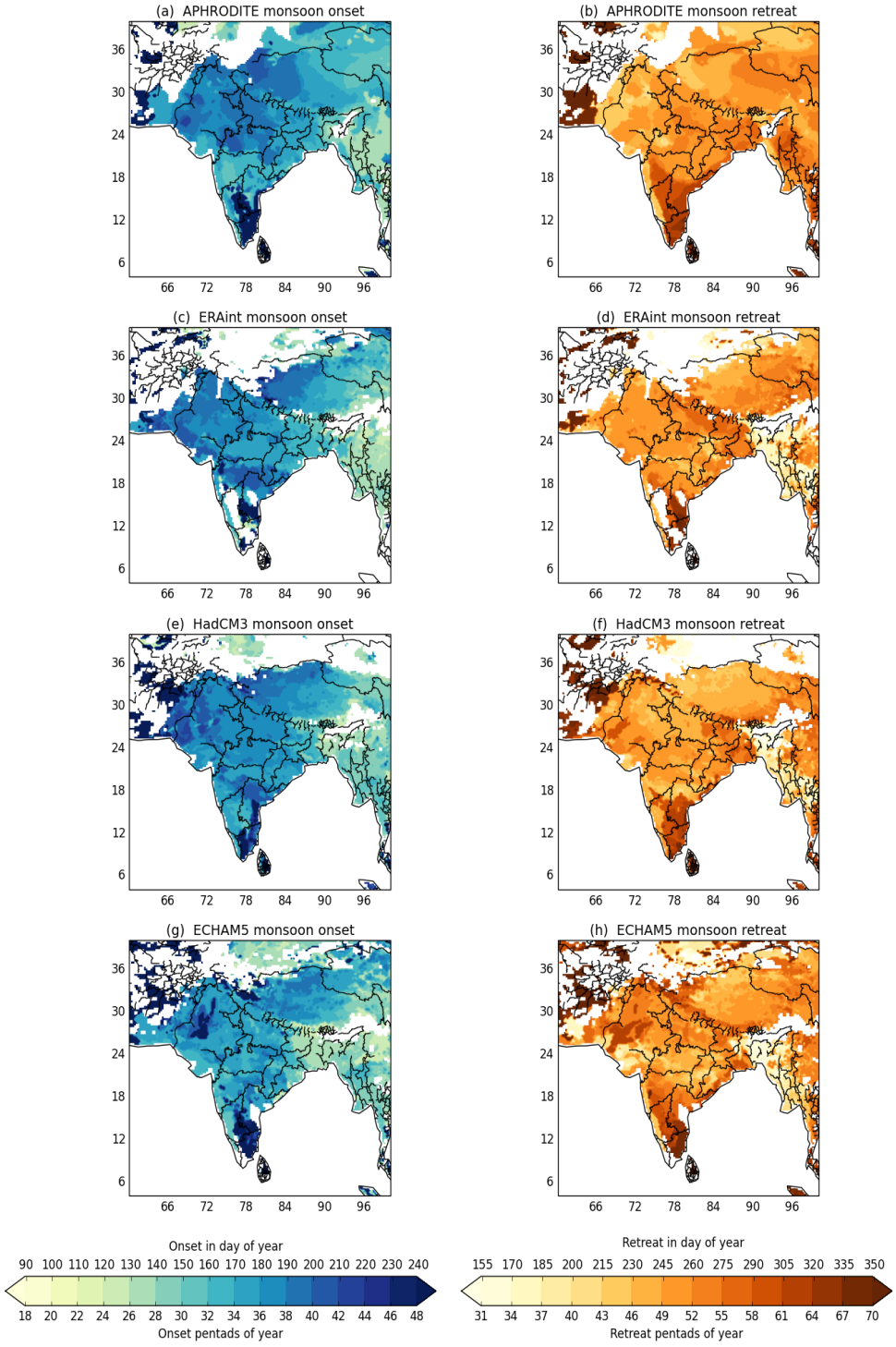

Figure 3.3: Plots of the 1990–2007 monsoon statistics; monsoon onset (left column) and retreat (right column). The APHRODITE precipitation observations (a and b) are shown and the three model simulations; ERAint (c and d), HadCM3 (e and f) and ECHAM5 (g and h) calculated using the NPPI metric. White areas are the regions where the model precipitation exceeds the threshold indicating the start of the monsoon at the initial pentad, this does not imply early monsoon but more likely a model bias in the precipitation at this location.

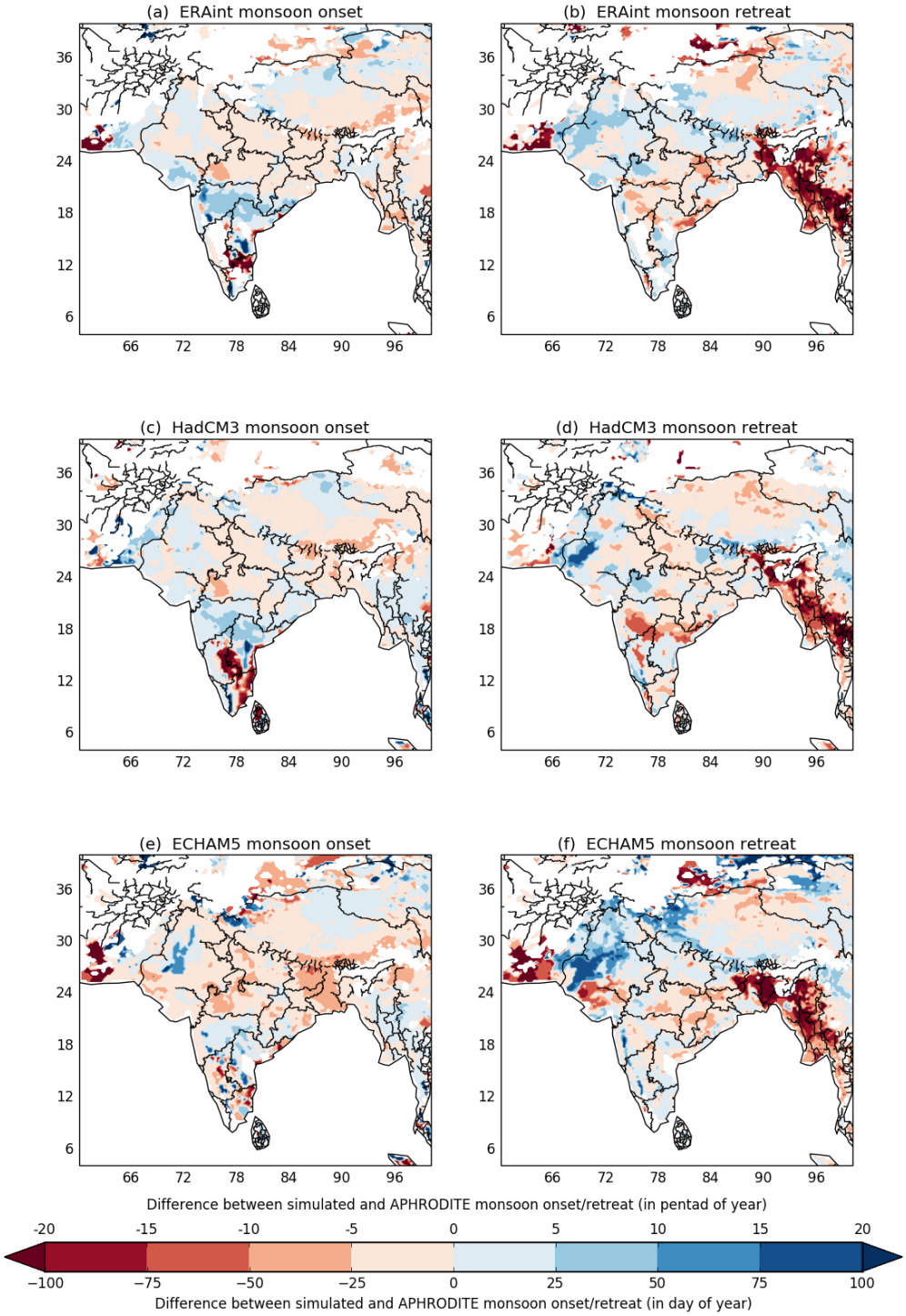

Figure 3.4: Plots of the 1990–2007 difference between model simulations and APHRODITE observations for the monsoon statistics; monsoon onset (left column) and retreat (right column); ERAint (a and b) HadCM3 (c and d) and ECHAM5 (e and f) calculated using the NPPI metric.

simulations. These sowing and harvest dates are not really intended to offer advice to farmers on when to sow or harvest on a year to year basis, rather it provides a way for sowing and harvest dates to remain relevant to this major climatological feature. A key assumption is that the monsoon remains a defining feature of the crop seasons for South Asia in the future.

3.2.3.1 Calculation of monsoon derived estimates of sowing and harvest dates for rice and wheat

We use the precipitation climatologies from APHRODITE precipitation observations and each of the HNRCM simulations (Fig. 3.2) by calculating the difference between the monsoon onset (or retreat) and the observed MinAg sowing (or harvest) dates for each crop (Fig. 3.2). These differences are per gridbox. We then calculate a weighted area average (using the *Met Office* (2018) package) to produce a crop rule for the whole region for each crop and stage; these are listed in Eq. 3.2. Collectively the crop rules given in Eq. 3.2 are referred to as $RelMonsoon_{croprule}$. This provides a simple rule that can be applied across the region, even where observations are not available. Although calculating a rule per gridbox would provide excellent results where observations were available, it would limit the usefulness of the method where observations were not available, which is one of the main aims of this approach.

$$\begin{aligned} RiceSowingCroprule &= AreaAverage(MonsoonOnset - RiceSowing) \\ RiceHarvestCroprule &= AreaAverage(MonsoonRetreat - RiceHarvest) \\ WheatSowingCroprule &= AreaAverage(MonsoonRetreat - WheatSowing) \\ WheatHarvestCroprule &= AreaAverage(MonsoonOnset - WheatHarvest) \end{aligned} \tag{3.2}$$

The $RelMonsoon_{croprule}$ is then applied to the monsoon onset and retreat field to provide an estimate of sowing and harvest dates for rice and wheat based on the monsoon. We refer to these estimates of sowing and harvest dates as 'monsoon derived crop dates' for brevity.

$$MonsoonDerivedCropDate = MonsoonStatistic - RelMonsoon_{croprule} \tag{3.3}$$

where the $MonsoonStatistic$ can be monsoon onset or retreat and the $RelMonsoon_{croprule}$ is one of the four crop rules given in Eq. 3.2

The spatial variability of the monsoon derived sowing and harvest dates is accounted for by the monsoon onset and retreat in the climatology used to calculate the $RelMonsoon_{croprule}$. The monsoon derived sowing and harvest dates for both the APHRODITE and HNRCM simulations are provided and compared against MinAg

observed sowing and harvest dates in Sect. 3.3.2.

The calculation of the $RelMonsoon_{croprule}$ is based on observations for India (from MinAg and *ICRISAT*, 2015) and therefore the analysis for the present day in Sect. 3.3.2 focuses on these areas. On the basis that most of the South Asia region is dominated by the ASM, the $RelMonsoon_{croprule}$, though tuned using India observations, can be applied to any region dominated by the ASM in order to estimate sowing and harvest dates for larger areas with a rice-wheat rotation (Sect 3.3.3). The method does not currently perform as well for parts of southern India where the climate is influenced by the Northeast monsoon but could be modified to provide better results for these areas. In Sect. 3.3.2, we compare the monsoon derived estimates of sowing and harvest dates for the period 1990–2007 with the MinAg range of sowing and harvest dates to establish if the method shown in Fig. 3.2 gives good results. There are four datasets used throughout this analysis; APHRODITE and the three HNRCMS. Where three of the four datasets provide sowing or harvest dates that are within the MinAg range the method is said to give good results, where two of the four datasets are within the MinAg range the results from the method are said to be fair. If no datasets are within the MinAg range the method is classed as poor. The sowing and harvest dates are presented for each state in Sect. 3.3.2.

3.2.4 Demonstration using monsoon derived estimates of sowing and harvest dates for two future periods

The method summarized in Fig. 3.2 is applied to two future periods using the ECHAM5 and HadCM3 RCM simulations (described in Sect. 3.6 of the Appendix). Global mean temperatures are used (within the High-End cLimate Impacts and eXtremes project – HELIX) to define the future climate in terms of specific warming levels (SWLs), i.e considering a 2°C, 4°C and 6°C world. The use of time periods is much more common than SWLs; however SWLs enable the analysis to focus less on the climate scenarios and more on what the world will look like at 2°C, 4°C and 6°C (*Gohar et al.*, 2017). This will differ depending on when the threshold is passed. The SWL approach is therefore a benefit as it means that new scenarios that are developed as part of new model intercomparison projects can be compared against older ones from previous projects. Although the older scenarios may not contain the most up-to-date socio-economic information, they are no less likely than the newer scenarios. The simulations used here are for the period 1965 to 2100 and therefore only the 2°C threshold for global mean temperature is actually passed during these simulations. For HadCM3 this occurs in 2047 and for ECHAM5, 2055. Therefore the two future periods used in this analysis are 2040–2057 and 2080–2097. The 2040–2057 period is chosen because it includes the year that the global mean temperature exceeds 2°C in the two simulations and the 2080–2097 period is chosen because it is furthest into the

future in these simulations and therefore likely to show the greatest warming. The length of the two future analyses periods has been chosen for consistency with the ERAint RCM simulation which is only available for the period 1990–2007. Although the threshold of 2°C is exceeded globally it is important to note that the relationship between the projected global mean change in temperature and the regional climate change in temperature for South Asia is complicated. Heat and moisture and how they vary across the globe are not evenly distributed with land warming faster than the ocean (*Christensen et al.*, 2013); therefore the actual temperature change experienced in South Asia may be higher than the global mean change.

3.3 Results

We compare the model monsoon to the monsoon calculated from precipitation observations to demonstrate that the model is able to reproduce the monsoon (Sect. 3.2.2.1) and therefore the methodology summarized in Fig. 3.2 and Sect. 3.2 is viable. In Sect. 3.3.1 we compare the simulated monsoon with the observed sowing and harvest dates in order to calculate the monsoon derived sowing and harvest dates and compare these new simulated sowing and harvest dates with the observations. We then show results from applying the method in Sect. 3.3.2. As a demonstration, we also apply the method to two future periods in Sect. 3.3.3.

3.3.1 Comparing observed sowing and harvest dates with estimates of monsoon onset and retreat

The climatology shown in Fig. 3.1 shows that on average the observed rice and wheat sowing and harvest dates from MinAg align well with the monsoon onset and retreat in the simulations. Observed rice sowing dates generally compare well with the monsoon onset in the model as shown in Fig. 3.5 and Fig. 3.6.

The monsoon onset and retreat estimates are provided in days of year (pentads) therefore with a range of plus or minus 2.5 days. The MinAg observations are also provided in days of year with a range that varies from plus or minus 15 days depending on the location. Figure 3.8 shows the range of the MinAg sowing and harvest observations for each state; the full sowing or harvest window is shown by the downward grey triangles, with the midpoints shown by black triangles joined by a black line. Figure 3.6 considers the midpoints of these two ranges in order to summarize how well aligned the monsoon onset range is to the observed range of rice sowing dates i.e. how the 5-day onset windows coincide with the observed sowing window. If the monsoon onset range is completely within the range of sowing days provided by the observations then this is classed as a 'hit' (shown by the blue regions). If the monsoon onset range is completely outside the range of observed sowing days then this is classed as a 'miss' (shown by the red regions). The yellow regions in Fig. 3.6 show the places where the

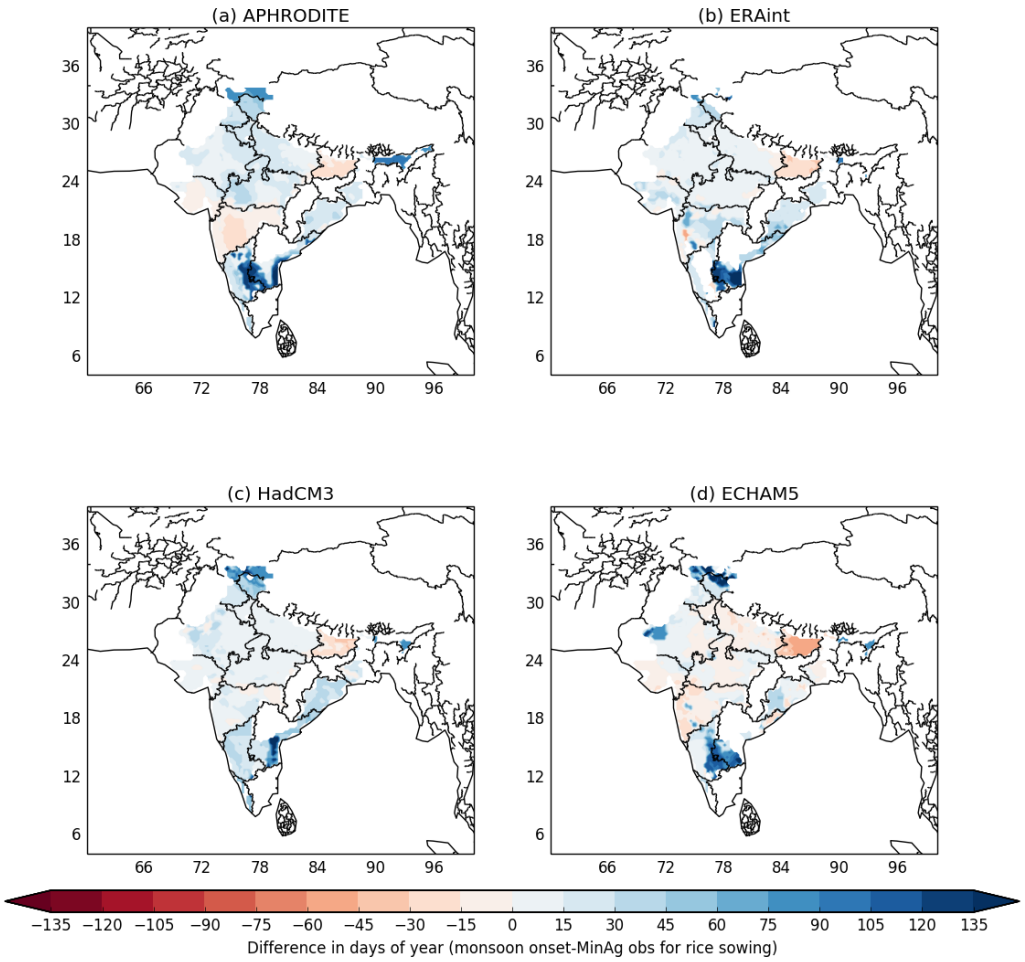

Figure 3.5: Plots of the difference between the midpoint of the monsoon onset in the model and the midpoint of the observed rice sowing period for 1990–2007.

monsoon onset overlaps the range of observed sowing days but does not completely fall within it; these regions are labelled 'Overlaps'. Figure 3.6 has only a small area of red indicating that monsoon onset is, for large parts of India, within the range of days of rice sowing. In each plot shown in Fig. 3.6 the region that is red or yellow is different; this makes it difficult to say if one dataset is better than another. ECHAM5 appears to have the smallest total area of red/yellow, which is probably because ECHAM5 tends to have an earlier onset than the other datasets and in general that makes it closer to the rice sowing dates.

Table 3.1 lists the differences between the monsoon statistics (onset and retreat) and the relevant sowing and harvest dates for each crop calculated for each of the simulations and the APHRODITE observations and averaged for India. Table 3.1 shows that on average across India rice sowing occurs between 10 and 20 days prior to the averaged modelled monsoon onset (third block, Table 3.1). We would not expect the different datasets to give the same results, however Table 3.1 shows that they are

relatively consistent with each other and importantly with observations as is illustrated by the APHRODITE data. Table 3.1 highlights that on average APHRODITE requires a larger croprule than the simulations for rice sowing; however, this is not always the case for sowing or harvest and rice or wheat. The croprules used here are based on the 1990–2007 period for which ERAint has the earliest onset (Fig. 3.10). ECHAM5 has the smallest croprule to move it towards the rice sowing date, but the highest variance in the mean difference between the monsoon onset and the MinAg rice sowing date. APHRODITE has the largest crop rule for rice sowing, indicating that the weighted average of the APHRODITE monsoon onset is further from the rice sowing date than for other datasets.

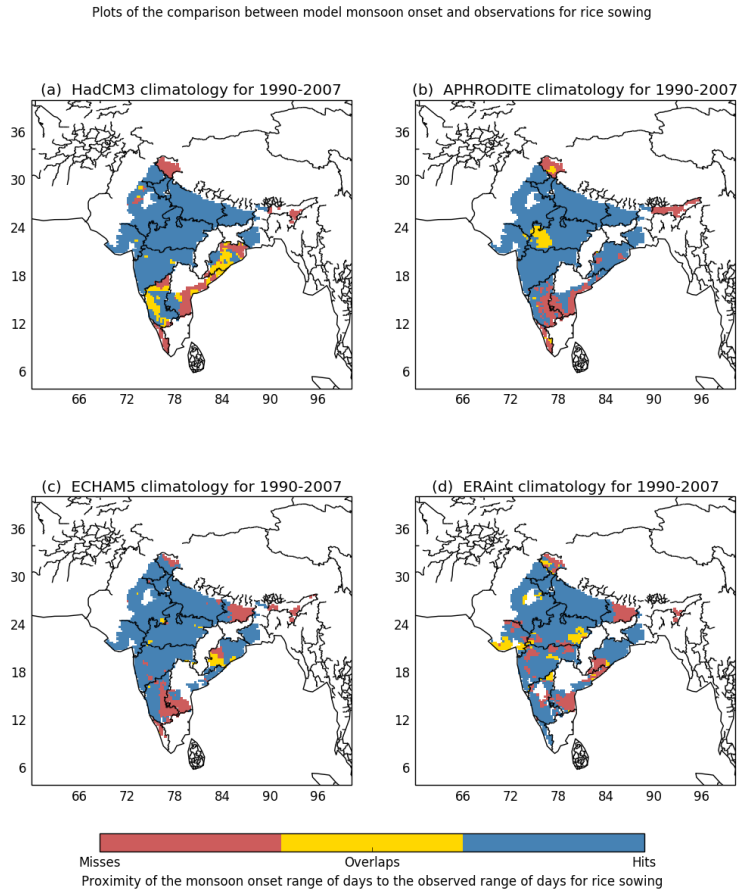

Figure 3.6: The comparison of the model monsoon onset in terms of the days of the year (to within the pentad) and the range of days of the year for the observed sowing date for rice. This is shown in terms of hit (blue) and overlap (yellow) or if there was no overlap this is shown as a miss (red)

In general the differences between rice harvest and monsoon retreat are larger but still consistent across the region (Fig. B.1), with rice harvest occurring on average 30–40 days after monsoon retreat (fourth block, Table 3.1). Wheat sowing tends to occur approximately 60–70 days after monsoon retreat (Fig. B.2 and first block, Table 3.1)

and wheat harvest tends to occur approximately 90–101 days before monsoon onset (Fig. B.3 and second block Table 3.1). These values (given in Table 3.1) provide the $RelMonsoon_{croprule}$ values introduced in Sect. 3.2.3.1 used to adjust the monsoon statistics and calculate the new sowing and harvest dates based on the monsoon. There are small regions with different monsoon characteristics and therefore much earlier sowing days, for example for rice sowing in the southern and far north of India. These regions have a direct impact on the values (minimum, maximum, mean and standard deviation - SD) given in Table 3.2 which are averages for the whole of India and are discussed in more detail in Sect. 3.4. Fig 3.1 highlights that the the average sowing and harvest dates for rice and wheat are closely aligned with the monsoon precipitation from all three RCM simulations.

crop	**stage**	Mon_{stat}	**source**	$RelMonsoon_{croprule}$ **(India average)**
wheat	sowing	retreat	APHRODITE	-63.5
wheat	sowing	retreat	ERAint	-62.8
wheat	sowing	retreat	HadCM3	-67.9
wheat	sowing	retreat	ECHAM5	-63.6
wheat	harvest	onset	APHRODITE	**98.5**
wheat	harvest	onset	ERAint	**100.4**
wheat	harvest	onset	HadCM3	**98.9**
wheat	harvest	onset	ECHAM5	**91.4**
rice	sowing	onset	APHRODITE	**19.7**
rice	sowing	onset	ERAint	**17.3**
rice	sowing	onset	HadCM3	**17.2**
rice	sowing	onset	ECHAM5	**10.1**
rice	harvest	retreat	APHRODITE	-32.7
rice	harvest	retreat	ERAint	-35.4
rice	harvest	retreat	HadCM3	-38.5
rice	harvest	retreat	ECHAM5	-34.7

Table 3.1: Table of $RelMonsoon_{croprule}$ for each dataset, crop and stage. The $RelMonsoon_{croprule}$ is the value subtracted from the monsoon onset/retreat in order to calculate a new sowing/harvest date based on the monsoon onset/retreat. In each case the new estimate of the sowing and harvest dates is calculated by subtracting the $RelMonsoon_{croprule}$ from the Mon_{stat} where Mon_{stat} is Monsoon onset or Monsoon retreat from a HNRCM or APHRODITE precipitation observations. Where the sowing/harvest is **before** the monsoon statistic, the crop rule is in **bold** with normal type indicating that sowing/harvest occurs after the monsoon statistic.

3.3.2 Monsoon derived estimates of sow/harvest dates for rice and wheat

The monsoon derived sowing and harvest dates are calculated from applying the $RelMonsoon_{croprule}$ for each model (Table 3.1) to the simulated monsoon onset and retreat fields (Fig. 3.2). Here we compare these with the gridded observations to see

crop	stage	monsoon stat	source	min	max	mean	SD
wheat	sowing	retreat	APHRODITE	-122.0	53.0	-63.5	23.6
wheat	sowing	retreat	ERAint	-160.0	36.0	-62.8	19.8
wheat	sowing	retreat	HadCM3	-185.0	33.0	-67.9	26.7
wheat	sowing	retreat	ECHAM5	-187.5	53.0	-63.6	34.6
wheat	harvest	onset	APHRODITE	32.5	216.5	98.5	26.5
wheat	harvest	onset	ERAint	22.0	216.5	100.4	26.8
wheat	harvest	onset	HadCM3	-3.0	216.5	98.9	23.0
wheat	harvest	onset	ECHAM5	-18.0	217.5	91.4	33.7
rice	sowing	onset	APHRODITE	-24.5	156.5	19.7	32.8
rice	sowing	onset	ERAint	-49.5	196.5	17.3	30.5
rice	sowing	onset	HadCM3	-40.0	226.5	17.2	25.4
rice	sowing	onset	ECHAM5	-65.0	186.5	10.1	36.7
rice	harvest	retreat	APHRODITE	-91.5	110.5	-32.7	30.4
rice	harvest	retreat	ERAint	-116.5	73.5	-35.4	23.3
rice	harvest	retreat	HadCM3	-111.5	78.5	-38.5	29.3
rice	harvest	retreat	ECHAM5	-141.5	98.5	-34.7	35.9

Table 3.2: Analysis of the differences between the midpoints of the MinAg data and Monsoon onset/retreat for rice/wheat sowing and harvest dates: The table shows the minimum, maximum, mean and standard deviation (SD) averaged across South Asia where wheat or rice are planted.

how well the method performs for the present day. The monsoon derived sowing and harvest dates are compared with the MinAg observations using regional maps and an analysis for each state area in order to show the differences in the method across India.

Figure 3.7 shows the monsoon derived estimates of rice sowing dates (left column) and compared with MinAg observations (right column). Fig. C.1 shows the same plots for rice harvest, with plots for wheat shown in Fig. C.2 and Fig. C.3 for sowing and harvest respectively. The $RelMonsoon_{croprule}$ for wheat for both sowing and harvest are much larger than those for rice but there is still good agreement between the monsoon derived estimates and the MinAg observations across the region. On average the monsoon derived estimates of sowing and harvest dates are within four days of the midpoints for the sowing and harvest dates for rice and within seven days of the midpoints for sowing and harvest dates for wheat. There is some variation across India with some regions showing some larger differences but generally the monsoon derived estimates for sowing and harvest dates are within the range provided by the observations across much of the region for both crops.

Figure 3.8 shows the average crop duration for each state where MinAg observations were available for the 1990 to 2007 period alongside the crop duration for each of the four sets of monsoon derived estimates using the Fig. 3.2 method. In the majority of states shown in Fig. 3.8 the sowing and harvest dates calculated using the Fig. 3.2 method were within the range of the MinAg observations for rice and wheat sowing and harvest dates; however, the overall performance was better for rice compared with

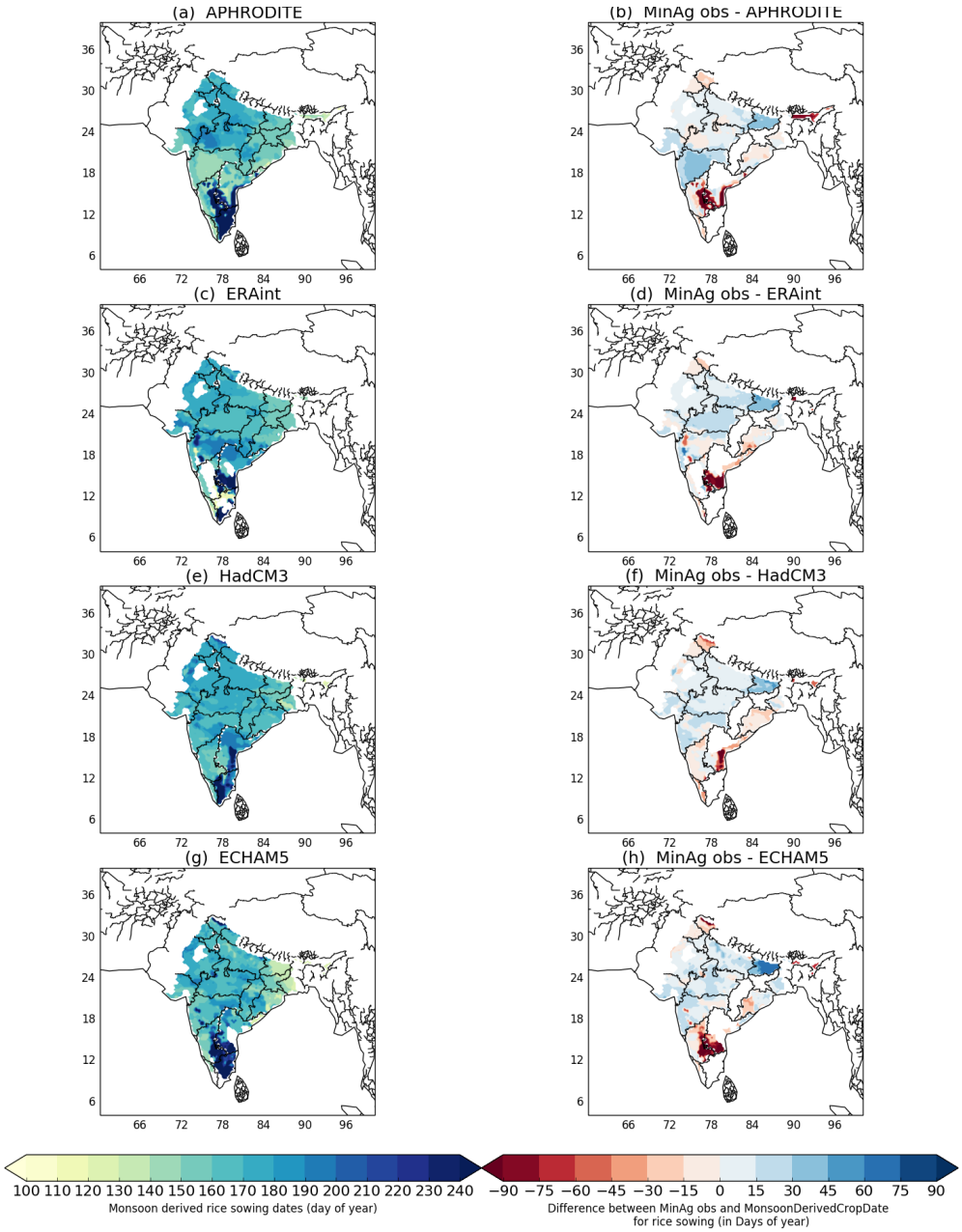

Figure 3.7: The monsoon derived rice sowing dates (left) and the difference between the MinAg observations and the monsoon derived rice sowing dates (right) for the period 1990–2007.

wheat and sowing compared with harvest in each crop. Figure 3.8 also highlights the difference in both the observed and simulated crop duration between the two crops with rice having a shorter season than wheat. In general across most of the states with available data the method provides a reasonable estimate of the sowing, harvest date and crop duration. Even where the method does not quite capture the observed sowing and harvest dates, the method is often just outside the observed range.

In order to establish how well the method performs over all, we use Fig. 3.8 to

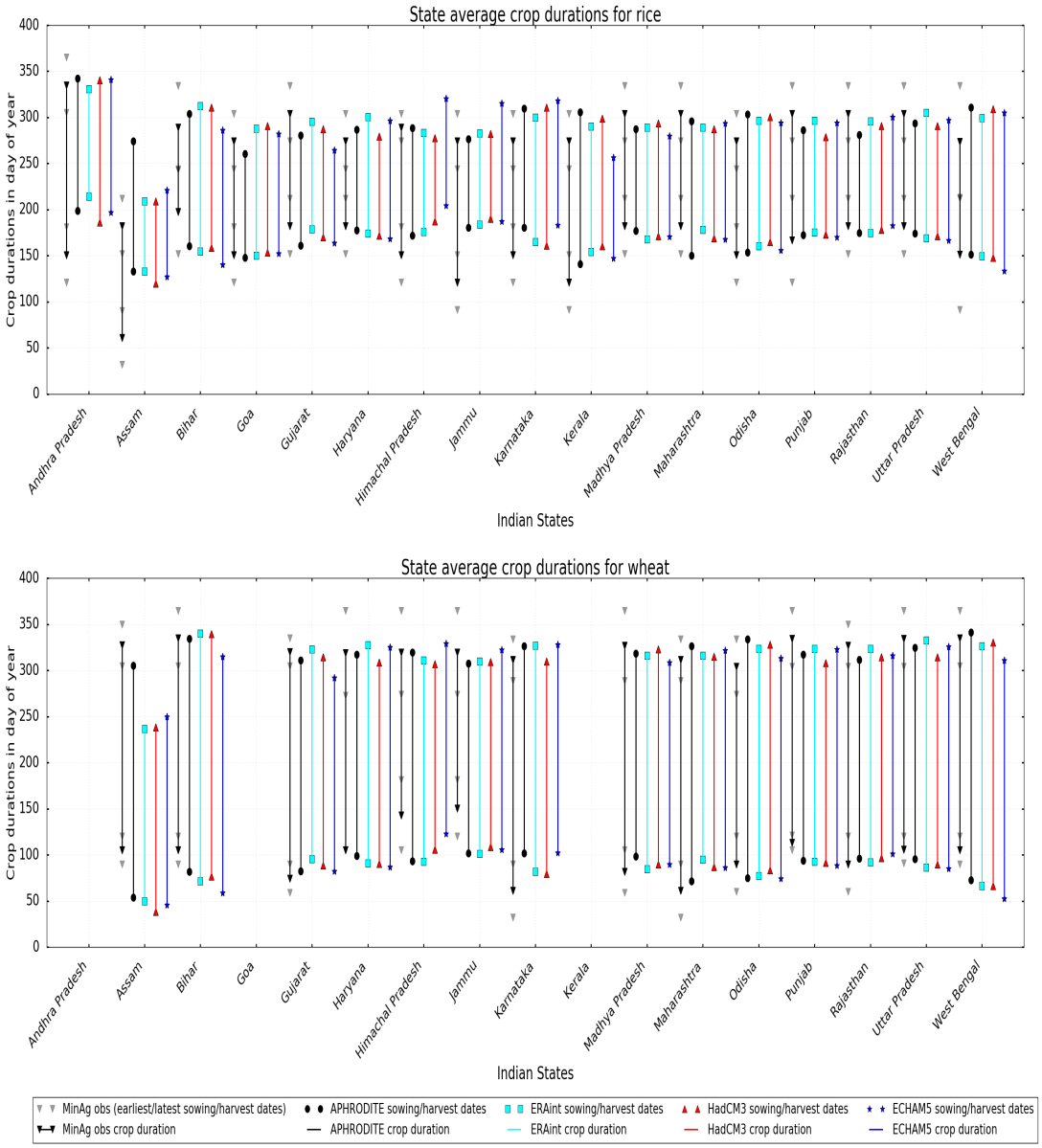

Figure 3.8: The state averaged crop durations for each dataset are shown by the lines for each state together with the sowing and harvest dates shown by the different shapes at the end of each line. The MinAg observations are shown by the black line and downward triangles, with the paler triangles representing the full range of sowing and harvest days for that state. The APHRODITE observations are also shown by black lines and filled circles for the sowing and harvest dates. ERAint is shown by cyan lines and squares, ECHAM5 by blue lines and asterisks, HadCM3 by red lines and upward triangles.

assess if the results using the method are good, poor or fair compared to the MinAg data. Where the monsoon derived sowing and harvest dates from three of the four datasets using the method are within the range of the MinAg data as shown in Fig. 3.8, the results of the method are said to be 'good' for a state. The results of the method are said to be 'fair' where two datasets are within the range of the MinAg data

and 'poor' where the sowing and harvest dates fall outside the observed range. In this analysis only the state of Assam did not have any 'good' scores for rice or wheat sowing or harvest. Most of the scores for most of the states for both sowing and harvest, and wheat and rice had a score of good or fair.

In general the regions where the monsoon derived sowing and harvest dates are not as close to the MinAg observations tends to be for the states in the south, such as Andhra Pradesh and Karnataka or to the north of India, such as Jammu and Himachal Pradesh. This is supported by the maps, particularly for rice for these regions (in Fig. 3.7 and Fig. C.1) which show that the method does not perform as well for some of these states. These differences may be explained by the differing monsoon characteristics in these regions compared to the rest of India; these are highlighted in Fig. 3.3 and discussed further in Sect. 3.3.1 and Sect. 3.4. Assam in the north east of India is also noticeable compared with the other states in Fig. 3.8 with the rice crop season in the MinAg data displaced to an earlier part of the year. Assam tends to plant predominantly rice, tending to have three distinct rice seasons (autumn, winter and summer) rather than a rice-wheat rotation (*Sharma and Sharma*, 2015). In this analysis we use data for the Kharif paddy rice crop from the MinAg dataset which is planted and harvested earlier in Assam than in other states, with sowing in Feb/March and harvest in June/July (*Bodh et al.*, 2015).

3.3.3 Analysis of future monsoon onset and retreat

As a demonstration of the method summarized in Fig. 3.2, the HELIX SWLs (described in Sec. 3.2.4) are used to select two future periods: 2040–2057 and 2080–2097. Considering only these future periods, spatially HadCM3 and ECHAM5 show quite different future climates. HadCM3 shows a similar onset to the present day for 2040–2057 (Fig. 3.9a and c) but later onset compared with the present day for 2080–2097 (Fig. D.1a and c). ECHAM5 shows an earlier onset compared with the present day for the 2040–2057 period (Fig. 3.9b and d) but much later for the 2080–2097 period (Fig. D.1b and d). This suggests high variability in monsoon onset in these simulations. In fact all of monsoon onset, peak, retreat and duration show a large degree of variability as shown in Fig. 3.10 where each statistic has been averaged for South Asia. Each point in Fig. 3.10 represents a 17-year timeslice from between 1970 and 2097 for each of the APHRODITE, ECHAM5, HadCM3 and ERAint datasets. Figure 3.10 supports the points made regarding the spatial plots and also shows how the four monsoon statistics change between the 17 year timeslices. The 2040–2057 period has a much earlier onset for ECHAM5 than all the other periods except the 2000–2017 period, which is similar (Fig. 3.10a. For most of the periods ECHAM5 has an earlier onset than HadCM3, this is also true of the retreat (Fig. 3.10b), the duration is usually longer for ECHAM5 compared with HadCM3 (Fig. 3.10d).

In order to illustrate the method for deriving sowing and harvest dates, Fig. 3.11

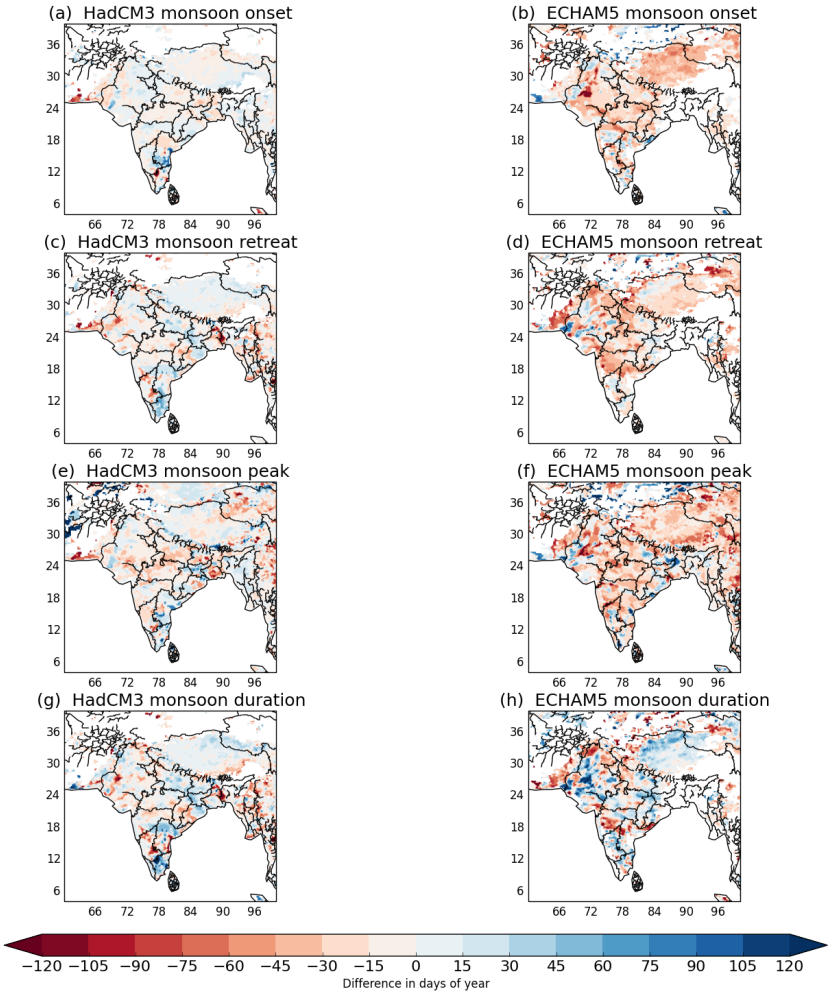

Figure 3.9: The difference between the monsoon statistics for the 2040–2057 future period and the present day 1990–2007 for HadCM3 (left) and ECHAM5 (right).

shows the annual cycle of precipitation averaged for South Asia for the two future periods (plot a shows 2040–2057 and plot b shows 2080–2097) in the same way as the present day is shown in Fig. 3.1. The crop sowing and harvest dates used to provide the growing season durations in each of the plots shown in Fig. 3.11 for each of the simulations are calculated using the method described in Fig. 3.2. This shows that the proposed method provides an estimate of sowing and harvest dates that ensures the crops can continue to be grown, in the simulation, when the climate is most appropriate rather than being fixed to the present day observed values.

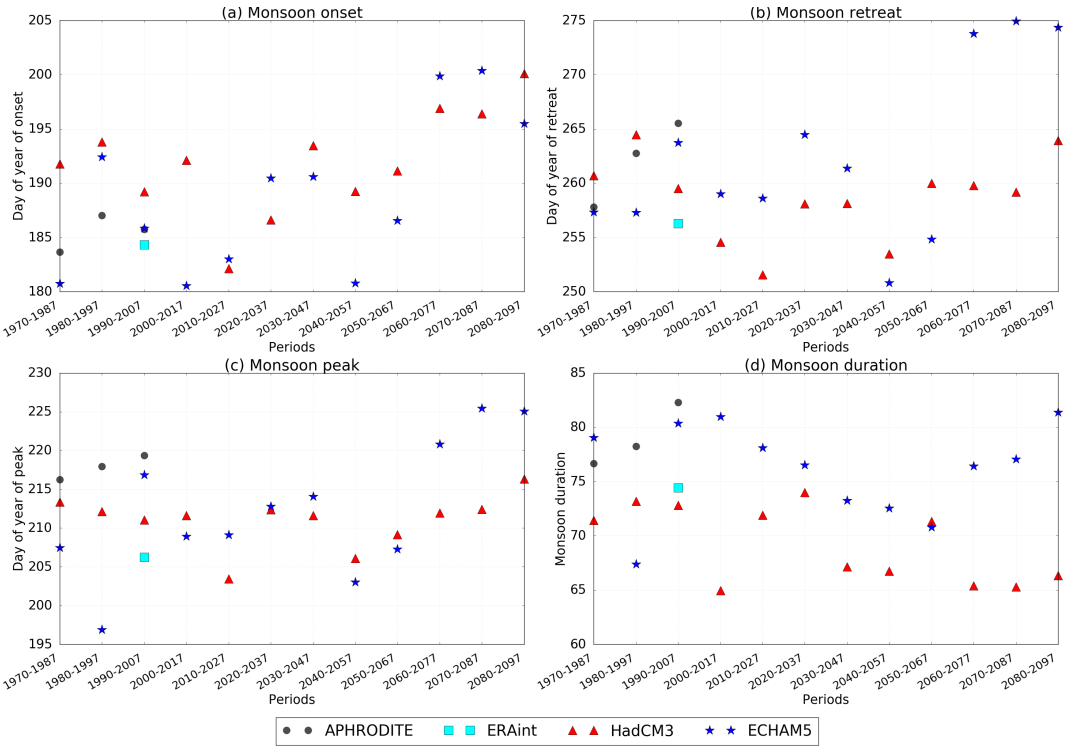

Figure 3.10: Monsoon statistics; onset (a), retreat (b), peak (c) and duration (d) averaged for South Asia for twelve 17-year timeslices between 1970–2097 to provide a timeseries of values for the region to assess the variability of the monsoon

3.4 Discussion

Recent climate impact studies such as AgMIP (*Rosenzweig et al.*, 2013, 2014) and ISIMIP (*Warszawski et al.*, 2013, 2014) have highlighted the importance of reliable input data for models. Section 3.1.1 highlights the scale of the uncertainties present when solely using a global sowing and harvest dataset to simulate region specific cropping patterns. We have therefore proposed a new method for generating sowing and harvest dates for South Asia based on the ASM. The method reproduces observed sowing and harvest dates for much of India. These results are discussed further in Sect. 3.4.1. This method will also be useful in other monsoon regions where data are scarce, unreliable or unavailable such as in future climate simulations. The future results are discussed further in Sect 3.4.2.

3.4.1 Present day analysis

In general the method described by Fig. 3.2 works well across most of India for the present day, with the monsoon derived estimates of sowing and harvest dates falling within the range of days for sowing given by the observations and therefore providing a good estimate of the crop duration for most states (Fig. 3.8). However, there are regions where the estimated sowing and harvest dates do not compare as well against

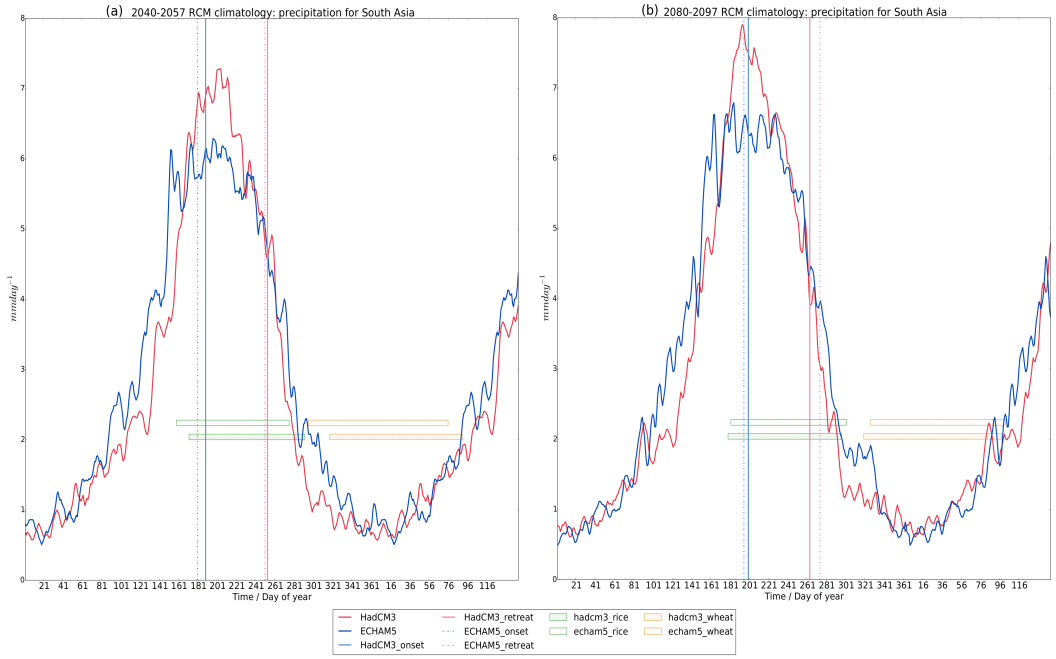

Figure 3.11: The one and a half year precipitation climatology for the period 2040–2057 (a) and the 2080–2097 (b) averaged for the whole of South Asia for each simulation (HadCM3-red line, ECHAM5-blue line) using a 5-day smoothed rolling mean. Also shown are the monsoon derived growing seasons for wheat (orange) and rice (green) calculated using the method described in Fig. 3.2 for HadCM3 (perpendicular hatching) and ECHAM5 (diagonal hatching). The monsoon onsets for each simulation are shown using blue vertical lines and retreat pink vertical lines (ECHAM5-dash dot lines, HadCM3-solid

present day observations. Rice sowing is generally closely associated with ASM onset across most of central India; however, in the south of India, there is a small region where the differences between the observations of sowing dates and the monsoon are larger than everywhere else (Fig. 3.5). In Sect. 3.3.1 this region is shown to have different monsoon characteristics to the rest of India. This part of India includes the state of Tamil Nadu, this state is located on the lee side of the Western Ghats and therefore does not receive the large amounts of ASM rainfall that is more commonly associated with this part of the world. Tamil Nadu receives up to 50 percent of its annual rainfall during October–December via the less stable North Eastern (NE) Monsoon. The NE monsoon is therefore more important for water resources for this part of India than the ASM which accounts for approximately 30 percent of the annual rainfall for this region (*Dhar et al.*, 1982). These differing monsoon characteristics mean different agricultural practices are required to cultivate rice in this part of the country. This is illustrated by Fig. 3.12 (left plot) which shows that the southern region of India with differing monsoon characteristics irrigates rice more intensively than other parts of India. In the Tamil Nadu region, rivers are usually dry except during the monsoon months and the flat gradients mean there are few locations for building reservoirs,

therefore approximately one third of the paddy rice crop is irrigated from a large network of water tanks (*Anbumozhi et al.*, 2001). The Southern states of India have the highest density of irrigation tanks with large numbers also found in Andhra Pradesh and Karnataka, these are also regions shown to have a high irrigation intensity in Fig. 3.12. Rice harvest is typically not as closely associated with the monsoon onset as rice sowing, which usually requires the monsoon to be fully established before planting.

The widespread irrigation of wheat shown in Fig. 3.12 (right plot) has less of an impact on the estimates of wheat sowing/harvest dates because this crop is less closely linked to the monsoon onset than rice. Therefore the regional differences between the MinAg observations and the monsoon derived sowing and harvest dates for wheat are not as large as some of those for rice (Sect. 3.3.2). Given that the method has provided reasonable estimates of sowing and harvest dates for most of India, it would be useful and interesting to extend this method to improve it for the South of India.

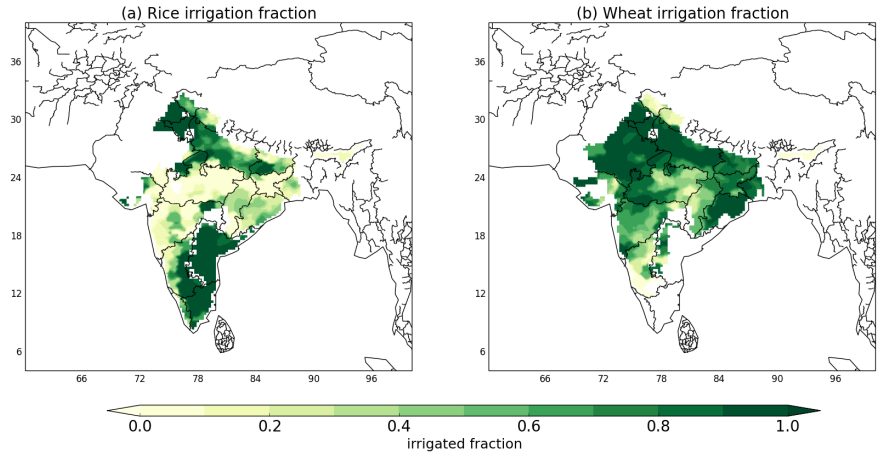

Figure 3.12: The average irrigation fraction for rice (a) and wheat (b) calculated from the ICRISAT observations of irrigation area and area planted

3.4.2 Analysis of future periods

Analysis of the future monsoon onset, retreat, peak and duration shown in Sect. 3.3.3 shows how changeable the ASM is for these simulations between time periods. *Christensen et al.* (2013) shows that there is a high model agreement within the ensemble from the 5th Coupled Model Intercomparison Project (CMIP5) for an earlier onset and later withdrawal in the future and therefore indicates a lengthening monsoon duration. However the simulations presented here do not show this with Fig. 3.10, instead, highlighting the large amount of variability in the ASM for this region. It is possible that an increase in the monsoon duration does occur in these simulations for some parts of South Asia, but this detail is lost through averaging over the region or as a result of the time periods selected. *Christensen et al.* (2013) also suggest that there is medium confidence within the CMIP5 ensemble that the ASM rainfall will increase to the end

of the century. The simulations presented do indicate this as shown by the timeseries in Fig. 3.13.

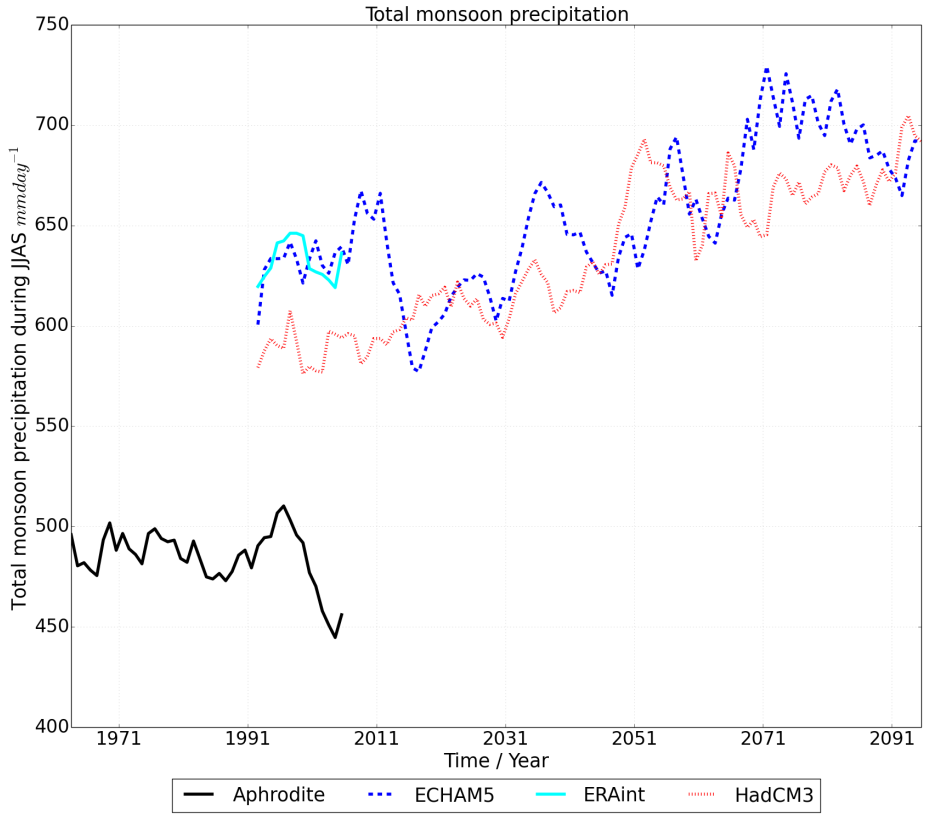

Figure 3.13: The annual timeseries of total monsoon precipitation, smoothed using 5-year averaging, averaged for the whole of South Asia for all simulations; APHRODITE-solid black line, ERAint-solid cyan line, ECHAM5-blue dashed line and HadCM3-red dotted line.

Assuming that crops continue to be grown in accordance with the monsoon, Sect. 3.3.3 shows that the method described in Sect. 3.2 provides a good estimate of sowing and harvest dates for the two future periods shown. Spatial plots of the sowing and harvest dates for the two future periods (not shown) are similar to those in Sect. 3.3.2 for the present day with the south of the Indian peninsula continuing to show different monsoon characteristics (Sect. 3.4.1) to the rest of India in the future, resulting in later estimated sowing and harvest dates for this region.

The proposed method successfully adjusts the sowing and harvest dates where the monsoon begins earlier in the future simulations and therefore provides a good estimate of sowing and harvest dates for the two future periods considered. This is a key benefit of using this method as it simulates the decision a farmer might take to sow before the usual observed date if the monsoon arrived early. This method therefore provides the capability for climate simulations to replicate the type of adaptation response that would happen in the real world. This method would also be useful for other regions

that have a crop calendar that is similarly defined such as the SSA; this is a multiple cropping region with sowing and harvest dates closely associated with the main rainy season (*Waha et al.*, 2013).

3.5 Conclusions and future work

Sowing and harvest dates are an important input within crop models but are a source of considerable uncertainty. Global datasets, such as *Sacks et al.* (2010), cannot always distinguish when wheat is grown in tropical and sub-tropical regions therefore driving a requirement for higher resolution regional datasets. Crops across much of South Asia are heavily dependent on the ASM and therefore sowing and harvest dates tend to be closely linked to this climatological phenomenon. We have therefore presented a new method for deriving sowing and harvest dates for rice and wheat for South Asia from the ASM onset and retreat. For the present day, the method generally shows good results for most areas of India with the derived sowing and harvest dates within the range of the observations for most states. The method does not work as well for the south of the Indian peninsular, this region receives a lower proportion of annual rainfall from the ASM than much of the rest of South Asia and irrigates intensively. Monsoon derived estimates of sowing and harvest dates for rice and wheat are useful for regions where data are scarce, unreliable or in future climate impact assessments. The method presented assumes that the agricultural practices remain dependent on the monsoon in the future. Given this assumption, the method presented successfully estimates the sowing and harvest dates for two future periods by adjusting the sowing and harvest dates according to the timing of the monsoon. Future work in this area could investigate refinements to the method to take into account the different characteristics of the monsoon in the regions where the method does not work as well and the differing agricultural practices there. It would also be interesting to investigate how well the method works for different crop rotations in different monsoon regions.

3.5.1 Addendum: Conclusions and future work

This paper focuses on the South Asia region and the ASM. Applying the method to another part of the world influenced by a different monsoon would require analysis similar to that presented here. In the first instance a model, either an RCM or GCM, would need to show skill in simulating the monsoon for that region. The monsoon onset and retreat would also need to be aligned with the sowing and harvest dates for that region. Currently in this method there is no estimate of interannual variability. South Asia is a highly variable region, which means that metrics used to estimate the monsoon typically use climatological information, as used in the analysis presented here. In order to estimate the interannual variability of the monsoon, many ensembles are needed. A large ensemble of simulations would enable an annual estimate of the monsoon rather

than a climatological estimate, thus allowing an estimate of the interannual variability to be included in the estimate of sowing and harvest dates. CMIP5 suggests that in the future, the ASM will be longer, with increasing rainfall towards the end of the century. There are also questions over its reliability, with more breaks in the rainfall during the monsoon. Therefore, including interannual variability could be an important development of the original method, especially for the application of the method to future periods.

3.6 Appendix A: Details of the models used

This analysis uses two General Circulation Models (GCMs) selected to capture a range of temperatures and variability in precipitation similar to the AR4 ensemble for Asia (*Christensen et al.*, 2007) and the main features of the ASM (*Kumar et al.*, 2013, *Annamalai et al.*, 2007, *Mathison et al.*, 2013, 2015). HadCM3; the Third version of the Met Office Hadley Centre Climate Model (HadCM3 – *Pope et al.*, 2000, *Gordon et al.*, 2000; a version of the Met Office Unified Model) provides the positive variation in precipitation and ECHAM5, (*Roeckner et al.*, 2003; 3rd realization–) the negative variation in order to estimate the uncertainty in the sign of the projected change in precipitation over the coming century.

One RCM, the HadRM3 RCM (*Jones et al.*, 2004) is used to downscale the GCM data to provide more regional detail to the global datasets. HadRM3 has 19 atmospheric levels and the lateral atmospheric boundary conditions are updated 3 hourly and interpolated to a 150 s timestep. These simulations include a detailed representation of the land surface in the form of version 2.2 of the Met Office Surface Exchange Scheme which includes a full physical energy-balance snow model (MOSESv2.2, *Essery et al.*, 2003). MOSESv2.2 treats subgrid land-cover heterogeneity explicitly with separate surface temperatures, radiative fluxes (long wave and shortwave), heat fluxes (sensible, latent and ground), canopy moisture contents, snow masses and snowmelt rates computed for each surface type in a grid box (*Essery et al.*, 2001). However the air temperature, humidity and wind speed above the surface are treated as homogenous across the gridbox and precipitation is applied uniformly over the different surface types of each gridbox (*Mathison et al.*, 2015). This RCM was included in an assessment of four RCMs conducted by *Lucas-Picher et al.* (2011) for the South Asia region which demonstrated that RCMs were able to capture the monsoon.

HadRM3 is driven by boundary data from the two GCMs (Fig. 3.2) to provide 25 km resolution regional climate modelling of the Indian sub-continent (25° N, 79° E–32° N, 88° E) for the period 1960–2100. These RCM simulations are from the EU-HighNoon project (referred to hereafter as HNRCMs), representing currently the finest resolution climate modelling available for this region (*Mathison et al.*, 2013, *Moors et al.*, 2011, *Kumar et al.*, 2013).

The HNRCMs use the SRES A1B scenario which represents a future world of very rapid economic growth, global population that peaks in mid-century and declines thereafter, and rapid introduction of new and more efficient technologies. The A1B scenario specifically, represents this future world where there is balance across energy sources i.e. a mixture of fossil and non-fossil fuels (*Nakicenovic et al.*, 2000).

3.7 Appendix B: Comparing observed sowing and harvest dates with estimates of monsoon onset and retreat

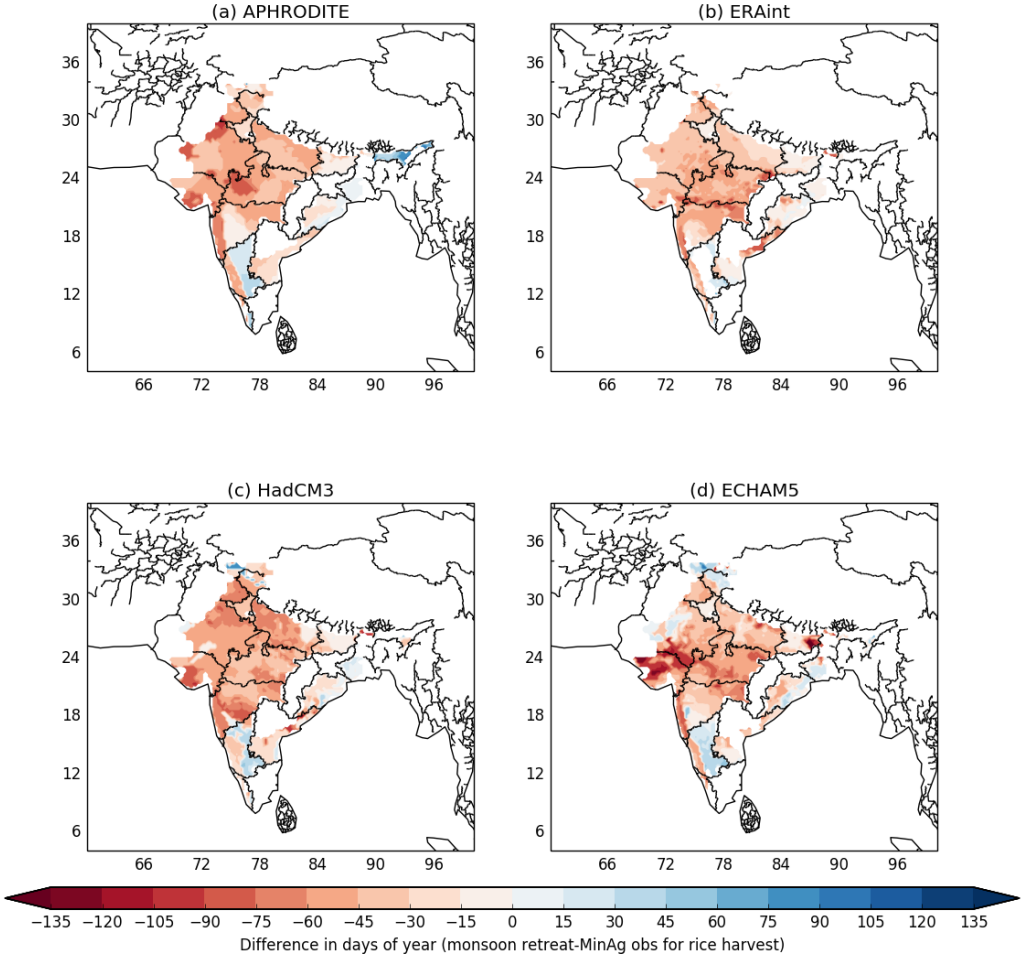

Figure B.1: The difference between the midpoint of the monsoon retreat in the model and the midpoint of the observed rice harvest period for 1990–2007.

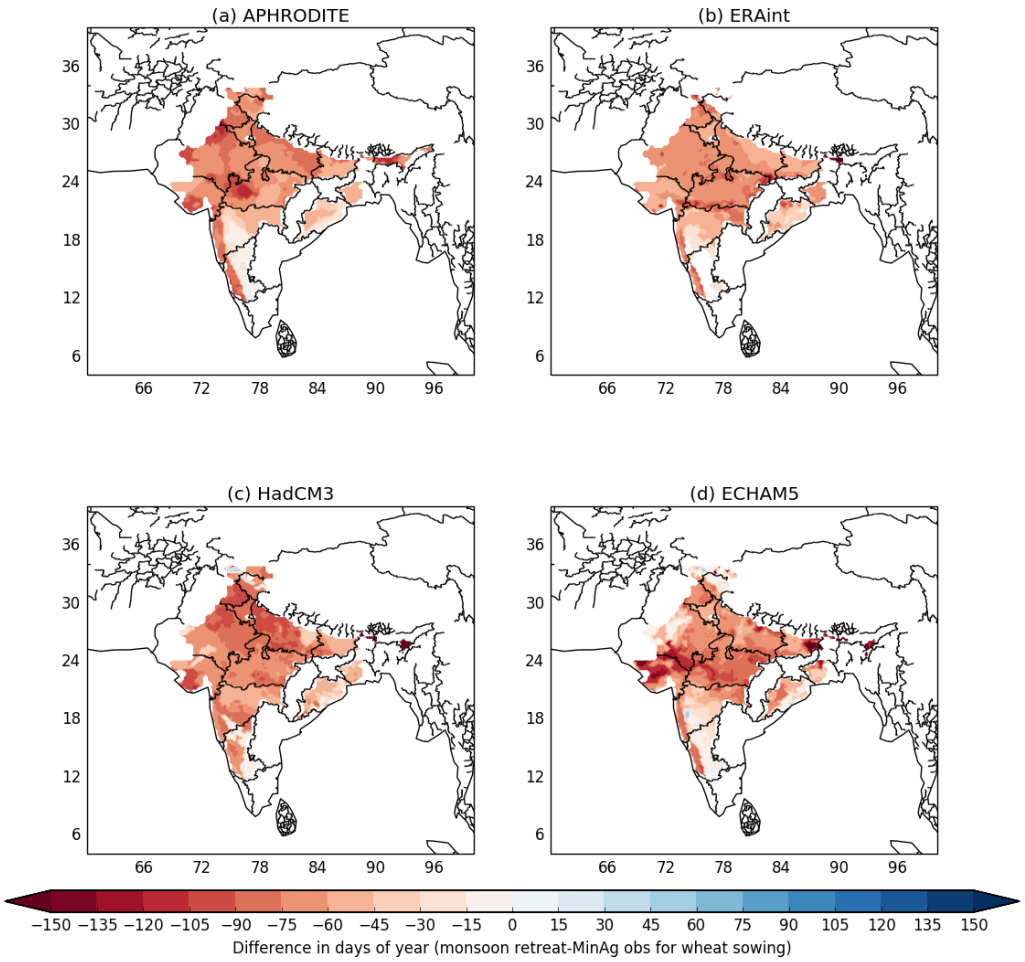

Figure B.2: The difference between the midpoint of the monsoon retreat in the model and the midpoint of the observed wheat sowing period for 1990–2007.

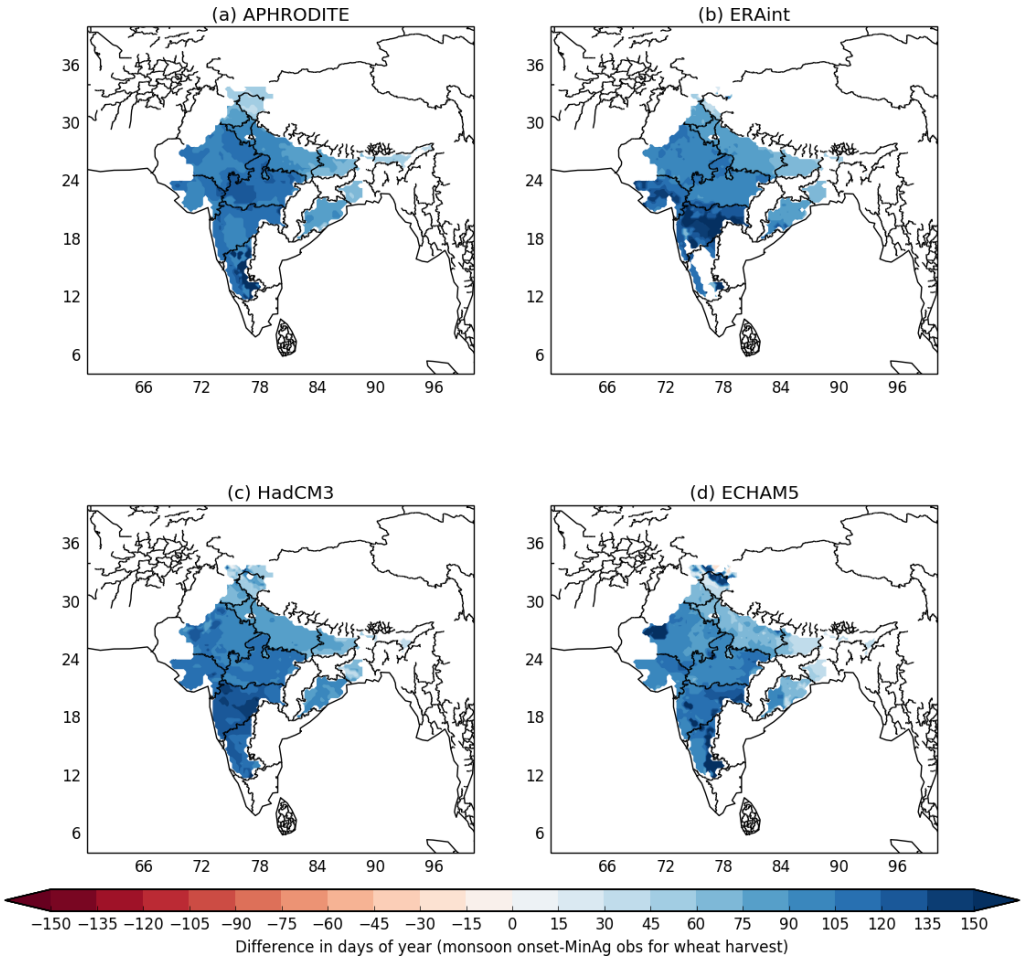

Figure B.3: The difference between the midpoint of the monsoon onset in the model and the midpoint of the observed wheat harvest period for 1990–2007.

3.8 Appendix C: Monsoon derived estimates of sow/harvest dates for rice and wheat

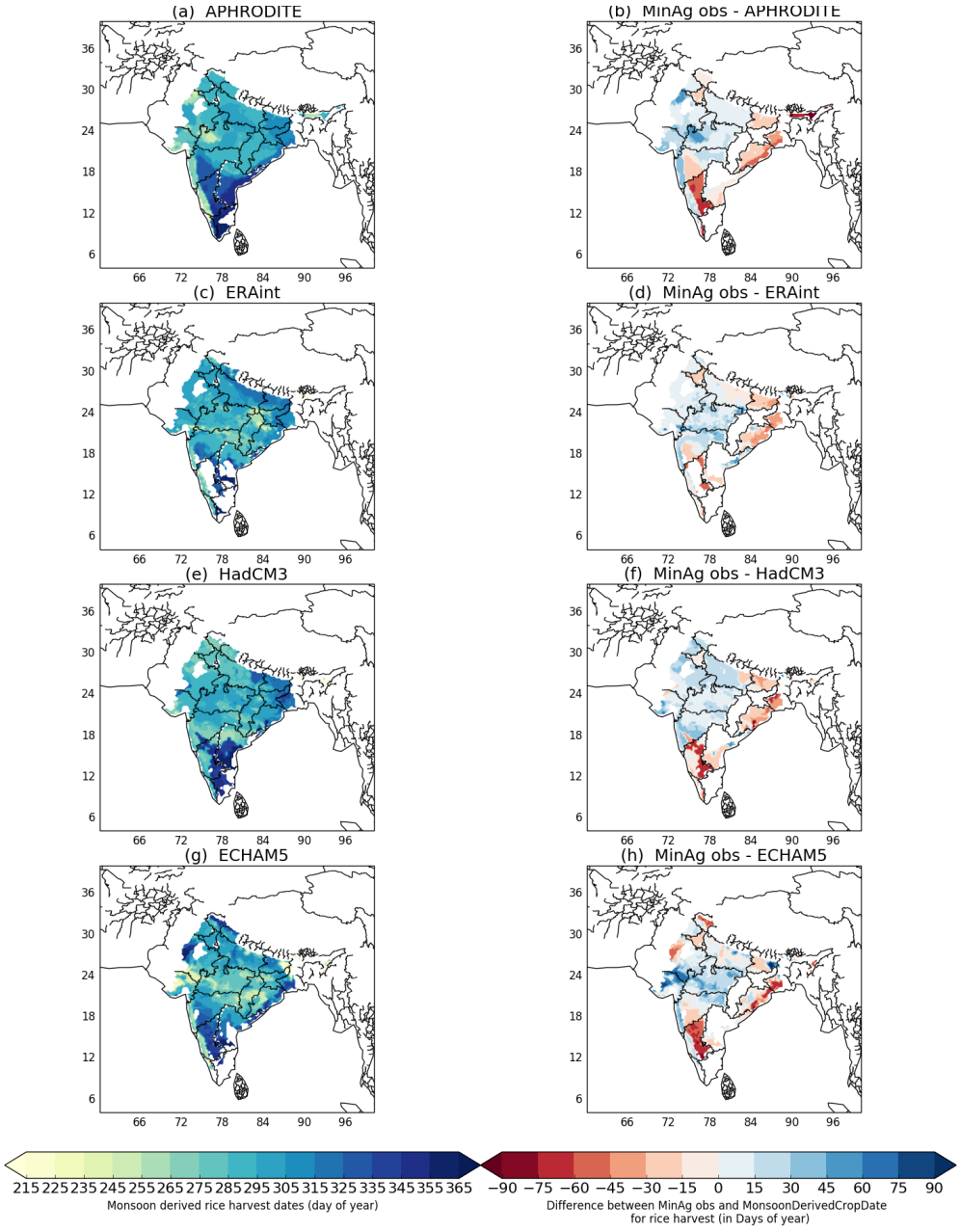

Figure C.1: The monsoon derived rice harvest dates (left) and the difference between the MinAg observations and the monsoon derived rice harvest dates (right) for the period 1990–2007.

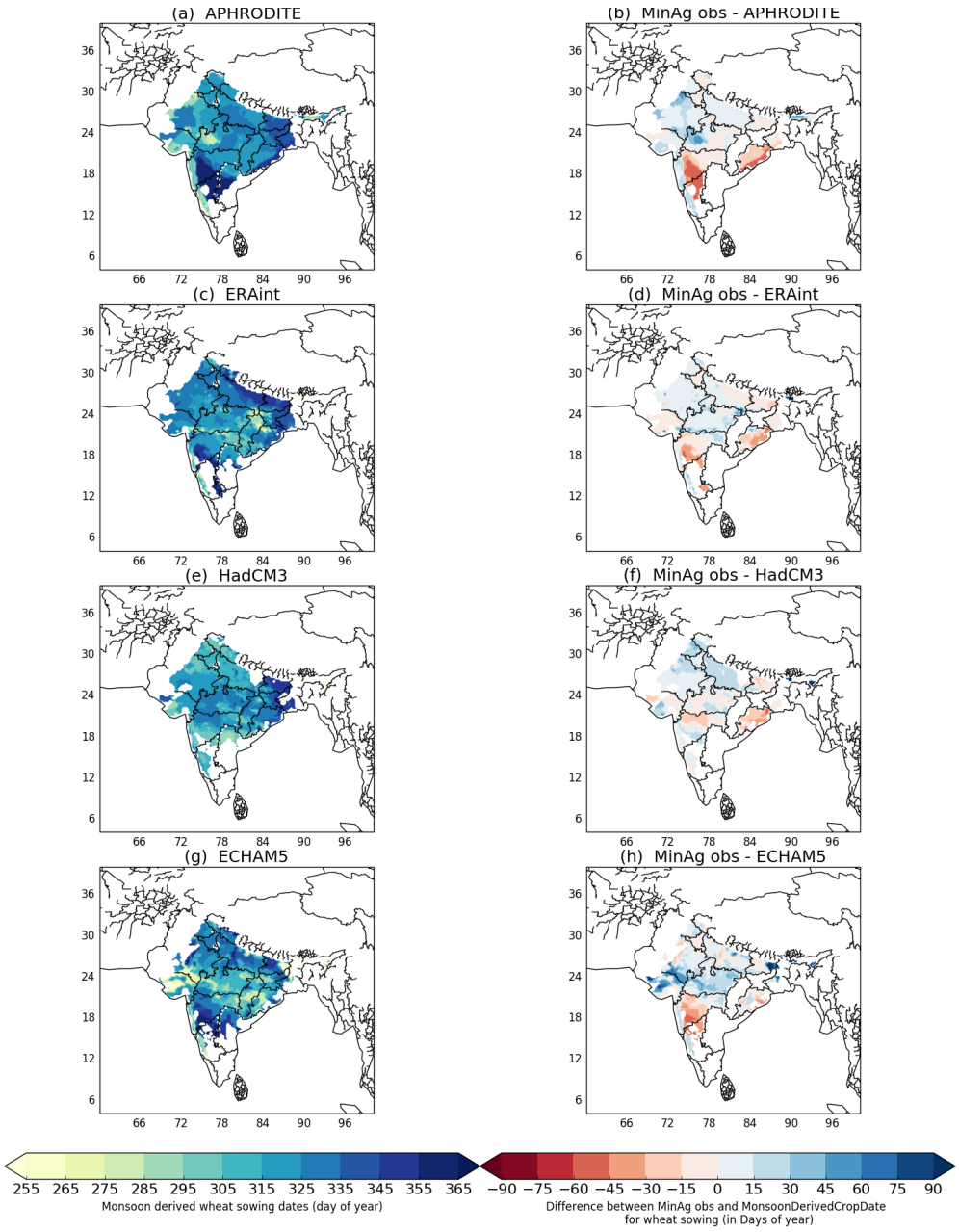

Figure C.2: The monsoon derived wheat sowing dates (left) and the difference between the MinAg observations and the monsoon derived wheat sowing dates (right) for the period 1990–2007.

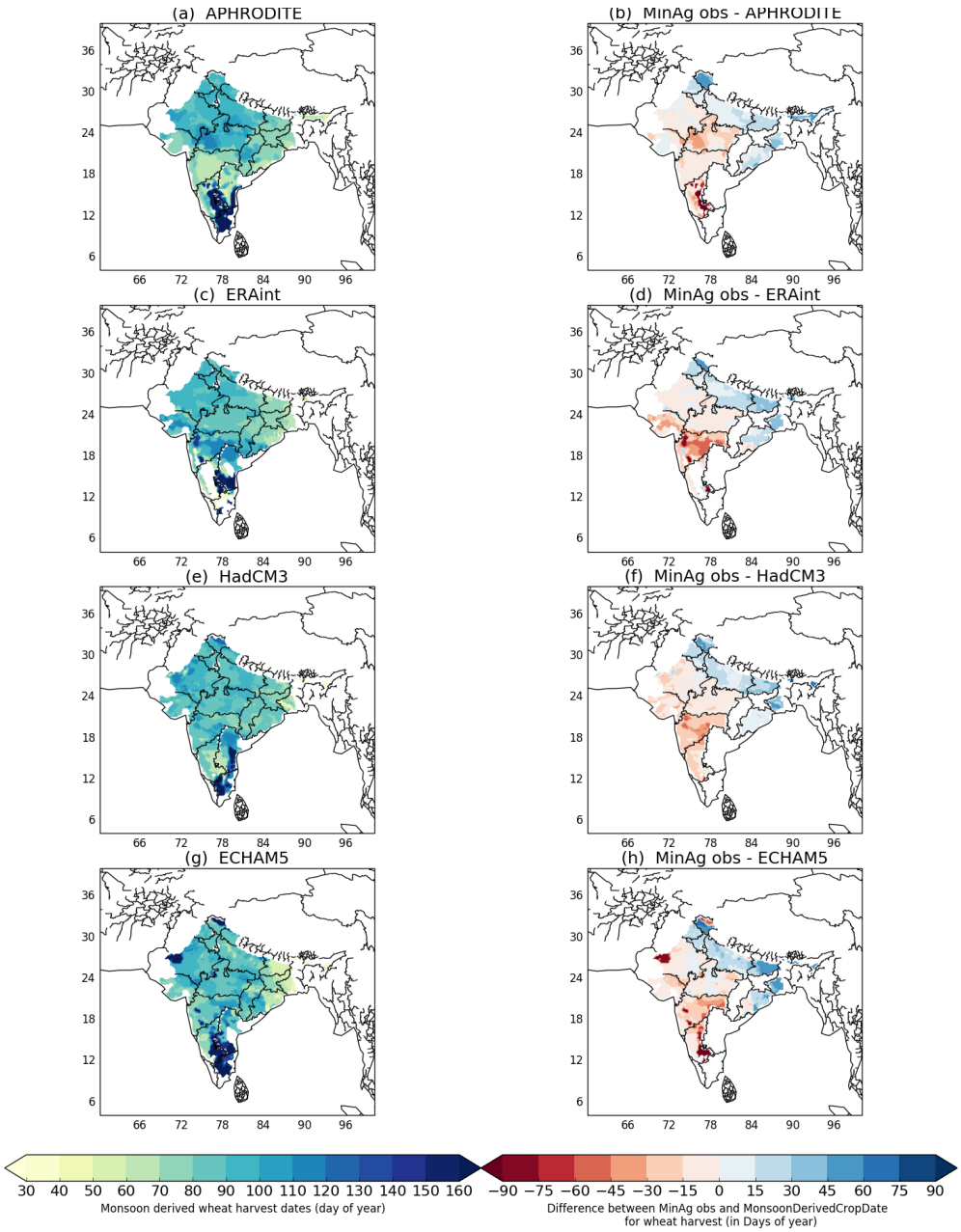

Figure C.3: The monsoon derived wheat harvest dates (left) and the difference between the MinAg observations and the monsoon derived wheat harvest dates (right) for the period 1990–2007.

3.9 Appendix D: Analysis of future monsoon onset and retreat

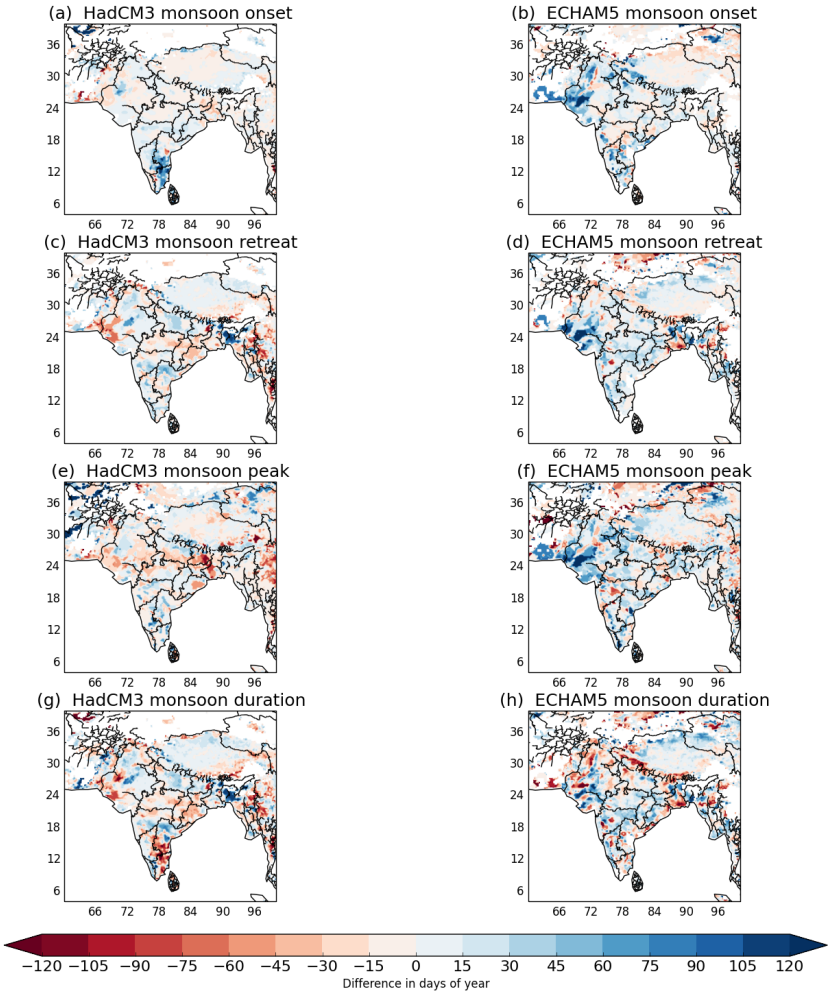

Figure D.1: The difference between the monsoon statistics for the 2080–2097 future period compared with the present day 1990–2007 for HadCM3 (left) and ECHAM5 (right).

References

Anbumozhi, V., K. Matsumoto, and E. Yamaji (2001), Sustaining agriculture through modernization of irrigation tanks: An opportunity and challenge for Tamilnadu, India, *Agricultural Engineering International, vol. III (2001)*, 1–11. 3.4.1

Annamalai, H., K. Hamilton, and K. Sperber (2007), The South Asian summer monsoon and its relationship with ENSO in the IPCC AR4 simulations, *Journal of Climate*, *20*(6), 1071–1092, doi:10.1175/JCLI4035.1. 3.6

Bodh, S. P. C., S. J. P. Rai, S. A. Sharma, S. P. Gajria, S. M. Yadav, S. S. Virmani, and S. R. Pandey (2015), Agricultural statistics at a glance 2015, *Ministry of Agriculture & Farmers welfare, Directorate of Economics and Statistics*. (document), 3.1.1, 3.1, 3.2.1, 3.3.2

Cannell, M. G. R., and R. I. Smith (1983), Thermal time, chill days and prediction of budburst in picea sitchensis, *Journal of Applied Ecology*, *20*(3), 951–963. 3.1.1

Challinor, A., T. Wheeler, P. Craufurd, J. Slingo, and D. Grimes (2004), Design and optimisation of a large-area process-based model for annual crops, *Agricultural and Forest Meteorology*, *124*(1-2), 99–120, doi:10.1016/j.agrformet.2004.01.002. 3.1, 3.1.1

Challinor, A. J., J. M. Slingo, T. R. Wheeler, P. Q. Craufurd, and D. I. F. Grimes (2003), Toward a combined seasonal weather and crop productivity forecasting system: Determination of the working spatial scale, *Journal of Applied Meteorology and Climatology*, *42*, 175–192. 3.1.1

Challinor, A. J., C. Müller, S. Asseng, C. Deva, K. J. Nicklin, D. Wallach, E. Vanuytrecht, S. Whitfield, J. Ramirez-Villegas, and A.-K. Koehler (2018), Improving the use of crop models for risk assessment and climate change adaptation, *Agricultural Systems*, *159*, 296–306, doi:10.1016/j.agsy.2017.07.010. 3.1

Christensen, J., B. Hewitson, A. Busuioc, A. Chen, X. Gao, I. Held, R. Jones, R. Kolli, W.-T. Kwon, R. Laprise, V. M. na Rueda, L. Mearns, C. Menendez, J. Räisänen, A. Rinke, A. Sarr, and P. Whetton (2007), Regional climate projections. in: Climate change 2007: The physical science basis. contribution of working group i, *Fourth Assessment Report of the Intergovernmental Panel on Climate Change*. 3.6

Christensen, J., K. Krishna-Kumar, E. Aldrian, S.-I. An, I. Cavalcanti, M. de Castro, W. Dong, P. Goswami, A. Hall, J. Kanyanga, A. Kitoh, J. Kossin, N.-C. Lau, J. Renwick, D. Stephenson, S.-P. Xie, and T. Zhou (2013), *Climate Phenomena and their Relevance for Future Regional Climate Change*, book section 14, pp. 1217–1308, Cambridge University Press, doi:10.1017/CBO9781107415324.028. 3.2.4, 3.4.2

Dhar, O. N., P. R. Rakhecha, and A. K. Kulkarni (1982), Fluctuations in northeast monsoon rainfall of tamil nadu, *Journal of Climatology*, *2*(4), 339–345, doi:10.1002/joc.3370020404. 3.4.1

Elliott, J., C. Müller, D. Deryng, J. Chryssanthacopoulos, K. Boote, M. Büchner, I. Foster, M. Glotter, J. Heinke, T. Iizumi, R. C. Izaurralde, N. D. Mueller, D. K. Ray, C. Rosenzweig, A. C. Ruane, and J. Sheffield (2015), The global gridded crop

model intercomparison: data and modeling protocols for phase 1 (v1.0), *Geoscientific Model Development*, *8*(2), 261–277, doi:10.5194/gmd-8-261-2015. 3.1

Erenstein, O., and V. Laxmi (2008), Zero tillage impacts in india's rice-wheat systems: A review, *Soil and Tillage Research*, *100*, 1–14, doi:10.1016/j.still.2008.05.001. 3.1

Erenstein, O., U. Farooq, R. Malik, and M. Sharif (2008), On-farm impacts of zero tillage wheat in south asia's rice-wheat systems, *Field Crops Research*, *105*(3), 240–252, doi:10.1016/j.fcr.2007.10.010. 3.1

Essery, R. L. H., M. J. Best, and P. M. Cox (2001), Moses 2.2 technical documentation, *Hadley Centre Technical Note*, *30*. 3.6

Essery, R. L. H., M. J. Best, R. A. Betts, P. M. Cox, and C. Taylor (2003), Explicit representation of subgrid heterogeneity in a GCM land surface scheme, *Journal of Hydrometeorology*, *4*, 530–543. 3.6

Frieler, K., S. Lange, F. Piontek, C. P. O. Reyer, J. Schewe, L. Warszawski, F. Zhao, L. Chini, S. Denvil, K. Emanuel, T. Geiger, K. Halladay, G. Hurtt, M. Mengel, D. Murakami, S. Ostberg, A. Popp, R. Riva, M. Stevanovic, T. Suzuki, J. Volkholz, E. Burke, P. Ciais, K. Ebi, T. D. Eddy, J. Elliott, E. Galbraith, S. N. Gosling, F. Hattermann, T. Hickler, J. Hinkel, C. Hof, V. Huber, J. Jägermeyr, V. Krysanova, R. Marcé, H. Müller Schmied, I. Mouratiadou, D. Pierson, D. P. Tittensor, R. Vautard, M. van Vliet, M. F. Biber, R. A. Betts, B. L. Bodirsky, D. Deryng, S. Frolking, C. D. Jones, H. K. Lotze, H. Lotze-Campen, R. Sahajpal, K. Thonicke, H. Tian, and Y. Yamagata (2017), Assessing the impacts of $1.5°c$ global warming – simulation protocol of the inter-sectoral impact model intercomparison project (isimip2b), *Geoscientific Model Development*, *10*(12), 4321–4345, doi:10.5194/gmd-10-4321-2017. 3.1

Gohar, L., J. Lowe, and D. Bernie (2017), The impact of bias correction and model selection on passing temperature thresholds, *Journal of Geophysical Research: Atmospheres*, *122*(22), 12,045–12,061, doi:10.1002/2017JD026797, 2017JD026797. 3.2.4

Gordon, C., C. Cooper, C. A. Senior, H. Banks, J. M. Gregory, T. C. Johns, J. F. B. Mitchell, and R. A. Wood (2000), The simulation of sst, sea ice extents and ocean heat transports in a version of the hadley centre coupled model without flux adjustments, *Climate Dynamics*, *16*(2-3), 147–168, doi:10.1007/s003820050010. 3.6

Hodson, D., and J. White (2007), Paper presented at international workshop on increasing wheat yield potential, cimmyt, obregon, mexico, 20-24 march 2006 use of spatial analyses for global characterization of wheat-based production systems, *The Journal of Agricultural Science*, *145*(2), 115–125, doi:10.1017/S0021859607006855. 3.1.1

Huffman, G. J., R. F. Adler, M. M. Morrissey, D. T. Bolvin, S. Curtis, R. Joyce, B. McGavock, and J. Susskind (2001), Global precipitation at one-degree daily resolution from multisatellite observations, *Journal of Hydrometeorology*, *2*(1), 36–50, doi:10.1175/1525-7541(2001)002¡0036:GPAODD¿2.0.CO;2. 3.2.2

ICRISAT (2015), District Level Database Documentation, *Tech. rep.*, International Crops Research Institute for the Semi-Arid Tropics, Hyderabad. 3.2.1, 3.2.3.1

Jat, R. K., T. B. Sapkota, R. G. Singh, M. Jat, M. Kumar, and R. K. Gupta (2014), Seven years of conservation agriculture in a rice-wheat rotation of eastern gangetic plains of south asia: Yield trends and economic profitability, *Field Crops Research*, *164*, 199 – 210, doi:10.1016/j.fcr.2014.04.015. 3.1

Jones, R. G., M. Noguer, D. C. Hassell, D. Hudson, S. S. Wilson, G. J. Jenkins, and J. F. Mitchell (2004), Generating high resolution climate change scenarios using PRECIS, *Met Office Hadley Centre, Exeter, UK*, pp. 0–40. 3.6

Joshi, A., G. Ortiz-Ferrara, J. Crossa, G. Singh, R. Sharma, R. Chand, and R. Parsad (2007), Combining superior agronomic performance and terminal heat tolerance with resistance to spot blotch (bipolaris sorokiniana) of wheat in the warm humid gangetic plains of south asia, *Field Crops Research*, *103*(1), 53–61, doi:10.1016/j.fcr.2007.04.010. 3.1

Kotera, A., K. D. Nguyen, T. Sakamoto, T. Iizumi, and M. Yokozawa (2014), A modeling approach for assessing rice cropping cycle affected by flooding, salinity intrusion, and monsoon rains in the mekong delta, vietnam, *Paddy and Water Environment*, *12*(3), 343–354, doi:10.1007/s10333-013-0386-y. 3.1

Kumar, P., A. Wiltshire, C. Mathison, S. Asharaf, B. Ahrens, P. Lucas-Picher, J. H. Christensen, A. Gobiet, F. Saeed, S. Hagemann, and D. Jacob (2013), Downscaled climate change projections with uncertainty assessment over India using a high resolution multi-model approach, *Science of The Total Environment*, *468-469, Supplement*(0), S18–S30, doi:10.1016/j.scitotenv.2013.01.051, changing water resources availability in Northern India with respect to Himalayan glacier retreat and changing monsoon patterns: consequences and adaptation. 3.6

Laik, R., S. Sharma, M. Idris, A. Singh, S. Singh, B. Bhatt, Y. Saharawat, E. Humphreys, and J. Ladha (2014), Integration of conservation agriculture with best management practices for improving system performance of the rice-wheat rotation in the eastern indo-gangetic plains of india, *Agriculture, Ecosystems & Environment*, *195*, 68–82, doi:10.1016/j.agee.2014.06.001. 3.1

Laux, P., H. Kunstmann, and A. Bardossy (2008), Predicting the regional onset of the rainy season in west africa, *International Journal of Climatology*, *28*(3), 329–342, doi:10.1002/joc.1542. 3.1

Laux, P., G. Jaeckel, R. M. Tingem, and H. Kunstmann (2010), Impact of climate change on agricultural productivity under rainfed conditions in cameroon - a method to improve attainable crop yields by planting date adaptations, *Agricultural and Forest Meteorology*, *150*(9), 1258–1271, doi:10.1016/j.agrformet.2010.05.008. 3.1

Lobell, D. B. (2014), Climate change adaptation in crop production: Beware of illusions, *Global Food Security*, *3*(2), 72–76, doi:10.1016/j.gfs.2014.05.002. 3.1

Lucas-Picher, P., J. H. Christensen, F. Saeed, P. Kumar, S. Asharaf, B. Ahrens, A. J. Wiltshire, D. Jacob, and S. Hagemann (2011), Can regional climate models represent the Indian monsoon?, *Journal of Hydrometeorology*, *12*, 849–868, doi:10.1175/2011JHM1327.1. 3.2.2, 3.2.2, 3.6

Martin, G., K. Arpe, F. Chauvin, L. Ferranti, K. Maynard, J. Polcher, D. Stephenson, and P. Tschuck (2000), Simulation of the asian summer monsoon in five european general circulation models, *Atmospheric Science Letters*, *1*(1), 37–55, doi:10.1006/asle.2000.0004. 3.2.2

Mathison, C., A. Wiltshire, A. Dimri, P. Falloon, D. Jacob, P. Kumar, E. Moors, J. Ridley, C. Siderius, M. Stoffel, and T. Yasunari (2013), Regional projections of North Indian climate for adaptation studies, *Science of The Total Environment*, *468-469, Supplement*(0), S4–S17, doi:10.1016/j.scitotenv.2012.04.066. 3.6

Mathison, C., A. J. Wiltshire, P. Falloon, and A. J. Challinor (2015), South asia river-flow projections and their implications for water resources, *Hydrology and Earth System Sciences*, *19*(12), 4783–4810, doi:10.5194/hess-19-4783-2015. 3.2, 3.2.1, 3.6

McMaster, G. S., and W. W. Wilhelm (1997), Growing degree-days: one equation, two interpretations, *Agricultural and Forest Meteorology*, *87*(4), 291–300, doi:10.1016/S0168-1923(97)00027-0. 3.1.1

Met Office (2018), *Iris: A Python library for analysing and visualising meteorological and oceanographic data sets*, Exeter, Devon, v2.0 ed. 3.2.3.1

Moors, E. J., A. Groot, H. Biemans, C. T. van Scheltinga, C. Siderius, M. Stoffel, C. Huggel, A. Wiltshire, C. Mathison, J. Ridley, D. Jacob, P. Kumar, S. Bhadwal, A. Gosain, and D. N. Collins (2011), Adaptation to changing water resources in the Ganges basin, northern India, *Environmental Science & Policy*, *14*(7), 758–769, doi:10.1016/j.envsci.2011.03.005, adapting to Climate Change: Reducing Water-related Risks in Europe. 3.6

Moron, V., and A. W. Robertson (2014), Interannual variability of indian summer monsoon rainfall onset date at local scale, *International Journal of Climatology*, *34*(4), 1050–1061, doi:10.1002/joc.3745. 3.2.2

Nakicenovic, N., J. Alcamo, A. Grubler, K. Riahi, R. Roehrl, H.-H. Rogner, and N. Victor (2000), Special report on emissions scenarios (SRES), *A Special Report of Working Group III of the Intergovernmental Panel on Climate Change*, Last access April 2017editor:Nebojsa Nakicenovic and Rob Swart. 3.6

Osborne, T., J. Gornall, J. Hooker, K. Williams, A. Wiltshire, R. Betts, and T. Wheeler (2015), Jules-crop: a parametrisation of crops in the joint uk land environment simulator, *Geoscientific Model Development*, *8*(4), 1139–1155, doi:10.5194/gmd-8-1139-2015. 3.1.1

Pope, V., M. L. Gallani, P. R. Rowntree, and R. A. Stratton (2000), The impact of new physical parametrizations in the hadley centre climate model: Hadam3, *Climate Dynamics*, *16*(2-3), 123–146, doi:10.1007/s003820050009. 3.6

Portmann, F. T., S. Siebert, and P. Döll (2010), Mirca2000-global monthly irrigated and rainfed crop areas around the year 2000: A new high-resolution data set for agricultural and hydrological modeling, *Global Biogeochemical Cycles*, *24*(1), doi:10.1029/2008GB003435, gB1011. 3.1

Rivington, M., and J. Koo (2010), Report on the meta-analysis of crop modelling for climate change and food security survey, *Climate Change, Agriculture and Food Security Challenge Program of the CGIAR*. 3.1

Roeckner, E., G. Bäuml, L. Bonaventura, R. Brokopf, M. Esch, M. Giorgetta, S. Hagemann, I. Kirchner, L. Kornblueh, E. Manzini, A. Rhodin, U. Schlese, U. Schulzweida, and A. Tompkins (2003), The atmospheric general circulation model ECHAM 5. PART I: Model description, *Max Planck Institute for Meteorology Rep. 349*. 3.6

Rosenzweig, C., J. Jones, J. Hatfield, A. Ruane, K. Boote, P. Thorburn, J. Antle, G. Nelson, C. Porter, S. Janssen, S. Asseng, B. Basso, F. Ewert, D. Wallach, G. Baigorria, and J. Winter (2013), The agricultural model intercomparison and improvement project (agmip): Protocols and pilot studies, *Agricultural and Forest Meteorology*, *170*, 166–182, doi:10.1016/j.agrformet.2012.09.011, agricultural prediction using climate model ensembles. 3.1, 3.4

Rosenzweig, C., J. Elliott, D. Deryng, A. C. Ruane, C. Müller, A. Arneth, K. J. Boote, C. Folberth, M. Glotter, N. Khabarov, K. Neumann, F. Piontek, T. A. M. Pugh, E. Schmid, E. Stehfest, H. Yang, and J. W. Jones (2014), Assessing agricultural risks of climate change in the 21st century in a global gridded crop model intercomparison, *Proceedings of the National Academy of Sciences*, *111*(9), 3268–3273, doi:10.1073/pnas.1222463110. 3.1, 3.4

Sacks, W. J., D. Deryng, J. A. Foley, and N. Ramankutty (2010), Crop planting dates: an analysis of global patterns, *Global Ecology and Biogeography*, *19*(5), 607–620. (document), 3.1, 3.1.1, 3.1, 3.2.1, 3.5

Sharma, B., and H. Sharma (2015), Status of rice production in assam, india, *Journal of Rice Research: Open Access*, *3*(4), 3–e121, doi:10.4172/2375-4338.1000e121. 3.3.2

Singh, D. K., P. Kumar, and A. K. Bhardwaj (2014), Evaluation of agronomic management practices on farmers' fields under rice-wheat cropping system in northern india, *International Journal of Agronomy*, *2014*, 5, doi:10.1155/2014/740656. 3.1

Sperber, K. R., H. Annamalai, I.-S. Kang, A. Kitoh, A. Moise, A. Turner, B. Wang, and T. Zhou (2013), The asian summer monsoon: an intercomparison of cmip5 vs. cmip3 simulations of the late 20th century, *Climate Dynamics*, *41*(9), 2711–2744, doi:10.1007/s00382-012-1607-6. 3.2.2, 3.2.2

van Bussel, L. G. J., E. Stehfest, S. Siebert, C. Müller, and F. Ewert (2015), Simulation of the phenological development of wheat and maize at the global scale, *Global Ecology and Biogeography*, *24*(9), 1018–1029, doi:10.1111/geb.12351. 3.1

Waha, K., L. G. J. van Bussel, C. Müller, and A. Bondeau (2012), Climate-driven simulation of global crop sowing dates, *Global Ecology and Biogeography*, *21*(2), 247–259, doi:10.1111/j.1466-8238.2011.00678.x. 3.1

Waha, K., C. Müller, A. Bondeau, J. Dietrich, P. Kurukulasuriya, J. Heinke, and H. Lotze-Campen (2013), Adaptation to climate change through the choice of cropping system and sowing date in sub-saharan africa, *Global Environmental Change*, *23*(1), 130–143, doi:10.1016/j.gloenvcha.2012.11.001. 3.1, 3.4.2

Waongo, M., P. Laux, S. B. Traore, M. Sanon, and H. Kunstmann (2014), A crop model and fuzzy rule based approach for optimizing maize planting dates in burkina faso, west africa, *Journal of Applied Meteorology and Climatology*, *53*(3), 598–613, doi:10.1175/JAMC-D-13-0116.1. 3.1

Warszawski, L., A. Friend, S. Ostberg, K. Frieler, W. Lucht, S. Schaphoff, D. Beerling, P. Cadule, P. Ciais, D. B. Clark, R. Kahana, A. Ito, R. Keribin, A. Kleidon, M. Lomas, K. Nishina, R. Pavlick, T. T. Rademacher, M. Buechner, F. Piontek, J. Schewe, O. Serdeczny, and H. J. Schellnhuber (2013), A multi-model analysis of risk of ecosystem shifts under climate change, *Environmental Research Letters*, *8*(4), 044,018. 3.1, 3.4

Warszawski, L., K. Frieler, V. Huber, F. Piontek, O. Serdeczny, and J. Schewe (2014), The inter-sectoral impact model intercomparison project (isi-mip):project framework, *Proceedings of the National Academy of Sciences*, *111*(9), 3228–3232, doi:10.1073/pnas.1312330110. 3.1, 3.4

Yan, L., G. Li, M. Yu, T. Fang, S. Cao, and B. F. Carver (2015), *Genetic Mechanisms of Vernalization Requirement Duration in Winter Wheat Cultivars*, pp. 117–125, Springer Japan, doi:10.1007/978-4-431-55675-6_13. 3.1.1

Yatagai, A., K. Kamiguchi, O. Arakawa, A. Hamada, N. Yasutomi, and A. Kitoh (2012), Aphrodite: constructing a long-term daily gridded precipitation dataset for asia based on a dense network of rain gauges., *Bulletin of the American Meteorological Society*, *93*, 1401–1415, doi:10.1175/BAMS-D-11-00122.1. 3.2.1, 3.2.2.1

Chapter 4

Developing a Sequential cropping capability in JULESvn5.2

Camilla T. Mathison[1,2], Andrew J. Challinor[2], Chetan Deva[2], Pete Falloon[1], Sëbastien Garrigues[3,4], Sophie Moulin[3,4] , Karina Williams[1] and Andy J. Wiltshire [1]

[1] *Met Office Hadley Centre, FitzRoy Road, Exeter, EX1 3PB, UK*
[2] *School of Earth and Environment, Institute for Climate and Atmospheric Science, University of Leeds, Leeds, LS2 9AT, UK*
[3] *EMMAH (UMR1114), INRA, Avignon, France*
[4] *Université d'Avignon et des Pays de Vaucluse, UMR1114 – EMMAH, 84000 Avignon, France*

Sequential cropping (also known as multiple or double cropping) is common in tropical regions, where the crop seasons are largely dictated by the main wet season. The Asian summer monsoon (ASM) provides the water resources for crops grown for the whole year, thereby influencing crop production outside the ASM period. Land surface models (LSMs) typically simulate a single crop per year. However, in order to understand how sequential cropping influences demand for resources, we simulate all of the crops grown within a year in a seamless way. In this paper we implement sequential cropping in a branch of the Joint UK Land Environment Simulator (JULES) and demonstrate its use at Avignon, a site that uses the sequential cropping system. Avignon provides over 15-years of continuous flux observations which we use to evaluate JULES with sequential cropping. In order to implement the method in future regional simulations where there may be large variations in growing conditions, we apply the same method to four locations in the North Indian states of Uttar Pradesh and Bihar to simulate the rice–wheat rotation and compare model yields to observations at these locations. The results show that JULES is able to simulate sequential cropping at Avignon and the four India locations, representing both crops within one growing

season in each of the crop rotations presented. At Avignon the maxima of LAI, above ground biomass and canopy height occur at approximately the correct time for both crops. The magnitudes of biomass, especially for winter wheat, are underestimated and the leaf area index is overestimated. The JULES fluxes are a good fit to observations (r-values greater than 0.7), either using grasses to represent crops or the crop model, implying that both approaches represent the surface coverage correctly. For the India simulations, JULES successfully reproduces observed yields for the eastern locations; however, yields are under estimated for the western locations. This development is a step forward in the ability of JULES to simulate crops in tropical regions, where this cropping system is already prevalent. It also provides the opportunity to assess the potential for other regions to implement sequential cropping as an adaptation to climate change.

4.1 Introduction

Climate change is likely to impact all aspects of crop production affecting plant growth, development and crop yield (*Hatfield and Prueger*, 2015) as well as cropping area and cropping intensity (*Iizumi and Ramankutty*, 2015). The impact of climate change on agriculture has been the focus of several large collaborative projects such as the Agricultural Model Intercomparison and Improvement Project (AgMIP; *Rivington and Koo*, 2010, *Rosenzweig et al.*, 2013, 2014) and the Inter-Sectoral Impact Model Intercomparison Project (*Warszawski et al.*, 2013, 2014; ISIMIP;). These projects have highlighted the likelihood of competition between crops grown for food and those grown for bio-energy in order to mitigate climate change (*Frieler et al.*, 2015). *Petrie et al.* (2017) discuss how the use of sequential cropping systems may have made it possible for populations in some areas to adapt to large changes in monsoon rainfall between 2200–2100 BC. These ancient agricultural practices are common today across most tropical countries but may also be a useful adaptation, especially where traditionally mono-crop systems are currently used, in order to meet a future rising demand for food (*Hudson*, 2009) or the demand for bio-fuels. This sort of adaptation is already happening in some locations. *Mueller et al.* (2015) show that longer growing seasons in the extratropics have made the cultivation of multiple crops in a year at northern latitudes more viable. Warmer spring temperatures in the Brahmaputra catchment have allowed earlier planting of a winter crop, leaving time for a second crop (*Zhang et al.*, 2013).

Intercropping or sequential cropping allow farmers to make the most efficient use of limited resources and space in order to maximize yield potential and lower the risk of complete crop failure. These techniques also influence ground cover, soil erosion and chemical properties, albedo and pest infestation (*Waha et al.*, 2013). Intercropping is the simultaneous cultivation of multiple crop species in a single field (*Cong et al.*, 2015) while sequential cropping (also called multiple or double cropping) involves growing two

or more crops on the same field in a given year (*Liu et al.*, 2013, *Waha et al.*, 2013). We use the term sequential cropping from here on to avoid confusion with other cropping systems. Sequential cropping systems are common in Brazil where the soybean–maize or soybean–cotton rotations are used (*Pires et al.*, 2016) and for South Asia where the rice–wheat systems are the most extensive, dominating in many Indian states (*Mahajan and Gupta*, 2009), across the Indo-Gangetic Plain (IGP) (*Erenstein and Laxmi*, 2008) and Pakistan (*Erenstein et al.*, 2008). States such as Punjab, Haryana, Bihar, Uttar Pradesh and Madhya Pradesh (*Mahajan and Gupta*, 2009) account for approximately 75 % of national food grain production for India. Rice-rice rotations are the second most prevalent crop rotation to rice-wheat rotations, these are typically found in the north eastern regions of India and Bangladesh (*Sharma and Sharma*, 2015) with some regions cultivating as many as three rice crops per year. The South Asia economy is highly dependent on the agricultural industry and other industries also with a high demand for water (*Mathison et al.*, 2015). The most important source of water for this part of the world is the Asian Summer Monsoon (ASM), which typically occurs between June and September (*Goswami and Xavier*, 2005); this phenomenon provides most of the water resource for any given year. The South Asia crop calendar is defined by the ASM which therefore has an important influence on the productivity across the whole year (*Mathison et al.*, 2018) and therefore on crop production outside the Monsoon period.

The modelling of crop rotations is a common feature in soil carbon simulations (*Bhattacharyya et al.*, 2007). *Bhattacharyya et al.* (2007) found that the rice–wheat rotation, common across the IGP, has helped maintain carbon stocks. However, in recent years, the yields of rice and wheat have plateaued, leading farmers to diversify and include other additional crops in the rotation, potentially depleting carbon stocks. The modelling of crop rotations has also been common in the field of agricultural economics with work regarding sequential cropping being mainly to understand influences on decision-making; therefore focusing on short timescales and at the farm management level (*Dury et al.*, 2012, *Caldwell and Hansen*, 1993).

Many dynamic global vegetation models (DGVMs), commonly used to study the effects of climate change, simulate a single crop per year, both for individual sites and gridded simulations. This may be due in part to some global observation datasets such as *Sacks et al.* (2010) reporting only one growing period per year for most crops (*Waha et al.*, 2012). MIRCA2000 (*Portmann et al.*, 2010) include different cropping calendars for different regions; however, rice and wheat are divided equally between the kharif and rabi seasons, when in reality wheat is only grown during the rabi season (*Biemans et al.*, 2016).

Waha et al. (2013) extend the LundPotsdamJena managed Land model (LPJml-*Bondeau et al.*, 2007) to consider sequential cropping in Africa for two different crops. LPJml is able to simulate sequential cropping in monoculture systems such as the rice–

rice system grown in Bangladesh (*Sharma and Sharma*, 2015). In order to implement sequential cropping in LPJml, *Waha et al.* (2013) specify different growing season periods for each crop in the rotation, where the growing period is given by the sum of the daily temperatures above a crop specific temperature threshold. They also specify the onset of the main rainy season as the start of the growing season using the *Waha et al.* (2012) method. *Waha et al.* (2013) find that when considering the impact of climate change, the type of cropping system is important because yields differ between crops and cropping systems. *Biemans et al.* (2016) also use a version of LPJml, refined for South Asia, to estimate water demand and crop production for South Asia. *Biemans et al.* (2016) simulate sequential cropping by combining the output from two simulations with different kharif and rabi land-use maps and zonal sowing and harvest dates based on observed monsoon patterns. *Biemans et al.* (2016) find that accounting for the use of sequential cropping in this South Asia version of LPJml improved the simulations of the demand for water from irrigation, particularly the timing of the demand. There are few land-surface models that are able to simulate sequential cropping but both *Waha et al.* (2013) and *Biemans et al.* (2016) have highlighted its importance in their simulations. It would be beneficial for more land-surface models to develop the capability to simulate different cropping systems and link crop production with irrigation both to improve the representation of the land surface in coupled models and to improve climate impacts assessments.

The JULES model is the land-surface scheme used by the UK Met Office for both weather and climate applications. It is also a community model and can be used in standalone mode; which is how it is used in the work presented here. JULES-crop, as described in *Osborne et al.* (2015) is a dual-purpose crop model intended for use both within standalone JULES, enabling a focus on food production and water availability applications, as well as being the land-surface scheme within climate and earth system models. JULES in these larger models allows feed-backs from regions with extensive croplands and irrigation systems, like South Asia, to have an effect on the atmosphere e.g. via Methane emissions from rice paddies or evaporation from irrigated fields (*Betts*, 2005).

In this paper we describe and demonstrate the development and implementation of sequential cropping in JULES. This is part of a larger project to develop simulations for South Asia to understand the integrated impacts of climate change (*Mathison et al.*, 2015, 2018) using state of the art RCM projections (*Kumar et al.*, 2013, *Mathison et al.*, 2013). This will improve understanding of the impacts of climate change and how they affect each other. There are many reasons for doing this including:

- improvement of simulations of those regions that use this cropping system currently,
- to understand the impact future climate change may have on this cropping system,

for example in terms of water resources,

- and to consider the impact of adopting this cropping system for regions where it is not currently used but could be in the future.

The purpose of this study is to use the site in Avignon (France) described in *Garrigues et al.* (2015, 2018) to illustrate and evaluate the sequential cropping method implemented in JULES. The method is summarized by Fig. 4.1 and described in Sect 4.3. We aim to show that the method is able to produce two crops in a single growing period and therefore provide a better representation of the real land surface at Avignon than previously possible using the crop model, rather than perform a detailed tuning exercise. Avignon is chosen because it has been observed and documented over several years (2001 to 2014), growing a range of crops throughout this period. The continuous measurements of surface fluxes provided by this dataset are a unique resource for evaluating land surface models (LSMs) and for testing and implementing crop rotations in LSMs. *Garrigues et al.* (2015) use this dataset to evaluate LSM simulations of evapotranspiration using the interactions between soil, biosphere, and atmosphere scheme (ISBA) LSM (*Noilhan and Planton*, 1989) specifically, the version from *Calvet et al.* (1998); ISBA-A-gs.

We focus on a two-crop-rotation between 2005 and 2012. In order to implement the method in a tropical region where there is large variation in growing conditions, we apply the same method to four locations in the North Indian states of Uttar Pradesh and Bihar to simulate the rice-wheat rotation. These states are key producers of these crops using the sequential cropping system. The paper is structured as follows, Section 4.2 describes the JULES model and the method for implementing the sequential cropping system in JULES is outlined in Sect. 4.3. The simulations are described in Sect. 4.4, the observations used in Sect. 4.5, the results in Sect. 4.6 and Sect. 4.7 provides the discussion and conclusions.

4.2 Model description

JULES is a process-based model that simulates the fluxes of carbon, water, energy and momentum between the land-surface and the atmosphere. The model and the equations it is based on are described in detail in *Best et al.* (2011) and *Clark et al.* (2011). JULES treats each vegetation type as a separate tile within a gridbox with each one represented individually with its own set of parameters, independent fluxes and interactions with the atmosphere. Prognostics such as leaf area index (LAI) and canopy height are therefore available for each tile. However the air temperature, humidity and windspeed are treated as homogenous across a gridbox and precipitation is applied uniformly over the different surface types of each gridbox. Below the surface the soil type is also uniform across each gridbox. The parametrisation of crops in JULES (JULES-crop) is

described in detail in *Osborne et al.* (2015) and *Williams et al.* (2017); the main aim of JULES-crop is to improve the simulation of land-atmosphere interactions where crops are a major feature of the land-surface (*Osborne et al.*, 2015).

The development of the crop is controlled by the cardinal temperatures, these define the temperature range within which each crop is able to develop; these are the base temperature (T_b), maximum temperature (T_m) and optimum temperature (T_o) and specific for each crop. The cardinal temperatures and the 1.5m tile temperature (T) are used to calculate the thermal time i.e. the accumulated effective temperature (T_{eff}) to which a crop is exposed, as defined in Eq. 4.1 (*Osborne et al.*, 2015). Table 4.3 summarises the settings for these temperatures used in this analysis.

$$T_{eff} = \begin{cases} 0 & \text{for} \quad T < T_b \\ T - T_b & \text{for} \quad T_b \leq T \leq T_o \\ (T_o - T_b)\left(1 - \dfrac{T - T_o}{T_m - T_o}\right) & \text{for} \quad T_o < T < T_m \\ 0 & \text{for} \quad T \geq T_m \end{cases} \tag{4.1}$$

Crop development can also be affected by the length of the day; this is called photoperiod sensitivity and is controlled by two parameters in the model: the critical photoperiod (P_{crit}) and the sensitivity of a specific crop development rate to photoperiod (P_{sens}). The critical photoperiod defines the threshold optimum photoperiod for crop development, this typically only affects the crop during the vegetative phase, ie. before flowering (*Penning de Vries et al.*, 1989). For some crops progress toward flowering is slowed if the day length is less than or greater than this specific photoperiod (*Osborne et al.*, 2015). These parameters are used to define the overall effect of the photoperiod on the crop called the relative photoperiod effect, RPE described by Eq. 4.2. In these simulations, as in (*Osborne et al.*, 2015), the effect of photoperiod is not included i.e P_{sens} is set to 0 and therefore RPE is equal to 1.0.

$$RPE = 1 - (P - P_{\text{crit}})P_{\text{sens}} \tag{4.2}$$

The RPE is then used to calculate the rate of crop development described by Eq. 4.3.

$$\frac{dDVI}{dt} = \begin{cases} \frac{T_{\text{eff}}}{TT_{\text{emr}}} & \text{for} \quad -1 \leq DVI < 0 \\ \left(\dfrac{T_{\text{eff}}}{TT_{\text{veg}}}\right) RPE & \text{for} \quad 0 \leq DVI < 1 \\ \frac{T_{\text{eff}}}{TT_{\text{rep}}} & \text{for} \quad 1 \leq DVI < 2 \end{cases} \tag{4.3}$$

where TT_{emr} is the thermal time between sowing and emergence, TT_{veg} and TT_{rep} are the thermal time between emergence and flowering and between flowering and maturity respectively. These are calculated using a temperature climatology from the

driving data and sowing dates from observations or a reliable dataset to ensure that the crop reaches maturity on average by the harvest date, the values used in these simulations are given in Tables 4.4 and 4.5.

In order to simulate the characteristics of a typical sequential cropping location using JULES we have implemented modifications to both JULES-crop and the irrigation code, these are described here. In order to simulate crops in sequence on the same gridbox, the first crop must no longer be in the ground so that the second one can be sown. The use of a latest harvest date forces the harvest of the first crop regardless of whether it has reached maturity or not to make certain of this. These modifications are controlled using the l_croprotate switch (see table 4.1). Therefore l_croprotate ensures the following:

- All crops are initialized at the start of a simulation so that they can be used later when they are needed within the crop rotation being modelled.
- If JULES is simulating a crop rotation, the user must supply a latest harvest date so that the first crop is harvested before the second crop is sown (a latest harvest date can also be specified without using l_croprotate).

The current JULES default for irrigation allows individual tiles to be specified (when frac_irrig_all_tiles is set to false) but the irrigation is applied as an average across a gridbox and therefore actually occurs across tiles. The flag set_irrfrac_on_irrtiles restricts the irrigation to the tiles specified by irrigtiles only (see table 4.1). This new functionality is needed because many locations that include crop rotations include crops that both do and do not require irrigation.

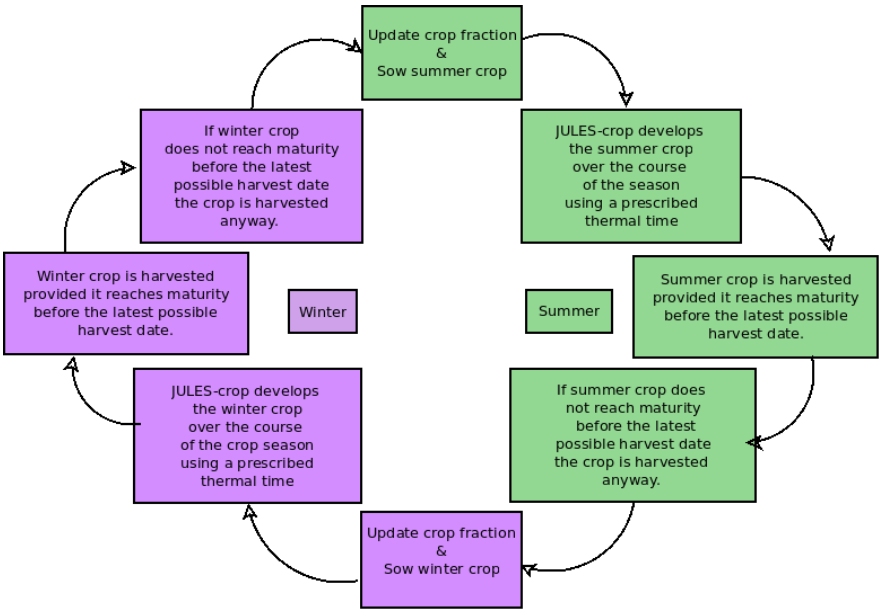

Figure 4.1: A flow chart showing the process followed to carry out the crop rotation in JULES.

4.3 Method for sequential cropping in JULES

The sequential cropping method implemented into JULES as part of this study is illustrated by the flow chart in Fig. 4.1 and described here using the Avignon site simulation. The Avignon site is a point run which is assumed to be entirely used to grow sorghum (in summer) and winter wheat (in winter). JULES updates the fraction of the site that is allocated to sorghum (winter wheat) just before the sowing date so that the appropriate crop occupies the whole of the site. The fraction of the site that is sorghum (winter wheat) is prescribed in the Avignon case using observed sowing and harvest dates. Once the fraction is updated the crop is sown, it then develops between the stages of: sowing and emergence, emergence and flowering and flowering and maturity.

The crop model integrates an effective temperature over time as the crop develops through these stages with the carbon partitioned according to the DVI (see Sect. 4.2). The effective temperature (see Eq. 4.1) is a function of air or leaf temperature and differs between models. The DVI is a function of the thermal time since emergence, therefore DVI=-1 is sowing, 0 is emergence and 1 is flowering. Maturity and therefore harvest occurs at a DVI of 2 (*Osborne et al.*, 2015). The integrated effective temperature in each development stage is referred to as the thermal time of that development stage (see Sect. 4.2, Eq. 4.1 and *Osborne et al.* (2015), *Mathison et al.* (2018)).

It is recommended for sequential cropping to prescribe a latest possible harvest date for those instances where the crop does not develop quickly enough and therefore does not reach maturity before the next crop in the rotation is due to be sown. The latest possible harvest date forces the removal of the first crop before the crop fraction is reassigned, ensuring that crops that are adjacent in time do not occupy the same area at the same time. This value can be assigned an observed harvest date if this is known or it can be the day before the next crop in the rotation is due to be sown. The flow chart shown in Fig. 4.1 is equally applicable to the India simulations. Rice is therefore represented by the summer crop (green boxes) and wheat is represented by the winter crop (purple boxes). This method could be extended to include as many crops as occurs in a rotation at a particular location.

4.4 Model simulations

The simulations are divided into two sections. Section 4.4.1 applies the method to a well observed site in order to describe and demonstrate how the sequential cropping method works and evaluate it against observations at this location. Section 4.4.2 applies the method to points in Northern India where this cropping system is commonly used. The parameter settings and switches used in JULES for the simulations in this study are provided in tables 4.1, 4.2 and 4.3. The Avignon and India simulations use the same

settings wherever possible; these are provided in Table 4.1 (see Avignon settings and India settings columns).

The plant functional type (PFT) parameter settings are also broadly the same between simulations, with the majority of these from *Osborne et al.* (2015) and therefore based on natural grasses. The crops are different between the two sets of simulations with winter wheat and sorghum at the Avignon site and spring wheat and rice at the India locations. The PFT parameters used in this study that govern V_{cmax}: including the lower (T_{low}) and upper (T_{upp}) temperatures for photosynthesis, n_{eff} and $n_l(0)$ are tuned to the maximum leaf assimilation expression from *Penning de Vries et al.* (1989) (see Table 4.2) for each crop. These values are consistent with the wider literature (*Hu et al.*, 2014, *Sinclair et al.*, 2000, *Olsovska et al.*, 2016, *Xue*, 2015, *Makino*, 2003, *Ogbaga*, 2014). The respiration parameters, μ_{rl} and μ_{sl} are from nitrogen concentrations given in *Penning de Vries et al.* (1989). The crop parameters are mainly from *Osborne et al.* (2015), with maize parameters used for sorghum (see Sect 4.4.1) except for the cardinal temperatures which are from *Nicklin* (2013) (see Table 4.3).

The calculation of the soil moisture availability factor (see Table 4.2) is different between the Avignon and India simulations. In the Avignon simulations we assume that the total depth of the rootzone d_r is 1.5 m, equivalent to the observed average maximum root depth over all of the years at the Avignon site. The soil moisture availability factor is then calculated using this maximum root depth together with the average properties of the soil. The India point simulations assume an exponential root distribution with an e-folding depth d_r of 0.5 m because we do not have an observed root depth for these locations. The individual simulations are described in more detail in Sect. 4.4.1 and Sect. 4.4.2 for the Avignon and India simulations respectively.

4.4.1 Avignon site simulation

The Avignon "remote sensing and flux site" of the National Institute Agronomic Research (INRA) described in *Garrigues et al.* (2015, 2018), provides a well studied location with several years of crop rotation data. We focus on the period with a rotation of just two crops: winter wheat and sorghum between 2005 and 2012. The aim of simulating the crops at this site is to illustrate that the new sequential cropping functionality in JULES can simulate more than one crop within a year and reproduce the correct growing seasons for each crop. We evaluate JULES with sequential crops and grasses representing crops against the observed fluxes. We are not aiming to provide a perfect representation of the two crops at this site; this would require significant further work and model tuning. We have therefore not added specific parameterizations for the crops at Avignon, but used existing crops within the model. Therefore Sorghum is largely based on the maize crop (as discussed earlier) as this is also a C4 crop and it is already available in JULES. We also use the existing spring wheat parameterization to represent the C3 winter wheat crop at Avignon.

Flag	JULES notation	Avignon settings	India settings	Effect of switch
Canopy radiation scheme	can_rad_mod	6	6	Selects the canopy radiation scheme.
Irrigation demand	l_irrig_dmd	F	T	Switches on irrigation demand.
Irrigation scheme	irr_crop	-	2	Irrigation occurs when the development index of the crop is greater than 0.
Physiology	l_trait_phys	F	F	Switches on trait based physiology when true.
Sowing	l_prescsow	T	T	Selects prescribed sowing.
Plant maintenance respiration	l_scale_resp_pm	F	F	Switch to scale respiration by water stress factor. If false this is leaf respiration only but if true includes all plant maintenance respiration.
Crop rotation	l_croprotate	T	T	A new switch to use the sequential cropping capability.
Irrigation on tiles	frac_irrig_all_tiles	-	F	Switch to allow irrigation on all or specific tiles
Irrigation on specific tiles	set_irrfrac_on_irrtiles	-	T	A new switch to set irrigation to only occur on a specific tile.
Specify irrigated tile(s)	irrigtiles	-	6	Setting to set the value(s) of the specific tile(s) to be irrigated.
Number of tiles irrigated	nirrtile	-	1	Setting to set how many tile(s) to be irrigated.
Set a constant irrigation fraction	const_irrfrac_irrtiles	-	1.0	A new setting to set the value(s) of the irrigation fraction for specific tile(s) to be irrigated in the absence of a file of irrigation fractions.

Table 4.1: JULES flags used that are new or different from those in *Osborne et al.* (2015)

The Avignon JULES simulation (referred to from here on using AviJUL) is driven using the meteorological site observations outlined in Section 4.5.1 and *Garrigues et al.* (2015, 2018) using a half hourly timestep. The irrigation is only applied to the summer Sorghum crop; this is included in the rainfall observations used to drive Avi-JULES. Therefore the irrigation and other settings governing irrigation are not switched on in JULES for the Avignon site simulations (See Table 4.1, column 'Avignon settings'). We include simulations for the Avignon site where the crops are represented by grasses (AviJUL-grass) for comparison with the simulations that use the new sequential cropping method implemented in the JULES-crop model (AviJUL-sqcrop). In the AviJUL-grass simulations the LAI and the canopy height are prescribed from observations in order to capture the growing seasons correctly without the crop model and the PFT parameters are adjusted to be the same as the crops. In the AviJUL-sqcrop simula-

Parameter	JULES notation	Description	Winter wheat	Sorghum	Spring wheat	Rice
T_{low}	t_low_io	Lower temperature for photosynthesis (° C).	5	18	5	15
T_{upp}	t_upp_io	Upper temperature for photosynthesis (° C).	30	53	30	40
n_{eff}	neff_io	Scale factor relating V_{cmax} with leaf nitrogen concentration.	0.8e-3	0.75e-3	0.8e-3	0.95e-3
$n_l(0)$	nl0_io	Top leaf nitrogen concentration (kg N/kg C).	0.073	0.07	0.073	0.073
fsmc method	fsmc_mod_io	When equal to 0 we assume an exponential root distribution with depth.			0	0
		When equal to 1, the soil moisture availability factor, fsmc, is calculated using average properties for the root zone.	1	1		
d_r	rootd_ft_io	If fsmc_mod_io = 0 d_r is the e-folding depth.			0.5	0.5
		If fsmc_mod_io = 1 d_r is the total depth of the root zone.	1.5	1.5		
$p0$	fsmc_p0_io	Parameter governing the threshold at which the plant starts to experience water stress due to lack of water in the soil.	0.5	0.5	0.5	0.5
μ_{rl}	nr_nl_io	Ratio of root nitrogen concentration to leaf nitrogen concentration.	0.39	0.39	0.39	0.39
μ_{sl}	ns_nl_io	Ratio of stem nitrogen concentration to leaf nitrogen concentration.	0.43	0.43	0.43	0.43
$Q_{10,leaf}$	q10_leaf_io	Q_{10} factor in the V_{cmax} calculation.	1.0	1.0	1.0	1.0

Table 4.2: JULES plant functional type (PFT) parameters and values modified for use in this study. We include only the values that have been changed or are new in JULES since *Osborne et al.* (2015)

tions the LAI and the canopy height are calculated by the model. Observed sowing and harvest dates from *Garrigues et al.* (2015) are used to calculate the thermal time requirements for each crop, these are provided in Table 4.4. During the periods between each crop, the ground is mostly bare (*Garrigues et al.*, 2018).

4.4.2 India Simulations

The India simulations focus on the north Indian states of Uttar Pradesh and Bihar. These states are key producers of rice and wheat in India and the use of a rice-wheat

Parameter	JULES notation	Description	Winter wheat	Sorghum	Spring wheat	Rice
T_b	t_bse_io	Base temperature (° K).	273.15	284.15	273.15	278.15
T_m	t_max_io	Max temperature (° K).	303.15	317.15	308.15	315.15
T_o	t_opt_io	Optimum temperature (° K).	293.15	305.15	293.15	303.15
TT_{emr}	tt_emr_io	Thermal time between sowing and emergence (° Cd).	35	80	35	60
TT_{veg}	tt_veg_io	Thermal time between emergence and flowering (° Cd).	Table 4.4	Table 4.4	Table 4.5	Table 4.5
TT_{rep}	tt_rep_io	Thermal time between flowering and maturity (° Cd).	Table 4.4	Table 4.4	Table 4.5	Table 4.5
T_{mort}	t_mort_io	Soil temperature (2^{nd} level) at which to kill crop if DVI¿1 (° K).	273.15	281.15	273.15	281.15
f_{yield}	yield_frac_io	Fraction of the harvest carbon pool converted to yield carbon.	1.0	1.0	1.0	1.0
DVI_{init}	initial_c_dvi_io	DVI at which the crop carbon is set to C_{init}.	0.0	0.0	0.0	0.0
DVI_{sen}	sen_dvi_io	DVI at which leaf senescence begins.	1.5	1.5	1.5	1.5
C_{init}	initial_carbon_io	Carbon in crop at emergence in kgC/m^2.	0.01	0.01	0.01	0.01

Table 4.3: JULES crop parameters used in this study. The Sorghum cardinal temperatures are from *Nicklin* (2013) with the other parameters those used for Maize in *Osborne et al.* (2015). We include only the values that have been changed or added since *Osborne et al.* (2015). Table 3 of *Osborne et al.* (2015) provides the original PFT parameters and Table 4 of *Osborne et al.* (2015) provides the original crop parameters).

Year	Crop	Sowing date	Harvest date	Emergence-flowering	Flowering-maturity	Sowing DOY
2005	Winter wheat	27 Oct 2005		1301.3	867.5	300
2006			27 Jun 2006			
2007	Sorghum	10 May 2007	16 Oct 2007	647.6	791.5	130
2007	Winter wheat	13 Nov 2007		1401.0	934.0	317
2008			1 Jul 2008			
2009	Sorghum	25 Jun 2009	22 Sep 2009	462.5	565.3	176
2009	Winter wheat	19 Nov 2009		1308.6	872.4	323
2010			13 Jul 2010			
2011	Sorghum	22 Apr 2011	22 Sep 2011	679.5	830.5	112
2011	Winter wheat	19 Oct 2011		1559.6	1039.7	292
2012			25 Jun 2012			

Table 4.4: Thermal times in degree days used in this study for the Avignon site, these are based on the observed sowing and harvest dates from *Garrigues et al.* (2015).

rotation is prevalent in this part of India (*Mahajan and Gupta*, 2009). The sequential cropping system in this region involves growing rice during the wet monsoon months and an irrigated wheat crop during the dry winter. The wheat varieties grown in this region are spring wheat, this is an important distinction as spring wheat does not require a vernalization period which is important for winter wheat varieties (*Griffiths et al.*, 1985, *Robertson et al.*, 1996, *Mathison et al.*, 2018). We select four points across these two states in order to gain understanding of the model response, particularly in terms of yield, to the variation in the conditions across the two states. Point simulations allow more in depth analysis than a complete regional simulation, in order to inform future regional simulations using this sequential cropping method.

The locations of the selected points are shown on a map of the surface altitude for South Asia in Fig. 4.2 (a). The driving data used for these four point simulations is from an RCM simulation run for South Asia for the period 1991–2007 as described below. Figure 4.2 (b, c and d) show a close-up view of the locations selected. Map (b) in 4.2 shows the average total monsoon precipitation for the 1991-2007 period while (c) and (d) show the average minimum and maximum temperatures respectively to illustrate that these four points are representative of the climate of the wider Uttar Pradesh/Bihar region.

In these simulations JULES is run using a 3-hourly timestep using driving data from ERA-interim (*Dee et al.*, 2011, *Simmons et al.*, 2007) downscaled to 25 km using the HadRM3 regional climate model (RCM- *Jones et al.*, 2004). This RCM simulation is one of an ensemble of simulations produced for the EU-HighNoon FP7 project for the whole of the Indian subcontinent (25 N, 79 E–32 N, 88 E) for the period 1991-2007. The HighNoon simulations are described in detail in previous publications such as *Kumar et al.* (2013) and *Mathison et al.* (2013, 2015). HadRM3 provides more regional detail to the global data with lateral atmospheric boundary conditions updated 3-hourly and interpolated to a 150 s timestep. These simulations include a detailed representation of the land surface in the form of version 2.2 of the Met Office Surface Exchange Scheme (*Essery et al.*, 2001; MOSESv2.2;). JULES has been developed from the MOSESv2.2 land surface scheme and therefore the treatment of different surface types is consistent between the RCM and JULES (*Essery et al.*, 2001, *Mathison et al.*, 2015). Sowing dates are prescribed using climatologies calculated from the observed dataset, *Bodh et al.* (2015), from the government of India, Ministry of Agriculture and Farmers welfare. Thermal times are calculated using these climatological sowing and harvest dates from *Bodh et al.* (2015) and a thermal climatology from the model simulation as described in *Osborne et al.* (2015), the values used in the simulations here are provided in Table 4.5. In the JULES point simulations only wheat is irrigated, the settings used for this are provided in Table 4.1 (column 'India settings').

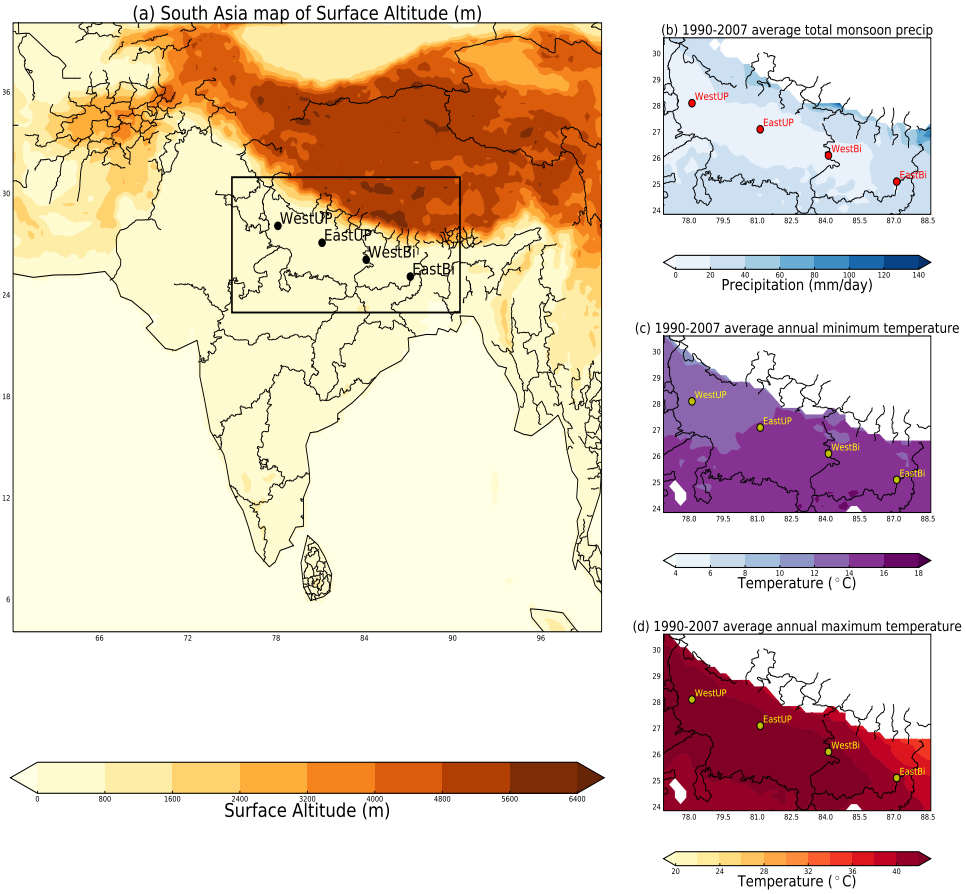

Figure 4.2: A map showing the location of the point simulations in the wider context of India on a map of the surface altitude (a) from the regional climate model that is used in the JULES simulations. The same points are shown in three smaller maps (b,c,d) that zoom in on the two states of Uttar Pradesh and Bihar. Map (b) shows the total monsoon precipitation, map (c) shows the minimum temperature, and map (d) the maximum temperature averaged for the period 1991-2007.

4.5 Observations

4.5.1 Avignon observations

The length and detail of the observation record at the Avignon site means it is an ideal site to demonstrate the method being implemented in JULES for simulating sequential cropping. High resolution meteorological data, important for the practicalities of running the JULES model is available on a half hourly basis; this includes air temperature, humidity, windspeed and atmospheric pressure at a height of 2m above the surface. Cumulative rainfall, radiation measurements and sensible (H) and latent heat (LE) fluxes are also available, with the latter flux measurements enabling the evaluation of the JULES fluxes. Cumulative evapotranspiration (ET) are derived from the half hourly LE measurements. The observations for evaluating the model include soil measurements of soil moisture along with plant measurements including canopy

Location	Crop	Sowing DOY	Emergence-flowering	Flowering-maturity
WestUP	Spring wheat	335	1007.6	671.1
	Rice	150	1759.4	1181.3
EastUP	Spring wheat	335	993.55	662.5
	Rice	150	1865.5	1243.5
WestBi	Spring wheat	335	991.54	661.6
	Rice	150	1907.55	1271.7
EastBi	Spring wheat	335	1019.21	679.1
	Rice	150	1976.96	1300.64

Table 4.5: The sowing day of year (Sowing DOY) and thermal times in degree days used in this study for the locations in Uttar Pradesh and Bihar, India (see 4.2 for a map of the locations), the values given here are based on the observed sowing and harvest dates from *Bodh et al.* (2015)

.

height (measured every 10 days), above ground dry weight biomass (taken at four field locations) and LAI; biomass and LAI are destructive measurements repeated up to six times per crop cycle (*Garrigues et al.*, 2015). More information is documented in *Garrigues et al.* (2015) regarding the site and the observations available.

4.5.2 India observations

Crop yield observations from the International Crops Research Institute for the Semi-Arid Tropics (*ICRISAT*, 2015) provides seasonal yields for each crop for each district for comparison with the point simulations. We also show average crop yield observations from *Ray et al.* (2012a) for three, 5-year periods between 1993 and 2007 (1993–1997, 1997–2003, 2003–2007) via *Ray et al.* (2012b). These data are based on previous publications *Monfreda et al.* (2008) and *Ramankutty et al.* (2008) and include the period of the point simulations which are from 1991–2007. We show both of these datasets to highlight that there is a range in the estimates of yield for this region.

4.6 Results

4.6.1 Avignon site simulation

Figure 4.3 shows the timeseries of total above ground biomass (a), LAI (b) and canopy height (c) for the AviJUL-grass and AviJUL-sqcrop simulations. Figure 4.3 shows that the crops are developing throughout the crop seasons with maxima of biomass, LAI and canopy height occurring at approximately the correct time for both crops. The total above ground biomass from JULES is calculated from the sum of the stem, leaf and

harvest carbon pools for each crop and plotted as a time series (dashed lines). Biomass observations are provided as a single timeseries with the crop type confirmed from the timing of the observations. These are plotted alongside the model represented by purple asterisks (see plot (a), Fig. 4.3). It is noticeable that the 2009 observed growing season for sorghum is much shorter than for the other two sorghum crop seasons (shown by the red solid line in Fig. 4.3 a, b and c). The 2009 sorghum crop is planted much later in the year compared to the other two sorghum seasons (2007 and 2011) but harvested at a similar time. This is because the variety of sorghum planted in 2009 is different to the variety planted 2007 and 2011 seasons. The 2009 variety is a fodder crop with a much larger LAI and a shorter growing season.

JULES fits the biomass observations for 2009 well (see Fig. 4.3 plot a). JULES also closely fits the leaf area (see Fig. 4.3 plot b) and canopy height observations (see Fig. 4.3 plot c) for the 2009 Sorghum season, with differences between the simulations and observations maximum values of approximately 1 m^2 m^{-2} and 0.1 m respectively. In the 2007 sorghum season JULES overestimates the maximum LAI and canopy height by approximately two times the observations (see Fig. 4.3 plots b and c) and underestimates the total biomass (see Fig. 4.3 plot a) by about 30 %. For the 2011 season the JULES sorghum biomass equals the magnitude of the observations; however, the maximum LAI is overestimated by four times in the model (similar to 2007) and the maximum canopy height is approximately two times the observed maximum. The canopy height is very close to observations for wheat in all four seasons; however, the wheat LAI is overestimated and the biomass is underestimated in all years. The two wheat seasons of 2006 and 2010 are closer to the LAI observations than 2008 and 2012. However the underestimation of the biomass is greater for these seasons. For 2008 and 2012 the wheat biomass is closer to the observations, but the overestimation in the LAI is greater. The increase in biomass for both crops through the start of the season follows the observations quite closely but in most years, especially for wheat, JULES does not accumulate enough biomass later in the crop season to reach the observed maxima.

The level of soil moisture that a plant begins to experience water stress at is reduced by the introduction of the variable $p0$; this is a scaling factor used in the soil moisture stress calculation (*Williams et al.*, 2018). The setting of $p0$ and how this affects GPP at the First ISLSCP Field Experiment (FIFE) site in Kansas is discussed in detail in *Williams et al.* (2018). In addition *Williams et al.* (2017) suggest modifying the $p0$ parameter to be 0.65 for the Mead site in Nebraska. In the simulations shown here $p0$ is set to 0.5 (see Table 4.2) modified from the default setting of 0, as recommended by *Allen et al.* (1998). The way that vegetation in JULES uses water and its response to drought conditions is currently under investigation within the wider JULES community as described in *Williams et al.* (2018) and *Harper et al.* (in preparation). The canopy height does not really change with the modification of $p0$ from 0 to 0.5 (not shown),

however biomass and LAI are more sensitive to changes in this parameter. This is apparent from comparison of Fig. 4.3, plots (a) and (b) with those from simulations that use the default setting provided in the Appendix (see Fig. A.5 plots (a) and (b). Setting $p0$ to 0.5 marginally improves the JULES biomass fit to observations but results in a large over estimation of the wheat LAI compared with a setting of 0 which gives an LAI that is closer to the observations (see Fig. A.5 plot b). The years with a large (small) LAI are also represented more closely for $p0 = 0$.

Garrigues et al. (2015) highlight that 2006 and 2008 are two atypical years with 2006 being very dry (256 mm of rain) and 2008 being very wet (500 mm of rain); these differing conditions could explain the large differences in observed LAI and biomass between the two years (*Garrigues et al.*, 2015). The peaks in productivity shown in the LAI in Fig. 4.3, (b) are consistent with the two years (2006 and 2007) of observations of GPP, shown by the black line in Fig. 4.4, plot (a). The wheat crop is clearly shown in the GPP for 2006, although it is underestimated in all simulations (see Fig. 4.4). The decline in GPP at the end of the wheat season is quite close to the observations with AviJUL-grass (red line) being slightly early and AviJUL-sqcrop (blue line) being slightly late. In the sorghum season of 2007 the magnitude and timing of the maximum GPP for the AviJUL-sqcrop simulation are a good fit to observations (see Fig. 4.4, plot a and Fig. A.1 plot b), although the increase in GPP for both simulations begins too early the decline is very close to the observations. The decline is very close to observations for the AviJUL-grass simulations too, although the maxima are slightly too low and a little later than observed (see Fig. 4.4, plot a). This is quantified in Fig. A.1 each of the simulations show a strong linear correlation with r_values of above 0.7 (see Fig. A.1 plots (a) and (b) and the values in the GPP row of Table 4.6).

On the basis that $p0$ has a positive impact on some aspects of the Avignon simulations it is likely that water stress is a factor in the simulations shown here. However there may be other factors not considered here, for example, the long periods of bare soil between between the winter and summer crops (e.g. July of 2006 to April of 2007). This could have a more significant impact on the crops grown in the following year in the model than in reality.

The H and LE fluxes are shown in Fig. 4.4, plots (b) and (c) respectively. The AviJUL-sqcrop (blue line) and the AviJUL-grass (red line) simulations follow each other closely which is reflected in the RMSE values and bias values for each simulation (see Table 4.6 and Figures A.2 and A.3 for H and LE comparisons respectively), these are generally comparable to those from Table 5 in *Garrigues et al.* (2015), which are LE: rmse of 52.4, bias of -11.8, and H: rmse of 56.2, bias of 17.6. The linear correlations shown for H and LE in Fig. A.2 and Fig. A.3 respectively, are strong for these simulations with r_values above 0.7, (see plots a and b). These values are comparable to those from Table 5 in *Garrigues et al.* (2015), which provides values of 0.8 for LE and 0.85 for H. The annual cycle of LE and H are shown in Fig. A.4, a and b respectively.

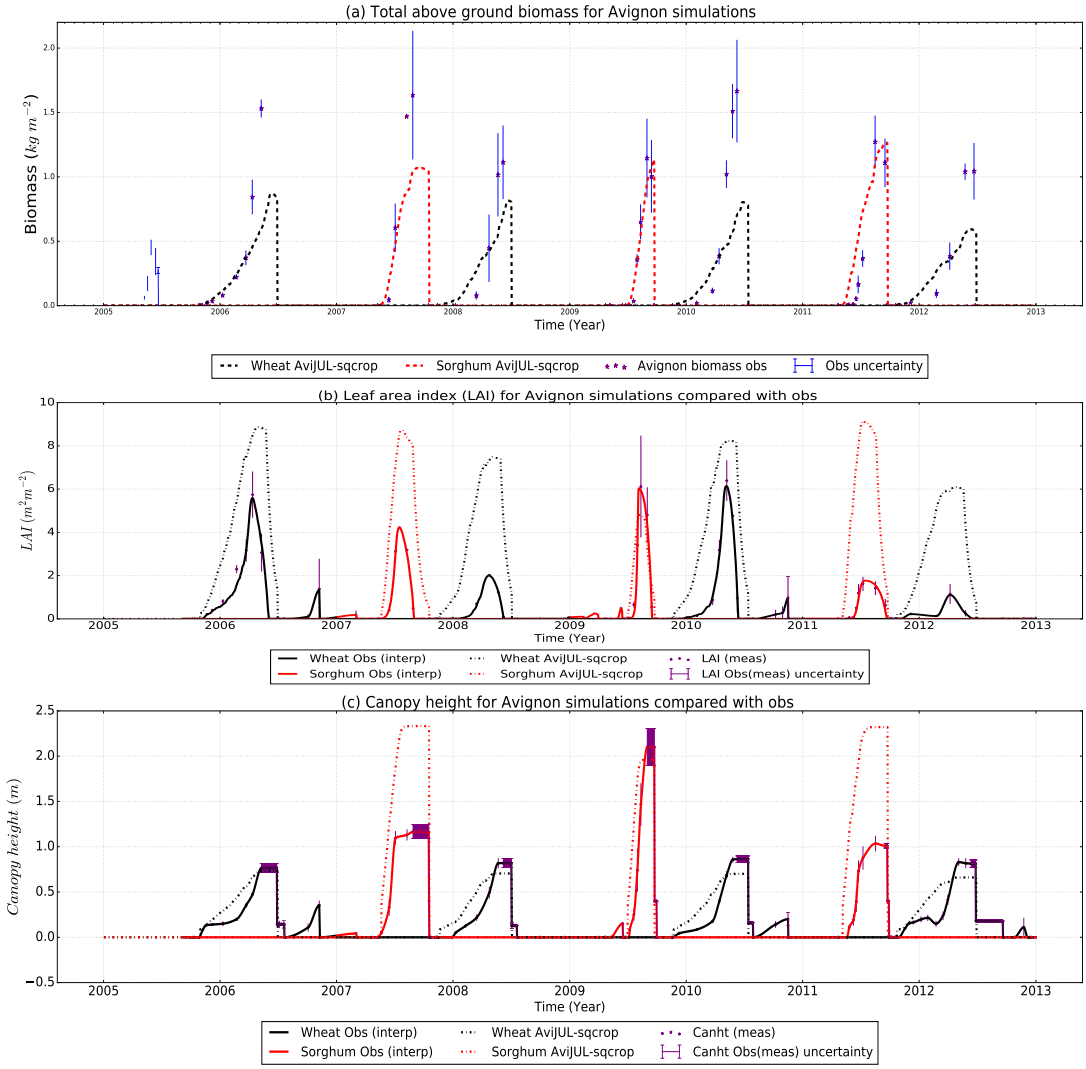

Figure 4.3: The timeseries of total above ground biomass (a), leaf area index (LAI) (b) and canopy height (c) for the Avignon site for wheat (black) and sorghum (red) for observations (solid lines) and simulations using the observed sowing and harvest dates: AviJUL-sqcrop and modelled soil moisture (dashed) for the period between 2005 and 2013 using observed sowing and harvest dates. Simulations with prescribed LAI and canopy height are not shown here as these follow the observed LAI and canopy height. Observed above ground biomass in plot (a) shown by purple asterisks

Figure A.4 highlights how well the simulations capture the seasonal cycle; this is also evident in the timeseries shown in Fig. 4.4, plot b and c.

Given that the soil moisture is important for these JULES simulations at Avignon, Fig. 4.5 plot (a) and (b) summarize the soil moisture conditions in these simulations. Figure 4.5, Plot (a) shows the available soil moisture in the top 1.0 m of the soil. The observations are generally lower than the soil moisture in the simulations throughout most of the timeseries. The AviJUL-sqcrop simulation captures some of the larger dips in the available soil moisture but mostly follows the same patterns as AviJUL-grasses. The soil moisture availability factor shown in Fig. 4.5 plot b, shows that there

Variable	Simulation type	RMSE	Bias	r_value
GPP ($gCm^{-2}day^{-1}$)	AviJUL-grass	2.0	-1.0	0.95
	AviJUL-sqcrop	3.0	0.0	0.82
H (Wm^{-2})	AviJUL-grass	37.0	13.0	0.76
	AviJUL-sqcrop	38.0	6.0	0.71
LE (Wm^{-2})	AviJUL-grass	28.0	-3.0	0.81
	AviJUL-sqcrop	33.0	0.0	0.73

Table 4.6: Table of statistics comparing the JULES simulations with and without soil moisture prescribed to observations

are periods where the soil moisture stress is higher in the observations. Additional simulations that prescribe the soil moisture using these site observations (shown in Fig. 4.5) have an early decline in GPP (not shown). This is due to water stress acting as a scaling factor on net leaf assimilation. A closer look at the soil moisture timeseries on each of the four levels reveals that the top soil layer (not shown), with a depth of 10 cm, is much too variable in the model compared with the observations, which are very stable. The AviJUL-sqcrop simulations follow the observations more closely in the other three soil layers capturing the timing of periods where the soil moisture is lower although not the magnitude. There is also a period in the second half of 2009 where the models simulate a drop in soil moisture in levels 1,2 and 3 that is not in the observations; this is evident in the available soil moisture in the top 1.0 m of the soil shown in Fig. 4.5, plot (a).

The Avignon simulation has shown that the method implemented for simulating sequential cropping in JULES provides two crops per year for several years. The representation of crops either using the crop model or using grasses to represent crops has a similar effect on the surface fluxes. The representation of soil moisture has a large effect in these simulations. As previously discussed the representation of soil moisture stress on vegetation in JULES is a known issue which is the subject of a large international collaborative effort (*Williams et al.*, 2018, *Harper et al.*, in preparation). The representation of individual crops at Avignon in JULES could probably be improved by having sorghum and winter wheat specific parameterizations in JULES, which are tuned to the crop varieties at this location. Such parameterizations are not available at the time of writing and would require significant further work to implement. It is clear that the 2009 variety of sorghum would also require different parameters to those for 2007 and 2011. However, the aim of presenting this simulation is to demonstrate the method rather than provide a perfect representation of either of these crops. This site at Avignon is a valuable resource that will help develop and test future specific parameterizations for these crops and others that are also grown at this site. It is hoped that the suite that runs JULES at Avignon with and without sequential crops could become one of the 'golden' sites that is referred to in *Williams et al.* (2018) and thereby

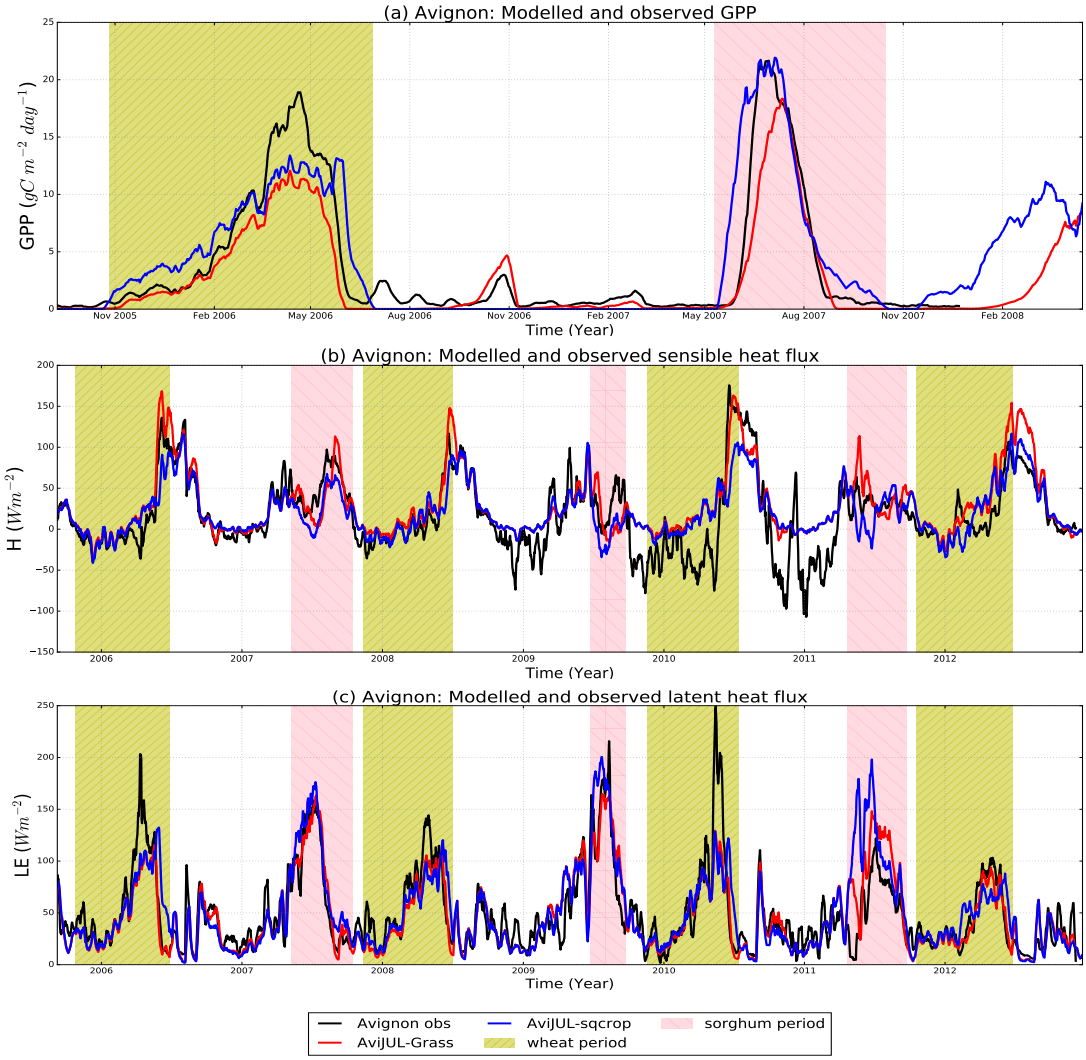

Figure 4.4: The timeseries of GPP (a), H (b) and LE (c) for the Avignon site compared with observations (black lines). H (b) and LE (c) heat fluxes show the whole period from 2005-2012, while GPP shows the period 2005-2008 due to availability of observations. The following model simulations are also shown: AviJUL-grass with prescribed LAI and modelled soil moisture (red), AviJUL-sqcrop with both soil moisture and LAI modelled (blue). In each plot a 10-day smoothing has been applied to the daily data.

aid future development of JULES and other land surface and crop models to include a sequential cropping capability. In the following section we apply this same method to a range of locations that use the sequential cropping system in the north of India in order to implement this method for a regional tropical simulation.

4.6.2 India simulations

The four India points selected for analysis in this study are shown on a map of South Asia in Fig. 4.2 (plot a) with smaller inset plots (b, c and d) focusing on the sequential cropping region being considered across the states of Uttar Pradesh and Bihar. Figure

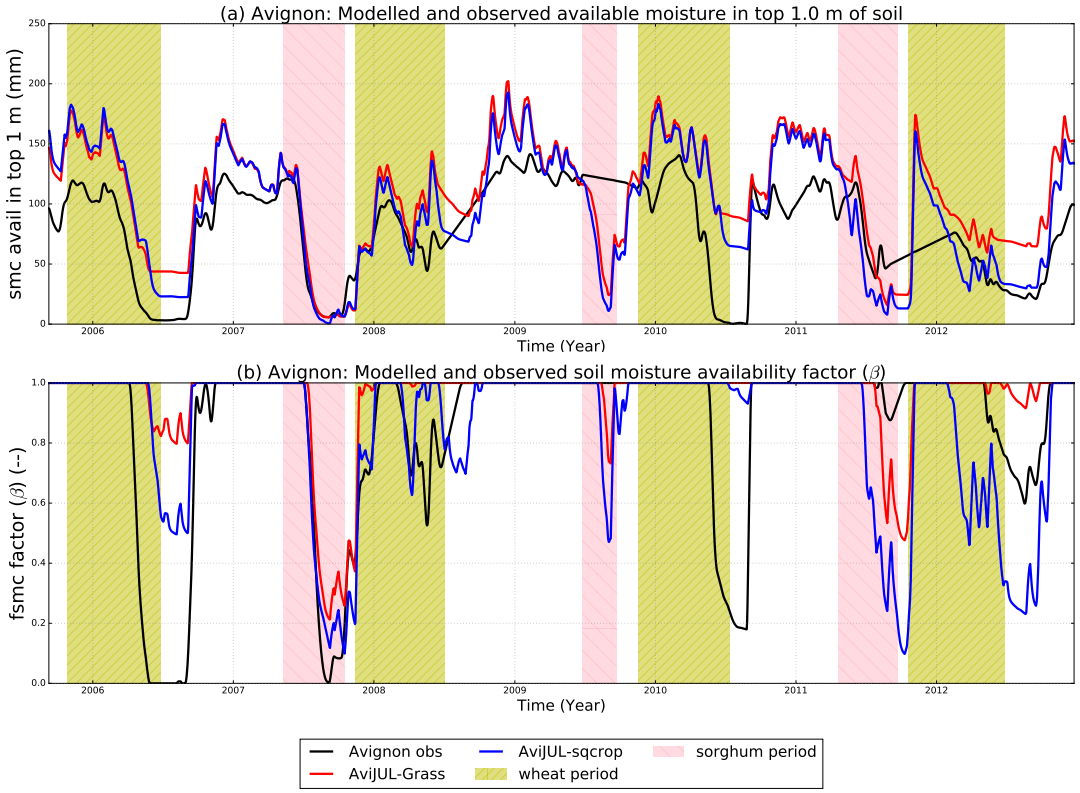

Figure 4.5: The timeseries of the available soil moisture in the top 1.0 m of soil and the soil moisture availability factor (Beta) for the Avignon site for 2005 to 2013 using observed sowing and harvest dates (black line). AviJUL-grass with modelled soil moisture shown in (red), AviJUL-sqcrop with modelled LAI and soil moisture (blue).

4.6 shows the differences in the timeseries of the average precipitation (a), temperatures (b), and vapour pressure deficit (VPD) (c) at each of these four points with the different crop seasons emphasized by the different colour shading (yellow for wheat and pink for rice) on each of the plots. The temperatures rarely reach the low temperatures of the t_{base} cardinal temperatures set in the model shown for rice (green) or wheat (orange) on Fig. 4.6 (b); however the high temperatures do exceed the maximum cardinal temperatures for these crops, especially those set for wheat. In general EastBi is cooler than the other points in more of the years, with the two locations in Uttar Pradesh often being the warmest. The precipitation at each location is variable (see Fig. 4.6 plot a) and there appears to be a variation in the distribution of precipitation through the monsoon period which could be important for crop yields. *Challinor et al.* (2004), for example, found that in two seasons with similar rainfall totals, the distribution of the rainfall during the growing season strongly affected groundnut crop yield. There is also a clear seasonal cycle in the vapour pressure deficit (VPD), increasing toward the end of the wheat season and decreasing into the rice season. EastBi generally has the lowest VPD, with WestUP and EastUP usually the highest throughout the timeseries shown (see Fig. 4.6). These plots suggest that there is a gradual change in conditions

from west to east across Uttar Pradesh and Bihar with increasing humidity and rainfall and decreasing maximum temperatures from west to east.

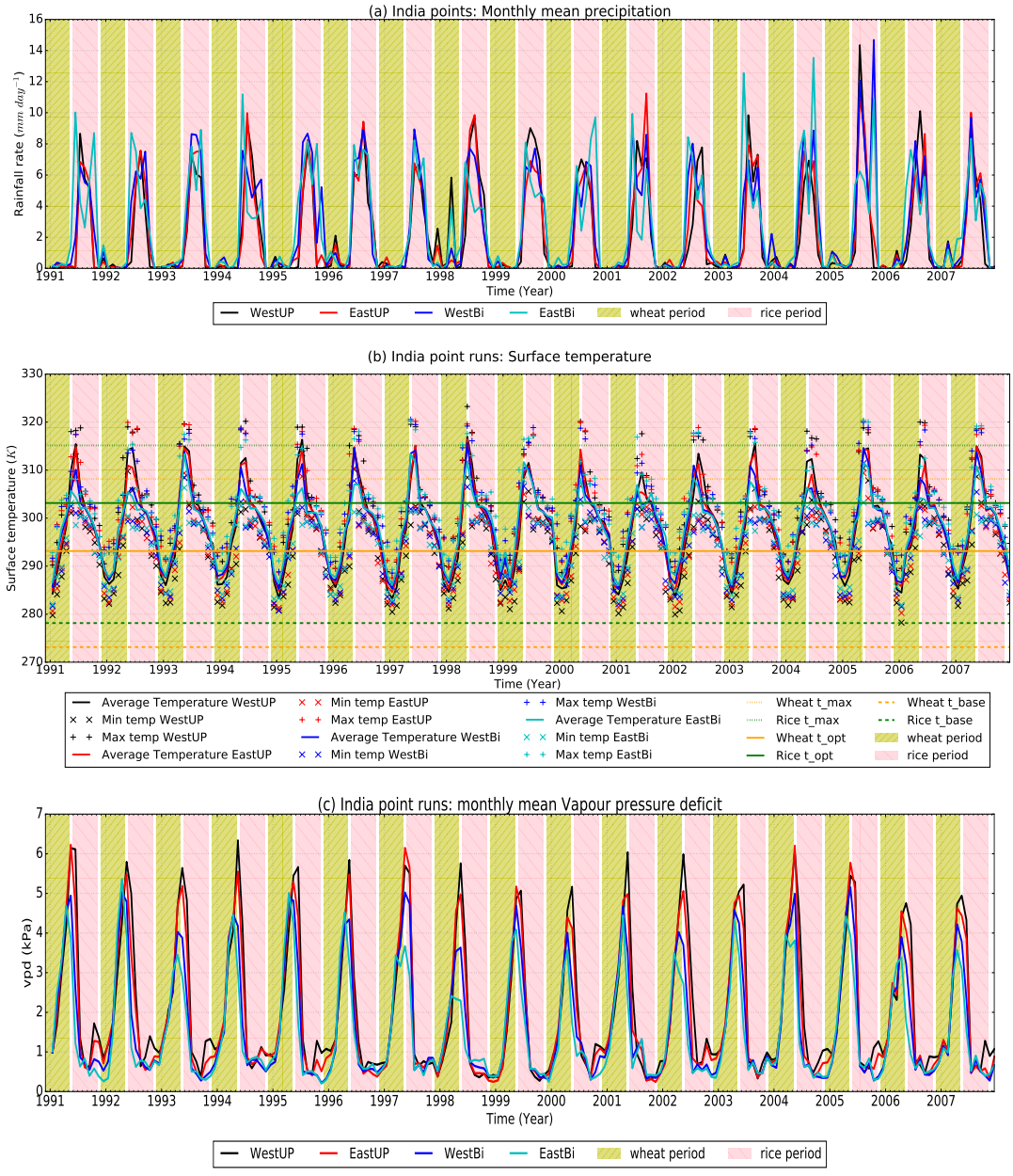

Figure 4.6: Timeseries of monthly precipitation (a), temperature (b), and vapour pressure deficit (c) at each of the India sites shown by the solid lines (WestUP-black, EastUP-red, WestBi-blue and EastBi-cyan). Plot (b) also shows the minimum ('x') and maximum ('+') temperatures for each of the locations for each month together with the JULES cardinal temperatures (horizontal lines) for rice (green) and wheat (orange): Max temperatures (dotted line), optimum temperatures (solid line) and base temperatures (dashed line).

The sequential cropping simulations at these India sites produce both a rice and wheat crop (see Fig. 4.7, with red representing rice and black representing wheat),

and a crop DVI regularly showing that the crop reaches 2 (see Fig. B.2), indicating maturity. JULES is growing both wheat and rice at each of these locations within one growing season and is therefore simulating the sequential cropping rotation. We first consider if the main crop characteristics such as LAI and canopy height are realistic. This is important, especially where the results are to be applied to analysis of future water resource requirement, where an overestimation (underestimation) of size or leaf area for a crop could skew the results towards a higher (lower) resource requirement. In these simulations the canopy height (see Fig. B.3) for both rice and wheat at each location is between 0.5 and 0.7 m (see Fig. B.3) which is an expected value for a typical crop, as described in (*Penning de Vries et al.*, 1989). Figure 4.8 shows the LAI for each of the four locations, indicating that the wheat LAI from JULES is between 5 and 7 $m^2 m^{-2}$ across the locations; this is also an expected value for a crop according to *Penning de Vries et al.* (1989). Rice LAI is lower (between 2 and 4 $m^2 m^{-2}$) with the lowest values for WestUP, slightly increasing from west to east locations. For WestUP particularly, rice (red solid line) has a small LAI (see Fig. 4.8) but it generates a yield (red asterisks Fig. 4.7) that falls within the range of the observations for each year. However, wheat (black solid line) generates a LAI that is closer to expected values but a smaller yield compared with observations (see Fig. 4.7, black asterisks). WestUP has the least available soil moisture, lowest rainfall and higher temperatures than the other locations, yet the observed yields and therefore the actual productivity are higher than the other locations.

Figure 4.10, plot (c) shows the NPP for each of the locations. The stage at which leaf senescence begins is given by a user defined parameter in JULES (sen_dvi_io). In these simulations this is set to be when the DVI is equal to 1.5. At this stage the carbon from the leaves starts to be remobilized to the harvest pool (Fig. 4.9). During this period where the leaves are senescing, they continue to respire (Fig. B.5) but are no longer photosynthesizing. This results in a decline in NPP, which begins relatively early in the season (Fig.4.10c). This decline in NPP appears to have a direct impact on the yield. In JULES the partitioning of carbon to the different parts of the crop is controlled by allometric coefficients. The values assigned to these allometric coefficients in these JULES simulations are those from *Osborne et al.* (2015); it is possible that the results could be improved for South Asia if these were tuned to more appropriate values for the crops there.

Figure 4.7 shows the yields from JULES (asterisks) overlaid on the curve of the harvest pool (solid lines) for each crop together with two observation datasets. The datasets are from *ICRISAT* (2015) shown by the filled circles and *Ray et al.* (2012a) by filled triangles (see Fig. 4.7) highlight that there is a spread between yield estimates for this region. The model (asterisks on Fig. 4.7) tends to underestimate the wheat yield for most years at the WestUP location (average bias across both datasets of -0.13 $kg\ m^{-2}$). Rice is more mixed for WestUP, falling within the range of the observations

in more than half of the years (average bias -0.064 $kg\ m^{-2}$). The average bias across both observation datasets is much smaller for the other locations with rice and wheat yields within the range of the observations for most years for both EastUP and WestBi (average bias across both crops at these locations ranges from -0.07 to 0.02 $kg\ m^{-2}$). During the second half of the simulation the wheat yield is underestimated by the model more often at EastUP but this is just the occasional year for WestBi and does not occur at all for EastBi. For EastBi the rice yields are often toward the top of the range provided by the two observed datasets but still within the range of the observations (see Fig. 4.7); this gives on average a positive bias of 0.06 for rice and 0.02 for wheat. However the observed yields at EastBi are lower than the other locations, where the cooler wetter conditions should be more conducive to achieving higher yields but these are neither observed nor modelled.

The wheat crop is irrigated in these simulations and therefore the soil moisture availability factor is equal to 1.0 during the wheat season (see Fig. 4.11). This suggests, therefore it is not water stress that influences the wheat yields in these JULES simulations. In JULES the irrigation is applied to the top two layers. However, if the roots at these India locations are deeper or shallower at these India locations, the irrigation may not be as effective at preventing water stress. The models underestimation of the high WestUP wheat yield (compared to EastBi) is therefore likely to be due to a combination of factors. One explanation is likely to be the differing management practices between the two states of Uttar Pradesh and Bihar. Uttar Pradesh is characterized by high agricultural productivity with effective irrigation systems (*Kumar et al.*, 2005) and early adoption of new management practices (*Erenstein and Laxmi*, 2008). Bihar on the other hand has lower agricultural productivity, farms tend to be smaller and more fragmented, irrigation systems are less effective (*Laik et al.*, 2014) and adoption of new technology is also slower due to the lack of available machinery (*Erenstein and Laxmi*, 2008). Yield gap parameters are included in many crop models in order to account for the impact of differing nutrient levels, pests, diseases and non-optimal management (*Challinor et al.*, 2004), thus explaining the difference between potential and actual yield under the same environment *Fischer* (2015). This is not included in these simulations.

At the western locations, the humidity is lower (higher VPD) and the temperatures are higher; these conditions may provide another contributory factor for the model underestimating the yields there. The humidity in the simulations could be lower in these simulations than in reality for two reasons: firstly we are running JULES in standalone mode. This means that the land-surface and therefore the crop is unable to influence the atmosphere through evaporation because the humidity is prescribed by the driving data at each timestep. Secondly the driving data is from an RCM that does not include irrigation (*Mathison et al.*, 2015) so the humidity in the driving data is not modified by evaporation due to irrigation. We are therefore missing the part

of the water cycle that allows evaporation from the surface to affect the humidity. This region is intensively irrigated (*Biemans et al.*, 2013) which means that there is a significant contribution from the evaporation due to irrigation and the recycling of water into precipitation (*Harding et al.*, 2013, *Tuinenburg et al.*, 2014) that cannot be accounted for here. *Tuinenburg et al.* (2014) estimate that as much as 35 % of the evaporation moisture from the Ganges basin is recycling within the river basin. We hypothesize that the VPD may be too high in our forcing data and this could be affecting the model yields at this location (*Ocheltree et al.*, 2014). An additional simulation, completed as a sensitivity test to see if low humidity in the driving data could be affecting the model yields, did have the effect of increasing NPP and yield for WestUP, suggesting this hypothesis is worthy of further investigation. However, how plants respond to high VPD is still the source of a great deal of debate (*Medina et al.*, 2019). There are two theories for the plant response to high VPD; the first is stomatal conductance decreases as VPD increases because of an increase in transpiration that lowers the leaf water potential (*Streck*, 2003, *Ocheltree et al.*, 2014, *Medina et al.*, 2019) rather than a direct response to the humidity. In this first theory if the rate of movement of moisture out of the stomata cannot be met by the vascular structure of the plant then the plant will become water stressed (*Streck*, 2003). The second theory is that there is a direct stomatal response to high VPD where stomatal conductance decreases as VPD increases, with abscisic acid (ABA) in the leaves probably triggering the response (*Streck*, 2003). However, *Streck* (2003) suggest that a direct response to VPD is probably contingent on the plant being exposed previously to water stressed conditions. (*Medina et al.*, 2019) investigate the response to high VPD of both irrigated and rainfed C3 and C4 grasses and find evidence of the direct response to VPD in some species; in fact there are published results that support both of these hypotheses. Further investigation is needed to confirm exactly why the simulation at WestUP does not achieve the observed yields.

The total above ground biomass for both crops shown in Fig. B.1 are comparable with each other and with the values simulated for wheat at Avignon. Figure 4.9 shows the evolution of the carbon pools for wheat and rice at each of the India locations for the years between 1998 and 2001, in order to examine the evolution of the carbon pools more closely by looking at a smaller number of crop seasons. The root carbon pool is a significant proportion of the total wheat biomass, larger than the rice root carbon pool. For rice it is the stem carbon pool that constitutes the larger proportion of the total biomass. As expected the leaf carbon drops away during senescence (this occurs when the DVI reaches 1.5 in these simulations) and the leaf carbon is remobilized to the harvest pool but the stem (for rice) and the roots (for wheat) remain high until harvest. Where the level of carbon remains high for a particular carbon pool, the respiration also remains high. It is therefore possible that the carbon partitioning after flowering requires some revision for JULES-crop simulations, especially for wheat. The

carbon partitioning in the model may also be affecting the model wheat yields and may provide another avenue for investigation in addition to those discussed so far. The temperatures during the wheat season shown in Fig. 4.6 rise rapidly, often reaching temperatures that are well above the maximum for the development of wheat by the expected harvest date. These high temperatures may speed up the rate at which wheat matures and therefore shorten the senescence period too much in the model bringing forward the harvest date without giving the yield carbon pool time to increase. The total plant respiration is also shown in Fig. B.5, with the respiration for each crop and carbon pool shown in Fig. B.4. Usually toward the end of the wheat season the plant respiration declines, as carbon is remobilized to the harvest pool which does not respire and the leaves senesce; this results in a decline in the respiring biomass. The rice plant respiration (see Fig. B.5) has a dip in the middle of the 2001 season that only occurs in EastBi; this is caused by a drop in the leaf respiration shown in Fig. B.4 plot (d). The drop in leaf respiration is related to changes in temperature, precipitation and VPD at this location. Usually the temperature timeseries shows an increase through the wheat season, which peaks during the short period between the two crops and then declines into the rice season. In 2001 there is an initial decline, but then a sharp rise in temperature before it then follows its usual decline into the winter wheat season. The rise in temperature is at the same time as the spike in VPD at EastBi (see Fig. 4.6 plot c). The usual fall in temperature is therefore much later in the 2001 rice season, which is accompanied by a significant drop in precipitation in the middle of the monsoon for EastBi, which does not occur at the other locations for this year.

The fluxes of heat (LE and H), NPP and GPP are shown for each of the four India locations (see Fig. 4.2) in Fig. 4.10, plots (a) to (d), with the moisture fluxes shown in Fig. 4.11, plot(c). They show the influence of the sequential crop rotation of wheat and rice on the fluxes at each location by the presence of a first peak for wheat and a secondary smaller peak during the rice season. This is most obvious in the plots of NPP and GPP (see Fig. 4.10, plot (c) and (d) respectively). In general the timeseries of the fluxes shown in Fig. 4.10 and Fig. 4.11, plot(c) are quite similar between locations. The timeseries (see Fig. 4.10) and the annual cycles (Fig. B.6 and Fig. B.7) show that on average, all the locations have minima and maxima occurring at the same time. The drier hotter location, WestUP usually has a lower LE, moisture flux and higher H than the other three locations. Although there are two short periods in 1998 and 2001, where EastBi has the lowest available soil moisture, these periods correspond with a lower monsoon rainfall at this location (see Fig. 4.6). The available soil moisture in the top 1.0 m of soil and the soil moisture availability factor (Beta) are shown in Fig. 4.11, plot a and b respectively). They show that for several years of the simulation WestUP has the lowest available soil moisture and soil moisture availability factor, suggesting this location is likely to be the most water stressed. WestBi on the other hand often has the highest soil moisture availability factor and the most consistent available soil

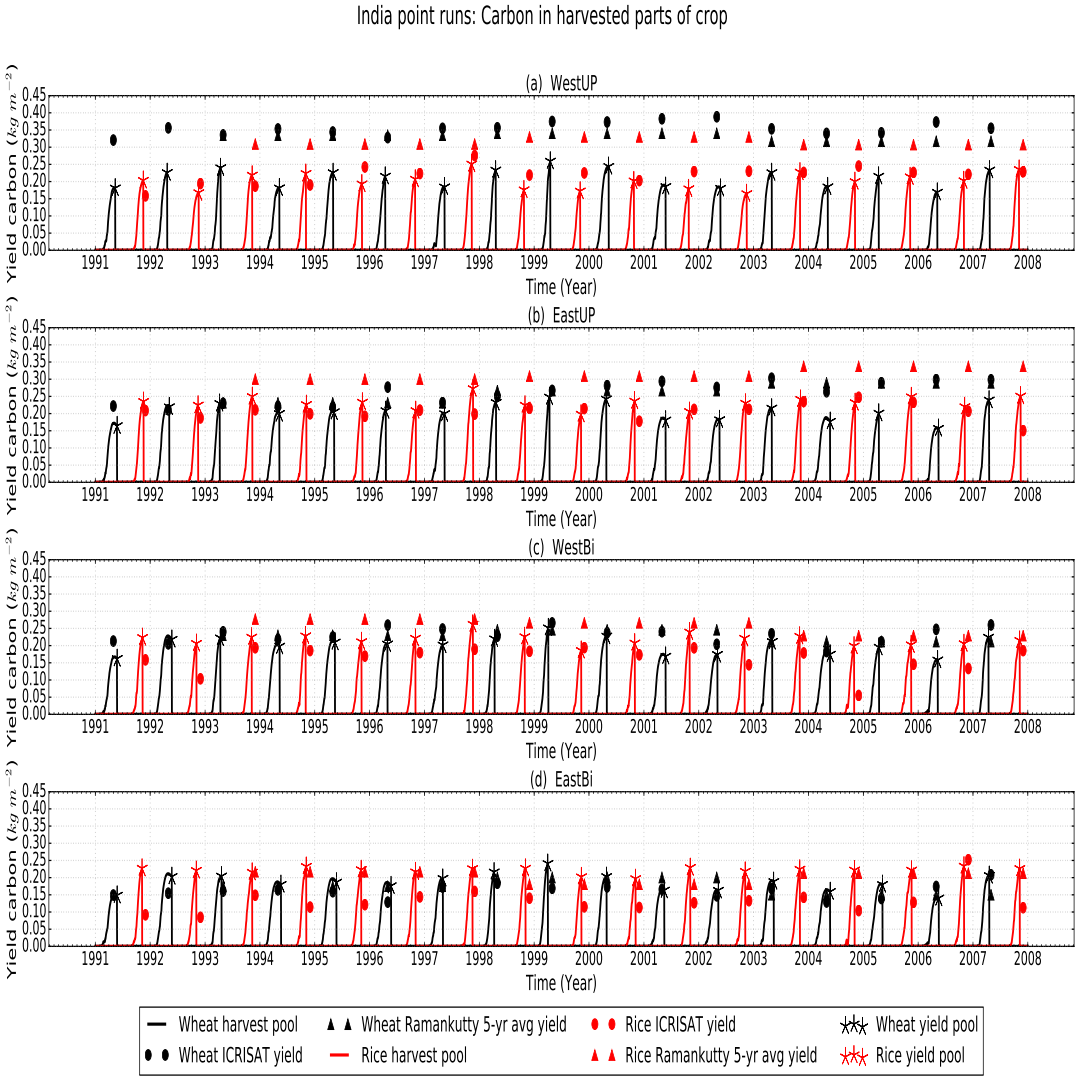

Figure 4.7: Timeseries of crop harvest pool (solid lines) with the JULES yield at the time it is output by the model (asterisks) for rice (red) and wheat (black) at each of the India sites shown in Fig. 4.2. Also shown are two sets of observations; annual yields from *ICRISAT* (2015) shown by the filled circles and 5 year averages from *Ray et al.* (2012a) shown by the filled triangles (following the same colours with rice shown in red and wheat in black)

moisture in the top 1.0 m across the year of the four locations. This is consistent with the temperature and precipitation timeseries shown in Fig. 4.6 where the locations become wetter and cooler from west to east. This means there is more available soil moisture in the top 1.0 m for the eastern locations compared with the western locations.

We have shown that JULES simulates wheat and rice across the four locations, however the varying conditions across these locations affect the model response which subsequently affects the yields produced by JULES. In general the model produces a similar amount of wheat biomass to Avignon but produces yields that are closer to those observed than for Avignon. This could be due to the JULES wheat parameterization

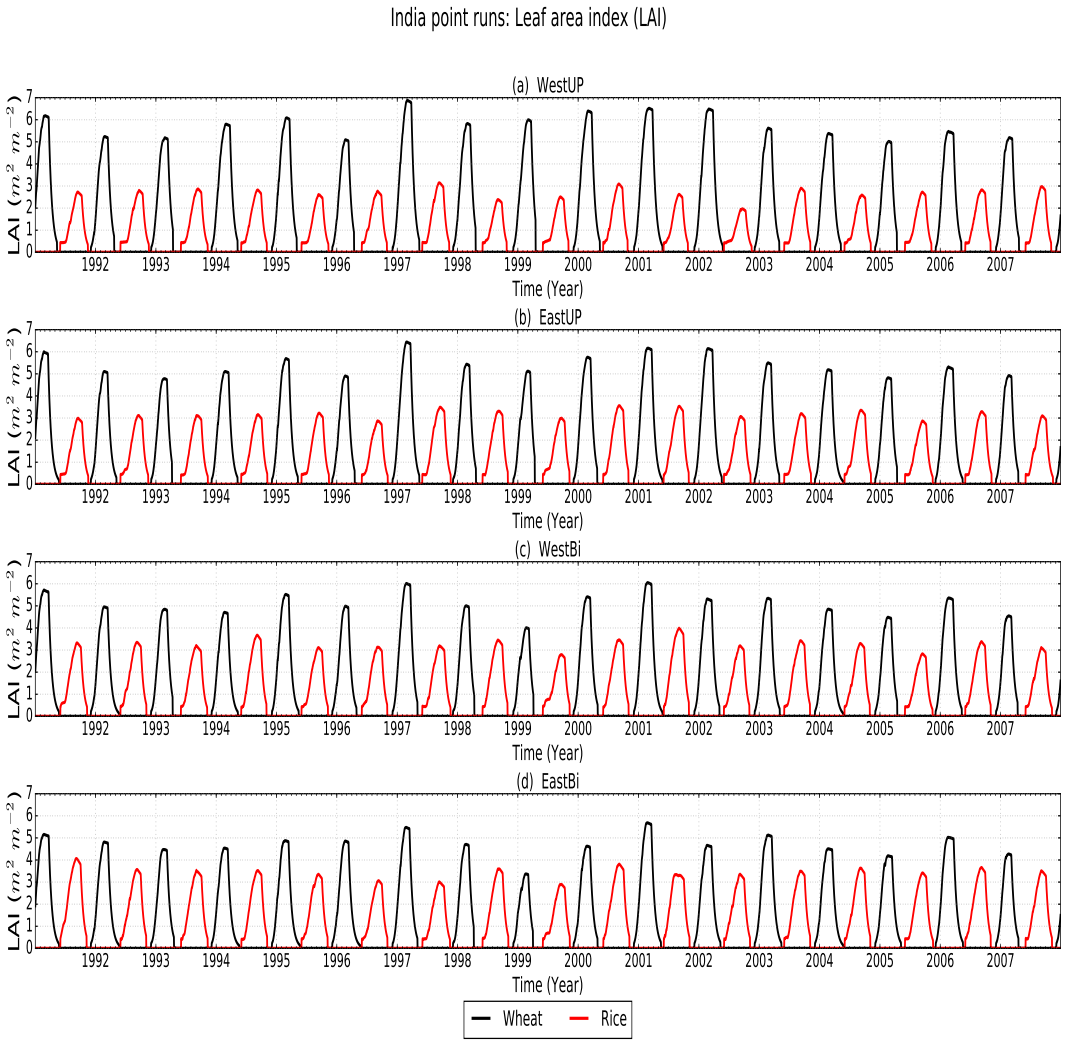

Figure 4.8: Timeseries of the leaf area index rice (red) and wheat (black) at each of the India sites shown in Fig. 4.2.

being more appropriate for modelling Indian spring wheat than Avignon winter wheat varieties.

4.7 Discussion and Conclusions

In this paper we describe and demonstrate a new development for JULES enabling more than one crop to be simulated at a given location during a particular growing season, thereby including a sequential cropping capability. There are relatively few models that are able to simulate sequential cropping, but there is a growing need as more regions of the world adopt this cropping system as a viable way of adapting to climate change (*Hudson*, 2009). We demonstrate the method and evaluate its impact for a site in

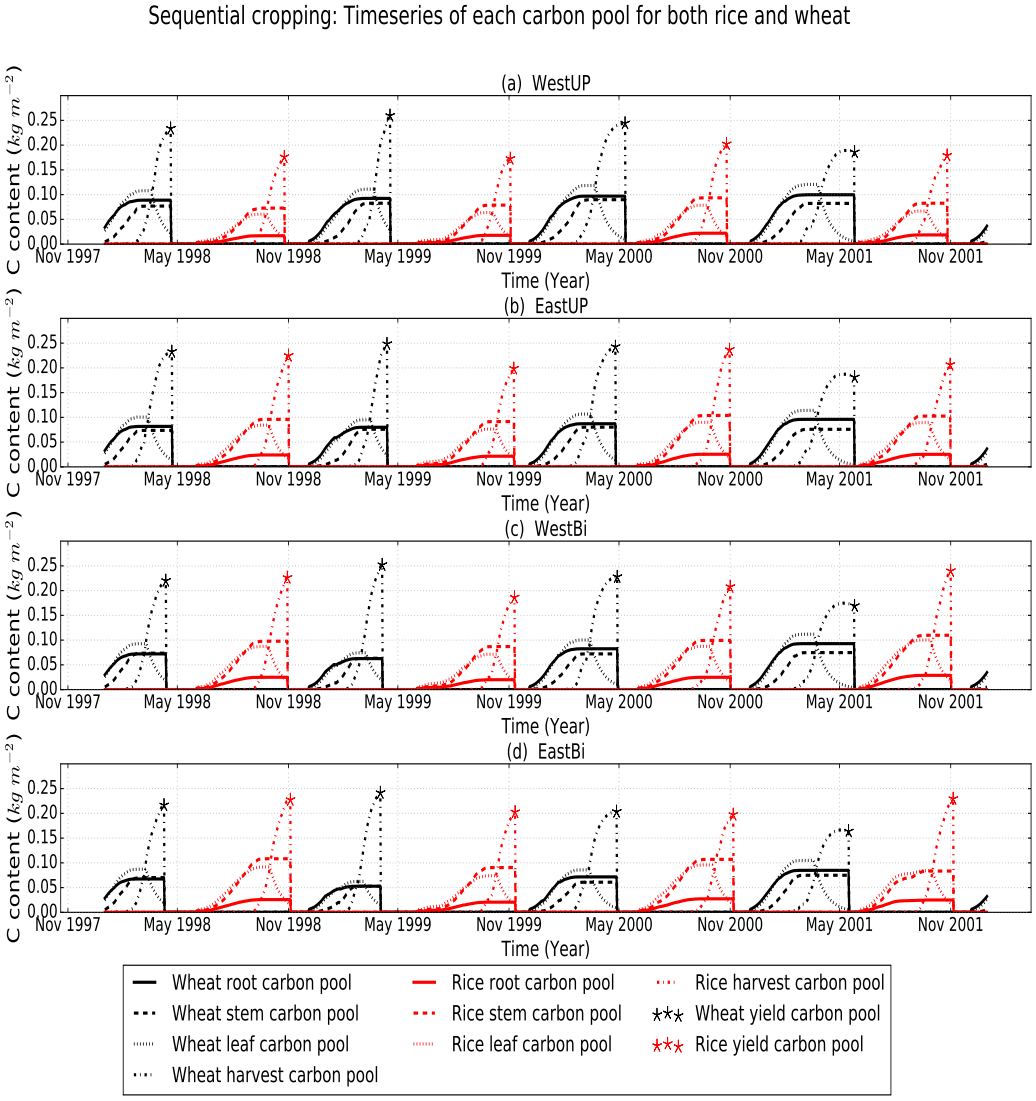

Figure 4.9: Timeseries of each crop carbon pool: leaf (solid lines), root (dashed), stem (dotted) and harvest (dash-dot) with the JULES yield at the time it is output by the model (asterisks) for rice (red) and wheat (black) at each of the India sites shown in Fig. 4.2 for a subset of years of the simulation between 1998 and 2001.

Avignon; this a site that has grown crops in rotation for several years and therefore has a lengthy and detailed observation record. We use this site to simulate a winter wheat–sorghum rotation in JULES approximated using spring wheat and maize. We apply this same method to four locations that use the sequential cropping system in the northern Indian states of Uttar Pradesh and Bihar, in order to inform its implementation for a regional simulation of South Asia.

We show that JULES is able to simulate two crops in a year both at Avignon and the four locations across Uttar Pradesh and Bihar, producing maxima of LAI, canopy height and biomass at approximately the correct times of the year. The wealth of

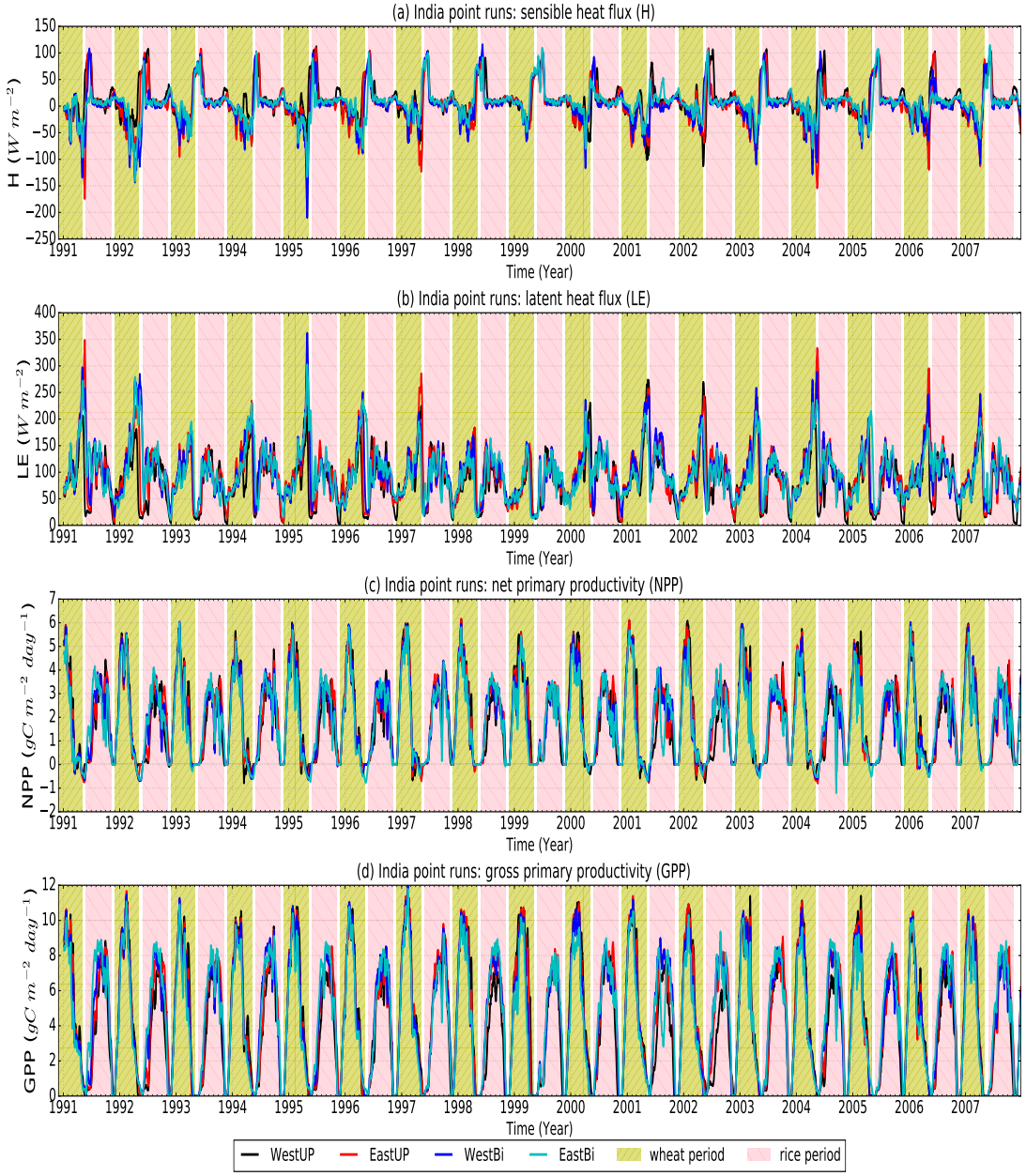

Figure 4.10: Timeseries of LE (a), H (b), gridbox NPP (c) and gridbox gpp (d) at each of the India sites shown in Fig. 4.2. Each location is represented by a solid line of a different colour: WestUP - black, EastUP - red, WestBi - blue and EastBi - cyan

observations at Avignon also provide the opportunity to gain a better understanding of the effect of sequential cropping on the surface fluxes. For Avignon, the representation of GPP and fluxes (H and LE) correlate well with observations with r_values of above 0.7. However the magnitude of the biomass for wheat is underestimated and LAI is overestimated compared with Avignon observations. The aim of showing the method for Avignon was not to produce perfect representations of the crops but show that the method is able to produce two crops in a single growing period and therefore provide a

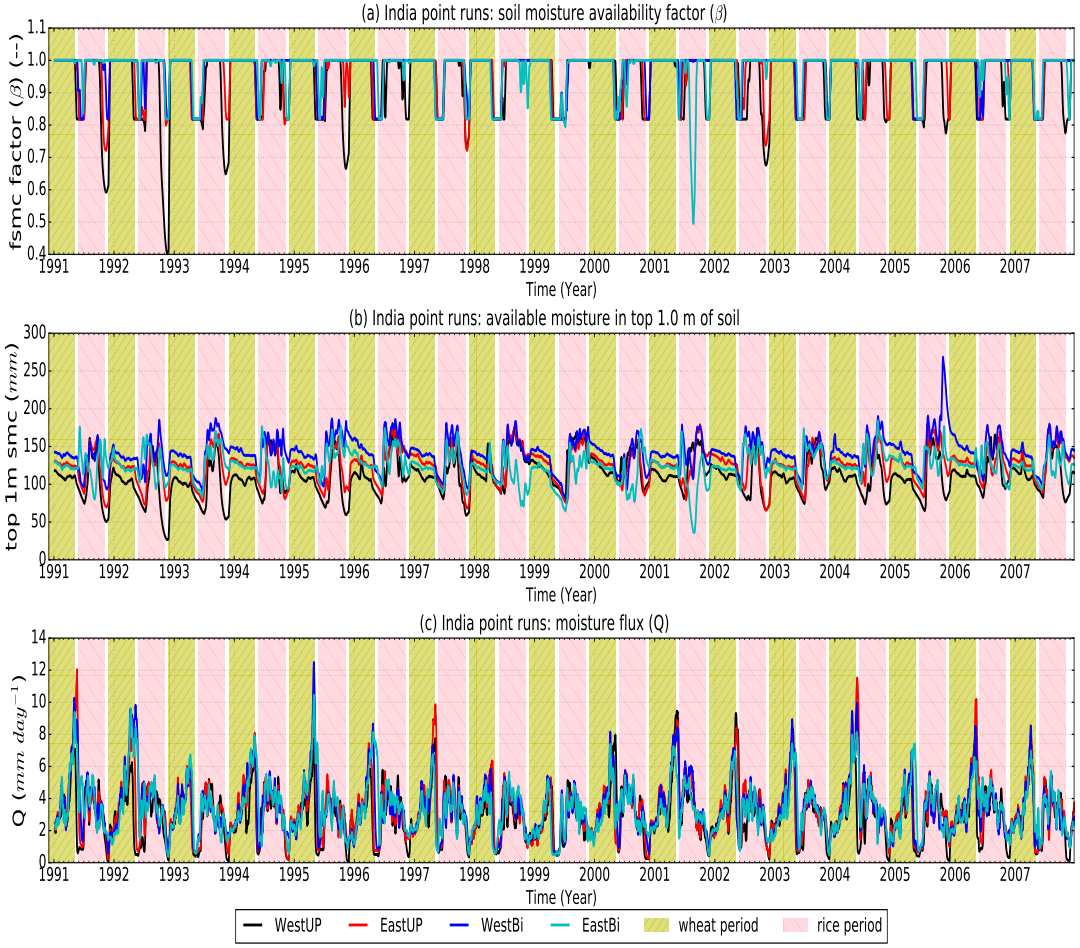

Figure 4.11: Timeseries of moisture fluxes including the gridbox soil moisture availability factor (beta) (a), the gridbox available moisture in the top 1.0 m of soil (b) and moisture flux across the gridbox (c) at each of the India sites shown in Fig. 4.2. Each location is represented by a solid line of a different colour: WestUP - black, EastUP - red, WestBi - blue and EastBi - cyan

better representation of the real land surface at Avignon than previously possible using the crop model. In general there are only small differences between using the crop model and using grasses to represent the crops at this site, indicating that both provide a similar representation of the surface fluxes. There are two varieties of sorghum grown at this site and this is apparent from the differences in the JULES simulations presented. Using maize as an approximation for sorghum provides a better representation for the variety grown in 2009 than in either of the 2007 or 2011 seasons. The representation of crops at Avignon could be improved by including crop specific parameterizations of winter wheat and sorghum in the model, although sorghum would probably require two different sets of parameters for a significant improvement because the two varieties grown at the site are so different. The soil moisture observations for Avignon show that there are periods where the soil moisture is very low. In additional simulations with prescribed soil moisture (not shown) soil moisture stress causes a significant drop

in GPP which is much earlier than shown in the observations, this is the subject of a wider modelling effort (*Williams et al.*, 2018, *Harper et al.*, in preparation) that aims to improve the response to soil moisture stress in JULES.

The sequential cropping system is used widely in the Tropics, especially regions such as Pakistan, India and Bangladesh. In order to apply this method to tropical regions we run JULES at four locations across the Indian states of Uttar Pradesh and Bihar; these are two of the main producers of rice and wheat in India and use of the rice–spring wheat rotation is prevalent in this region. This region is highly variable, both in terms of temperatures (ranging from 7 to 52 ° C) and rainfall (between 0 and 15 $mm\ day^{-1}$) with these locations showing a cooling moistening trend from west to east making conditions for growing crops very different across a relatively limited area. JULES produces both a rice and wheat crop at each of the four locations, with yields for the locations in the cooler, wetter east of the region closer to observed yields than those in the warmer drier west. We propose two possible reasons for this difference, although in reality both could be contributing factors. One explanation for the differences in observed yields between WestUP and EastBi is the differing management practices between the two states of Uttar Pradesh and Bihar. The western locations are typically more effective at adopting new technology and therefore have higher yields than the eastern locations. This difference from west to east may therefore be reduced by a yield gap parameter.

The difference between the observed and model yields at WestUP may be exacerbated by the lack of irrigation in the forcing data, which means that evaporation from surface water due to irrigation is missing in these simulations. *Tuinenburg et al.* (2014) highlight that this makes a considerable contribution to the overall moisture budget for this region. On this basis we hypothesize that this missing evaporative process has a drying effect on the RCM atmosphere driving JULES; particularly at the already arid western locations. This could be affecting the yields there. In addition, it is possible that revising the carbon partitioning especially for wheat could have a positive impact on yields. Further investigation is needed to establish the reasons for the model yields at these locations. It would be interesting and useful to follow up this study with further simulations which attempt to account for this missing process, for example, by using alternative driving data that includes irrigation and the subsequent surface evaporation. This would demonstrate if the influence of the evaporation of irrigation water from the surface is a large enough effect to increase the modelled yields for WestUP and maintain the yields for EastBi, where the humidity is usually higher and therefore maybe less influenced by this process.

The work presented here has shown that sequential cropping is an important addition to JULES, providing a closer representation of the land surface where crops are grown in rotation. Therefore the code modifications presented as part of this analysis, currently in a branch of JULES at vn5.2, are intended for inclusion in a future official version of JULES. This analysis has provided valuable information for using

this sequential cropping method for future regional crop simulations; these regional simulations will be the focus of work that follows this paper. Model intercomparison projects such as AgMIP (*Rivington and Koo*, 2010, *Rosenzweig et al.*, 2013, 2014) and ISIMIP (*Warszawski et al.*, 2013, 2014) have hugely benefited the crop and land-surface modelling communities by accelerating development and understanding of land surface models. On the basis that this cropping system is likely to be a feature of the future land-surface, not just in the tropics but globally as an adaptation to climate change, we encourage other modelling communities to develop their models to include a sequential cropping capability so that future model intercomparisons can include this and find ways to improve it further.

4.8 Appendix A: Avignon comparison

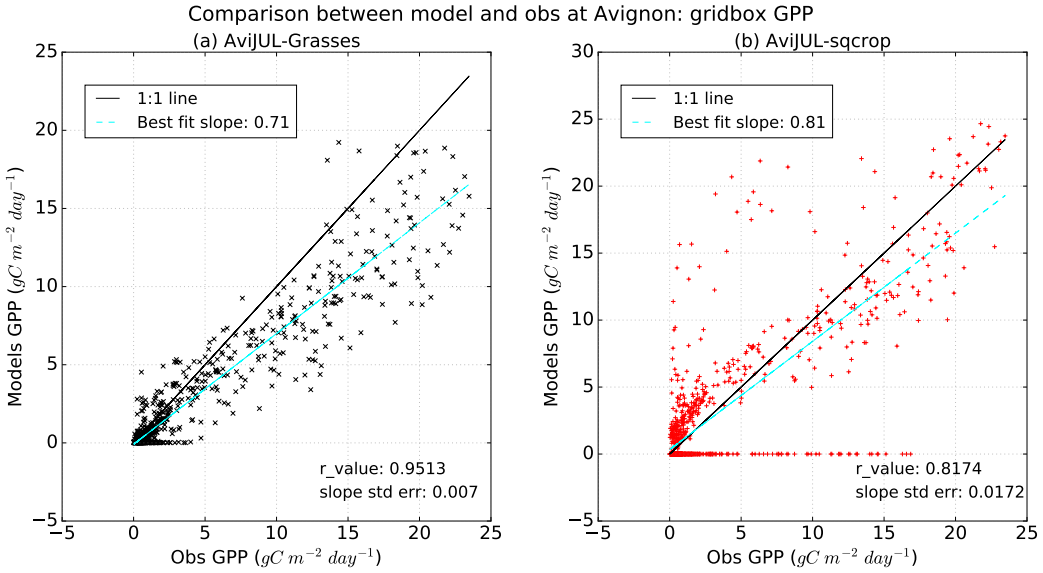

Figure A.1: Comparison of Observed GPP at the Avignon site against the modelled GPP between 2005 and 2008 for AviJUL-grass (a) and AviJUL-sqcrop (b)

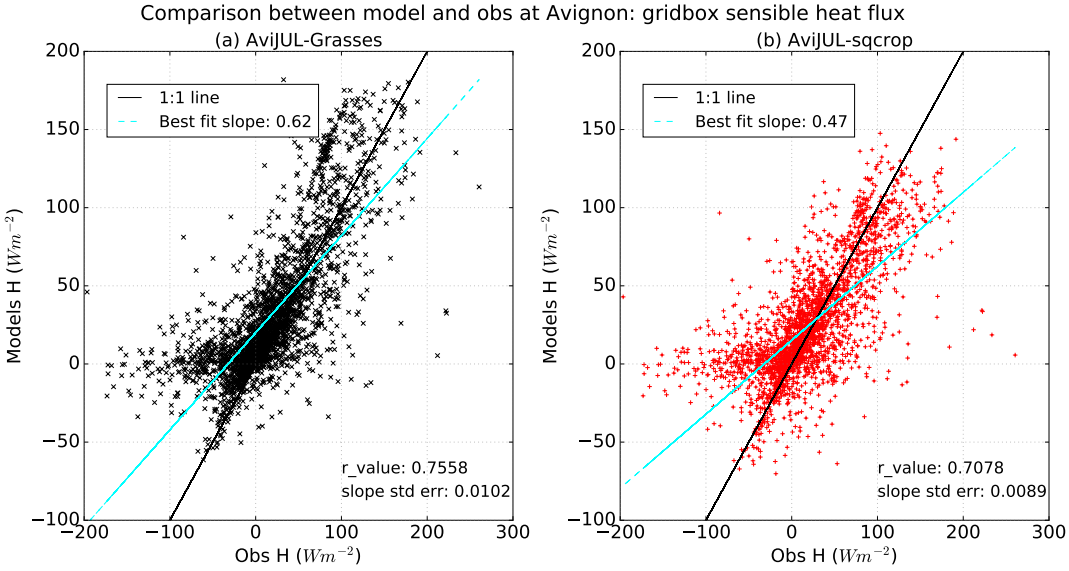

Figure A.2: Comparison of observed H at the Avignon site against the modelled H between 2005 and 2013 for AviJUL-grass (a) and AviJUL-sqcrop (b)

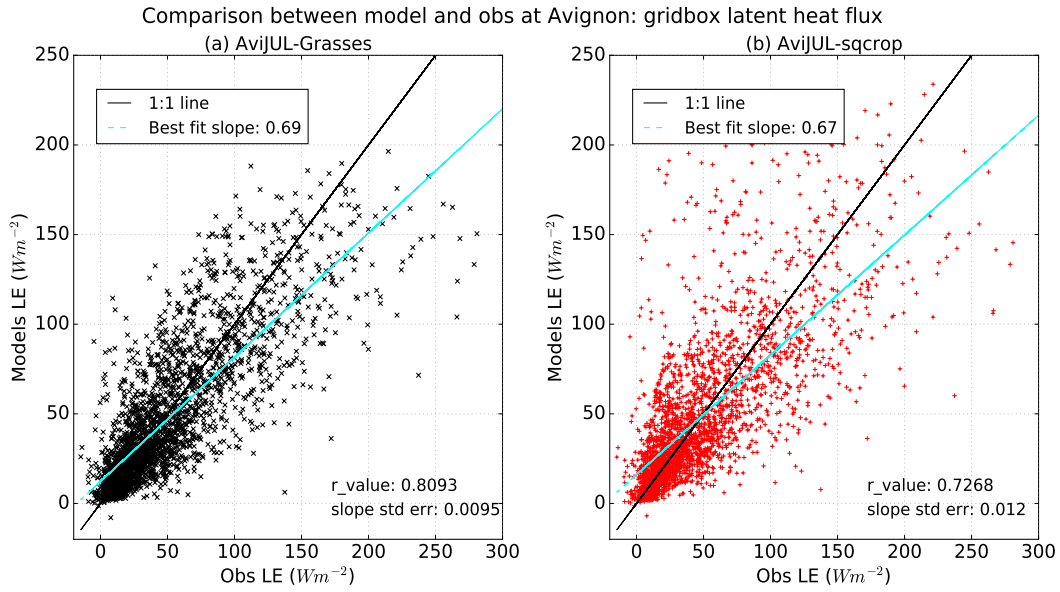

Figure A.3: Comparison of observed LE at the Avignon site against the modelled LE between 2005 and 2013 for AviJUL-grass (a) and AviJUL-sqcrop (b).

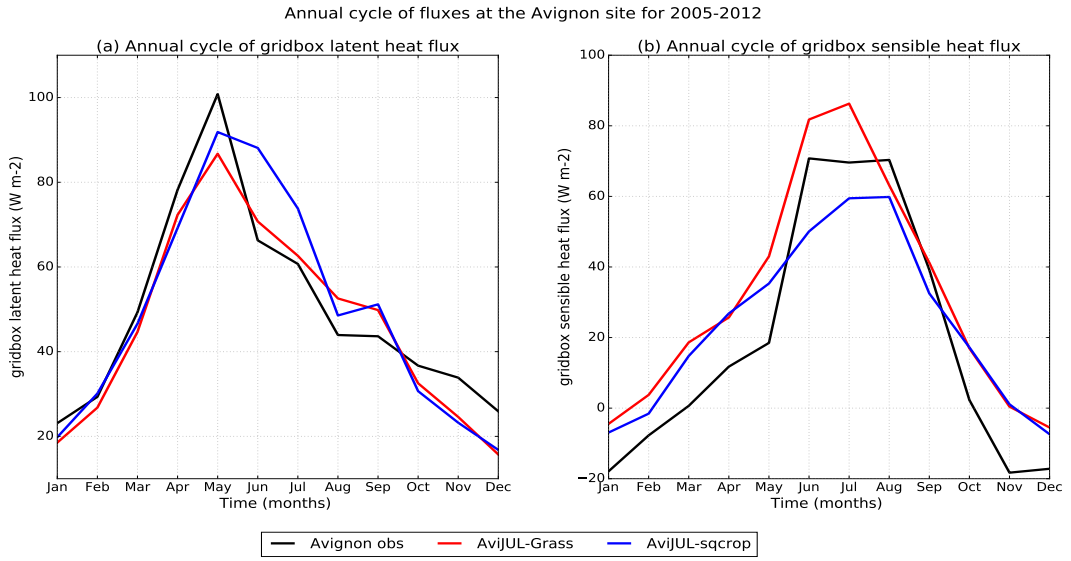

Figure A.4: Annual cycle of the H and LE compared with observations (black line) at the Avignon site for between 2005 and 2013. Annual cycles for the simulations are also shown: AviJUL-grass (red line). AviJUL-sqcrop (blue line).

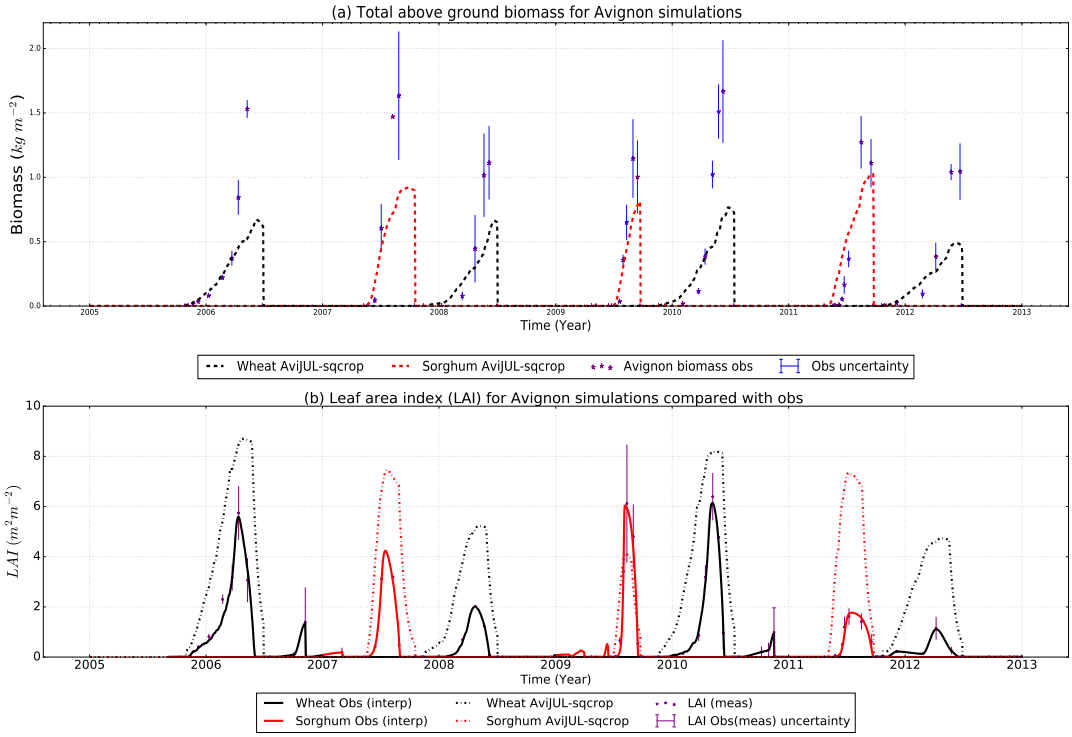

Figure A.5: The timeseries of total biomass (a) and leaf area index (LAI) (b) for simulations with a setting of 0 for $p0$ for the Avignon site for wheat (black) and sorghum (red) for observations (solid lines) and simulation using the observed sowing and harvest dates: AviJUL-sqcrop (dashed) for the period between 2005 and 2013 using observed sowing and harvest dates. AviJUL-grass simulations are not shown here as these follow the observed LAI and canopy height.

4.9 Appendix B: India comparison

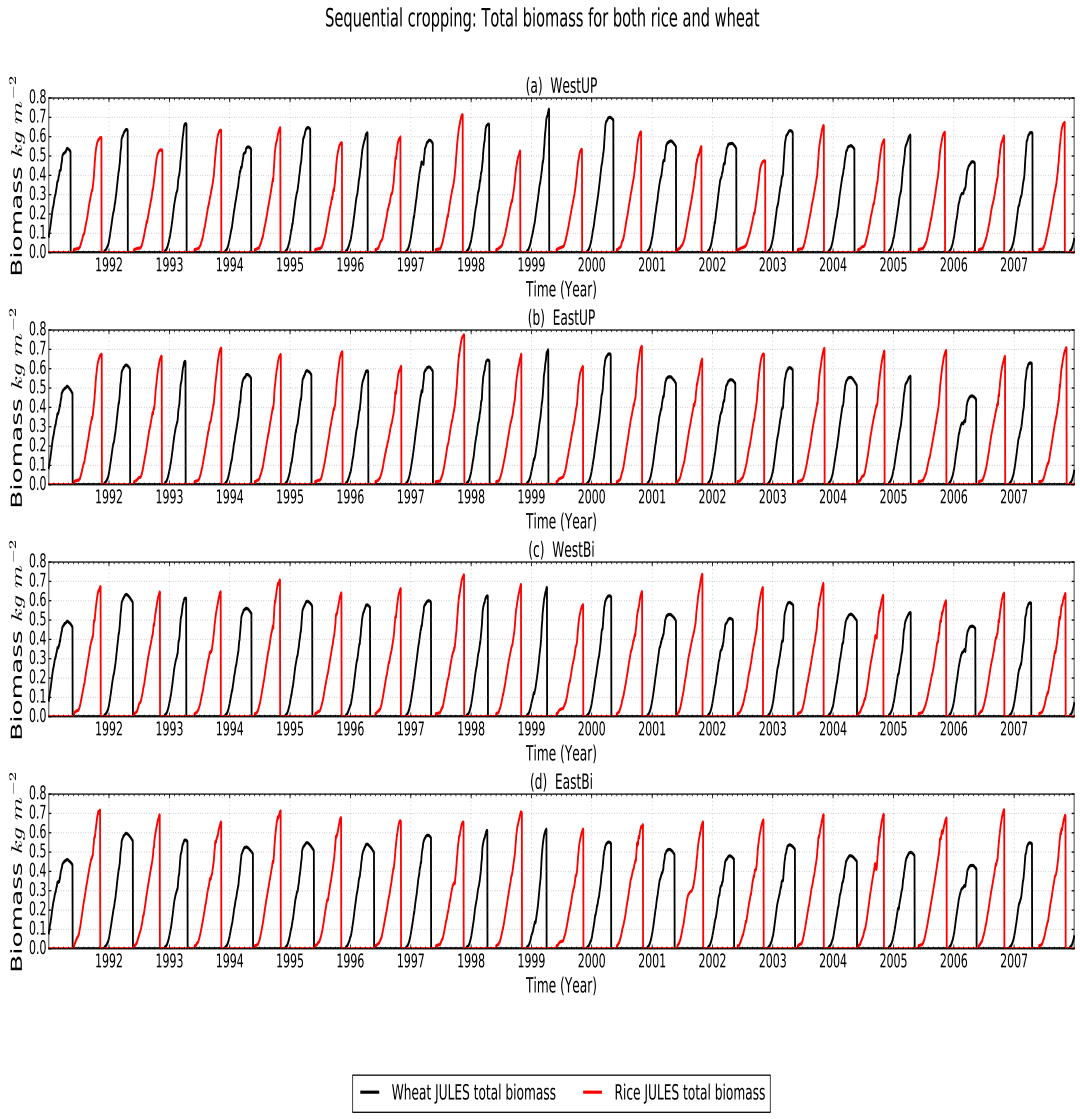

Figure B.1: Timeseries of total biomass for rice (red) and wheat (black) at each of the India sites shown in Fig. 4.2.

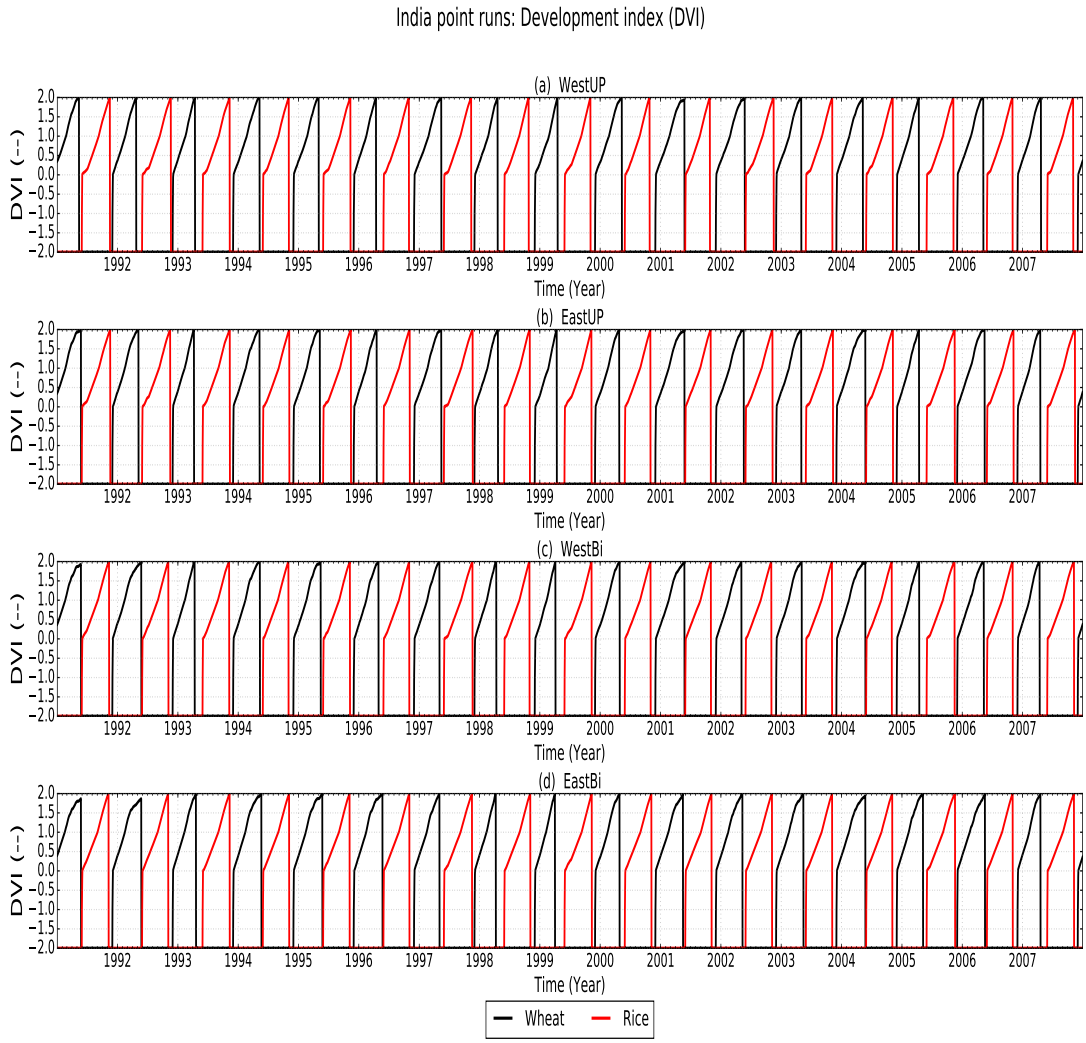

Figure B.2: Timeseries of the development index (DVI) for rice (red) and wheat (black) at each of the India sites shown in Fig. 4.2.

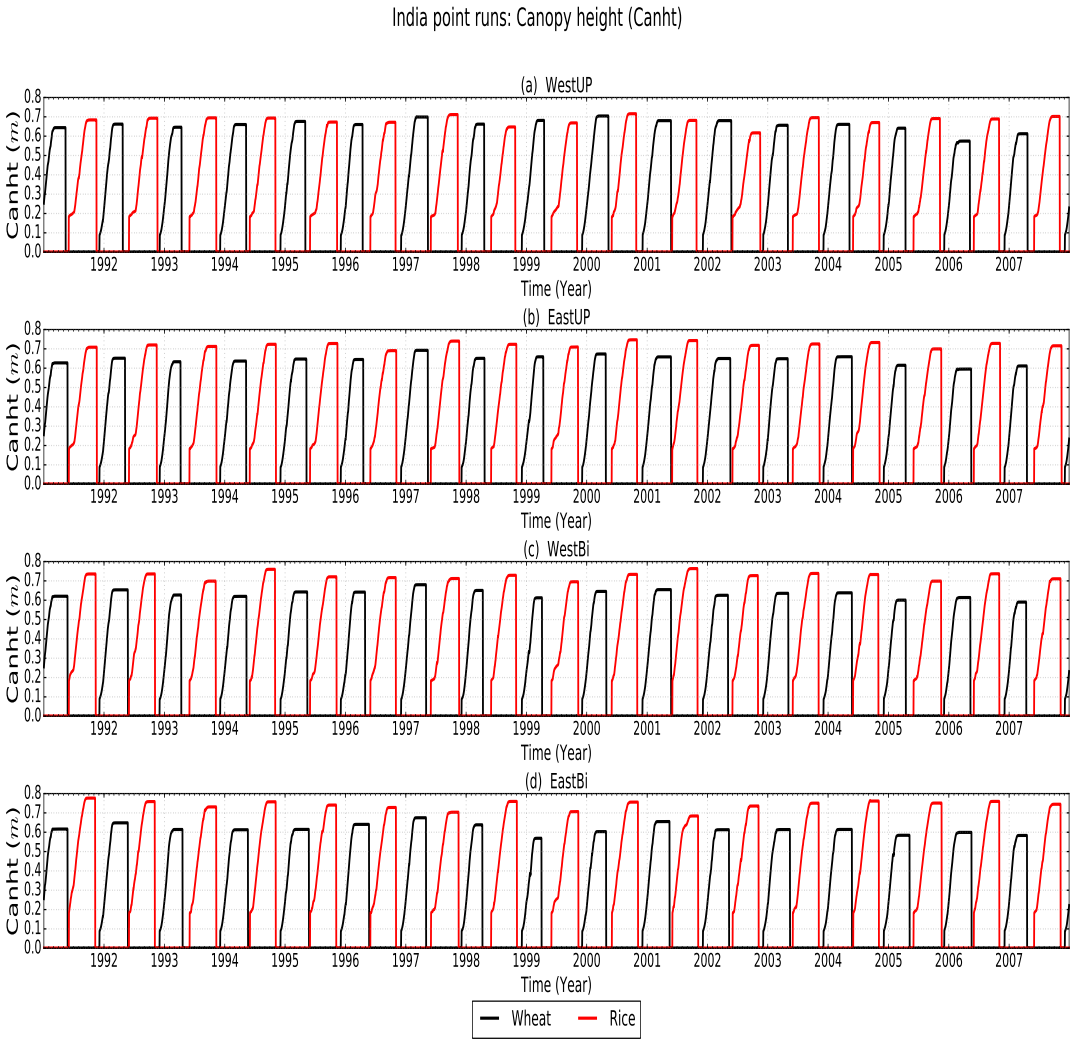

Figure B.3: Timeseries of canopy height for rice (red) and wheat (black) at each of the India sites shown in Fig. 4.2.

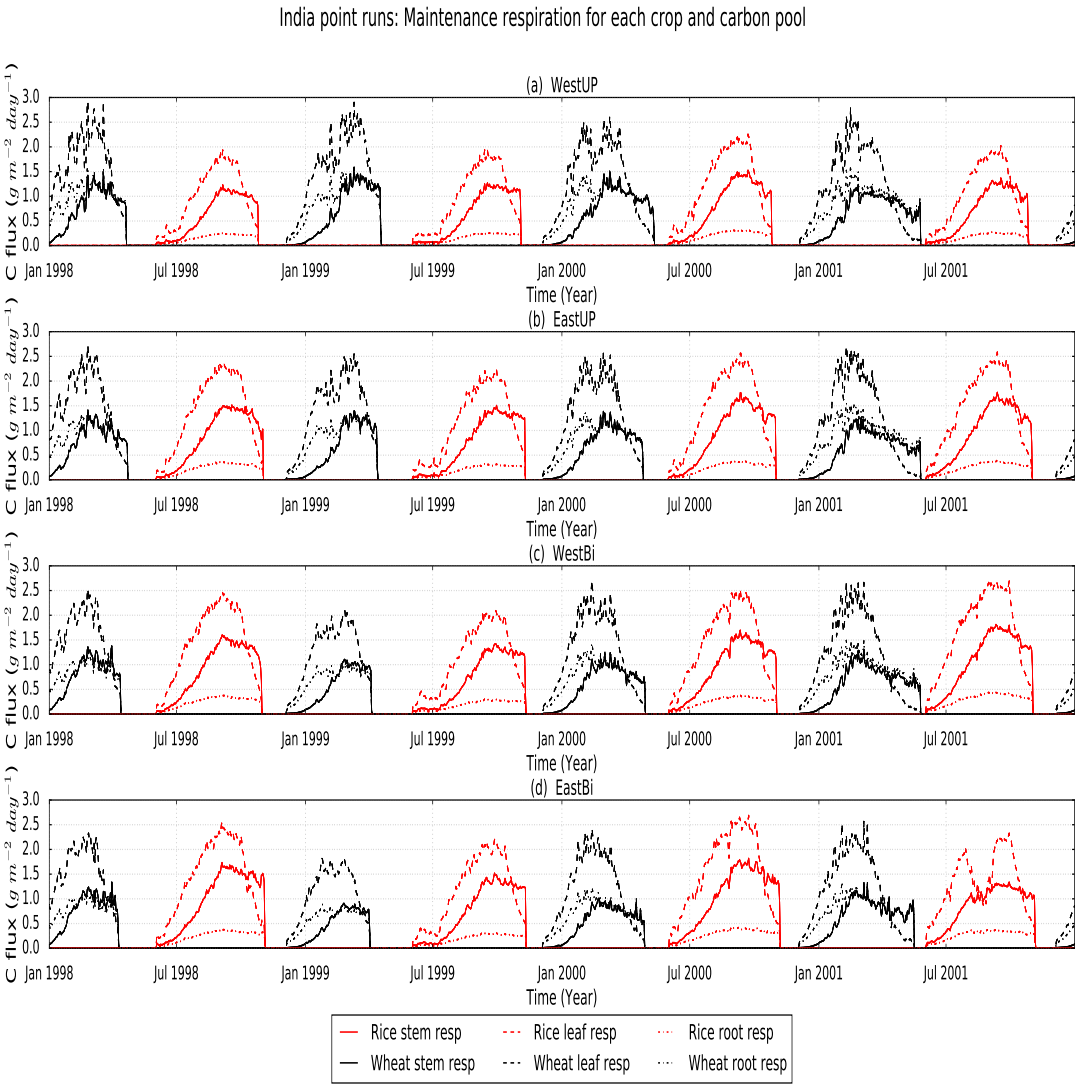

Figure B.4: Timeseries of leaf, stem and root leaf respiration for rice (red) and wheat (black) at each of the India sites shown in Fig. 4.2.

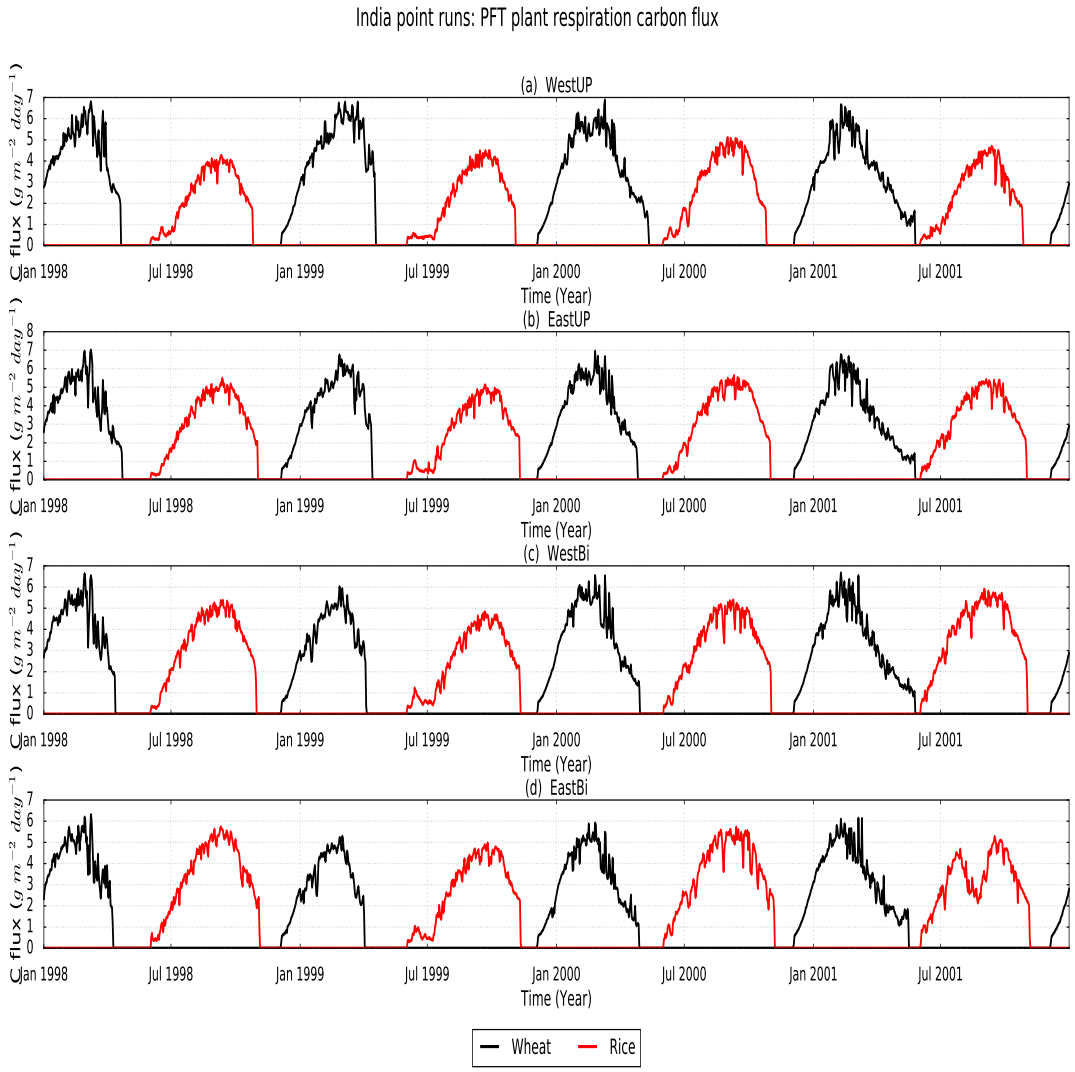

Figure B.5: Timeseries of plant respiration for rice (red) and wheat (black) at each of the India sites shown in Fig. 4.2.

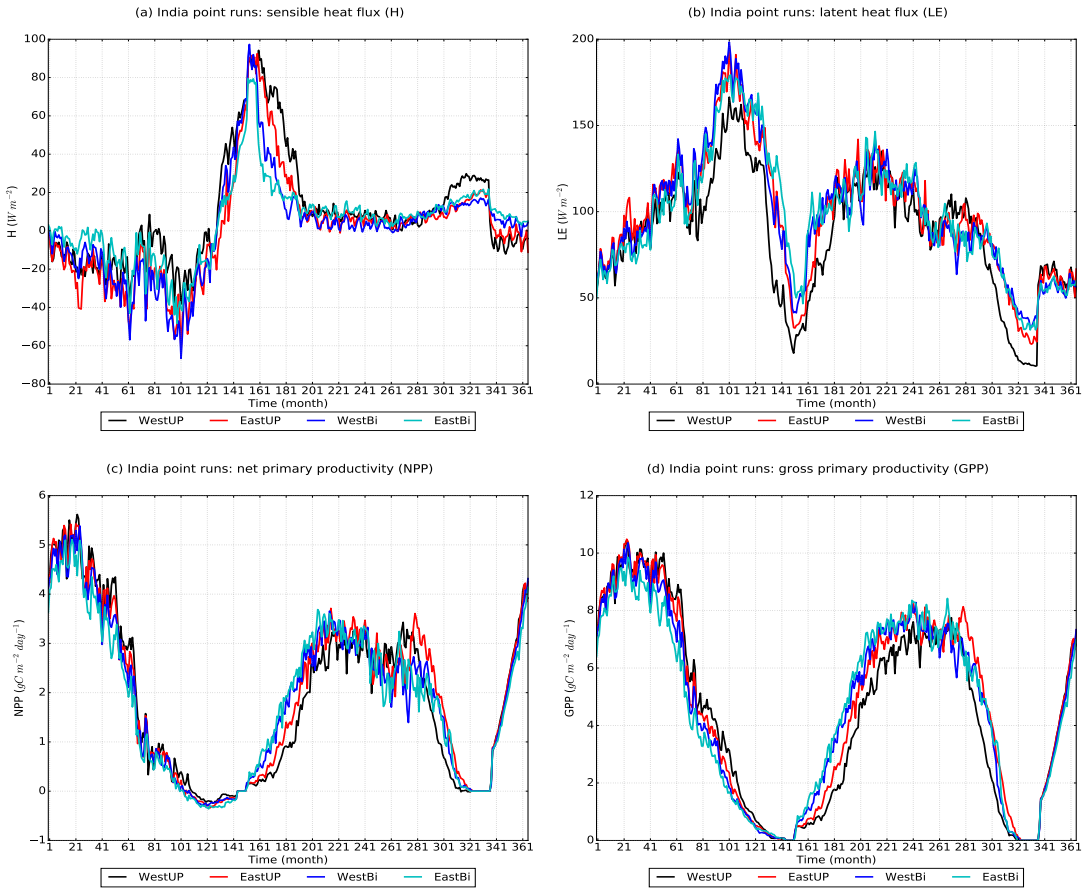

Figure B.6: Annual climatology (in day of year) of H (a), LE (b), gridbox NPP (c) and gridbox gpp (d) at each of the India sites shown in Fig. 4.2. Each location is represented by a solid line of a different colour: WestUP - black, EastUP - red, WestBi - blue and EastBi - cyan

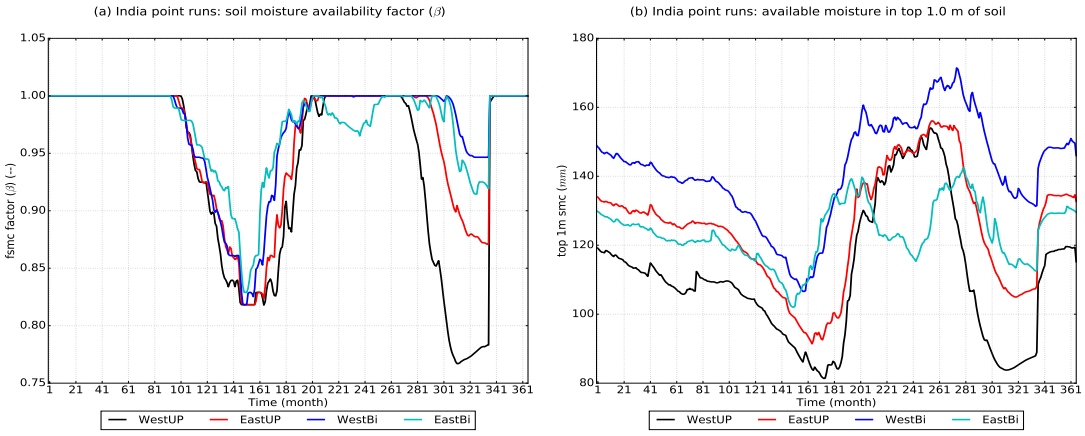

Figure B.7: Annual climatology of moisture fluxes including the gridbox soil moisture availability factor (beta) (a) and the gridbox available moisture in the top 1.0 m of soil (b) at each of the India sites shown in Fig. 4.2. Each location is represented by a solid line of a different colour: WestUP - black, EastUP - red, WestBi - blue and EastBi - cyan

References

Allen, R. G., L. S. Pereira, D. Raes, and M. Smith (1998), Crop evapotranspiration - guidelines for computing crop water requirements - fao irrigation and drainage paper 56, *Food and Agriculture Organization of the United Nations*. 4.6.1

Best, M. J., M. Pryor, D. B. Clark, G. G. Rooney, R. L. H. Essery, C. B. Ménard, J. M. Edwards, M. A. Hendry, A. Porson, N. Gedney, L. M. Mercado, S. Sitch, E. Blyth, O. Boucher, P. M. Cox, C. S. B. Grimmond, and R. J. Harding (2011), The joint uk land environment simulator (JULES), model description, part 1: Energy and water fluxes, *Geoscientific Model Development*, *4*(3), 677–699, doi:10.5194/gmd-4-677-2011. 4.2

Betts, R. A. (2005), Integrated approaches to climate-crop modelling: needs and challenges, *Philosophical transactions of the Royal Society of London. Series B, Biological sciences*, *360*, 2049–65, doi:10.1098/rstb.2005.1739. 4.1

Bhattacharyya, T., D. Pal, M. Easter, N. Batjes, E. Milne, K. Gajbhiye, P. Chandran, S. Ray, C. Mandal, K. Paustian, S. Williams, K. Killian, K. Coleman, P. Falloon, and D. Powlson (2007), Modelled soil organic carbon stocks and changes in the indo-gangetic plains, india from 1980 to 2030, *Agriculture, Ecosystems & Environment*, *122*(1), 84 – 94, doi:10.1016/j.agee.2007.01.010, soil carbon stocks at regional scales. 4.1

Biemans, H., L. Speelman, F. Ludwig, E. Moors, A. Wiltshire, P. Kumar, D. Gerten, and P. Kabat (2013), Future water resources for food production in five South Asian river basins and potential for adaptation - a modeling study, *Science of The Total Environment*, *468-469, Supplement*(0), S117–S131, doi:10.1016/j.scitotenv.2013.05.092. 4.6.2

Biemans, H., C. Siderius, A. Mishra, and B. Ahmad (2016), Crop-specific seasonal estimates of irrigation-water demand in south asia, *Hydrology and Earth System Sciences*, *20*(5), 1971–1982, doi:10.5194/hess-20-1971-2016. 4.1

Bodh, S. P. C., S. J. P. Rai, S. A. Sharma, S. P. Gajria, S. M. Yadav, S. S. Virmani, and S. R. Pandey (2015), Agricultural statistics at a glance 2015, *Ministry of Agriculture & Farmers welfare, Directorate of Economics and Statistics*. (document), 4.4.2, 4.5

Bondeau, A., P. C. Smith, S. Zaehle, S. Schaphoff, W. Lucht, W. Cramer, D. Gerten, H. Lotze-Campen, C. Müller, M. Reichstein, and B. Smith (2007), Modelling the role of agriculture for the 20th century global terrestrial carbon balance, *Global Change Biology*, *13*(3), 679–706, doi:10.1111/j.1365-2486.2006.01305.x. 4.1

Caldwell, R. M., and J. W. Hansen (1993), *Simulation of multiple cropping systems with CropSys*, pp. 397–412, Springer Netherlands, Dordrecht, doi:10.1007/978-94-011-2842-1_24. 4.1

Calvet, J.-C., J. Noilhan, J.-L. Roujean, P. Bessemoulin, M. Cabelguenne, A. Olioso, and J.-P. Wigneron (1998), An interactive vegetation svat model tested against data from six contrasting sites, *Agricultural and Forest Meteorology*, *92*(2), 73–95, doi:10.1016/S0168-1923(98)00091-4. 4.1

Challinor, A., T. Wheeler, P. Craufurd, J. Slingo, and D. Grimes (2004), Design and optimisation of a large-area process-based model for annual crops, *Agricultural and Forest Meteorology*, *124*(1-2), 99–120, doi:10.1016/j.agrformet.2004.01.002. 4.6.2, 4.6.2

Clark, D. B., L. M. Mercado, S. Sitch, C. D. Jones, N. Gedney, M. J. Best, M. Pryor, G. G. Rooney, R. L. H. Essery, E. Blyth, O. Boucher, R. J. Harding, C. Huntingford, and P. M. Cox (2011), The joint uk land environment simulator (JULES), model description, part 2: Carbon fluxes and vegetation dynamics, *Geoscientific Model Development*, *4*(3), 701–722, doi:10.5194/gmd-4-701-2011. 4.2

Cong, W.-F., E. Hoffland, L. Li, J. Six, J.-H. Sun, X.-G. Bao, F.-S. Zhang, and W. V. D. Werf (2015), Intercropping enhances soil carbon and nitrogen, *Global Change Biology*, *21*(4), 1715–1726, doi:10.1111/gcb.12738. 4.1

Dee, D. P., S. M. Uppala, A. J. Simmons, P. Berrisford, P. Poli, S. Kobayashi, U. Andrae, M. A. Balmaseda, G. B. P., Bauer, P. Bechtold, A. C. M. Beljaars, L. van de Berg, J. Bidlot, N. Bormann, C. Delsol, R. Dragani, M. Fuentes, A. J. Geer, L. Haimberger, S. B. Healy, H. Hersbach, E. V. Hólm, L. Isaksen, P. Kållberg, M. Köhler, M. Matricardi, A. P. McNally, B. M. Monge-Sanz, J.-J. Morcrette, B.-K. Park, C. Peubey, P. de Rosnay, C. Tavolato, J.-N. Thépaut, and F. Vitart (2011), The era-interim reanalysis: configuration and performance of the data assimilation system, *Quarterly Journal of the Royal Meteorological Society*, *137*(656), 553–597, doi:10.1002/qj.828. 4.4.2

Dury, J., N. Schaller, F. Garcia, A. Reynaud, and J. E. Bergez (2012), Models to support cropping plan and crop rotation decisions. a review, *Agronomy for Sustainable Development*, *32*(2), 567–580, doi:10.1007/s13593-011-0037-x. 4.1

Erenstein, O., and V. Laxmi (2008), Zero tillage impacts in india's rice-wheat systems: A review, *Soil and Tillage Research*, *100*, 1–14, doi:10.1016/j.still.2008.05.001. 4.1, 4.6.2

Erenstein, O., U. Farooq, R. Malik, and M. Sharif (2008), On-farm impacts of zero tillage wheat in south asia's rice-wheat systems, *Field Crops Research*, *105*(3), 240–252, doi:10.1016/j.fcr.2007.10.010. 4.1

Essery, R. L. H., M. J. Best, and P. M. Cox (2001), Moses 2.2 technical documentation, *Hadley Centre Technical Note*, *30*. 4.4.2

Fischer, R. (2015), Definitions and determination of crop yield, yield gaps, and of rates of change, *Field Crops Research*, *182*, 9–18, doi:10.1016/j.fcr.2014.12.006. 4.6.2

Frieler, K., A. Levermann, J. Elliott, J. Heinke, A. Arneth, M. F. P. Bierkens, P. Ciais, D. B. Clark, D. Deryng, P. Döll, P. Falloon, B. Fekete, C. Folberth, A. D. Friend, C. Gellhorn, S. N. Gosling, I. Haddeland, N. Khabarov, M. Lomas, Y. Masaki, K. Nishina, K. Neumann, T. Oki, R. Pavlick, A. C.Ruane, E. Schmid, C. Schmitz, T. Stacke, E. Stehfest, Q. Tang, D. Wisser, V. Huber, F. Piontek, L. Warszawski, J. Schewe, H. Lotze-Campen, and H. J. Schellnhuber (2015), A framework for the cross-sectoral integration of multi-model impact projections: land use decisions under climate impacts uncertainties, *Earth System Dynamics*, *6*(2), 447–460, doi:10.5194/esd-6-447-2015. 4.1

Garrigues, S., A. Olioso, J. Calvet, E. Martin, S. Lafont, S. Moulin, A. Chanzy, O. Marloie, S. Buis, V. Desfonds, N. Bertrand, and D. Renard (2015), Evaluation of land surface model simulations of evapotranspiration over a 12-year crop succession: impact of soil hydraulic and vegetation properties, *Hydrology and Earth System Sciences*, *19*(7), 3109–3131, doi:10.5194/hess-19-3109-2015. (document), 4.1, 4.4.1, 4.4, 4.5.1, 4.6.1, 4.6.1

Garrigues, S., A. Boone, B. Decharme, A. Olioso, C. Albergel, J.-C. Calvet, S. Moulin, S. Buis, and E. Martin (2018), Impacts of the soil water transfer parameterization on the simulation of evapotranspiration over a 14-year mediterranean crop succession, *Journal of Hydrometeorology*, *19*(1), 3–25, doi:10.1175/JHM-D-17-0058.1. 4.1, 4.4.1

Goswami, B., and P. K. Xavier (2005), Dynamics of "internal" interannual variability of the Indian summer monsoon in a GCM, *Journal of Geophysical Research: Atmospheres*, *110*(D24), doi:10.1029/2005JD006042. 4.1

Griffiths, F. E. W., R. Lyndon, and M. Bennett (1985), The effects of vernalization on the growth of the wheat shoot apex, *Annals of Botany*, *56*, 501–511, doi:10.1093/oxfordjournals.aob.a087035. 4.4.2

Harding, R., E. Blyth, O. Tuinenburg, and A. Wiltshire (2013), Land atmosphere feedbacks and their role in the water resources of the ganges basin, *Science of The Total Environment*, *468-469, Supplement*(0), S85–S92, doi:10.1016/j.scitotenv.2013.03.016, changing water resources availability in Northern India with respect to Himalayan glacier retreat and changing monsoon patterns: consequences and adaptation. 4.6.2

Harper, A. B., K. Williams, J. Team, and F. Team (in preparation), Toward an improved representation of soil moisture stress: disentangling causes and effects, *to be decided*, *00*, 0–34. 4.6.1, 4.6.1, 4.7

Hatfield, J. L., and J. H. Prueger (2015), Temperature extremes: Effect on plant growth and development, *Weather and Climate Extremes*, *10*, 4–10, doi:10.1016/j.wace.2015.08.001, uSDA Research and Programs on Extreme Events. 4.1

Hu, S., X. Mo, and Z. Lin (2014), Optimizing the photosynthetic parameter vcmax by assimilating modis-fpar and modis-ndvi with a process-based ecosystem model, *Agricultural and Forest Meteorology*, *198-199*, 320–334, doi:10.1016/j.agrformet.2014.09.002. 4.4

Hudson, R. (2009), *Management of Agricultural, Forestry, Fisheries and Rural Enterprise - Volume I*, 254–265 pp., EOLSS Publications, 2009. 4.1, 4.7

ICRISAT (2015), District Level Database Documentation, *Tech. rep.*, International Crops Research Institute for the Semi-Arid Tropics, Hyderabad. (document), 4.5.2, 4.6.2, 4.7

Iizumi, T., and N. Ramankutty (2015), How do weather and climate influence cropping area and intensity?, *Global Food Security*, *4*, 46–50, doi:10.1016/j.gfs.2014.11.003. 4.1

Jones, R. G., M. Noguer, D. C. Hassell, D. Hudson, S. S. Wilson, G. J. Jenkins, and J. F. Mitchell (2004), Generating high resolution climate change scenarios using PRECIS, *Met Office Hadley Centre, Exeter, UK*, pp. 0–40. 4.4.2

Kumar, P., A. Wiltshire, C. Mathison, S. Asharaf, B. Ahrens, P. Lucas-Picher, J. H. Christensen, A. Gobiet, F. Saeed, S. Hagemann, and D. Jacob (2013), Downscaled climate change projections with uncertainty assessment over India using a high resolution multi-model approach, *Science of The Total Environment*, *468-469, Supplement*(0), S18–S30, doi:10.1016/j.scitotenv.2013.01.051, changing water resources availability in Northern India with respect to Himalayan glacier retreat and changing monsoon patterns: consequences and adaptation. 4.1, 4.4.2

Kumar, R., R. Singh, and K. Sharma (2005), Water resources of India, *Current Science*, *89*(5), 794–811. 4.6.2

Laik, R., S. Sharma, M. Idris, A. Singh, S. Singh, B. Bhatt, Y. Saharawat, E. Humphreys, and J. Ladha (2014), Integration of conservation agriculture with best management practices for improving system performance of the rice-wheat rotation in the eastern indo-gangetic plains of india, *Agriculture, Ecosystems & Environment*, *195*, 68–82, doi:10.1016/j.agee.2014.06.001. 4.6.2

Liu, L., X. Xu, D. Zhuang, X. Chen, and S. Li (2013), Changes in the potential multiple cropping system in response to climate change in china from 1960–2010, *PLoS ONE*, *8*(12), doi:10.1371/JOURNAL.PONE.0080990. 4.1

Mahajan, A., and R. D. Gupta (Eds.) (2009), *The Rice–Wheat Cropping System*, pp. 109–117, Springer Netherlands, Dordrecht, doi:10.1007/978-1-4020-9875-8_7. 4.1, 4.4.2

Makino, A. (2003), Rubisco and nitrogen relationships in rice: Leaf photosynthesis and plant growth, *Soil Science and Plant Nutrition*, *49*(3), 319–327, doi:10.1080/00380768.2003.10410016. 4.4

Mathison, C., A. Wiltshire, A. Dimri, P. Falloon, D. Jacob, P. Kumar, E. Moors, J. Ridley, C. Siderius, M. Stoffel, and T. Yasunari (2013), Regional projections of North Indian climate for adaptation studies, *Science of The Total Environment*, *468-469, Supplement*(0), S4–S17, doi:10.1016/j.scitotenv.2012.04.066. 4.1, 4.4.2

Mathison, C., A. J. Wiltshire, P. Falloon, and A. J. Challinor (2015), South asia river-flow projections and their implications for water resources, *Hydrology and Earth System Sciences*, *19*(12), 4783–4810, doi:10.5194/hess-19-4783-2015. 4.1, 4.4.2, 4.6.2

Mathison, C., C. Deva, P. Falloon, and A. J. Challinor (2018), Estimating sowing and harvest dates based on the asian summer monsoon, *Earth System Dynamics*, *9*(2), 563–592, doi:10.5194/esd-9-563-2018. 4.1, 4.3, 4.4.2

Medina, S., R. Vicente, M. T. Nieto-Taladriz, N. Aparicio, F. Chairi, O. Vergara-Diaz, and J. L. Araus (2019), The plant-transpiration response to vapor pressure deficit (vpd) in durum wheat is associated with differential yield performance and specific expression of genes involved in primary metabolism and water transport, *Frontiers in Plant Science*, *9*, 1994, doi:10.3389/fpls.2018.01994. 4.6.2

Monfreda, C., N. Ramankutty, and J. A. Foley (2008), Farming the planet: 2. geographic distribution of crop areas, yields, physiological types, and net primary production in the year 2000, *Global Biogeochemical Cycles*, *22*(1), doi:10.1029/2007GB002947. 4.5.2

Mueller, B., M. Hauser, C. Iles, R. H. Rimi, F. W. Zwiers, and H. Wan (2015), Lengthening of the growing season in wheat and maize producing regions, *Weather and Climate Extremes*, *9*, 47–56, doi:10.1016/j.wace.2015.04.001, the World Climate Research Program Grand Challenge on Extremes-WCRP-ICTP Summer School on Attribution and Prediction of Extreme Events. 4.1

Nicklin, K. J. (2013), Seasonal crop yield forecasting in semi-arid west africa, *PhD thesis, University of Leeds*, *1*, Chapter 4. (document), 4.4, 4.3

Noilhan, J., and S. Planton (1989), A simple parameterization of land surface processes for meteorological models, *Monthly Weather Review*, *117*(3), 536–549, doi:10.1175/1520-0493(1989)117¡0536:ASPOLS¿2.0.CO;2. 4.1

Ocheltree, T. W., J. B. Nippert, and P. V. V. Prasad (2014), Stomatal responses to changes in vapor pressure deficit reflect tissue-specific differences in hydraulic conductance, *Plant, Cell & Environment*, *37*(1), 132–139, doi:10.1111/pce.12137. 4.6.2

Ogbaga, C. (2014), Regulation of photosynthesis in sorghum in response to drought, *PhD Thesis, University of Manchester*, *1*, 1–186, doi:10.13140/RG.2.1.4756.5208. 4.4

Olsovska, K., M. Kovar, M. Brestic, M. Zivcak, P. Slamka, and H. B. Shao (2016), Genotypically identifying wheat mesophyll conductance regulation under progressive drought stress, *Frontiers in Plant Science*, *7*, 1111, doi:10.3389/fpls.2016.01111. 4.4

Osborne, T., J. Gornall, J. Hooker, K. Williams, A. Wiltshire, R. Betts, and T. Wheeler (2015), Jules-crop: a parametrisation of crops in the joint uk land environment simulator, *Geoscientific Model Development*, *8*(4), 1139–1155, doi:10.5194/gmd-8-1139-2015. (document), 4.1, 4.2, 4.2, 4.3, 4.4, 4.1, 4.2, 4.3, 4.4.2, 4.6.2

Penning de Vries, F. W. T., D. Jansen, H. ten Berge, and A. Bakema (1989), *Simulation of Ecophysiological Processes of Growth in Several Annual Crops*, Simulation monographs, Pudoc. 4.2, 4.4, 4.6.2

Petrie, C. A., R. N. Singh, J. Bates, Y. Dixit, C. A. I. French, D. A. Hodell, P. J. Jones, C. Lancelotti, F. Lynam, S. Neogi, A. K. Pandey, D. Parikh, V. Pawar, D. I. Redhouse, and D. P. Singh (2017), Adaptation to variable environments, resilience to climate change: Investigating land, water and settlement in indus northwest india, *Current Anthropology*, *58*(1), 1–30, doi:10.1086/690112. 4.1

Pires, G. F., G. M. A. ao, L. M. Brumatti, L. J. Oliveira, M. H. Costa, S. Liddicoat, E. Kato, and R. J. Ladle (2016), Increased climate risk in brazilian double cropping agriculture systems: Implications for land use in northern brazil, *Agricultural and Forest Meteorology*, *228-229*, 286 – 298, doi:10.1016/j.agrformet.2016.07.005. 4.1

Portmann, F. T., S. Siebert, and P. Döll (2010), Mirca2000-global monthly irrigated and rainfed crop areas around the year 2000: A new high-resolution data set for agricultural and hydrological modeling, *Global Biogeochemical Cycles*, *24*(1), doi:10.1029/2008GB003435, gB1011. 4.1

Ramankutty, N., A. T. Evan, C. Monfreda, and J. A. Foley (2008), Farming the planet: 1. geographic distribution of global agricultural lands in the year 2000, *Global Biogeochemical Cycles*, *22*(1), doi:10.1029/2007GB002952. 4.5.2

Ray, D. K., N. Ramankutty, and N. D. M. and (2012a), Recent patterns of crop yield growth and stagnation., *Nature Communications*, *3*, 1293–1300, doi:10.1038/ncomms2296. (document), 4.5.2, 4.6.2, 4.7

Ray, D. K., N. Ramankutty, N. D. Mueller, P. C. West, and J. A. Foley (2012b), Harvested area and yield for 4 crops (1995-2005), doi:10.1038/ncomms2296. 4.5.2

Rivington, M., and J. Koo (2010), Report on the meta-analysis of crop modelling for climate change and food security survey, *Climate Change, Agriculture and Food Security Challenge Program of the CGIAR*. 4.1, 4.7

Robertson, M., I. Brooking, and J. Ritchie (1996), Temperature response of vernalization in wheat: Modelling the effect on the final number of mainstem leaves, *Annals of Botany*, *78*(3), 371–381, doi:10.1006/anbo.1996.0132. 4.4.2

Rosenzweig, C., J. Jones, J. Hatfield, A. Ruane, K. Boote, P. Thorburn, J. Antle, G. Nelson, C. Porter, S. Janssen, S. Asseng, B. Basso, F. Ewert, D. Wallach, G. Baigorria, and J. Winter (2013), The agricultural model intercomparison and improvement project (agmip): Protocols and pilot studies, *Agricultural and Forest Meteorology*, *170*, 166–182, doi:10.1016/j.agrformet.2012.09.011, agricultural prediction using climate model ensembles. 4.1, 4.7

Rosenzweig, C., J. Elliott, D. Deryng, A. C. Ruane, C. Müller, A. Arneth, K. J. Boote, C. Folberth, M. Glotter, N. Khabarov, K. Neumann, F. Piontek, T. A. M. Pugh, E. Schmid, E. Stehfest, H. Yang, and J. W. Jones (2014), Assessing agricultural risks of climate change in the 21st century in a global gridded crop model intercomparison, *Proceedings of the National Academy of Sciences*, *111*(9), 3268–3273, doi:10.1073/pnas.1222463110. 4.1, 4.7

Sacks, W. J., D. Deryng, J. A. Foley, and N. Ramankutty (2010), Crop planting dates: an analysis of global patterns, *Global Ecology and Biogeography*, *19*(5), 607–620. 4.1

Sharma, B., and H. Sharma (2015), Status of rice production in assam, india, *Journal of Rice Research: Open Access*, *3*(4), 3–e121, doi:10.4172/2375-4338.1000e121. 4.1

Simmons, A., S. Uppala, D. Dee, and S. Kobayashi (2007), Era-interim: New ecmwf reanalysis products from 1989 onwards., *ECMWF Newsletter - Winter 2006/07*, *110*, 25–35. 4.4.2

Sinclair, T., P. P. Jr, B. Kimball, F. Adamsen, R. LaMorte, G. Wall, D. Hunsaker, N. Adam, T. Brooks, R. Garcia, T. Thompson, S. Leavitt, and A. Matthias (2000), Leaf nitrogen concentration of wheat subjected to elevated CO_2 and either water or n deficits, *Agriculture, Ecosystems & Environment*, *79*(1), 53 – 60, doi:10.1016/S0167-8809(99)00146-2. 4.4

Streck, N. A. (2003), Stomatal response to water vapor pressure deficit: an unsolved issue, *Current Agricultural Science and Technology*, *9*(4). 4.6.2

Tuinenburg, O. A., R. W. A. Hutjes, T. Stacke, A. Wiltshire, and P. Lucas-Picher (2014), Effects of irrigation in india on the atmospheric water budget., *Journal of Hydrometeorology*, *15*, 1028–1050, doi:10.1175/JHM-D-13-078.1. 4.6.2, 4.7

Waha, K., L. G. J. van Bussel, C. Müller, and A. Bondeau (2012), Climate-driven simulation of global crop sowing dates, *Global Ecology and Biogeography*, *21*(2), 247–259, doi:10.1111/j.1466-8238.2011.00678.x. 4.1

Waha, K., C. Müller, A. Bondeau, J. Dietrich, P. Kurukulasuriya, J. Heinke, and H. Lotze-Campen (2013), Adaptation to climate change through the choice of cropping system and sowing date in sub-saharan africa, *Global Environmental Change*, *23*(1), 130–143, doi:10.1016/j.gloenvcha.2012.11.001. 4.1

Warszawski, L., A. Friend, S. Ostberg, K. Frieler, W. Lucht, S. Schaphoff, D. Beerling, P. Cadule, P. Ciais, D. B. Clark, R. Kahana, A. Ito, R. Keribin, A. Kleidon, M. Lomas, K. Nishina, R. Pavlick, T. T. Rademacher, M. Buechner, F. Piontek, J. Schewe, O. Serdeczny, and H. J. Schellnhuber (2013), A multi-model analysis of risk of ecosystem shifts under climate change, *Environmental Research Letters*, *8*(4), 044,018. 4.1, 4.7

Warszawski, L., K. Frieler, V. Huber, F. Piontek, O. Serdeczny, and J. Schewe (2014), The inter-sectoral impact model intercomparison project (isi-mip):project framework, *Proceedings of the National Academy of Sciences*, *111*(9), 3228–3232, doi:10.1073/pnas.1312330110. 4.1, 4.7

Williams, K., J. Gornall, A. Harper, A. Wiltshire, D. Hemming, T. Quaife, T. Arkebauer, and D. Scoby (2017), Evaluation of jules-crop performance against site observations of irrigated maize from mead, nebraska, *Geoscientific Model Development*, *10*(3), 1291–1320, doi:10.5194/gmd-10-1291-2017. 4.2, 4.6.1

Williams, K. E., A. B. Harper, C. Huntingford, L. M. Mercado, C. T. Mathison, P. D. Falloon, P. M. Cox, and J. Kim (2018), Revisiting the first islscp field experiment to evaluate water stress in julesv5.0, *Geoscientific Model Development Discussions*, *2018*, 1–47, doi:10.5194/gmd-2018-210. 4.6.1, 4.6.1, 4.7

Xue, W. (2015), Evaluation of biophysical factors driving temporal variations in c gain, water use and yield production in rice, *PhD thesis, Department of Plant Ecology, University of Bayreuth*, *1*, 1–230. 4.4

Zhang, G., J. Dong, C. Zhou, X. Xu, M. Wang, H. Ouyang, and X. Xiao (2013), Increasing cropping intensity in response to climate warming in tibetan plateau, china, *Field Crops Research*, *142*, 36–46, doi:10.1016/j.fcr.2012.11.021. 4.1

Chapter 5

First integrated impacts simulations for South Asia

The impacts of climate are often studied separately by each sector, even though the effects of changes do not respect sectoral divides. A sectoral approach to climate impacts could miss important links between sectors that are both affected by climate and also each other. In this chapter a standalone model, which is also a land–surface model used in larger coupled simulations, is used with additional processes that cannot yet be included in larger coupled simulations. These additional processes enable the standalone model to provide a more complete representation of the land–surface. Two simulations are presented that include river flows and the developments completed within this thesis: estimated sowing and harvest dates from the ASM (Chapter 3), irrigation on specific crop tiles and sequential crops (Chapter 4). In one simulation the irrigation is limited according to availability, therefore taking water from groundwater and rivers; and in the other the resource is unlimited. The aim of this chapter is two-fold: firstly to demonstrate that a regional simulation with these processes included is now possible as a result of the work in this thesis; and secondly to show that it produces plausible results for a small region of India through comparison with similar analyses using a different model. These simulations will provide the basis for future work analysing the demand for water resources and food production for the whole of South Asia.

5.1 Introduction

Climate impact studies tend to be sector specific, with each sector using different methods to understand the likely impacts to that sector. A climate model provides forcing data for simulating the downstream impacts of the land-surface using different models for each sector, such as crops and hydrology. This unidirectional approach limits the links between impacts of related sectors that are known to affect each other and misses

feedbacks between the land–surface and the atmosphere; for example by allowing the croplands to modify the atmosphere through evaporation (*Betts*, 2005). A key recommendation by *Betts* (2005) and *Slingo et al.* (2005) is for land-surface schemes that are routinely used in coupled climate simulations to be developed into standalone impacts models that include these additional processes. This is a useful interim approach en-route to integrating crops and irrigation more fully into climate simulations. *Osborne et al.* (2007) show that using GLAM (*Challinor et al.*, 2004) integrated within the Met Office Hadley Centre atmospheric model, HadAM3 (*Pope et al.*, 2000) represents the impacts of weather and climate on crops and the feedbacks of growing crops on the environment. However the success of this approach depends on the skill of both the GCM and the crop parameterization.

The ISIMIP project, a community driven climate-impact modelling initiative. This project has actively encouraged more focussed studies of the land–surface, ultimately contributing to a better understanding of the impact of climate on the land–surface. As part of the ISIMIP project, the CMIP5 models were used to drive land–surface models to contribute to multi-model assessments of climate impacts. ISIMIP included JULES and covered a range of different sectors including flooding (*Dankers et al.*, 2014), runoff (*Davie et al.*, 2013), droughts (*Prudhomme et al.*, 2014), water stress (*Schewe et al.*, 2014), ecosystem distribution and multi-sectoral hot-spots (*Piontek et al.*, 2014).

Integrated Assessment Models (IAMs) are complex models that provide an integrated system perspective of human influences on climate change and mitigation of greenhouse gases (*Schwanitz*, 2013). They are a type of integrated impacts model that seek to combine environmental, social and economic factors to determine future climate change and the effectiveness of climate policy (*van Vuuren et al.*, 2011). They are highly complex because they need to include so many different components all of which have to be merged together but still be representative of the processes being simulated. A combination of user priority and available computing resources dictate the level of simplification required to represent the different processes which means compromises have to be made in terms of the complexity of the representation of each process (*Schwanitz*, 2013). For example, it is typical for IAMs to use simple climate models (SCMs) that are calibrated against more complex coupled ocean-atmosphere climate simulations but use a fraction of the computing power (*van Vuuren et al.*, 2011). In simplifying individual components, processes that occur on the timescales of a day or a month are often not considered even though they are important. Also, at times, regions are aggregated together using broad quantities such as GDP, despite the characteristics leading to these values varying considerably across a region (*Schwanitz*, 2013).

IAMS are often built with a specific purpose in mind; for example economists use IAMS to understand the economic feasibility of particular climate policies, i.e. the costs and benefits of mitigating climate change (*Ackerman et al.*, 2009). Fundamentally this involves attaching a numerical value to aspects of life today that are notoriously

difficult to put a value on, such as human health or biodiversity (*Ackerman et al.*, 2009). Therefore economists are more likely to require a complex economic component, whereas those IAMs used by the energy industry are more likely to have a complex representation of energy demand and usage. The variation in IAM construction means there is huge scope for the outputs of these models to be different; for example, *van Vuuren et al.* (2011) found from analysis of a number of IAMs that different representations of the carbon cycle and climate can lead to large differences in the climate outcomes.

Recognising the complexity in the relationships between climate change, agriculture and water resources *Zessner et al.* (2016) developed the integrated impacts modelling framework (IIMF). The IIMF aims to assess the impacts of climate on land use and water quality specifically focussing on crop choices, farming practices and fertilization levels. *Zessner et al.* (2016) focuses on water pollution in Austria by coupling models from different sectors together, using the outputs from one as an input for the next. The main challenge of this approach was the spatial and temporal aggregation and disaggregation of data to keep inputs and outputs for each of the component models consistent with each other. These problems with differing scales of application and the integration of submodels are also highlighted by *Ewert et al.* (2015). Crop models are a fundamental part of understanding climate impacts on food production. Therefore it is useful to align crop model development with the requirements of IAMS that are designed for completing climate change risk assessments of food security (*Ewert et al.*, 2015). These requirements include the need for crop models to simulate yield, biomass and water use while capturing any feedbacks as a result of climate change.

In this thesis the focus in on the impact of climate on the land-surface and consideration of socio-economic factors is limited to the use of the A1B SRES scenario. To look at the wider issue of food security it would be valuable to combine the JULES model or outputs from simulations with socioeconomic information; for example the social response to a climate event, to examine how different responses could amplify/dampen the impact of that event; or export/import information between major crop producing countries to understand supply chains (*Challinor et al.*, 2018).

In this chapter the aim is to run simulations that include hydrology, crops and irrigation as integral parts of a land surface model. Therefore we bring together the different elements of this thesis and consider the climate impacts on multiple sectors at once. The river routing described and implemented in Chapter 2 as a postprocessing step and the crop specific elements of this thesis, described in Chapters 3 and 4, are included in the simulations presented in this chapter. As these are the first simulations including the various elements from this project, these simulations focus on the same two states in northern India as in Chapter 4. The aim of these regional simulations is to demonstrate that it is both technically possible and the results for the present day are plausible. The results will highlight where development effort needs to be targeted

to be able to use JULES-IM for future simulations before fully integrating JULES-crop and hydrology models into larger more complicated climate simulations.

This chapter is structured as follows. The model simulations are described in Sect. 5.2. The observations used to evaluate JULES are provided in Sect. 5.3 and methods used to analyse the results in the absence of relevant observations are described in Sect. 5.4. The results of the simulations are discussed in Sect. 5.5 and summarized in Sect. 5.6.

5.2 Model simulation

The first regional simulations using all of the impacts components developed as part of this thesis continue to focus, as in Chapter 4, on the north Indian states of Uttar Pradesh and Bihar, to simulate the rice-wheat rotation. These states are key producers of these crops using the sequential cropping system (*Mahajan and Gupta*, 2009). The sequential cropping system in this region involves growing rice during the wet monsoon months and an irrigated wheat crop during the dry winter. The wheat varieties grown in this region are spring wheat which does not require a vernalization period which is required for winter wheat varieties (*Griffiths et al.*, 1985, *Robertson et al.*, 1996, *Mathison et al.*, 2018). In these simulations it is assumed that wheat and rice are grown everywhere within this subregion of India; this is a similar assumption to that made in ISIMIP simulations. In practice this will not be the case and simulations for the purpose of accurately calculating the demand for resources either for the present day or a future period would need realistic estimates of crop areas in each gridbox. Observations of crop area are available from *ICRISAT* (2015); however time constraints prevented these being used as input to JULES for this simulation.

As with previous simulations (Chapters 2, 3 and 4), JULES is run using a 3-hourly timestep using driving data from ERA-interim (*Dee et al.*, 2011, *Simmons et al.*, 2007) downscaled to 25 km using the HadRM3 regional climate model (RCM- *Jones et al.*, 2004). The ERA-interim RCM simulation is one of an ensemble of simulations produced for the EU-HighNoon FP7 project for the whole of the Indian subcontinent (25 N, 79 E–32 N, 88 E) for the period 1991-2007. The HighNoon simulations are described in Sect. 1.3 and also in previous publications such as *Kumar et al.* (2013) and *Mathison et al.* (2013, 2015). HadRM3 provides more regional detail to the global data with lateral atmospheric boundary conditions updated 3-hourly and interpolated to a 150 s timestep. These simulations include a detailed representation of the land surface in the form of version 2.2 of the Met Office Surface Exchange Scheme (*Essery et al.*, 2001; MOSESv2.2;). JULES has been developed from the MOSESv2.2 land surface scheme and therefore the treatment of different surface types is in principal consistent between the RCM and JULES (*Essery et al.*, 2001, *Mathison et al.*, 2015).

The two simulations in this chapter include river routing introduced in Chapter 2

which is now part of the official JULES code. Therefore the runoff is calculated from the precipitation prescribed by the forcing data (described above) and then routed through the TRIP river network in JULES. In the regional simulations in this chapter the JULES vn5.2 branch with sequential crops and extended irrigation code, described in Chapter 4 are used. The code included in this branch of JULES means that crops can be grown in rotation: here we use the rice–wheat rotation which is common across the IGP region. The changes to the irrigation code enable the irrigation to be limited to specific tiles, in this case wheat (Chapter 4).

The sowing and harvest dates from the method introduced in Chapter 3 are used to calculate the thermal time requirements for the rice and wheat crops. The main reason for using estimated sowing and harvest dates for this present day simulation is that they are very similar to the observations for this part of India and, unlike the observations, there is no missing data. The values of the sowing dates, harvest date and therefore the thermal times are allowed to vary across the region, in the same way as in *Osborne et al.* (2015). Maps of the inputs for JULES-crop including: the sowing day of year, the latest possible harvest date and the thermal times are shown for rice (Fig. 5.1) and wheat (Fig. 5.2). Figure 5.1a shows that the rice sowing dates are between the 140th and 180th day of the year, i.e. during May and June for these two states, with Bihar earlier than Uttar Pradesh. Figure 5.2a indicates that the wheat sowing dates are towards the end of the year between the 315th and 360th day, i.e. during November and December for these two states. These sowing dates for rice and wheat are within the observed sowing window from *ICRISAT* (2015) for both states.

The latest harvest dates represent the last day that the crop can be harvested in order to sow the next crop in the rotation are shown for rice (Fig. 5.1b) and wheat (Fig. 5.2b). Therefore the latest harvest date closely resembles the sowing dates for the other crop in the rotation, i.e. the wheat latest harvest (Fig. 5.2b) closely resembles the sowing dates for rice (Fig. 5.1a) and vice versa for the rice latest harvest dates (Fig. 5.1b) and the wheat sowing dates (Fig. 5.2a).

The simulations in this chapter use the same parameters and settings from the India simulations in Chapter 4, Tables 4.1, 4.2 and 4.3. However, in this chapter, in one simulation the irrigation is referred to as unlimited and in the other the irrigation is referred to as limited by water availability. The unlimited simulation represents an upper limit on how much irrigation can be applied to a crop in JULES, because the rivers and irrigation are not linked with one another. Therefore the irrigation cannot affect the river flow and the river flow cannot limit the amount of water available for irrigation. In the simulation with limited irrigation water is first taken from the surface groundwater store and then from the rivers when the groundwater source is exhausted. The limited simulation makes the link between the available water and irrigation demand which means that, provided JULES is correctly simulating the groundwater and river flow, the estimated use of water resources for crops should be realistic. Running

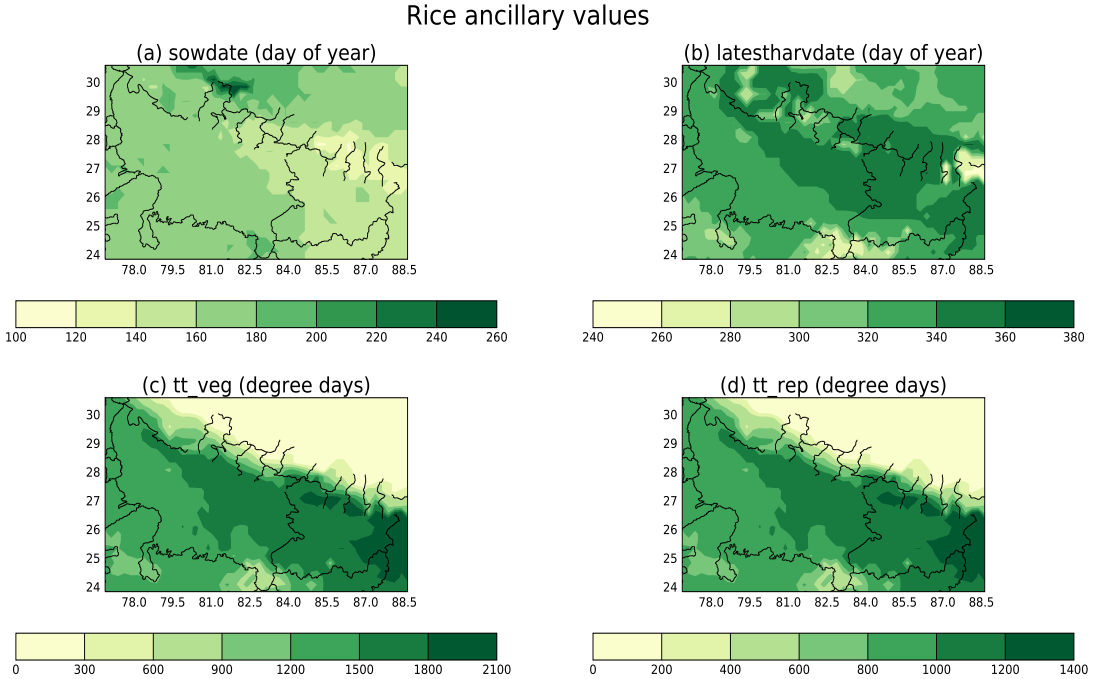

Figure 5.1: The values used in the model for rice for the sowing date (a), latest possible harvest date (b), thermal time for the vegetative stage (c), thermal time for the reproductive phase (d).

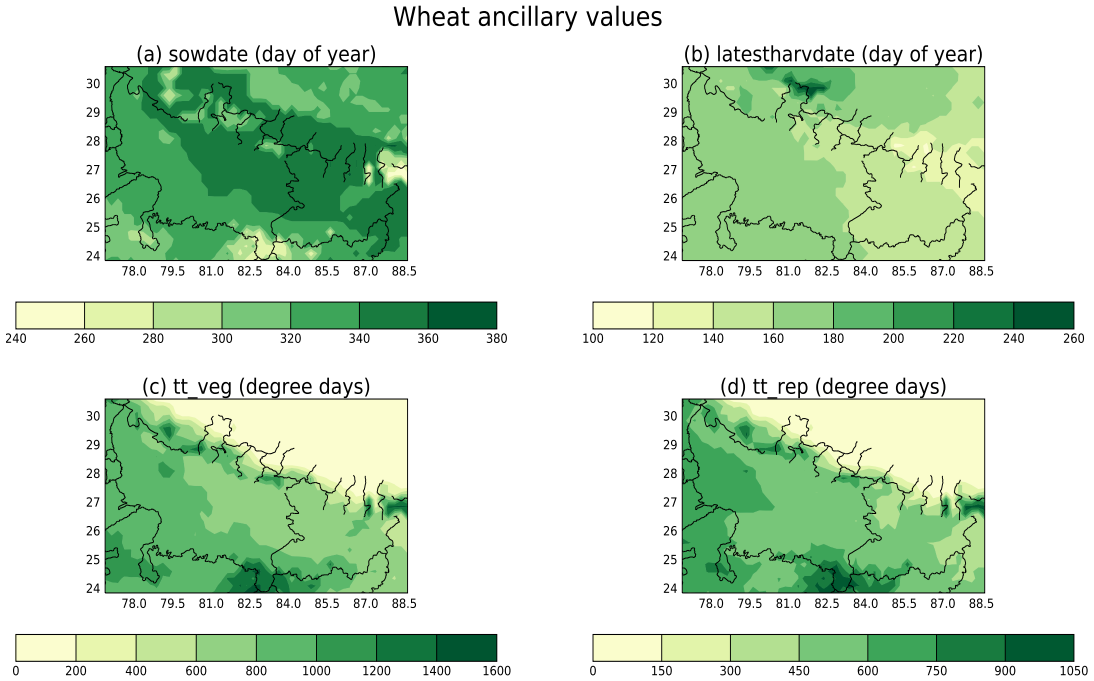

Figure 5.2: The values used in the model for Wheat for the sowing date (a), latest possible harvest date (b), thermal time for the vegetative stage (c), thermal time for the reproductive phase (d).

with limited or unlimited irrigation involves the very simple change of one switch from l_irrig_limit false (for unlimited irrigation) to true (for limited irrigation). The choice of running with limited or unlimited irrigation is likely to be important for simulating future resources where resource may not be sufficient to meet the demand. To date, no simulations have been completed where this occurs.

5.3 Observations

Crop yield observations are from the International Crops Research Institute for the Semi-Arid Tropics (*ICRISAT*, 2015) which provides seasonal yields for each crop for comparison with JULES. River flows for this region are unavailable as are the overall extractions from rivers and surface water. Groundwater extractions are available. However, in JULES the source of the irrigation is not separated and therefore it is not clear how much of the water extracted is from surface or groundwater. The lack of relevant observations for this region means that other comparisons have to be made to understand if the simulations are providing plausible results (see Sect. 5.4).

5.4 Analysis methods

Simulations that follow on from this will be for a larger domain where GRACE data can be used to estimate irrigation extraction. The prototype simulations presented here aim to demonstrate that these types of simulations are now possible for this region. Therefore, the initial evaluation of these simulations presented in this chapter is designed to check the plausibility of these results, rather than provide a rigorous comparison against observations, as this is an early stage in the development of the simulations. The JULES simulations presented in this chapter include estimates of irrigation demand. These are compared with similar simulations from another model because surface extractions are not readily available for this size of domain at this location. This does not replace the need for a more in depth evaluation using observed irrigation but provides a quick check that the values for irrigation demand simulated by JULES are plausible. Therefore the JULES simulated irrigation demand is compared against the simulations from LPJml in *Biemans et al.* (2013) and *Biemans et al.* (2016). LPJml is a well established model used to simulate the irrigation demand, including an estimate of the irrigation efficiency from both surface water (rivers and lakes) and groundwater separately. The analysis presented in both *Biemans et al.* (2013) and *Biemans et al.* (2016) includes the states of Uttar Pradesh and Bihar that are simulated by JULES in this chapter.

In LPJml groundwater is given a higher efficiency of 70 % (*Gupta and Deshpande*, 2004, *Biemans et al.*, 2016) than the surface water because it is more expensive and therefore farmers are likely to use it more sparingly. In the LPJml simulations shown

in *Biemans et al.* (2016), water resource is limited by availability but in *Biemans et al.* (2013) simulations with both limited and unlimited irrigation are shown. JULES does not account for irrigation efficiency which means the irrigation demand from JULES should be lower than the demand for LPJml.

5.5 Results

5.5.1 Rivers

Figure 5.3 shows maps of the JULES river flows for each simulation. In both simulations the driving data from a 25km climate simulation uses the 0.5° TRIP routing model within JULES; this is then regridded back to 25km to provide 25km resolution river flows. 25km is a coarse resolution for the size of the study area which is why the rivers look very broad in Fig. 5.3. The points A and B are two river locations in TRIP; one in Uttar Pradesh (A) and another in Bihar (B). There are several river channels represented by TRIP that run through Uttar Pradesh and merge into one in Bihar by point B. The river channels in Uttar Pradesh are likely to be the Karnali (Ghaghara), Gomati and the Ganges as these are the largest in this part of India, although the coarse resolution of TRIP makes it difficult to say for certain, as there are many tributaries in this region.

The simulation with limited irrigation (Fig. 5.3b) produces very similar river flows to the simulation with unlimited irrigation (Fig. 5.3a). However it is noticeable that with limited irrigation (Fig. 5.3b), the groundwater values are lower in the regions surrounding the main river channels and the river channels themselves are a lighter blue, indicating the river flows are being reduced by the demand for irrigation.

The seasonal cycle of river flow at each of the points A and B are shown in Fig. 5.4, a and b respectively. These seasonal cycles also indicate that the limited irrigation simulation reduces the river flows at each of these points. There are no GRDC gauges available for sites within this particular region and therefore no observations of river flow to compare against. However these seasonal river flows are plausible, based on the gauges at other locations in the same area. The seasonal cycles for the unlimited irrigation simulation are consistent with the river flow analysis shown in Chapter 2 with the river flows at the upstream point in Uttar Pradesh (point A) similar in magnitude to those for the Tehri dam, Benighat and Turkghat gauges and river flows at point B similar to those for the Chisapani and Devghat gauges. All of these are within the Ganges/Brahmaputra catchment but are to the north of Uttar Pradesh and Bihar.

There are no observational data available regarding the surface water extraction at these points, so no conclusions can be drawn regarding how well the surface extractions are simulated, or if they are reducing the river flow by the right amount. However the simulation with irrigation limited by availability (blue lines) is clearly taking water from

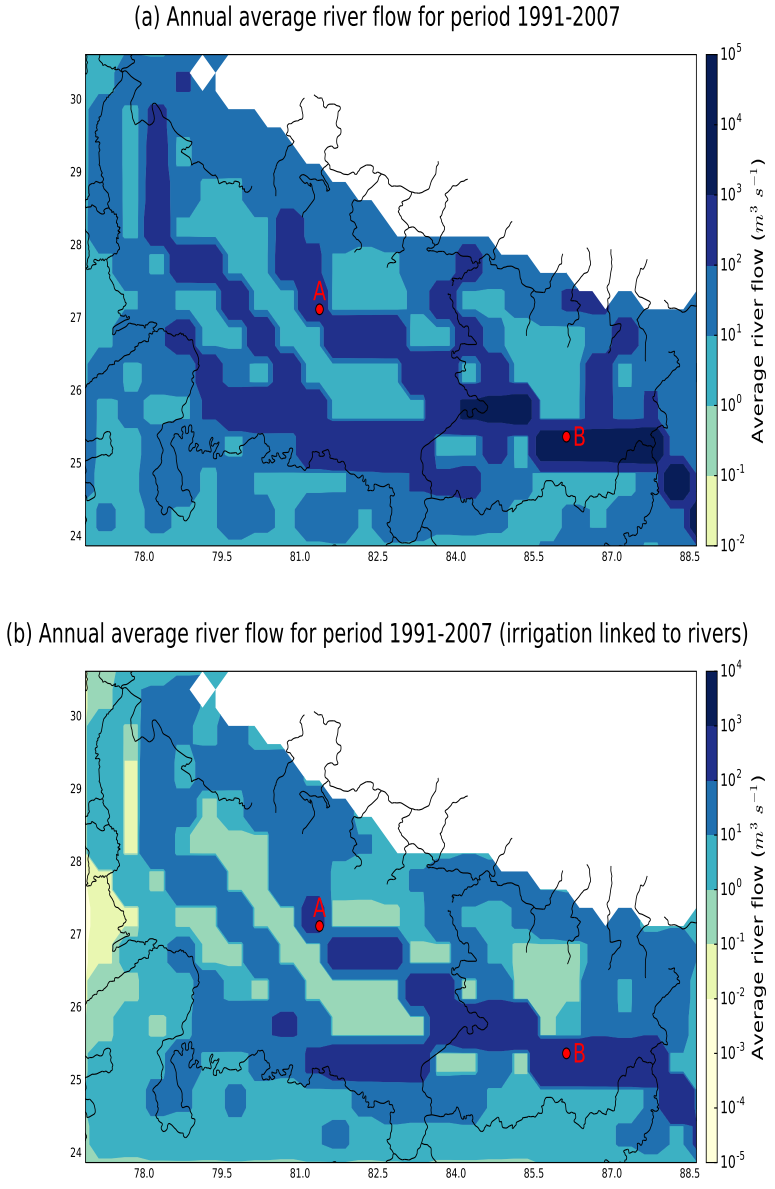

Figure 5.3: JULES river flows averaged for the period 1991-2007 for simulation with unlimited irrigation (a) and a simulation where irrigation is limited by availability from groundwater and rivers (b).

the groundwater and rivers and reducing the river flows compared with the simulation that is not limited by availability (red lines); this is a promising result for future work. There is little doubt that simulation of river flows in JULES would benefit from a higher resolution river routing map than the 0.5° resolution currently available and data regarding river flows and volumes extracted for irrigation are needed for evaluating the model performance.

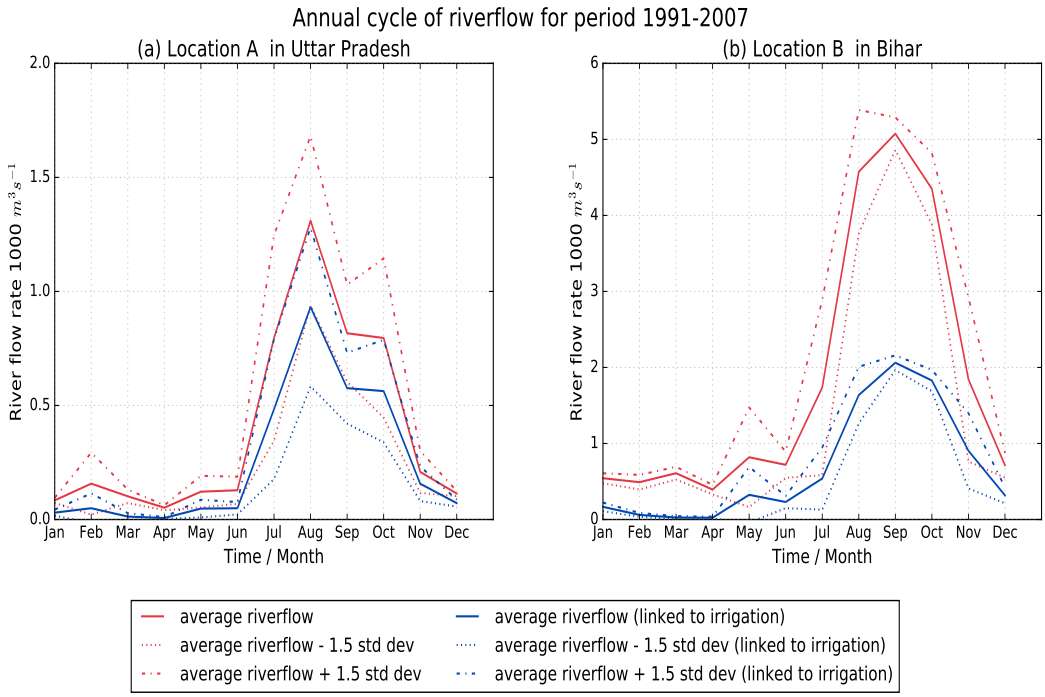

Figure 5.4: JULES river flows averaged for the period 1991-2007 at point A in Uttar Pradesh (a) and point B in Bihar (b) with unlimited irrigation (red lines) and irrigation limited by water availability (blue lines). Note the differing scales on the y-axis.

5.5.2 Irrigation demand

Figure 5.5 shows the regional irrigation demand simulated by JULES for the states of Uttar Pradesh and Bihar for the two main crop seasons: kharif during the monsoon season (Fig. 5.5a) and rabi the dry season (Fig. 5.5b) for an unlimited irrigation simulation, i.e. the irrigation is not linked to the rivers. JULES does not have an irrigation efficiency parameter to allow for losses of water through leaks or evaporation so the irrigation demand in JULES is assumed to be 100 % efficient. In reality India is known to have a relatively low irrigation efficiency for surface water of approximately 38 % (*Biemans et al.*, 2013). A simulation with limited irrigation, i.e. linked to rivers is also shown in Fig. 5.6. Although the spatial patterns change slightly, there is very little difference in the overall amounts between the simulation with limited irrigation and the simulation where irrigation is unlimited. Rice is usually cultivated during the wet kharif season in Bihar and Uttar Pradesh and is therefore not irrigated as much, if at all in some parts of this region. However wheat, which is cultivated during the dry winter in these states, usually requires irrigation. In these simulations JULES only irrigates the wheat crop. Therefore irrigation in these simulations mostly occurs during the rabi season with very little if any during the kharif season (Figs. 5.5 and 5.6). In the limited irrigation simulation the irrigation takes resource from the groundwater and then the rivers, which reduces the river flow across the region in Fig. 5.3b compared

with Fig. 5.3a.

In the absence of observations of surface water extraction, comparing a limited LPJml irrigation simulation (Fig. 6 from *Biemans et al.* (2016)) with the limited irrigation JULES simulation (Fig. 5.6) suggests that the irrigation demand is lower in JULES than LPJml. However it is difficult to establish more exactly because the colour scales in *Biemans et al.* (2016) represent a wide range of values.

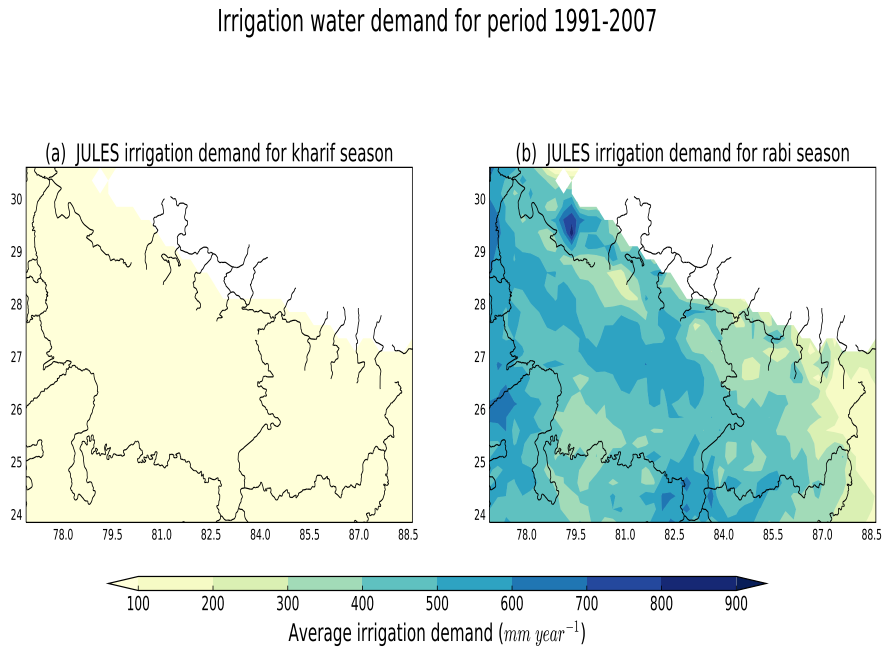

Figure 5.5: JULES crop average irrigation demand for an unlimited irrigation simulation for the kharif (a) and rabi (b) crop seasons for the period 1991-2007.

Biemans et al. (2013) estimate the total irrigation demand per year for individual states including Bihar and Uttar Pradesh for the period 1971-2000. LPJml estimates the total irrigation demand for Bihar to be just under 40 km^3 year^{-1} and Uttar Pradesh to be approximately 120 km^3 year^{-1}; again this includes an estimate of irrigation efficiency. However it is not clear if this estimate is for an unlimited or limited irrigation simulation, as both are mentioned but only one value is shown (in Fig A5 of *Biemans et al.* (2013)). The values simulated in the 1991-2007 simulation using JULES are comparable to these values, with a total irrigation demand for Bihar of between 37 and 42 km^3 year^{-1} and for Uttar Pradesh of between 117 and 119 km^3 year^{-1} for the two simulations with both unlimited and limited irrigation, respectively.

The similarity between the JULES results and those shown for LPJml in *Biemans et al.* (2013) and *Biemans et al.* (2016) are promising. However, given that JULES assumes perfect irrigation, it might be expected that the irrigation demand simulated by JULES should be considerably lower than those simulated for LPJml. This is likely to be due to the way the two simulations are set up rather than the actual simulated

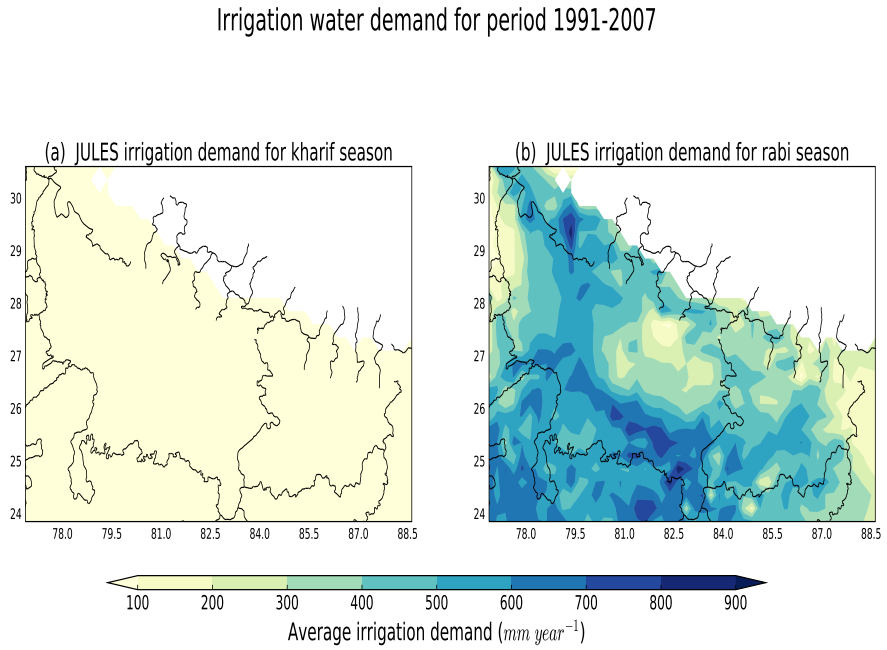

Figure 5.6: JULES crop average irrigation demand for a limited irrigation simulation for the kharif (a) and rabi (b) seasons for the period 1991-2007.

values. A key factor is the crop areas used: in LPJml the crop areas are from *Ramankutty et al.* (2008) but in this JULES simulation it is assumed that every gridbox in the two states is entirely used for the cultivation of rice and wheat. This, together with the shorter time period of the JULES simulation, could mean the values are a little higher than expected compared with the LPJml values. A cleaner comparison between models would be beneficial, setting up JULES for the same time period and WFDEI forcing data (*Weedon et al.*, 2014) as that shown by (*Biemans et al.*, 2016). In addition, comparison between the JULES simulations with unlimited and limited irrigation suggests that there are periods where the average regional irrigation demand is higher for the simulation with limited irrigation than for the simulation with unlimited irrigation (Fig. 5.7). Therefore it is also important to investigate this behaviour further, establish the reason for this and check that the irrigation in JULES is working correctly.

5.5.3 Crops

Figures 5.8 and 5.9 show the simulated crop LAI and canopy height respectively for rice and wheat across Bihar and Uttar Pradesh for the simulation with unlimited irrigation; as expected the limited irrigation plots are similar to these and are therefore not shown. These largely reflect the results from the India point simulations shown in Chapter 4. The canopy height for both crops is broadly similar to each other and to

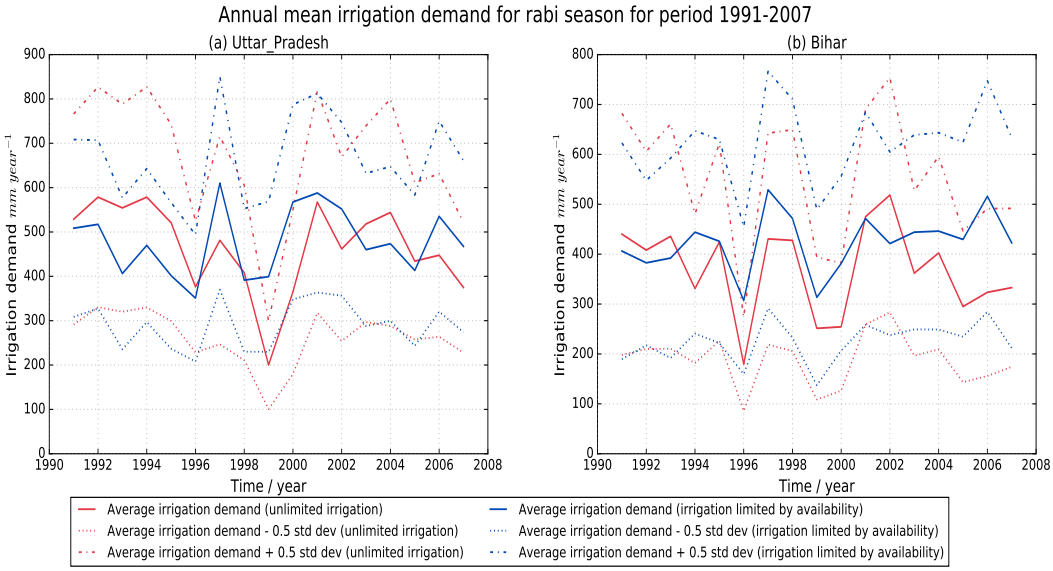

Figure 5.7: The average regional irrigation demand for the rabi season for the Uttar Pradesh region (a) and the Bihar region (b) for the simulation with limited irrigation simulation (blue) and the simulation with unlimited irrigation (red) for the period 1991-2007.

the results from Chapter 4 (approximately 0.5-0.7 m), from west to east the canopy height for rice increases while for wheat it reduces, but these differences are relatively small (approximately 0.1 m). The LAI shows a similar pattern for the two crops but the differences between crops are larger, with rice generally having a smaller LAI than wheat. The magnitudes of the LAI and canopy height are similar to those for the point simulations, i.e. JULES is producing wheat and rice crops with the broadly typical LAI and canopy heights suggested by *Penning de Vries et al.* (1989).

The yields from JULES are compared against seasonal observations of yield for this region from *ICRISAT* (2015) in Fig. 5.10 for the unlimited irrigation simulation. Fig. 5.10a shows the ICRISAT rice observations and Fig. 5.10b shows the simulation of rice from JULES, both averaged for 1991-2007. The magnitude of the rice yields is lower than the observations for Uttar Pradesh but higher than the observations for Bihar; highlighting that JULES does not capture the observed reduction in rice yields from west to east. The reduction in observed yields from west to east is also reflected in the annual averages of the rice yields shown for the two regions with Uttar Pradesh shown in Fig. 5.11a and Bihar in Fig. 5.11c. Figure 5.11 also highlights the variability in the observed rice yields for these two states from year to year.

The observed wheat yields (*ICRISAT*, 2015), averaged for 1991-2007 are shown in Fig. 5.10c with the JULES simulated wheat yield shown in Fig. 5.10d. JULES does capture the observed reduction in yields from west to east for wheat. Similar to the point simulations in Chapter 4, the wheat yields are underestimated for Uttar Pradesh, but closer to observations for Bihar; this is reflected in the annual average crop yields

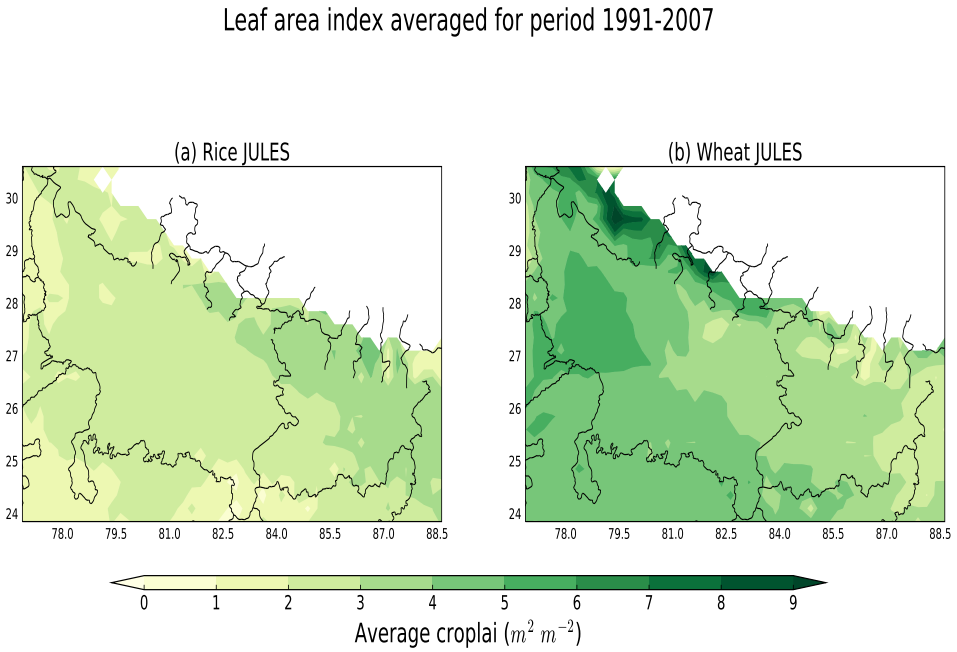

Figure 5.8: JULES crop estimated LAI for rice (a) and wheat (b) averaged for the period 1991-2007

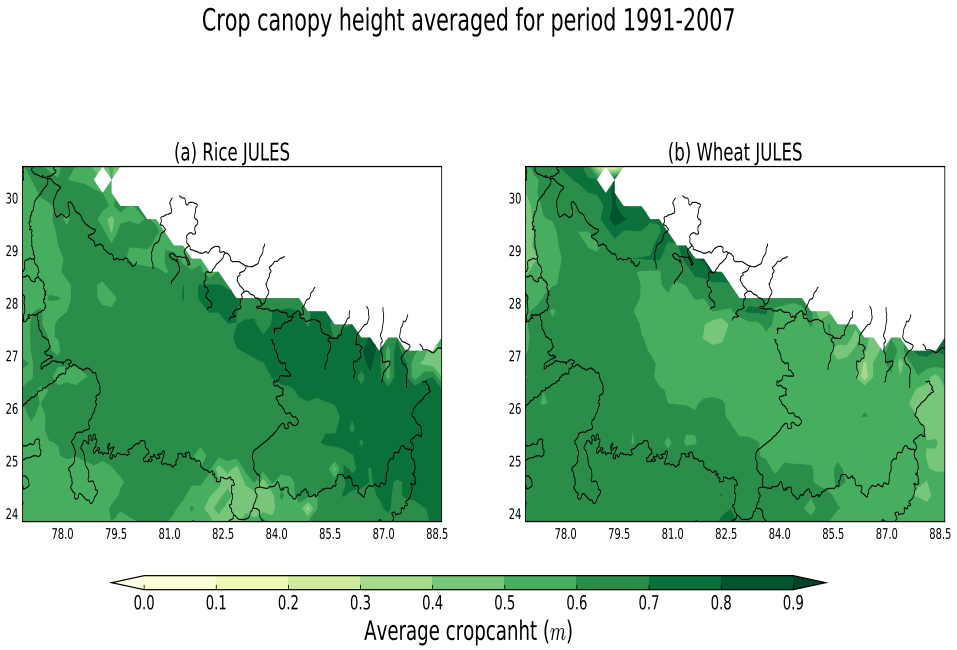

Figure 5.9: JULES crop estimated canopy height for rice (a) and wheat (b) averaged for the period 1991-2007

shown in Fig. 5.11b for Uttar Pradesh and Fig. 5.11d for Bihar.

Irrigation in these simulations is restricted to the wheat tile only, so differences

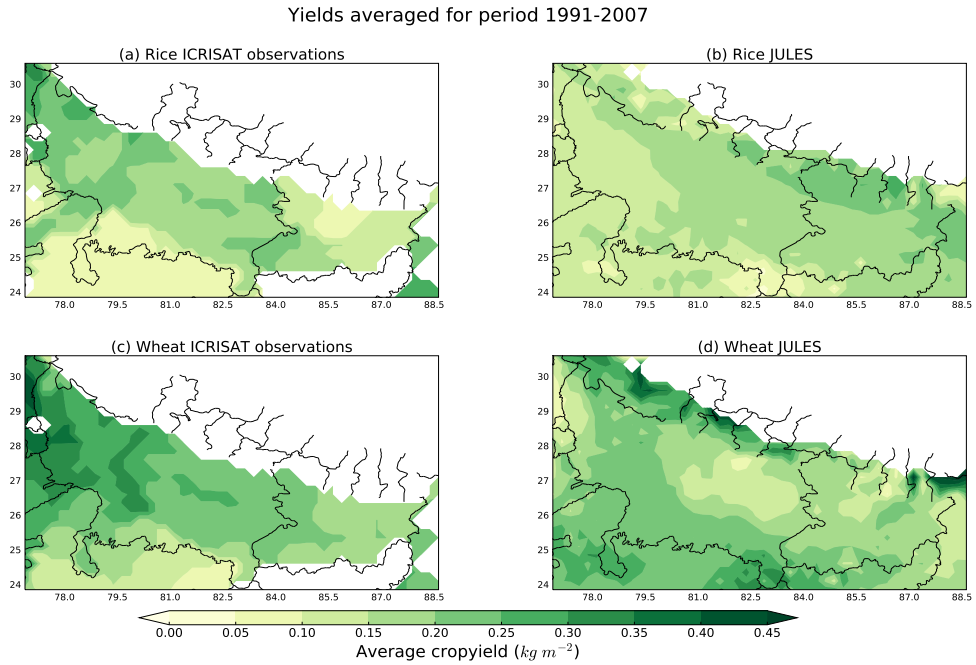

Figure 5.10: A comparison of observed rice yields from *ICRISAT* (2015) (a) with JULES rice yields (b) and observed wheat yields from *ICRISAT* (2015) (c) with JULES wheat yields (d) for the period 1991-2007.

between limited and unlimited irrigation yields for wheat are expected. The wheat yield for the irrigation simulation with limited irrigation returns typically lower yields than the unlimited simulation (Fig. 5.11b and d), which is also to be expected. However Fig. 5.11 also shows that there are small differences between the simulations of rice yields between the unlimited irrigation and limited irrigation simulations, even though rice is not irrigated at all in these simulations (Fig. 5.11 a and c). The differences are small for Bihar and larger for Uttar Pradesh with larger rice yields simulated by the unlimited irrigation simulation than the limited simulation. It is possible that the application of unlimited irrigation, which is applied during the wheat season throughout the crop season until harvest, means the soil remains wet into the rice crop season that follows; this may be having a positive impact on the JULES rice yields.

5.6 Summary and next steps

The simulations and brief analysis presented in this chapter show that regional JULES simulations that include: river flows, crop specific irrigation (both unlimited and limited by availability) and sequential crops, are possible and produce plausible results for the Uttar Pradesh and Bihar region. These simulations are a more complete representation of the South Asia cropping system and irrigation than was previously possible with JULES. Each of the components are an integral part of JULES, which will enable

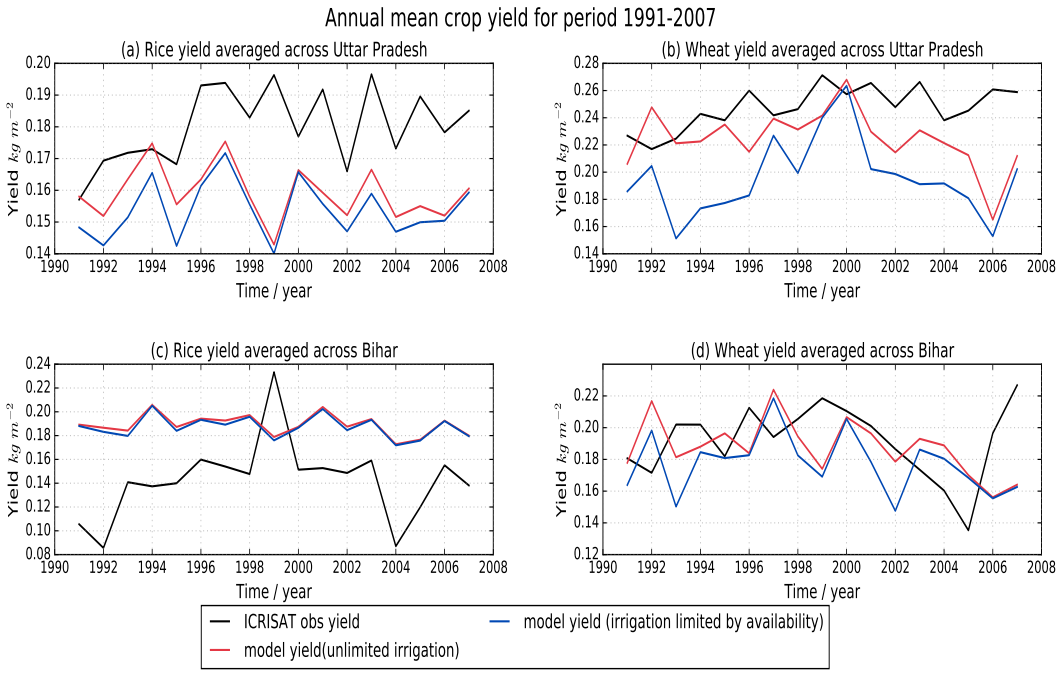

Figure 5.11: Annual average observed yields (*ICRISAT*, 2015) averaged for the state of Uttar Pradesh for rice (a) and wheat (b) and the state of Bihar also for rice (c) and wheat (d) (black lines). Two model simulations are also shown; a simulation with unlimited irrigation (red lines) and a simulation with irrigation limited by availability (blue lines) for the period 1991-2007.

the interactions between the irrigation, river flows and crops to be investigated. The regional analysis shown in this chapter has highlighted the next steps required to ensure that JULES can provide useful, reliable results for understanding interactions between the water and crop sectors (See Sect. 5.6.1). Ultimately the aim is to be able to use JULES to understand the implications of the interactions between the water and agriculture sectors on the demand for resources.

5.6.1 Next steps for regional impacts simulations

The first priority for furthering the work shown in this chapter is to estimate the areas where these crops are currently being grown in the present day. In the simulations presented in this chapter, wheat and rice are assumed to be planted everywhere. However, in order to provide a realistic estimate of the demand for resources, a more realistic representation of where the crops are actually grown is needed. Given that observations of crop area per district are available from *ICRISAT* (2015) and the area of each state is known, estimation of the crop fraction within each district should be possible for a large proportion of India for the present day.

Following this inclusion of a more accurate representation of crop areas, a second priority is a comprehensive evaluation of the model for each sector. In order to do this there is a need for more observations, either regional or site observations to ensure

that the different elements of the model are being simulated correctly and working as expected. Some examples of observations that would be useful for evaluating JULES for these sectors and this region are given in Table 5.1. Current day model evaluation is important for ensuring that the demands for resources are simulated correctly and for the appropriate reason; this is important for the interpretation of and having confidence in simulations of future climate change and the estimated demand for resources. For example if the irrigation demand for the present day is within the range of observational uncertainty, then assuming future demand is driven by the same mechanisms as today, future projections of demand would be more likely to be reliable.

The sparsity of observation data especially for surface water extractions means that comparison with other models is perhaps the only available option. Therefore another priority is to repeat the simulations in *Biemans et al.* (2016) using JULES, i.e. JULES simulations driven by WFDEI data (*Weedon et al.*, 2014) for the period 1979–2009. These WFDEI-JULES simulations would enable a cleaner comparison of the irrigation demand between the LPJml and JULES models. This comparison could be extended to include other models developed with a multisectoral approach in mind, thereby contributing to a model intercomparison project specifically designed for modelling the links between water and agriculture.

Finally, given that the ultimate aim is to use JULES to understand the implications of interactions between water and agriculture on resources, another priority should be the development of future simulations. Simulations of future resources require other information, including estimates of how crop area and population could change. These estimates rely on projections of future human behaviour, so several simulations that capture a range of possible future land use scenarios are required.

Sector	Observation type	Site Region	Location	frequency	Other information
Water	River flows	Sites - river gauges	Current river flows at known locations along SA rivers.	Daily, monthly	Including information on catchment area
Water	Water storage volume and capacity	Regional	District, state or country information	Annual, monthly	Including whether surface water or groundwater. GRACE useful on the country or catchment level
Water	Irrigation extractions	Both	Farm, district, state and country information	Annual, monthly, seasonal, daily	Daily useful for looking at the distribution of extractions through a crop season
Water	Irrigation applications	Both	Farm, district, state, country	Annual, monthly, seasonal, daily	Daily especially useful at the farm level ideally including number of days after sowing. ICRISAT provide irrigation area.
Water	Irrigation efficiency	Regional	District, state or country	Annual, seasonal	Specifying if from ground or surface water
Crops	Yields	Both	Farm, district, state or country	Annual or Seasonal (every crop)	ICRISAT useful at the regional scale
Crops	Biomass	Both	Farm, district, state or country	Daily, monthly, seasonal	
Crops	LAI	Both	Farm, district, state or country	Daily, monthly, seasonal	MODIS with ICRISAT for crop area of croptypes. Subseasonal information for crop development through the season.
Crops	Canopy height	Both	Farm, district state or country	Daily, monthly, seasonal	
Crops	Varieties of Crop	Both	Farm, district and state	Seasonal	Including thermal time information
Crops	Key development dates	Both	Farm, district and state	Daily through each season	Including number of days after sowing that crop emerges, flowers, reaches maturity, harvest

Table 5.1: A list of observations that would be helpful for model evaluation.

References

Ackerman, F., S. J. DeCanio, R. B. Howarth, and K. Sheeran (2009), Limitations of integrated assessment models of climate change, *Climatic Change*, *95*(3), 297–315, doi:10.1007/s10584-009-9570-x. 5.1

Betts, R. A. (2005), Integrated approaches to climate-crop modelling: needs and challenges, *Philosophical transactions of the Royal Society of London. Series B, Biological sciences*, *360*, 2049–65, doi:10.1098/rstb.2005.1739. 5.1

Biemans, H., L. Speelman, F. Ludwig, E. Moors, A. Wiltshire, P. Kumar, D. Gerten, and P. Kabat (2013), Future water resources for food production in five South Asian river basins and potential for adaptation - a modeling study, *Science of The Total Environment*, *468-469, Supplement*(0), S117–S131, doi:10.1016/j.scitotenv.2013.05.092. 5.4, 5.5.2, 5.5.2

Biemans, H., C. Siderius, A. Mishra, and B. Ahmad (2016), Crop-specific seasonal estimates of irrigation-water demand in south asia, *Hydrology and Earth System Sciences*, *20*(5), 1971–1982, doi:10.5194/hess-20-1971-2016. 5.4, 5.5.2, 5.5.2, 5.6.1

Challinor, A., T. Wheeler, P. Craufurd, J. Slingo, and D. Grimes (2004), Design and optimisation of a large-area process-based model for annual crops, *Agricultural and Forest Meteorology*, *124*(1-2), 99–120, doi:10.1016/j.agrformet.2004.01.002. 5.1

Challinor, A. J., W. N. Adger, T. G. Benton, D. Conway, M. Joshi, and D. Frame (2018), Transmission of climate risks across sectors and borders, *Philosophical Transactions of the Royal Society A: Mathematical, Physical and Engineering Sciences*, *376*, doi:10.1098/rsta.2017.0301. 5.1

Dankers, R., N. W. Arnell, D. B. Clark, P. D. Falloon, B. M. Fekete, S. N. Gosling, J. Heinke, H. Kim, Y. Masaki, Y. Satoh, T. Stacke, Y. Wada, and D. Wisser (2014), First look at changes in flood hazard in the inter-sectoral impact model intercomparison project ensemble, *Proceedings of the National Academy of Sciences*, *111*(9), 3257–3261, doi:10.1073/pnas.1302078110. 5.1

Davie, J. C. S., P. D. Falloon, R. Kahana, R. Dankers, R. Betts, F. T. Portmann, D. Wisser, D. B. Clark, A. Ito, Y. Masaki, K. Nishina, B. Fekete, Z. Tessler, Y. Wada, X. Liu, Q. Tang, S. Hagemann, T. Stacke, R. Pavlick, S. Schaphoff, S. N. Gosling, W. Franssen, and N. Arnell (2013), Comparing projections of future changes in runoff from hydrological and biome models in isi-mip, *Earth System Dynamics*, *4*(2), 359–374, doi:10.5194/esd-4-359-2013. 5.1

Dee, D. P., S. M. Uppala, A. J. Simmons, P. Berrisford, P. Poli, S. Kobayashi, U. Andrae, M. A. Balmaseda, G. B. P., Bauer, P. Bechtold, A. C. M. Beljaars, L. van de Berg, J. Bidlot, N. Bormann, C. Delsol, R. Dragani, M. Fuentes, A. J. Geer, L. Haimberger, S. B. Healy, H. Hersbach, E. V. Hólm, L. Isaksen, P. Kållberg, M. Köhler, M. Matricardi, A. P. McNally, B. M. Monge-Sanz, J.-J. Morcrette, B.-K. Park, C. Peubey, P. de Rosnay, C. Tavolato, J.-N. Thépaut, and F. Vitart (2011), The era-interim reanalysis: configuration and performance of the data assimilation system, *Quarterly Journal of the Royal Meteorological Society*, *137*(656), 553–597, doi:10.1002/qj.828. 5.2

Essery, R. L. H., M. J. Best, and P. M. Cox (2001), Moses 2.2 technical documentation, *Hadley Centre Technical Note*, *30*. 5.2

Ewert, F., R. Rötter, M. Bindi, H. Webber, M. Trnka, K. Kersebaum, J. Olesen, M. van Ittersum, S. Janssen, M. Rivington, M. Semenov, D. Wallach, J. Porter, D. Stewart, J. Verhagen, T. Gaiser, T. Palosuo, F. Tao, C. Nendel, P. Roggero, L. Bartošová, and S. Asseng (2015), Crop modelling for integrated assessment of risk to food production from climate change, *Environmental Modelling & Software*, *72*, 287–303, doi:10.1016/j.envsoft.2014.12.003. 5.1

Griffiths, F. E. W., R. Lyndon, and M. Bennett (1985), The effects of vernalization on the growth of the wheat shoot apex, *Annals of Botany*, *56*, 501–511, doi:10.1093/oxfordjournals.aob.a087035. 5.2

Gupta, S., and D. Deshpande (2004), Water for India in 2050: first order assessment of available options, *Current Science*, *86*(9), 1216–1224. 5.4

ICRISAT (2015), District Level Database Documentation, *Tech. rep.*, International Crops Research Institute for the Semi-Arid Tropics, Hyderabad. (document), 5.2, 5.3, 5.5.3, 5.5.3, 5.10, 5.11, 5.6.1

Jones, R. G., M. Noguer, D. C. Hassell, D. Hudson, S. S. Wilson, G. J. Jenkins, and J. F. Mitchell (2004), Generating high resolution climate change scenarios using PRECIS, *Met Office Hadley Centre, Exeter, UK*, pp. 0–40. 5.2

Kumar, P., A. Wiltshire, C. Mathison, S. Asharaf, B. Ahrens, P. Lucas-Picher, J. H. Christensen, A. Gobiet, F. Saeed, S. Hagemann, and D. Jacob (2013), Downscaled climate change projections with uncertainty assessment over India using a high resolution multi-model approach, *Science of The Total Environment*, *468-469, Supplement*(0), S18–S30, doi:10.1016/j.scitotenv.2013.01.051, changing water resources availability in Northern India with respect to Himalayan glacier retreat and changing monsoon patterns: consequences and adaptation. 5.2

Mahajan, A., and R. D. Gupta (Eds.) (2009), *The Rice–Wheat Cropping System*, pp. 109–117, Springer Netherlands, Dordrecht, doi:10.1007/978-1-4020-9875-8_7. 5.2

Mathison, C., A. Wiltshire, A. Dimri, P. Falloon, D. Jacob, P. Kumar, E. Moors, J. Ridley, C. Siderius, M. Stoffel, and T. Yasunari (2013), Regional projections of North Indian climate for adaptation studies, *Science of The Total Environment*, *468-469, Supplement*(0), S4–S17, doi:10.1016/j.scitotenv.2012.04.066. 5.2

Mathison, C., A. J. Wiltshire, P. Falloon, and A. J. Challinor (2015), South asia river-flow projections and their implications for water resources, *Hydrology and Earth System Sciences*, *19*(12), 4783–4810, doi:10.5194/hess-19-4783-2015. 5.2

Mathison, C., C. Deva, P. Falloon, and A. J. Challinor (2018), Estimating sowing and harvest dates based on the asian summer monsoon, *Earth System Dynamics*, *9*(2), 563–592, doi:10.5194/esd-9-563-2018. 5.2

Osborne, T., J. Gornall, J. Hooker, K. Williams, A. Wiltshire, R. Betts, and T. Wheeler (2015), Jules-crop: a parametrisation of crops in the joint uk land environment simulator, *Geoscientific Model Development*, *8*(4), 1139–1155, doi:10.5194/gmd-8-1139-2015. 5.2

Osborne, T. M., D. M. Lawrence, A. J. Challinor, J. M. Slingo, and T. R. Wheeler (2007), Development and assessment of a coupled crop-climate model, *Global Change Biology*, *13*(1), 169–183, doi:10.1111/j.1365-2486.2006.01274.x. 5.1

Penning de Vries, F. W. T., D. Jansen, H. ten Berge, and A. Bakema (1989), *Simulation of Ecophysiological Processes of Growth in Several Annual Crops*, Simulation monographs, Pudoc. 5.5.3

Piontek, F., C. Müller, T. A. M. Pugh, D. B. Clark, D. Deryng, J. Elliott, F. de Jesus Colón González, M. Flörke, C. Folberth, W. Franssen, K. Frieler, A. D. Friend, S. N. Gosling, D. Hemming, N. Khabarov, H. Kim, M. R. Lomas, Y. Masaki, M. Mengel, A. Morse, K. Neumann, K. Nishina, S. Ostberg, R. Pavlick, A. C. Ruane, J. Schewe, E. Schmid, T. Stacke, Q. Tang, Z. D. Tessler, A. M. Tompkins, L. Warszawski, D. Wisser, and H. J. Schellnhuber (2014), Multisectoral climate impact hotspots in a warming world, *Proceedings of the National Academy of Sciences*, *111*(9), 3233–3238, doi:10.1073/pnas.1222471110. 5.1

Pope, V., M. L. Gallani, P. R. Rowntree, and R. A. Stratton (2000), The impact of new physical parametrizations in the hadley centre climate model: Hadam3, *Climate Dynamics*, *16*(2-3), 123–146, doi:10.1007/s003820050009. 5.1

Prudhomme, C., I. Giuntoli, E. L. Robinson, D. B. Clark, N. W. Arnell, R. Dankers, B. M. Fekete, W. Franssen, D. Gerten, S. N. Gosling, S. Hagemann, D. M. Hannah, H. Kim, Y. Masaki, Y. Satoh, T. Stacke, Y. Wada, and D. Wisser (2014), Hydrological droughts in the 21st century, hotspots and uncertainties from a global multimodel ensemble experiment, *Proceedings of the National Academy of Sciences*, *111*(9), 3262–3267, doi:10.1073/pnas.1222473110. 5.1

Ramankutty, N., A. T. Evan, C. Monfreda, and J. A. Foley (2008), Farming the planet: 1. geographic distribution of global agricultural lands in the year 2000, *Global Biogeochemical Cycles*, *22*(1), doi:10.1029/2007GB002952. 5.5.2

Robertson, M., I. Brooking, and J. Ritchie (1996), Temperature response of vernalization in wheat: Modelling the effect on the final number of mainstem leaves, *Annals of Botany*, *78*(3), 371–381, doi:10.1006/anbo.1996.0132. 5.2

Schewe, J., J. Heinke, D. Gerten, I. Haddeland, N. W. Arnell, D. B. Clark, R. Dankers, S. Eisner, B. M. Fekete, F. J. Colón-González, S. N. Gosling, H. Kim, X. Liu, Y. Masaki, F. T. Portmann, Y. Satoh, T. Stacke, Q. Tang, Y. Wada, D. Wisser, T. Albrecht, K. Frieler, F. Piontek, L. Warszawski, and P. Kabat (2014), Multimodel assessment of water scarcity under climate change, *Proceedings of the National Academy of Sciences*, *111*(9), 3245–3250, doi:10.1073/pnas.1222460110. 5.1

Schwanitz, V. J. (2013), Evaluating integrated assessment models of global climate change, *Environmental Modelling & Software*, *50*, 120–131, doi:10.1016/j.envsoft.2013.09.005. 5.1

Simmons, A., S. Uppala, D. Dee, and S. Kobayashi (2007), Era-interim: New ecmwf reanalysis products from 1989 onwards., *ECMWF Newsletter - Winter 2006/07*, *110*, 25–35. 5.2

Slingo, J. M., A. J. Challinor, B. J. Hoskins, and T. R. Wheeler (2005), Introduction: food crops in a changing climate, *Philosphical Transactions of the Royal Society B: Biological Sciences*, *360*, 1983–1989, doi:10.1098/rstb.2005.1755. 5.1

van Vuuren, D. P., J. Lowe, E. Stehfest, L. Gohar, A. F. Hof, C. Hope, R. Warren, M. Meinshausen, and G.-K. Plattner (2011), How well do integrated assessment models simulate climate change?, *Climatic Change*, *104*(2), 255–285, doi:10.1007/s10584-009-9764-2. 5.1

Weedon, G. P., G. Balsamo, N. Bellouin, S. Gomes, M. J. Best, and P. Viterbo (2014), The wfdei meteorological forcing data set: Watch forcing data methodology applied to era-interim reanalysis data., *Water Resources Research*, *50*(9), 7505–7514, doi:10.1002/2014WR015638. 5.5.2, 5.6.1

Zessner, M., M. Schönhart, J. Parajka, H. Trautvetter, H. Mitter, M. Kirchner, G. Hepp, A. Blaschke, B. Strenn, and E. Schmid (2016), A novel integrated modelling framework to assess the impacts of climate and socio-economic drivers on land use and water quality, *Science of The Total Environment*, *579*, doi:10.1016/j.scitotenv.2016.11.092. 5.1

Chapter 6

Discussion, conclusions and future work

This final chapter begins by providing a thesis summary (Sect. 6.0.1) followed by discussion (Sect. 6.1), conclusions (Sect. 6.2) and suggestions for future work (Sect. 6.3).

6.0.1 Thesis summary

In Chapter 2, analysis of river flows in the climate model simulations for 1970-2100 showed a potential increase in water resources for the northern basins of India, with river flow rates at some of the gauges almost doubled by the end of the century. These increases in river flow occur for the gauges in the Ganges/Brahmaputra basin, which also shows an increasing trend in both evaporation and precipitation. Therefore the changes in river flow are likely to be mainly driven by precipitation on the annual scale which more than counters the evaporation caused by increasing temperatures in the model. This is consistent with other analyses of precipitation which also use the A1B climate scenario (*Nepal and Shrestha*, 2015) and more recent analyses by *Betts et al.* (2018). SA is a location of intensive agriculture with extensive irrigation systems. However the RCM in this analysis does not include irrigation and crops, these are needed to fully understand how the demand for water resources could change in this region in the future. JULES-IM includes representation of crops and irrigation; therefore using the RCM data within JULES it is possible to look at the effects of crops and irrigation on the land surface.

In Chapter 3, the close relationship between SA sowing and harvest dates and the ASM is exploited to propose and demonstrate a method for calculating the sowing and harvest dates for the SA region. Crop simulations require accurate input data that ensures the crops are being grown at the correct time of the year. This is usually in the form of a sowing window or sowing date together with a harvest date or an estimate of the growing period. Global datasets are often coarse resolution and make

compromises based on climatology. As a result these datasets are not always able to distinguish when wheat is grown in tropical and sub-tropical regions; leading to simulations growing crops during the wrong season, which affects the reliability of the simulated water use and crop yield. The crop calendar for the SA region is closely related to the monsoon period; for example, rice sowing dates particularly are very closely aligned with monsoon onset. Although there is more uncertainty regarding rice harvest and wheat sowing and harvest dates as these are not as closely associated with the monsoon rainfall, there is still a relationship. The method presented assumes that the agricultural practices remain dependent on the monsoon in the future. Given this assumption, the method can be used to estimate the crop seasons for future simulations; demonstrated in Chapter 3 for two future periods. The method adjusts the sowing and harvest dates according to the timing of the monsoon to ensure that the crops in the future simulations are still sown at the optimum time of year.

Most LSMs only simulate one crop per year, however there are many regions that use sequential cropping systems (also referred to as double or multiple cropping). These cropping systems make the most efficient use of limited resources and space to maximize yield potential and lower the risk of complete crop failure. Previously *Biemans et al.* (2016) represented sequential cropping in LPJml by joining two simulations together, while *Waha et al.* (2013) changed the growing seasons in LPJml so that there was no overlap between crops in Africa. In Chapter 4 a sequential cropping method is described and implemented in a branch of JULES at vn5.2 to enable the continuous simulation of two crops in each year. This method is demonstrated and evaluated at Avignon and four locations across Uttar Pradesh and Bihar, a major rice–wheat producing area of northern India. In Chapter 4 the results show that JULES successfully simulates two crops in rotation at the Avignon site and the four locations across Uttar Pradesh and Bihar, producing maxima of LAI, canopy height and biomass at approximately the correct times of the year. For Avignon, where detailed observations are available, the JULES fluxes correlate well with the observed fluxes of GPP, H and LE (r_values of above 0.7). In general JULES underestimates biomass and yields in these simulations, which is consistent with results shown in *Osborne et al.* (2015); this could be reduced in some cases, by implementing a yield gap parameter.

All of the developments within this thesis have been brought together in two integrated simulations presented in Chapter 5. These integrated simulations show the progress that has been made towards the representation of the impacts of climate on water (river flows and irrigation) and agriculture (crops) in a single simulation, i.e. modelling multiple related sectors at once and allowing them to affect each other. These first regional simulations include sequential cropping and selective irrigation for the same two states included in Chapter 4: Uttar Pradesh and Bihar. The method for estimating sowing and harvest dates (including for regions where observations are sparse), developed in Chapter 3, is used to calculate the thermal time requirement for

the rice–wheat crop rotation in which only wheat is irrigated (Chapter 4). In one simulation irrigation is limited which means it is linked to rivers and groundwater; in the other, irrigation is unlimited, which means it is not linked to the rivers.

These two 17-year regional simulations for Uttar Pradesh and Bihar have demonstrated that JULES is now closer to being able to simulate impacts for SA for multiple sectors. Although these initial simulations show some promising results, there are aspects that require further investigation, particularly regarding the representation of irrigation. More observation data is needed to evaluate each of the individual model components included in these regional simulations; for example river flows and surface extractions to ensure that the model is simulating both the present day demand and available water resource correctly. Water resource and usage data is difficult to acquire for SA. Area crop yields, crop areas and irrigation area data are available from *ICRISAT* (2015). However it would also be useful, in addition to this, to have site data for SA crop sites to evaluate modelled crop characteristics against observations for each of the growing stages. This would allow a thorough evaluation of the water and crop aspects of JULES to ensure they are simulating each of these elements correctly for the present day. Section 6.3 summarizes all of the recommendations for future work from all of the chapters.

6.1 Discussion

SA is a complex region, both in terms of its environment (specifically climate and orography) and socioeconomics. A large population and dependence on industries with a high demand for water, make SA vulnerable to changes in climate. SA depends on the ASM for much of its fresh water each year, with water resources for agriculture of key importance for economic prosperity and food security. However, the simulation of the monsoon remains a challenge for the climate modelling community, with a large spread in simulations and significant overlap between the CMIP3 and CMIP5 ensembles (*Sperber et al.*, 2013). *Sperber et al.* (2013) finds that no one model simulates the monsoon better than all the others, with different models able to simulate different aspects of the monsoon. In this thesis, GCMs that provide a reasonable estimate of the monsoon precipitation climatology (*Annamalai et al.*, 2007) are used to provide boundary conditions for an RCM. The RCM is then used to prescribe the SA climate and hence the monsoon, for simulations using both river routing and the JULES model. JULES in this context is the standalone land surface model also used in the UK Met Office models. There are now more model simulations available for this region, with the output variables needed to run JULES, which increases the opportunities for further analysis of this region.

The ASM provides the water resource for much of SA throughout the growing season, which begins with the start of the monsoon. A major feature of the SA growing

season is the cultivation of more than one crop per growing season; this is referred to as sequential or multiple cropping and can be simulated in JULES using outputs from this thesis (Chapter 4). The use of the sequential cropping system will have an impact on the amount of water needed for the crops to grow successfully. To understand water resources, there needs to be a seamless simulation of the whole SA growing season, incorporating all of the crops grown (and the resources they need), from the start of one monsoon to the next. This more integrated approach to simulating water and agriculture allows climate to affect both aspects of the land–surface simultaneously and for each to influence each other. Ultimately avoiding the need to arbitrarily separate out two aspects of the land-surface that are intrinsically linked, while improving understanding of the interactions between these climate impacts (*Betts*, 2005, *Falloon and Betts*, 2010).

The JULES developments presented in Chapter 4 also highlight the large number of parameters that define a range of other crop characteristics, which may also be important for simulating SA crops. For example, the stage of the crop development at which senescence begins. In Chapter 4 the start of senescence is defined as the point at which the development index (DVI) is 1.5, which is the same setting as used in *Osborne et al.* (2015). This DVI may not be appropriate for some crops grown in SA, particularly for wheat, which is grown during the rabi or dry season. Towards the end of the rabi season, the temperature increases rapidly. High temperatures tend to accelerate senescence (*Penning de Vries et al.*, 1989), thereby affecting the rate of grain filling and the rate of senescence in the model. Previously, the default setting for the start of senescence (DVI=1.5) was found by *Williams et al.* (2017) to be too late and the process progressed to quickly for a maize site in Nebraska (prior to tuning to observations from that site). The crop characteristics (such as LAI and canopy height) shown for both the point simulations (Chapter 4) and the regional simulations (Chapter 5) of Uttar Pradesh and Bihar are plausible compared with an average crop described in *Penning de Vries et al.* (1989). However, there may be specific characteristics of India spring wheat varieties that could modify the allocation of carbon to different parts of the crop, affecting for example: the number or density of leaves; the depths of the roots or the thickness of the stem.

In this thesis, the irrigation scheme is modified so that only one crop can be irrigated at once but the scheme itself is not changed, i.e., the irrigation season is determined by maximum dvi. Therefore the crop model must be switched on and the DVI must be greater than 0 for irrigation to occur. All schemes in JULES assume that crops access water from the top two soil layers and that this is sufficient to reduce water stress. In the regional simulations (Chapter 5), rice is not therefore irrigated during the monsoon. However, this is likely to depend on location, with some regions irrigated during monsoon breaks and also accessing water from deeper than the second soil layer. In addition, irrigation in JULES is applied consistently throughout the crop growing

season. However, irrigation in SA is often applied at particular times throughout the growing season. To facilitate more focussed development of the irrigation scheme and ensure that SA irrigation is being modelled correctly, knowledge of when and where water is applied through the growing season is needed. It may also be relevant to know the depth the water is being added, especially if it is not typically added to the top two soil levels.

The input data for SA crops in JULES is important to ensure that the crops are being grown at the appropriate time of the year, even where there are few observations available. The method shown in Chapter 3, is flexible, does not require much data and can be easily applied to a wide range of climate model data. This will be particularly useful for future climate simulations and looking at alternative adaptation options

The regional simulations that are presented as prototype simulations in Chapter 5 use ERAinterim to provide boundary conditions to the HadRM3 RCM. ERAinterim, like the other GCMS in this thesis (ECHAM5 and HadCM3) and the RCM, will have biases due to the representation of processes or resolution. Therefore, these data are often the focus of bias correction before being used in impacts models like JULES. In this thesis no bias correction is applied; therefore the outputs from JULES will carry the errors from the models further up the model chain, in the same way as they would if the process was completely integrated. In RCM simulations based on the HadGEM3 model, which use JULES as the land-surface scheme in place of MOSESv2.2, there will be more consistency between the RCM and JULES. As a first step to simulate crops and irrigation as an integrated part of the land-surface for policy relevance, it would be a major recommondendation for the design of the integrated impacts experiment to include an RCM with JULES as the land-surface.

6.2 Concluding remarks

This thesis has produced prototype regional integrated impact simulations (Chapter 5) focusing on two sectors: agriculture (crops) and water (river flows and irrigation). These integrated simulations allow the climate and irrigation to simultaneously affect both river flows and crops; these are some of the interactions summarized in Fig. 1.1. These simulations represents a significant step towards fully integrated impacts simulations. However the simulations presented in Chapter 5 do not allow the surface to influence the atmosphere as this would require a fully coupled climate model that includes hydrology and crops. The development of integrated SA simulations has required the inclusion of the sequential cropping system in JULES (Chapter 4); this makes JULES one of the few models with this capability. Including sequential cropping will improve the representation of surface fluxes over croplands that use this cropping system and when combined with accurate climate data and crop parameterizations will provide improved estimates of the use of resources.

Sequential cropping is a common cropping system across the world, making this development useful for many other regions; for example Brazil and Africa. However for regions like Africa, data for setting up crop models is often scarce. For these regions with limited data availability, the method for calculating sowing and harvest dates using dominating climate phenomena (Chapter 3) may also be applicable; especially where there is evidence that the crop seasons and regional climate are closely aligned. This thesis has focussed on SA but these developments could be applied to any relevant region, potentially shortening the time required for developing integrated impacts simulations. To develop simulations for another region where little or no observations are available, knowledge of the dominating climate phenomena and its relationship with crop seasons would be needed to calculate the sowing and harvest dates. The different crops that are used within a region would also need consideration; balancing the need for new crop parameterizations against using existing crops already in the model.

6.3 Recommendations and Future work

The next steps for developing understanding of the impact of climate for SA fall into three main categories. Broadly these areas are model evaluation, model development and simulations of future climate. This section discusses each of these in order of priority starting with model evaluation discussed in Sect. 6.3.1, followed by model development in Sect. 6.3.2 and finally future simulations in Sect. 6.3.3.

6.3.1 Model evaluation

Model evaluation is the one of the most immediate considerations for future work especially for the regional simulations presented in Chapter 5. This relies on having appropriate data with sufficient detail for a relevant period. This data may be a mixture of both site and regional data because the availability of data is not consistent across different geographical or subject areas. For SA particularly, past river flow data is available but rarely for the present day. Most rivers in SA flow through several countries, crossing many state borders. Each state is responsible for the river(s) in their jurisdiction, in terms of its use and development, which makes water resource and river flow a state subject (*Jain and Kumar*, 2014) and therefore not readily available. This restriction also applies to extractions for irrigation particularly regarding surface water extractions although there is more information available on groundwater and data is available from *GoI* (2011).

Observations of water extracted for irrigation or irrigation amounts applied would be useful for establishing that the irrigation is working correctly and to check that the model is applying a realistic amount of water to the soil. In Chapter 5 there were increases in rice yields for the unlimited irrigated simulation compared to the limited simulation despite only wheat being irrigated in both of these simulations. The

hypothesis proposed is that the soil, irrigated during the wheat season remains wet into the following rice season; increasing the following season rice yields. This is more likely to be the case if too much water is added to the soil during the wheat season. The regional analysis in Chapter 5 also highlighted that the irrigation demand is sometimes higher when irrigation is linked to the rivers compared with a simulation that includes irrigation that is not linked to rivers. Further work is needed to understand both of these aspects of irrigation in these simulations.

There is more information on crop yields from India particularly via *ICRISAT* (2015), which is a valuable resource. However yields can occur for a variety of reasons. It would be beneficial to have observations for all stages of the crop development throughout the crop cycle, to ensure that the model captures the observed stages of development; accurate simulation of the different development stages could be important for calculating the use of resources. Site information is also useful for model evaluation, although care must be taken in using it where a model is intended for regional or global use. *Challinor et al.* (2018) highlight the need for models to be evaluated using historical observations from a range of different sources to avoid overtuning to one site or crop characteristic; these observations should include, but not be limited to yields alone. Given the wealth of observations at the Avignon site used in Chapter 4, but with this note of caution in mind, the Avignon simulation of winter wheat and sorghum in Chapter 4 indicated some biases in the LAI and biomass for winter wheat. It would be interesting to revisit this work at Avignon, replacing the spring wheat parameterization used in Chapter 4 with a winter wheat parameterization to see if this reduces these biases and improves the simulations. However, additional sites would also be useful to evaluate the model for a wide range of environments, crops and conditions (*Challinor et al.*, 2018).

The analysis of four locations across the Indian states of Uttar Pradesh and Bihar in Chapter 4 highlighted differences both in observed and simulated yield from West to East that were also evident in the regional simulations of the same area (see Chapter 5). More crop specific data, similar to Avignon, but for individual locations across SA; such as those suggested in Table 5.1 would facilitate further investigation into the reasons for differences in both observed and modelled yields between locations. Understanding if the differences between yields are influenced more by differing land management practices than missing processes in the driving data would be useful for planning other similar simulations. For example, if the differences in the model yields are due to a lack of irrigation in the driving data this suggests that future simulations should take account of this; particularly given the potential influence that evaporation from irrigated croplands has on the regional climate (*Tuinenburg et al.*, 2014). However it would also be beneficial to separate out the influence of the differing management practices across these two states to quantify its effect on observed yields. *Williams et al.* (2017) describes using the f_{yield} parameter to account for different management

practises at different locations within JULES.

Large projects like ISIMIP and AgMIP are extremely useful for understanding how models differ and evaluation against other models. The focussed studies that are part of AgMIP are also a particularly useful resource in developing understanding of the more detailed processes in models. Although JULES was not included in the original AgMIP wheat pilot simulations (*Asseng et al.*, 2015) the availability of data to run these simulations retrospectively is a useful resource of site specific data. Ensuring JULES is included in future projects like ISIMIP and AgMIP in future would be beneficial in terms of furthering understanding of the JULES model and focussing model development. It would be also be interesting to explore using higher resolution driving data to run the regional integrated JULES simulations presented in this thesis. For example using the 12 km reanalysis data product described by *Mahmood et al.* (2018); this is an India reanalysis product that captures the main areas and the intensity of precipitation over India throughout the monsoon period.

6.3.2 Model development

This section focuses on the model developments that are needed for simulating the impacts of climate on the SA region; highlighted by the research presented in this thesis. It is not intended to be an exhaustive list of all the different model developments needed for the whole of JULES. For example further information on the JULES community wide effort to improve the representation of water stress in JULES are provided in *Harper et al.* (in preparation) and *Williams et al.* (2018). In addition, the particular development priorities for JULES-crop are provided in a number of deliverables from the Brazil Climate Science to Services Project (CSSP–Brazil; *Falloon et al.*, 2017, *Falloon*, 2018); these include for example linking JULES-crop to the nitrogen cycle and additional or improved crop parameterizations. Model developments useful for the SA region are:

- Including representation of glaciers: A representation of glaciers in JULES would be beneficial for simulating river flows more accurately for SA. Implementing the scheme presented by *Shannon et al.* (2019), currently in a branch of JULES into the main JULES code and incorporating it into regional simulations that included the high Himalaya would be important especially for the lower river flows outside of the monsoon period.

- A higher resolution river routing map: The current river routing map is 0.5°, which is quite coarse resolution. A higher resolution river routing map would improve the representation of river flows and possibly mean that JULES no longer needs to regrid the climate data onto the river grid and then back to the climate grid. Assuming the existing global river routing map is replaced this development would be beneficial across other regions too.

- Inundation and flooding are very important for large parts of SA, with parts of Bangladesh and north eastern India flooding almost annually. Therefore including representation of inundation in SA regional simulations for simulating the impacts of climate on agriculture and water would be an extremely useful next step for this work.

- The SA region has seen a great deal of development along the river network including the building of dams for purposes of hydroelectric power generation. Including this type of information in the model would also be beneficial for understanding the water resources available for people and agriculture. Global dam and reservoir information would have a positive impact across regions other than SA.

- Including representation of the irrigation efficiency in JULES either by country as in *Biemans et al.* (2016) or by state if available. This would allow comparison of JULES with extraction data. The irrigation scheme could also be developed to include management practices for a region where a specific amount of irrigation water is applied across a given area, with applications on particular days after sowing e.g an irrigation calendar. Setting up and evaluating a scheme like this would probably require detailed irrigation information and may not be applicable across large regions.

- Including representation of heat stress in the crop model. Currently crop yields are only affected by extreme temperatures in JULES through a slowing of the crop development. In reality extreme temperatures at critical times could actually cause complete crop failure and therefore no yield at all. Given that temperatures in SA already high and projected to increase further due to climate change this is likely to an important feature of crop models for future projections. This development is likely to be useful across multiple regions, especially where temperatures are already at or close to the biological maximum for crops (*Gornall et al.*, 2010).

Many of the developments described above are likely to be useful for other regions, particularly tropical regions with similar challenges to SA in terms of climate change, resources (e.g. water) and population growth. The order of priority for these developments would be different depending on the region and the question being asked. Unlike SA the representation of glaciers is not a priority for regions such as Africa or Brazil. The type of crops will also vary according to region, where rice/wheat dominate in SA, crops like sorghum/cassava may be the priority in Africa and maize/soybean/sugarcane for Brazil. The growing importance of heat stress is likely to improve the accuracy of simulations across the tropics helping to understand the likelihood of crop failures or years of lower yields for simulated crops; this is therefore a high priority development.

A better representation of water resources for a region will be possible by including higher resolution rivers, representation of flooding/inundation and including dams and water storage. For regions where flooding is almost an annual event such as Bangladesh, understanding the future frequency of inundation and flooding events could be a higher priority than heat stress on crops; having the potential to completely devastate not only crops but livelihoods, homes and infrastructure.

6.3.3 Simulations of future climate

Setting up future simulations, either for the Uttar Pradesh and Bihar region presented in Chapter 5 or for the whole SA region, would need to include additional input data to provide a realistic representation of the demand for resources. This is also not intended to be an exhaustive list but these have been highlighted by the research presented in this thesis.

- Crop areas: In the regional simulations presented in Chapter 5 it is assumed that wheat and rice are grown in every gridbox every year. For developing an understanding of demand for resources it is necessary to have a realistic estimate of where the crops are actually grown. Developing realistic crop areas for the present day using observed cropping areas is possible for SA using the *ICRISAT* (2015) data. However developing these into plausible future crop areas is a bigger challenge. Datasets do exist for this purpose for example the Land-use Harmonization 2 project (LUH2; *Hurtt et al.*, 2011), originally developed for the fifth Assessment Report (AR5) of the Intergovernmental Panel on Climate Change (IPCC) and now also being used in the coupled model intercomparison project (CMIP6) simulations.

- Crop thermal time requirements: JULES requires as input thermaltime requirements for each gridbox; these would need to be calculated for future simulations based on the temperature climatology in the driving data as described in *Osborne et al.* (2015).

- The 25km HighNoon simulations in use in this thesis are based on the HadCM3 GCM, an AR4 generation model. It therefore does not include many of the processes from more recent developments that have been implemented into newer ESMs (e.g. aerosols). *Janes et al.* (2019) describe new 25km simulations, for a larger domain (but including the HighNoon domain). These new RCMs use the same RCM (HadCM3) to downscale three CMIP5 models for the period 1970-2100. It would be interesting to add these new simulations to the HighNoon RCMs to produce a 5-model SA region ensemble for studying climate impacts.

References

Annamalai, H., K. Hamilton, and K. Sperber (2007), The South Asian summer monsoon and its relationship with ENSO in the IPCC AR4 simulations, *Journal of Climate*, *20*(6), 1071–1092, doi:10.1175/JCLI4035.1. 6.1

Asseng, S., F. Ewert, P. Martre, R. P. Rötter, D. B. Lobell, D. Cammarano1, B. A. Kimball, M. J. Ottman, G. W. Wall, J. W. White, M. P. Reynolds, P. D. Alderman, P. V. V. Prasad, P. K. Aggarwal, J. Anothai1, B. Basso1, C. Biernath, A. J. Challinor, G. D. Sanctis, J. Doltra, E. Fereres, M. Garcia-Vila, S. Gayler, G. Hoogenboom, L. A. Hunt, R. C. Izaurralde, M. Jabloun, C. D. Jones, K. C. Kersebaum, A.-K. Koehler, C. Müller, S. N. Kumar, C. Nendel, G. O'Leary, J. E. Olesen, T. Palosuo, E. Priesack, E. E. Rezaei, A. C. Ruane, M. A. Semenov, I. Shcherbak, C. Stöckle, P. Stratonovitch, T. Streck, I. Supit, F. Tao, P. J. Thorburn, K.Waha, E.Wang, D.Wallach, J.Wolf, Z. Zhao, Y. Zhu, A. Sibley, and J. I. Ortiz-Monasterio (2015), Rising temperatures reduce global wheat production, *Nature Climate Change*, *5*(2), 143–147, doi:10.1038/NCLIMATE2470. 6.3.1

Betts, R. A. (2005), Integrated approaches to climate-crop modelling: needs and challenges, *Philosophical transactions of the Royal Society of London. Series B, Biological sciences*, *360*, 2049–65, doi:10.1098/rstb.2005.1739. 6.1

Betts, R. A., L. Alfieri, C. Bradshaw, J. Caesar, L. Feyen, P. Friedlingstein, L. Gohar, A. Koutroulis, K. Lewis, C. Morfopoulos, L. Papadimitriou, K. J. Richardson, I. Tsanis, and K. Wyser (2018), Changes in climate extremes, fresh water availability and vulnerability to food insecurity projected at 1.5°c and 2°c global warming with a higher-resolution global climate model, *Philosophical Transactions of the Royal Society A: Mathematical, Physical and Engineering Sciences*, *376*, doi:10.1098/rsta.2016.0452. 6.0.1

Biemans, H., C. Siderius, A. Mishra, and B. Ahmad (2016), Crop-specific seasonal estimates of irrigation-water demand in south asia, *Hydrology and Earth System Sciences*, *20*(5), 1971–1982, doi:10.5194/hess-20-1971-2016. 6.0.1, 6.3.2

Challinor, A. J., C. Müller, S. Asseng, C. Deva, K. J. Nicklin, D. Wallach, E. Vanuytrecht, S. Whitfield, J. Ramirez-Villegas, and A.-K. Koehler (2018), Improving the use of crop models for risk assessment and climate change adaptation, *Agricultural Systems*, *159*, 296–306, doi:10.1016/j.agsy.2017.07.010. 6.3.1

Falloon, P. (2018), What is needed to switch on jules-crop in an existing non-crop gridded jules run?, *Climate Science to Services Project – Brazil, Met Office Hadley Centre, Exeter, UK*. 6.3.2

Falloon, P., and R. Betts (2010), Climate impacts on european agriculture and water management in the context of adaptation and mitigation – the importance of an integrated approach, *Science of The Total Environment*, *408*(23), 5667 – 5687, doi:10.1016/j.scitotenv.2009.05.002, special Section: Integrating Water and Agricultural Management Under Climate Change. 6.1

Falloon, P., K. E. Williams, K. Richardson, C. Kent, and E. Pope (2017), Preliminary assessment of crop modelling capability, for crops relevant to brazil, *Climate Science to Services Project - Brazil Met Office Hadley Centre, Exeter, UK*. 6.3.2

GoI, M. (2011), Dynamic ground water resources of India, *Central Ground Water Board, Ministry of Water Resources, River Development and Ganga Rejuvenation, Government of India*. 6.3.1

Gornall, J., R. Betts, E. Burke, R. Clark, J. Camp, K. Willett, and A. Wiltshire (2010), Implications of climate change for agricultural productivity in the early twenty-first century, *Philosphical Transactions of the Royal Society B: Biological Sciences*, *365*, 2973–2989, doi:10.1098/rstb.2010.0158. 6.3.2

Harper, A. B., K. Williams, J. Team, and F. Team (in preparation), Toward an improved representation of soil moisture stress: disentangling causes and effects, *to be decided*, *00*, 0–34. 6.3.2

Hurtt, G. C., L. P. Chini, S. Frolking, R. A. Betts, J. Feddema, G. Fischer, J. P. Fisk, K. Hibbard, R. A. Houghton, A. Janetos, C. D. Jones, G. Kindermann, T. Kinoshita, K. K. Goldewijk, K. Riahi, E. Shevliakova, S. Smith, E.Stehfest, A. Thomson, P. Thornton, D. P. van Vuuren, and Y. P. Wang (2011), Harmonization of land-use scenarios for the period 1500–2100: 600years of global gridded annual land-use transitions, wood harvest, and resulting secondary lands, *Climatic Change*, *109*(1), 117, doi:10.1007/s10584-011-0153-2. 6.3.3

ICRISAT (2015), District Level Database Documentation, *Tech. rep.*, International Crops Research Institute for the Semi-Arid Tropics, Hyderabad. 6.0.1, 6.3.1, 6.3.3

Jain, S. K., and P. Kumar (2014), Environmental flows in india: towards sustainable water management, *Hydrological Sciences Journal*, *59*(3-4), 751–769, doi:10.1080/02626667.2014.896996. 6.3.1

Janes, T., F. McGrath, I. Macadam, and R. Jones (2019), High-resolution climate projections for south asia to inform climate impacts and adaptation studies in the ganges-brahmaputra-meghna and mahanadi deltas, *Science of The Total Environment*, *650*, 1499–1520, doi:10.1016/j.scitotenv.2018.08.376. 6.3.3

Mahmood, S., J. Davie, P. Jermey, R. Renshaw, J. P. George, E. N. Rajagopal, and S. I. Rani (2018), Indian monsoon data assimilation and analysis regional reanalysis: Configuration and performance, *Atmospheric Science Letters*, *19*(3), e808, doi:10.1002/asl.808. 6.3.1

Nepal, S., and A. B. Shrestha (2015), Impact of climate change on the hydrological regime of the indus, ganges and brahmaputra river basins: a review of the literature, *International Journal of Water Resources Development*, *31*(2), 201–218, doi:10.1080/07900627.2015.1030494. 6.0.1

Osborne, T., J. Gornall, J. Hooker, K. Williams, A. Wiltshire, R. Betts, and T. Wheeler (2015), Jules-crop: a parametrisation of crops in the joint uk land environment simulator, *Geoscientific Model Development*, *8*(4), 1139–1155, doi:10.5194/gmd-8-1139-2015. 6.0.1, 6.1, 6.3.3

Penning de Vries, F. W. T., D. Jansen, H. ten Berge, and A. Bakema (1989), *Simulation of Ecophysiological Processes of Growth in Several Annual Crops*, Simulation monographs, Pudoc. 6.1

Shannon, S., R. Smith, A. Wiltshire, T. Payne, M. Huss, R. Betts, J. Caesar, A. Koutroulis, D. Jones, and S. Harrison (2019), Global glacier volume projections under high-end climate change scenarios, *The Cryosphere*, *13*(1), 325–350, doi:10.5194/tc-13-325-2019. 6.3.2

Sperber, K. R., H. Annamalai, I.-S. Kang, A. Kitoh, A. Moise, A. Turner, B. Wang, and T. Zhou (2013), The asian summer monsoon: an intercomparison of cmip5 vs. cmip3 simulations of the late 20th century, *Climate Dynamics*, *41*(9), 2711–2744, doi:10.1007/s00382-012-1607-6. 6.1

Tuinenburg, O. A., R. W. A. Hutjes, T. Stacke, A. Wiltshire, and P. Lucas-Picher (2014), Effects of irrigation in india on the atmospheric water budget., *Journal of Hydrometeorology*, *15*, 1028–1050, doi:10.1175/JHM-D-13-078.1. 6.3.1

Waha, K., C. Müller, A. Bondeau, J. Dietrich, P. Kurukulasuriya, J. Heinke, and H. Lotze-Campen (2013), Adaptation to climate change through the choice of cropping system and sowing date in sub-saharan africa, *Global Environmental Change*, *23*(1), 130–143, doi:10.1016/j.gloenvcha.2012.11.001. 6.0.1

Williams, K., J. Gornall, A. Harper, A. Wiltshire, D. Hemming, T. Quaife, T. Arkebauer, and D. Scoby (2017), Evaluation of jules-crop performance against site observations of irrigated maize from mead, nebraska, *Geoscientific Model Development*, *10*(3), 1291–1320, doi:10.5194/gmd-10-1291-2017. 6.1, 6.3.1

Williams, K. E., A. B. Harper, C. Huntingford, L. M. Mercado, C. T. Mathison, P. D. Falloon, P. M. Cox, and J. Kim (2018), Revisiting the first islscp field experiment to evaluate water stress in julesv5.0, *Geoscientific Model Development Discussions*, *2018*, 1–47, doi:10.5194/gmd-2018-210. 6.3.2